Electrical Network Design for Offshore Wind: Analysis, Mathematical Modelling, and Optimization

Pérez-Rúa, Juan-Andrés

Link to article, DOI:
10.11581/dtu:00000080

Publication date:
2020

Document Version
Publisher's PDF, also known as Version of record

Electrical Network Design for Offshore Wind: Analysis, Mathematical Modelling, and Optimization

Department of Wind Energy
PhD Report 2020

Juan-Andrés Pérez-Rúa

DTU Wind Energy PhD-0102(EN)
DOI number: : https://doi.org/10.11581/dtu:00000080

May 2020

Authors: Juan-Andrés Pérez-Rúa

Title: Electrical Network Design for Offshore Wind: Analysis, Mathematical Modelling, and Optimization

Department: Wind Energy

2020

Project Period:

15 May 2017 – 14 May 2020

Education:

PhD

Supervisor:

Professor MSO Nicolaos A. Cutululis

DTU Wind Energy

Co-supervisor:

Professor Mathias Stolpe, DTU Wind Energy

Professor Poul E. Sørensen, DTU Wind Energy

Researcher Kaushik Das, DTU Wind Energy

DTU Wind Energy is a department of the Technical University of Denmark with a unique integration of research, education, innovation and public/private sector consulting in the field of wind energy. Our activities develop new opportunities and technology for the global and Danish exploitation of wind energy. Research focuses on key technical-scientific fields, which are central for the development, innovation and use of wind energy and provides the basis for advanced education.

DTU Wind Energy has a staff of approximately 240 and a further 35 PhD-students, spread across 38 different nationalities. The variety of research, education, innovation, testing and consultancy is reflected in the employment profile which includes faculty with research and teaching responsibilities, researchers and technical academic staff, highly skilled technicians and administrative staff.

Our facilities are situated at DTU Risø Campus and at DTU Lyngby Campus. Furthermore the department is running the national test stations in Høvsøre and Østerild.

Technical University of Denmark
Department of Wind Energy
Frederiksborgvej 399
Building 118
4000 Roskilde
Denmark

www.vindenergi.dtu.dk

Technical University of Denmark
Department of Wind Energy
Frederiksborgvej 399
Building 118
4000 Roskilde
Denmark
Telephone 46 77 50 85

info@vindenergi.dtu.dk
www.vindenergi.dtu.dk

Summary

Ambitious targets set by the European Commission see offshore wind power reaching 450 GW by 2050. Economies of scale push offshore wind to be deployed with hundreds of Wind Turbines (WTs) in single projects. Likewise, the distance from the Onshore Connection Point (OCP) to the Offshore Substation (OSS), is also increasing as response for finding new sites with high wind power potential.

A conspicuous increment in the complexity to design (and optimize) the electrical network for modern OWFs is resulted. The export submarine cables are complex dynamic systems, exposed to time-varying conditions that need to be assessed and understood to optimally size their cross-sections. Besides, in the collection systems, the feasible set of connections between WTs increase exponentially as a function of the project size.

On the top of the technical challenges, the economics of electrical power cables play a significant role as well. Between 2020 and 2024 more than 6,750 km of export cables are estimated to be needed. Meanwhile, 19,000 km of submarine cables for collection systems are prognosed to be installed from 2018 to 2028, with an estimated worth of £5.36bn. This places power cables as one of the main components of the Balance of Plant (BoP), representing at least 11% of the overall Levelised Cost Of Energy (LCOE).

In order to address these challenges, several methods and mathematical optimization models are proposed in this PhD thesis. The problem of sizing optimally export cables is approached through a comprehensive single framework, supporting cost reduction and reliability. A probabilistic lifetime estimation model is implemented to calculate the effects of cumulative damage due to electro-thermal stress. This framework is benchmarked against industrial standards, demonstrating the capability to reduce the overall LCOE by optimizing the export cable.

The deterministic design of the cable layout for OWFs collection systems is studied through several proposed approaches, based on heuristics, metaheuristics, and global optimization methods. For the latter, benchmarking results indicate the superiority of the proposed method against a state-of-the-art approach published in the scientific literature, in terms of solution quality, computing time, and optimality gap. This is continued with the proposition of a MILP program to design simultaneously the collection and transmission systems, accounting for OSSs location and forbidden areas.

Finally, a stochastic global optimization method is proposed to design closed-loop topology for OWF collection systems. A comparative analysis between radial and closed-loop topologies is performed to calculate and compare the cost benefits from each of them.

Resumé på dansk

Europa-Kommissionen har sat et ambitiøst mål om, at Offshore vind skal være 450 GW i 2050. Stordriftsfordele gør, at de enkelte offshore parker bliver installeret med hundredvis af vindmøller (WTG'er). Derudover er afstanden fra Onshore Connection Point (OCP) til Offshore Substation (OSS) stigende for at finde nye steder med højt vindkraftpotentiale.

Et resultat af dette er en stigning i kompleksiteten med at designe og optimere elkablerne for en moderne OWF. Eksport-søkablerne er komplekse dynamiske systemer, som udsættes for forhold, der varierer over tid. Dette skal vurderes og forstås for at bestemme det optimale tværsnit af kablerne. Derudover stiger antallet af mulige kabelforbindelser (array-kabler) imellem vindmøllerne eksponentielt som funktion af antal vindmøller.

Ud over de tekniske udfordringer spiller økonomien i elkabler også en væsentlig rolle. Mellem 2020 og 2024 skønnes det, at mere end 6,750 km eksportkabler vil være nødvendige. Derudover forventes det at 19,000 km array-kabler, med en estimeret pris på £5.36bn vil blive installeret i perioden fra 2018 til 2028. Dette placerer elkabler som en væsentlig del af Balance of Plant (BoP) med ca. 11% af Levelised Cost Of Energy (LCOE).

For at løse disse udfordringer foreslås flere metoder og matematiske optimeringsmodeller i denne PhD-afhandling. Problemet med at dimensionere og optimere eksport-kabler tackles gennem et enkelt omfattende framework, der understøtter omkostningsreduktion og pålidelighed. Der implementeres en sandsynlighedsbaseret levetidsvurderingsmodel for at beregne kumulative skader som følge af elektro-termisk stress. Dette framework er sammenlignet med industrielle standarder og demonstrerer muligheden for at reducere den samlede LCOE ved at optimere eksportkablet.

Det deterministiske design af kabellayoutet for OWF arraykablerne undersøges gennem flere foreslåede tilgange, baseret på heuristik, metaheuristik og globale optimeringsmetoder. For sidstnævnte indikerer benchmarkingresultaterne, at den foreslåede metode er overlegen i forhold til en state-of-the-art tilgang offentliggjort i den videnskabelige litteratur. Dette er med hensyn til løsningskvalitet, computertid og optimality gap. Endvidere foreslås et MILP optimeringsprogram til samtidigt at designe arraykabler og eksportkabler, under hensyntagen til OSS placeringer og forbudte områder.

Til sidst foreslås en stokastisk global optimeringsmetode til at designe closed-loop topologi til OWF arraykabler. En sammenlignende analyse imellem radial og closed-loop topologier udføres for at beregne og sammenligne omkostningsfordelene ved hver af dem.

Acknowledgements

I wish to express my sincere appreciation to my supervisor, Nicolaos Antonio Cutululis, who has always been there to provide both scientific and moral support along the execution of this PhD project.

I also want to deeply thank my supervisor Mathias Stolpe, who showed me in many occasions, the way to go during tough moments when challenges came.

Likewise, thanks as well to my other supervisors, Poul Sørensen and Kaushik Das, for all the knowledge gained from them and their valuable advices.

Thanks to all my colleagues at DTU Wind Energy, especially those at the Integration and Planning section.

I wish to acknowledge the support and great love of my family, my mom, Zamarkanda, my father, Manuel, and my brother Juanma, without their persistent help and counseling, the goal of this project would not have been realized.

And, last but not least, thank you, Karina, for all your love and support.

Contents

Abbreviations

AC	Alternating Current
ACO	Ant Colony Optimization
AEP	Annual Energy Production
BIP	Binary Integer Linear Programming
BoP	Balance of Plants
C-MST	Capacitated Minimum Spanning Tree
CCCP	Capacitated Centred Clustering Problem
CIGRE	Conseil International des Grands Réseaux Électriques
DC	Direct current
DCF	Discounted Cash Flow
DT	DanTysk
DTE	Dynamic Temperature Estimation
DTS	Dynamic Temperature Sensing
EW	Esau-Williams
FCM	Fuzzy C-Means
FEM	Finite Element Method
GA	Genetic Algorithm
HR1	Horns Rev 1
HV	High Voltage
I	Investment
IEC	International Electrotechnical Commission
IP	Investment plus total Power losses

IR	Investment plus Reliability
IRL	Investment plus Reliability plus Losses
L	Length
LA	London Array
LCOE	Levelised Cost Of Energy
LP	Length plus total Power losses
MCFP	Minimum Cost Flow Problem
MILP	Mixed Integer Linear Programming
MINLP	Mixed Integer Non-Linear Programming
MIQP	Mixed Integer Quadratic Programming
MST	Minimum Spanning Tree
MTBF	Mean Time Between Failures
MTTR	Mean Time To Repair
MV	Medium Voltage
NP	Nondeterministic Polynomial time
NPV	Net Present Value
O	Ormonde
OCP(s)	Onshore Connection Point(s)
OSS(s)	Offshore Substation(s)
OWF(s)	Offshore Wind Farm(s)
OWiFDO	Offshore Wind Farms Design and Optimization
PCI	Progressive Contingency Incorporation
PSO	Particle Swarm Optimization
PVC	Poly Vinyl Chloride
QT	Quality Threshold
RBN	Ronne Bank North
RBS	Ronne Bank South

SA	Simulated Annealing
SCTEM	Single Core Thermal Equivalent Model
SR	Step Response
SY	Synthetic
TEE	ThermoElectric Equivalent
TH	Thanet
TSP	Travelling Salesman Problem
VAM	Vogels Approximation Method
VRP	Vehicle Routing Planning
WDS	West of Duddon Sands
WT(s)	Wind Turbine(s)
XLPE	Cross-Linked PolyEthylene

CHAPTER 1

Introduction

1.1 Motivation

Among the different technologies for power production using renewable resources, offshore wind energy is shaping up as one of the fastest and most steadily growing. In Figure 1.1 the evolution of offshore wind power in the world from 2011 until the year where this PhD started, 2017, is shown. It can be noted that the share grew almost five times in that period of six years, with Europe hosting almost 85% of the total capacity.

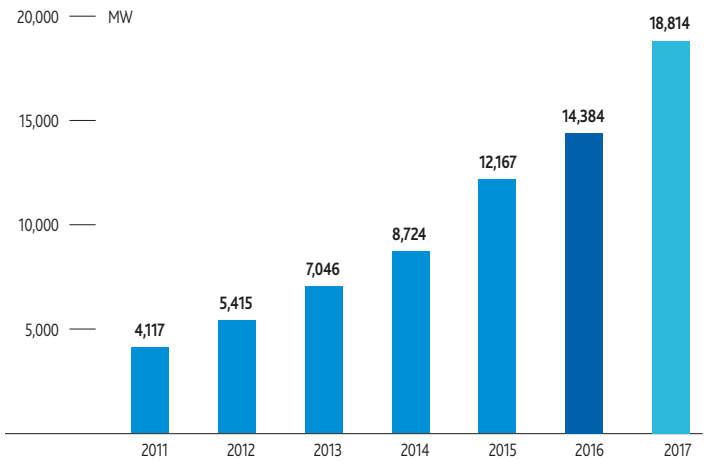

Figure 1.1: Cumulative offshore wind capacity 2011-2017 [1]

In the latest report published by the Global Wind Energy Council in 2020 [2], is evidenced that this growth rate is even higher, as quoting the international association "2019 was the best year ever for the global offshore wind industry", since the market has increased 6 GW in the course of 2019. Offshore wind is also spreading around the world, the percentage of projects located in Europe is currently of around 75%, having more participation from other continents, especially from Asia but as well from North America. The accelerated development of OWFs in the last decade casts a promising future for power systems fully based on renewable energy. The potential of this technology can be further unleashed; the European Commission estimates a total capacity of 450 GW by 2050 [3].

The evolution of offshore wind is reflected not only from the perspective of installation capacity, but also in economic terms. The LCOE has plummeted by around 50% on average in the last lustrum. Newly built project costs have declined by 33% from 2018

to 2019 alone [2]. The major drivers for this cost reduction have been mainly technology innovations in WTs and installation, reductions in financing costs, and economies of scale [4]. As a result, modern OWFs are typically composed by hundreds of WTs in single projects, with increasing connection distance from the OCPs to the OSSs to exploit new sites with high wind power potential [5].

Nevertheless, as a consequence of such scaling, the grid connection gains a bigger role, due to the electrical power cables and OSS costs. In Figure 1.2 is presented the LCOE evolution along with the grid connection cost share in some European countries. The main takeaway is that the grid connection costs are not following proportionally the overall LCOE reduction.

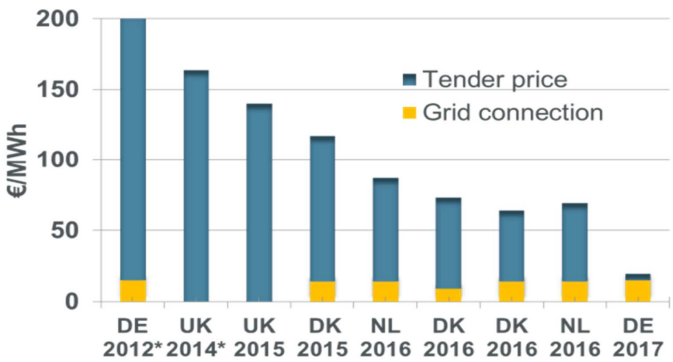

Figure 1.2: LCOE development of offshore wind [6]

Bigger OWFs causes a conspicuous increase in the mathematical complexity to design their electrical network, which has as a main component electrical power cables. The number of solutions for the interconnection system between WTs increase exponentially as a function of the project size [7], while longer cables are used to connect those projects to the grid, implying a higher level of vulnerability in front of the dynamics of the system [8].

Electrical power cables are one of the main components of the BoP, representing at least 11% of the overal LCOE [9], with comparable costs to those reported for the wind turbine nacelles, towers, and foundations. Between 2020 and 2024 more than 6,750 km of export cables are estimated to be needed. Meanwhile, 19,000 km of submarine cables for collection systems are prognosed to be installed from 2018 to 2028, with an estimated worth of £5.36bn [10]. However, electrical power cables do not only have a sizeable impact over capital expenses, but also affect greatly the operation and performance of OWFs projects. The total electrical power losses and potential single points of failure [11] may impact negatively the profitability of the project in the long-run.

This means that the challenge of designing the electrical network of OWFs, may provide a great potential for extra overall cost minimization by applying computational optimization and properly sizing components. Given the trend of constant grid connection costs in the

last years, and the accentuated weight of electrical power cables in the overall LCOE (in terms of capital and operational costs), this PhD work focuses on developing techniques and methods for further more cost reductions. The efforts are concentrated to the electrical network design for large-scale OWFs (in the order of hundred of WTs).

1.2 Scope

The PhD project was part of the project *Integrated Baltic Offshore Wind Electricity Grid Development* (Baltic InteGrid) [12].

The Baltic InteGrid project provided a research framework for assessing the feasibility to construct meshed grid in the Baltic Sea Region, optimizing efficiency and potential of offshore wind. The main goals were:

1. Contribute to sustainable indigenous electricity generation.
2. Further integration of electricity markets.
3. Enhance security of supply in the Baltic Sea Region.
4. Facilitate the development of offshore wind.

Part of the PhD work belonged to the Work Package 3, group of activities 3.3. Stemming from this work package, the aim was to design a tool for optimizing the electrical network for OWFs, supporting both deterministic and probabilistic modelling of electrical power cables, as a component and as a system (collection and transmission systems).

The Figure 1.3 depicts a simplified full picture of the problem addressed in the PhD project.

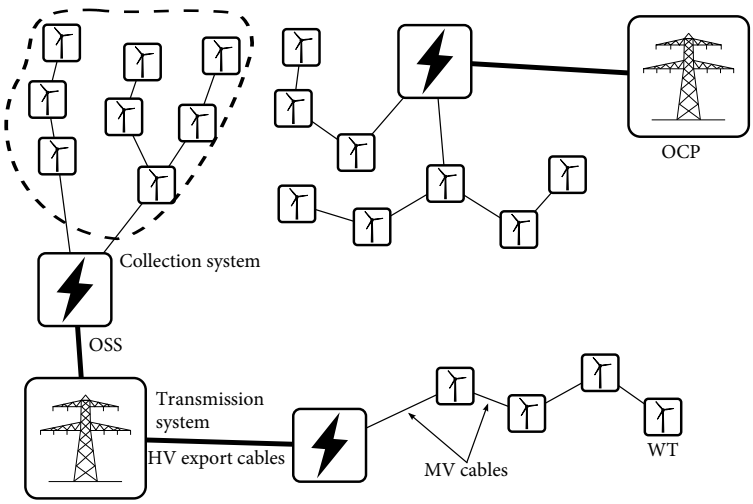

Figure 1.3: Electrical network design for offshore wind: An overview. Based on [7]

Electrical power cables are present in both the collection and transmission systems. The cable layout in the collection system corresponds to the interconnections between WTs through MV electrical power cables. The MV cables are usually rated at 33 kV in AC, but recent new technologies allow the use of 66 kV-rated components to decrease current ratings and total electrical power losses, since WT rated power is steadily increasing. The collection system is interfaced to the transmission system by means of an OSS, to subsequently connect the OWF to the OCP. The transmission (export) system rated voltage encompasses values in HV AC of 110 kV, 132 kV, 150 kV, 220 kV, and 275 kV [13]. AC technology for both the collection and transmission systems were considered in this doctoral thesis, albeit conceptually the models can be applied straightforwardly to DC technology as well.

The cable layout in the collection system may have different topologies. The most frequently used currently is a radial layout (without a redundant path from each WT to the OSS, as shown in Figure 1.3), albeit some project have a closed-loop layout (with a single redundancy from each WT to the OSS), resembling a sunflower. The underlying reasoning behind choosing either of them, comes from the modelling choice regarding the cables failures. If no failures are considered in the design phase, then a *deterministic* approach is used, generally resulting in radial layout; otherwise, if to each cable a failure probability is associated, then a *stochastic* approach is considered to design a closed-loop layout. The size of the cables failure rate, combined with the availability of proper methods, would ultimately decide the approach.

While a closed-loop layout can be designed considering a deterministic approach, the capability to exploit the benefits of this network type is contingent on the inclusion of cables failures [C5]. Similarly, a radial topology can also include reliability aspects and be optimized for it, but this would not make much sense as redundant paths are missing, and could result in expensive designs.

Since optimizing the placing of WTs is mostly driven by aerodynamic interactions, their location in Figure 1.3 is considered fixed and given, following a sequential divide-and-conquer approach [J1].

Based on the above, the objectives of the PhD project are:

1. Sizing (optimization) of the export power cable for a given OWF.
2. Design (and optimization) of the radial cable layout of the collection systems for large-scale OWFs, assuming fixed WT and OSS locations.
3. Simultaneous design (and optimization) of the collection and transmission systems, assuming fixed WT locations, variable OSS locations, and forbidden areas.
4. Design and compare closed-loop and radial cable layouts for the collection system of OWFs.

1.2.1 Research Questions

The main objectives of this work were further detailed into research questions summarised as:

1. Is it possible to decrease the LCOE-share of export power cables, ensuring minimum reliability requirements, accounting for the impact of the variable wind power production, and the transmission length?
2. What are pros and cons of the different methods for designing the radial cable layout of collection systems for OWFs?
3. What are the benefits for combining different conceptual methods for designing the radial cable layout of collection systems for large-scale OWFs?
4. Is it possible to improve the tractability and efficiency of state-of-the-art methods for designing the radial cable layout of collection systems for large-scale OWFs?
5. How can the collection and transmission systems be optimized simultaneously being handled with a global optimization method for large-scale OWFs?
6. What are the benefits of designing either radial or closed-loop topologies for the cable layout of collection system for OWFs, considering a stochastic approach?

1.3 List of Publications

The results of the PhD research were disseminated in several scientific publications, as listed below. They represent the basis of the PhD thesis and are included in the Appendix.

1.3.1 Journal Publications

[J1] J.A. Pérez-Rúa, and N. A. Cutululis, "Electrical Cable Optimization in Offshore Wind Farms - A review", in *IEEE Access*, Vol. 7, 85796–85811, July 2019, https://doi.org/10.1109/ACCESS.2019.2925873.

[J2] J.A. Pérez-Rúa, K. Das, and N. A. Cutululis, "Optimum Sizing of Offshore Wind Farm Export Cables", in *International Journal of Electrical Power & Energy Systems*, Vol. 113, 982–990, December 2019, https://doi.org/10.1016/j.ijepes.2019.06.026.

[J3] J.A. Pérez-Rúa, M. Stolpe, K. Das, and N. A. Cutululis, "Global Optimization of Offshore Wind Farm Collection Systems", in *IEEE Transactions on Power Systems*, Vol. 35, No. 3, 2256–2267, May 2020, https://doi.org/10.1109/tpwrs.2019.2957312.

[J4] J.A. Pérez-Rúa, M. Stolpe, and N. A. Cutululis, "Integrated Global Optimization Model for Electrical Cables in Offshore Wind Farms", accepted in *IEEE Transactions on Sustainable Energy*, October 2019, https://doi.org/10.1109/TSTE.2019.2948118.

[J5] J.A. Pérez-Rúa, S. Lumbreras, A Ramos, and N. A. Cutululis, "Reliability-based Topology Optimization for Offshore Wind Farm Collection System", submitted to *Wind Energy*, April 2020.

1.3.2 Conference Publications

[C1] J.A. Pérez-Rúa, K. Das, and N. A. Cutululis, "Lifetime estimation and performance evaluation for offshore wind farms transmission cables", in *Proceedings of the 15th IET International Conference on AC and DC Power Transmission (ACDC 2019)*, Coventry, UK, 5th–7th February 2019, https://doi.org10.1049/cp.2019.0062.

[C2] J.A. Pérez-Rúa, K. Das, and N. A. Cutululis, "Improved Method for Calculating Power-Transfer Capability Curves of Offshore Wind Farms Cables", in *Proceedings of the 2019 CIGRE International Symposium*, Aalborg, Denmark, 4th–7th June 2019.

[C3] J.A. Pérez-Rúa, D. Hermosilla, K. Das, and N. A. Cutululis, "Heuristics-based design and optimization of offshore wind farms collection systems", in *Journal of Physics: Conference Series*, Vol. 1356, 012014, 16th Deep Sea Offshore Wind R&D conference, Trondheim, Norway, 16th–18th January 2019, https://doi.org/10.1088/1742-6596/1356/1/012014.

[C4] D. Hermosilla, J.A. Pérez-Rúa, K. Das, and N. A. Cutululis, "Metaheuristic-based Design and Optimization of Offshore Wind Farms Collection Systems", in *Proceedings of the 13th IEEE PES PowerTech Conference*, Milan, Italy, 23rd–27th June 2019, https://doi.org/10.1109/PTC.2019.8810583.

[C5] J.A. Pérez-Rúa, S. Lumbreras, A. Ramos, and N. A. Cutululis, "Closed-Loop Two-Stage Stochastic Optimization of Offshore Wind Farm Collection System", under review in *Journal of Physics: Conference Series*, EAWE TORQUE 2020, Delft, Netherlands, https://arxiv.org/abs/2003.06598.

1.4 Contributions

The main contributions of the PhD project are:

1. Comprehensive state of the art review regarding electrical cable optimization in OWFs. Proposal of a general classification of the electrical network design problem, framed in the general context of the OWFs Design and Optimization.
2. Proposal of a method to improve the calculation of power-transfer capability of OWFs cables, accounting for variable production of wind power, and variable boundary conditions.
3. Proposal of a method to size optimally OWF export cables. It minimizes the LCOE-share corresponding to this component, by balancing out investment, losses and reliability requirements. It includes different concepts, considering realistic

operation conditions, such as: time varying cyclic power generation, electro-thermal stress, among others.

4. Development, testing, and application of heuristic algorithms to design the radial cable layout of collection system for OWFs.
5. Development, testing, and application of a metaheuristic algorithm based on a GA, to design the radial cable layout of collection system for OWFs.
6. Development, testing, and application of a global optimization model based on a MILP approach, to optimize the radial cable layout of collection systems for large-scale OWFs.
7. Development, testing, and application of a global optimization model based on a MILP approach, to optimize simultaneously the radial cable layout of collection systems, and transmission cables for large-scale OWFs.
8. Development, testing, and application of an algorithmic framework to design collection system with a closed-loop structure, using global optimization based on a MILP approach, integrated with analytical methods for reliability assessment.
9. Development of a common framework to assess and compare economically topology optimization for OWFs, namely closed-loop vs radial layouts.

1.5 Thesis Outline

The PhD thesis is organised as follows:

- The PhD project has been introduced in Chapter 1. The motivation, scope, research questions, publications, and contributions have been presented.
- The state of the art is presented and discussed in Chapter 2.
- The methods regarding electro-thermal analysis of cables and the optimization framework to design export cables for OWFs is presented in Chapter 3.
- The different method to design (and optimize) the radial cable layout of collection systems for OWFs are presented and demonstrated in Chapter 4.
- The global optimization program to design simultaneously the radial cable layout of collection systems, and transmission cables for large-scale OWFs is presented and demonstrated in Chapter 5.
- The global optimization program to closed-loop network for large-scale OWFs is presented and demonstrated in Chapter 6. In this chapter the comparison of this topology against radial layout is also examined using several case studies.
- Finally, concluding remarks and recommendations for future research are made in Chapter 7.

CHAPTER 2

State of The Art

This chapter is a summary of the review article [J1].

2.1 Introduction

Electrical network design for OWFs is a multidisciplinary problem. A wide variety of definitions, strategies, models, and frameworks to optimize performance metrics related to electrical infrastructure has been detected in the literature survey. Additionally, this is a relatively new research area, with no more than 15 years of studies by scientists from different fields, therefore plethora of methodologies and mathematical formulations have been proposed; that is reflected by a relatively large pallet of objectives and requirements identified in the scholar literature. In this sense, a literature review of the latest techniques for optimizing electrical cables in OWFs is performed, intending to provide a classification of the problem while underlying its most important aspects.

2.1.1 Design and Optimization of OWFs

The OWiFDO problem can be defined as the body of decisions to be made in order to design reliable, secure, and efficient OWFs, while maximizing their performance through the evaluation of a quantifiable target. The definition of the set of modelling options, constraints, objective function, variables and parameters, is up to the OWF developers, according to established and particular practices. The OWiFDO is a non-linear, non-convex problem with integer and continuous variables, laying in the category of NP class [14].

Due to the mathematical complexity of the problem, the full picture of it can be split following a sequential divide-and-conquer approach, such as the one illustrated in Figure 2.1. The main inputs are: minimum and maximum number of WTs, minimum and maximum OWF's total installed power, and definition of the objective, constraints, and other parameters. The sequential steps are described as follows:

1. Macrositing (site selection): It includes the analysis of the available infrastructure (power system capacity at OCP, logistic resources, accessibility, etc), the evaluation of the environmental suitability (especially relevant in marine spatial planning), the wind resource potential assessment, and the geographical adequacy (most importantly maximum water depths). The main output of this block is the selection of the OWF site, and the upper bound of project area. Important economic factors such as energy regulatory framework, financing and funding must be taken into

consideration in this stage as well, in order to assess the financial sustainability of the project.

2. Micrositing (WTs location): It involves the OWF layout design, where the arrangement of the individual WTs is decided. In this sub-problem the number and geographical locations of the WTs along with their sizing are defined.
3. Infrastructures: This stage regards the design of the BoP, encompassing structural, electrical, and civil infrastructures. Electrical infrastructure encompasses the network design and optimum sizing of transformers and converter stations. This PhD focuses on the electrical network design of OWFs.
4. Control/Protection/Operation: In this sub-problem the control, protection and operation schemes are designed.

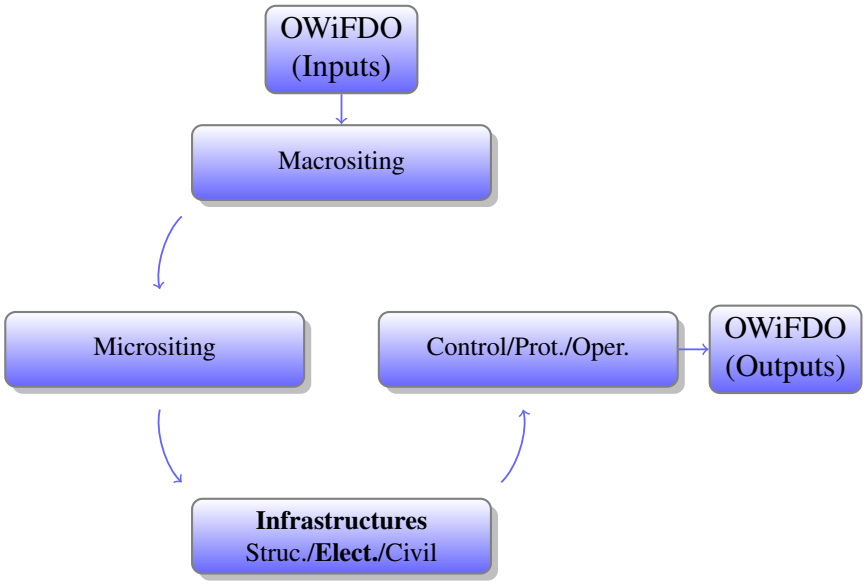

Figure 2.1: Overview of the OWiFDO problem [J1]

2.1.2 Electrical Network Design for OWFs: A classification

Since electrical power cable is the main component for the network design, the classification of the problem around this element is depicted in Figure 2.2.

In the left branch of the Figure 2.2, the topics corresponding to optimum sizing of electrical cables are presented, which answers the question of *How to* size individually these elements. The right branch of the figure represents the combinatorial optimization problem related to the electrical network topology optimization for OWFs; it deals with *Where to* allocate power cables in such a way that the produced power by the WTs is evacuated to the OCP. The latter problem feeds itself from the former, establishing the complementarity between them, and the possibility to combine them for more refined optimization.

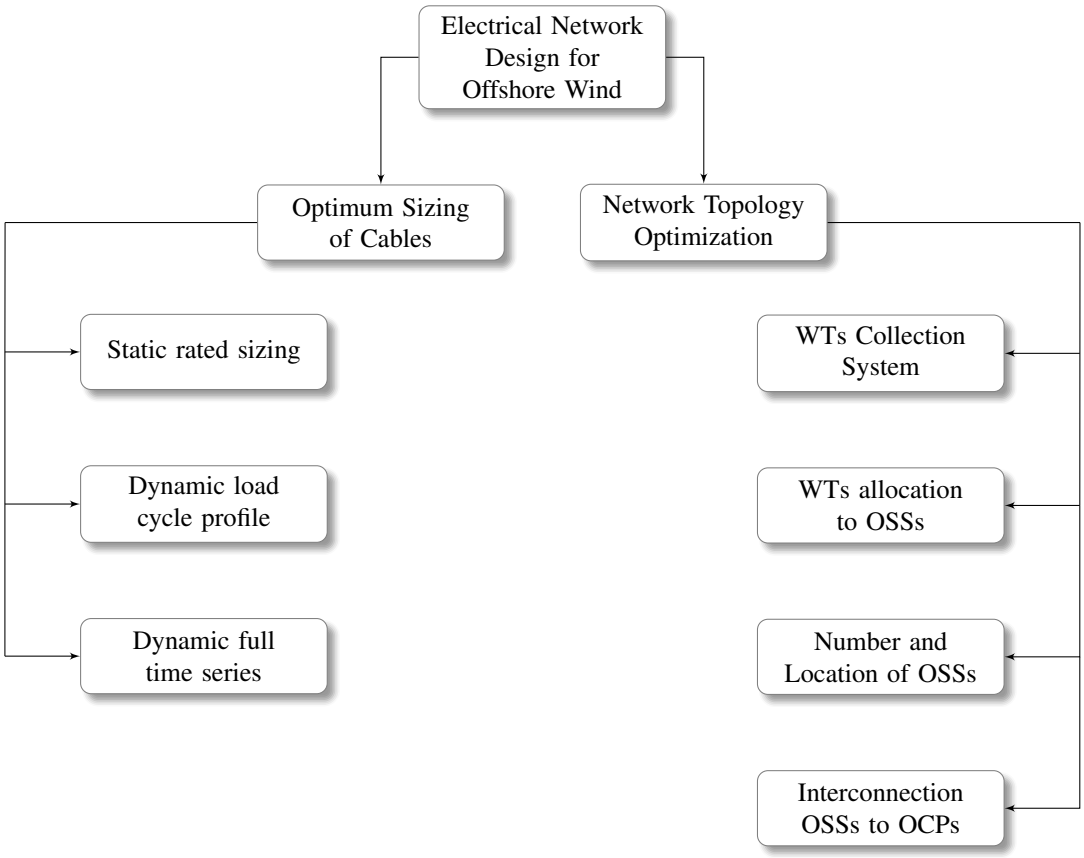

Figure 2.2: Electrical network design for offshore wind: A classification [J1]

2.2 Optimum Sizing of Cables

The definition of a cable's nominal current must take into account the variability of offshore wind power and its relatively low capacity factor [15]. This implies that a smaller nominal value can be chosen given certain conditions. The three main techniques used in OWFs cable sizing from the perspective of thermo-electrical conditions are presented in the following.

2.2.1 Static Rated Sizing

This is the classic technique recommended in [16], [17], and [18] (industrial technical standards). It is a straight-forward approach, consisting only a multi-parameter static equation for calculating the continuous current I_t, to be transmitted during infinite time, in order to obtain a continuous conductor temperature equal to 90°C. The smallest cable t, with I_t equal or greater than the total current (including capacitive currents) at hot spot, is selected. The aforementioned IEC and CIGRE industrial standards consider static conditions at rated operation, however OWFs are characterized by low capacity factors and high power production variability.

2.2.2 Dynamic Load Cycle Profile

This technique consists in finding the worst case dynamic load profiles, as presented in [19] (CIGRE: Working Group B1.40). This approach is taking into account the inherent variability of power production, representing a more sophisticated method that is emerging as industrial practice, as detailed in [19]. It consists of a four-step signal, calculated using the highest RMS values computed through different periods, sweeping through the yearly data set by means of a rolling RMS filter starting at each singular data point. Further details can be found in [J1].

2.2.3 Dynamic Full Time Series

This method encompasses the use of full and high resolution time series for performing electro-thermal analysis. The previous two methods exclude reliability analysis, therefore new advances and strategies requiring time series information, such as, generated power, seabed surface temperature, thermal parameters, among others, are necessitated. So far works have focused on: i) conductor temperature estimation, and ii) cables sizing considering a maximum instantaneous temperature never exceeding 90 °C (which also is assumed in the previous two approaches).

A review of articles dealing with this aspect is available in [J1]. Important progress has been done in this topic, however there is still room for new advancements, such as the application of lifetime methods and probabilistic techniques for sizing these components. The dynamics of the system must be considered holistically, being able to estimate fatigue factors to which a real operating cable is exposed to.

2.3 Network Topology Optimization

The main objective is to achieve an optimized cable layout, in terms of length and/or investment costs, and/or reliability (See Figure 1.3). Several variants of the problem compose the problem classification depicted in the right branch of the Figure 2.2. They are described as:

- WTs collection system design: This is to design the cable layout considering a single fixed OSS.
- WTs allocation to OSSs: This is to design the cable layout considering multiple fixed OSSs.
- Number and location of OSSs: This is to design the cable layout considering multiple movable OSSs.
- Interconnection of OSSs to OCPs: This is to design the export cables given fixed or movable OSSs and OCPs.

2.3.1 WTs Collection System Design

This problem resembles to historical mathematical problems such as MST and its constrained version, the C-MST, which classifies under the category of NP-hard class [20], and the TSP with all its variants [21], also NP-hard. Problems from other fields map to this one, like telecommunication networks design back in the 60's and 70's [22], or network planning [20]. However in the case of OWFs, *Ad hoc* methods are necessitated in function of particular spatial (nature reserve or occupied areas, seabed bathymetry, among others), planarity (no-crossing of cables, trenching requirements, and so on), and technical (stochasticity on power generation, cables capacities, topological structure, ancillary services support, etc) constraints. Figure 2.3 presents a decision flowchart to design the cable layout of a collection system.

The flowchart in Figure 2.3 explains the set of decisions to be taken during the design process; that includes the selection of the desired topology, followed by the required objective function. The selection in both aspects depends among other things, about the modelling approach for cables failures, i.e., deterministic (no failures) or stochastic. A deterministic approach generally results in radial layout, which in turn can be optimized for length, and investment with or without losses. Stochastic optimization permits to design redundant systems including costs in the objective function due to random energy curtailment. Some methods perform better than others for a particular topology and objective function, and therefore must be selected accordingly.

The solution methods can be classified in four main groups: i) Heuristics (Prim, Dijkstra, Kruskal, EW, VAM), ii) Metaheuristics (GA, PSO, SA, ACO), iii) Global optimization or exact formulations (BIP, MILP, MIQP, MINLP) and iv) Hybrids. A detailed analysis between them and their frequency of application in the scientific literature is presented in [J1]. In general, heuristics seem to be very fast but weak in the sense of low solutions quality, while metaheuristics, which are based on evolutionary operators, provide better solutions without optimality certificate. Mathematical formulations have the enormous advantage of being able to provide certified optimum solutions when the problem is convex and can be solved by means of commercial solvers. Hybrids methods combine different concepts, such as evolutionary algorithms and/or heuristic rules mixed with exact formulations.

After selecting the solution method, the modelling choices of the physics must be carried out, taking into account the inherent biased caused by the chosen methodology. Mainly five aspects needs to be examined: i) wake effects, ii) wind stochasticity, iii) power flow, iv) electrical losses, and v) reliability. A compromise between accuracy of the solution method and the fidelity of physics modelling must be carried out.

Each of the different topology options according to the literature (radial with and without branching, radial with splices, closed-loop, and tailored-made), are discussed in [J1], describing the most sound solution methods, modelling choices, and spatial/planarity constraints handling.

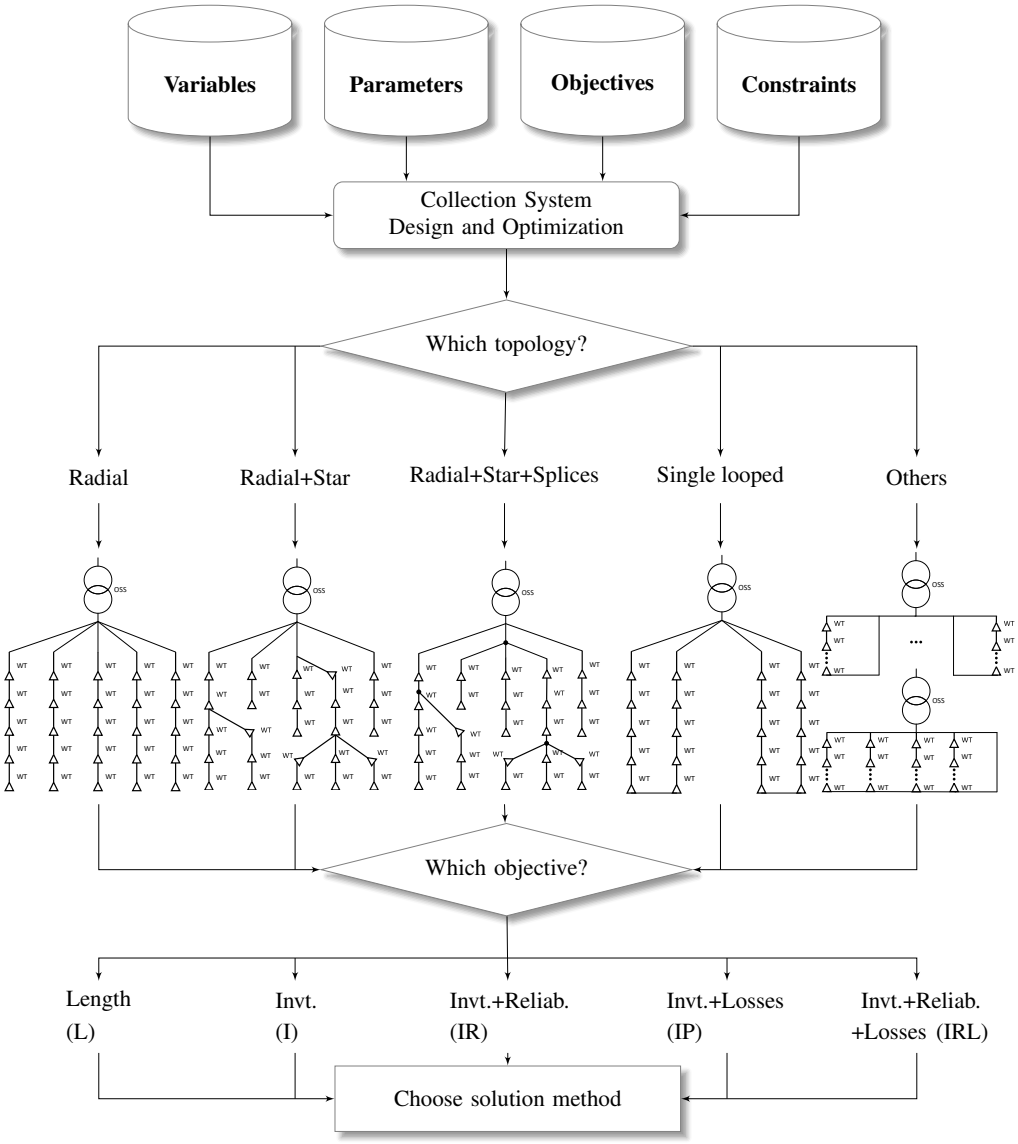

Figure 2.3: OWFs collection systems design and optimization: Decision flowchart [J1]

2.3.2 WTs Allocation to OSSs

This problem is an extension of the one analyzed in Section 2.3.1 but with the added complexity of considering a given number of multiple OSSs with fixed locations. The problem size is thus from medium (30 to 60 WTs) to very large-scale (hundreds of WTs). The WTs must be allocated unequivocally only to one OSS (i.e., no direct electrical coupling from one WT to more than one OSS), while guaranteeing the OSSs capacities (in terms of nominal power).

Three alternatives have been found out to address this problem:

- Single approach: WTs allocation is solved simultaneously with the collection

system problem. Mathematical formulations can be used transparently to leave the optimization set up to deal with the full problem, as in [23] or [24] (hybridized with heuristics). However, for very large OWFs this may be computationally expensive as presented in [7] and [24], pointing out the impossibility to solve them to optimality. Thus, scalability is the main challenge and exact methods with high tractability, efficiency and accuracy are demanded. Metaheuristics can also be designed to handle this issue as per in [25]; which may help in shortening computing time to obtain feasible points.

- Multi-step approach: WTs allocation is firstly handled, and then followed by a multi-thread optimization problem to design multiple collection systems using any of the methods described in Section 2.3.1. The WTs allocation tasks can be approached by clustering techniques such as QT (deterministic), K-means, and FCM (both unsupervised machine learning processes). Mathematical methods such as the one framed as a MCFP [26] is applicable as well. MCFP allows shaping the problem with an BIP mathematical formulation, and the network simplex algorithm can be applied to solve it to optimality by exploiting the problem structure and the duality conditions.
- Nested approach: WTs clustering is updated based on iterative calculations of collection systems searching for a cheaper solutions [27].

2.3.3 Number and Location of OSSs

This is an extension of the problem in Section 2.3.2, adding the flexibility of the number and location of OSSs. Two main variants for the task are identified:

- Variable number and location of OSSs: This has been coped by means of a multi-step approach in [28] (MILP formulation), [29] (GA), [30] (FCM plus Prim algorithm), and [31] (immune GA). A nested approach has been applied in [32] and in [33]. See more details in [J1].
- Fixed number and variable position of OSSs: This has been coped with single exact methods as in [34], and [35] for small-scale instances (maximum 30 WTs). A multi-step approach is proposed in [36], where a CCCP and a heuristic is used to find the OSS location. Lastly, a nested approach can be found in [27].

2.3.4 Interconnection of OSSs to OCPs

Two main variants for this task are identified:

- Point-to-point interconnection between a single (or few) OSS(s) to a single (or few) OCP(s): It basically consists on finding the proper balance between the collection system design (including the OSS positioning), and the transmission system design (export system to connect the OSS to the OCP), given that the shorter distance between OSS to OCP, the more expensive the collection system, but the cheaper

the transmission system. Most of the authors assume the influence of OSSs location to the transmission system costs inside of a given range negligible. Nevertheless, in works like [37] (onshore case), [38], multi-fidelity and heuristics approaches, respectively, are considered to analyze the trade-off between these two costs. Other works taking into consideration simultaneously the collection system design (with OSSs location), and the transmission system design are: [34] (MILP), [32] (PSO), [39] (GA), [33] (GA and clustering techniques), and others.

- Interconnection between multiple OSSs and multiple OCPs (large OWFs spread out in a large area): The OWFs are seen in an aggregated way, disconsidering the collection system design and calculating the total installed power of the OWF. This problem aims to find a balance between new OWFs project and the integration with new or reinforced interconnectors between countries, while having present other types of electricity generation connected to OCPs [40]. Electricity markets and power system planning aspects need to be considered.

2.4 Summary

A detailed review regarding the electrical network design for offshore wind, based on [J1], is carried out in this chapter. As a result, the full picture of the problem is divided in two main branches: optimum sizing of electrical cables, and network topology optimization.

For the electrical cable sizing, the three main techniques available today in the industry practices and scientific literature have been presented. They span from a lower to higher level of complexity as follows: static rated sizing, dynamic load cycle profile, and dynamic analysis with full time series. The dynamic load cycle profile is gaining popularity nowadays, given the relative low capacity factors of OWFs (of around maximum 50%), and the high variability of wind power.

Dynamic full time series analysis represents an attractive and important topic, which may allow offline or online lifetime estimation in order to ensure the selection of smaller cables while respecting reliability requirements. The development and application of electro-thermal-mechanical models for cables cumulative damage estimation promise important contributions for further OWFs cost minimization.

For the network topology optimization aspects, the wide set of different methods to study variants of the combinatorial problem to interconnect WTs to the OSSs, and these to the OCPs, have been described. The proper balance between the method complexity and physics modelling is one of the main task of the OWF designer. Thus, the main challenge is the development of exact methods incorporating high fidelity models to account for: wake effects, wind stochasticity, power flow, total electrical power losses, and reliability.

Additionally, since the trend for modern OWFs is to construct very large projects (in the order of hundreds of WTs), then tractability and efficiency of the solution approaches must be prioritized. Inclusion of real-world constraints is also becoming very relevant, like forbidden areas due to maritime restrictions, seabed bathymetry, cables bending

moment, etc. There is also space for new global optimization formulations including a probabilistic approach for reliability assessment to obtain closed-loop networks. Exact methods to approach the full picture of the network topology optimization problem are necessitated as well.

As a result of the literature review, the aforementioned scientific challenges have been identified, and these are the main motivation for the proposed methods presented in the next chapters. The methods seek to cover some of the identified gaps in the scientific literature.

CHAPTER 3
Sizing of Export Power Cables

This chapter is a summary of the articles [J2], [C1] and [C2].

3.1 Introduction

The distance to shore for modern OWFs is currently in the order of hundreds of kilometers. Inclusive, some projects with construction permit have been designed for 200 km of connection between the OSS and the OCP [4]. This unequivocally means that more and more export cables are needed, which in turn causes more attention towards the optimum sizing and understanding of the electro-thermal-mechanical dynamics (in transient and steady states) of this component.

The most prevalent types of HV AC and MV AC cables use XLPE technology for the insulation, as presented in Figure 3.1. The low dielectric loss factor of polyethylene allows its use at higher voltage levels than other type of insulation materials, such as PVC [41].

Figure 3.1: XLPE submarine cables for OWFs [13]

An electrical power cable is composed by several subcomponents, mainly, in inner to outer order: conductor, conductor shield, insulation, insulation shield, metallic screen, plastic sheath, filling material (three-core cables), tapes for assembling (three-core cables), armour and jacket. Optical fibers are installed for DTS.

The electrical current is transmitted through the conductor generally manufactured with copper, which is protected by a carbon doped XLPE shield to mitigate electric fields intensification; then the XLPE insulation is placed, useful for maintaining electrical distance between conductor and ground. This is followed by other polymer insulated shield to protect the insulation, and then the lead metallic screen is found, which carry ground potential and conduct fault currents; plastic shields isolate this material. Three-core cables require filling materials and tapes for being assembled. Finally a copper armour layer protects the cable against mechanical stress, and a PVC layer covers externally this component [42].

Cables' most critical element is the insulation layer, which according to manufacturers, has an associated lifetime with failure probability, that is described in terms of rated temperature, 90 °C, and rated electric field; since this material is in close contact to the conductor external layer, the conductor continuous temperature and electric field, under operation, must be fixed to the rated values.

There may be other factors fatiguing the cable, such as mechanical and environmental stress [43]. The former is present during manufacturing, assembling, and laying processes, but their impact is minimized considerably by following modern techniques throughout each process. The latter is caused by oxidation, radiation, and moisture; however submarine cables are implicitly protected against these threats, partly due to the buried depth, and partly due to the mechanical protective inner layers of the cable itself.

Traditionally, the sizing of offshore export cables has been done based on the CIGRE [18] and IEC [16]-[17] standards. The standards approach this with a classic point of view, considering steady state conditions under constant rated operation. Recently, a new approach as described in [19], consisting in worst case equivalent step-wise load profiles, is being increasingly used in the industry. This represents a strategy to minimize the cable's cross section, going towards a more refined, realistic, and simplified approach.

The deterministic, constant rated power operation implied in the standards is intuitively too conservative considering that OWFs have a typical capacity factor of 0.4 - 0.5 with high variability. Additionally, the increase of length of export cables lead to more potential failure points.

In this sense, in this chapter are proposed techniques for optimum sizing of HV export cables for offshore wind. The methods allow for:

- Correction of power-transfer capability. The impact of cables' thermal and geometrical parameters, site-dependent variables (wind power generation time series, soil temperature time series, soil thermal properties variation, etc), and installation conditions (total length, buried depth, compensation units, among others) over

the transmissible OWF installed power offered by export cables is quantified. Real operating conditions (thermal transients, capacitive currents, and cyclic generation) are considered. The output is the transmissible power for a given cable in function of the connection length. The results are fully available in [C1] and [C2].

- Sizing optimally export cables through a holistic framework. This method combines different concepts, considering operating conditions deemed realistic, such as: time varying cyclic power generation, electro-thermal stress, thermal transients, capacity currents, length-dependent failure probability, and variable external temperature. It also accounts for the ultimate strength limit of the insulation material and, proposing a holistic approach for optimizing the export cable utilization. The output is the cable's cross-section which presents the best balance between investment, losses, and reliability requirements. The results are fully available in [C1] and [J2].

3.2 Methods

The set of methods are: The DTE model, the power-transfer capability correction model, and the optimization framework for export cables. The last two use the DTE model for their analysis.

3.2.1 DTE Model

Dynamic loadability techniques calculate the current which can be carried for a limited period of time, without the physical limitations of any part of the cable being exceeded. Dynamic loadability requires the use of DTE in order to estimate the cable temperature either for real-time applications or for offline predictions given time-series of forecasted load current.

Nowadays, there are mainly three modelling principles for estimation of the cable temperature dynamically, those are: FEM, SR -used by CIGRE- and TEE. A comparison between those methods has been done in the papers [44]-[45], where it is remarked that TEE provides results which are within an acceptable range of the FEM simulations (nearly 1 °C) with a considerable computation time reduction. Additionally, SR provides good quality results but still around six times slower than TEE and requires to solve two set of equations for a specific calculation point, in contrast to the TEE method that solves the system for several radial distances at once [42]. TEE model also has proved to exhibit a correct estimation of the temperature as compared to real measured data in experimental tests, with deviations of around 3 °C. All in all, it has been concluded that a TEE model represents the best choice for performing DTE analysis.

The TEE method is easy to be understood from an electrical engineering point of view. It is based on a SCTEM [45], [46]. It basically consists in a direct translation of thermodynamic variables into electrical variables, i.e., considering the heat flow as electrical current and temperature as nodal voltages. Every subcomponent of the cable is then represented with a thermal resistance and a thermal capacitance (also known

as specific heat), and along with the electrical losses, the equivalent electrical circuit is formed from them as presented in [C1]. The surroundings, which in the case of submarine cables is the determined by the seabed where the cable is buried, can be divided into multiple layers, in order to evenly distribute its influence over the seabed volume, at cost of a higher computational time required. The TEE results in a system of ordinary differential equations. More details of the TEE model, its calibration and formulae are in [C1] and [C2].

The DTE model is depicted in Figure 3.2. The site-dependent inputs include OWF annual power time series [15], seabed temperature time series, and seabed thermal parameters (thermal resistivity and thermal specific heat). Project-dependant inputs are the project's electrical system data, such as nominal frequency, nominal voltage at OSS, power factor at OSS, compensation units, export cable type with all its geometrical, thermal, and electrical information, and cable installation conditions, like buried depth and phase spacing for single-core systems. The simulation setting is the number of layers to model the seabed terrain, typically a value of 10 is good enough [C1].

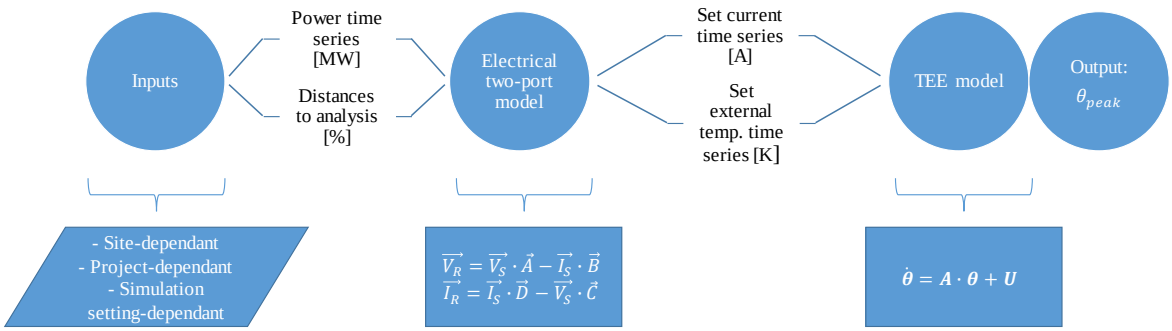

Figure 3.2: The DTE model [C2]

A fixed distance to analysis equal to 100% must be set in case no shunt-series compensation units are installed, as current increases monotonously with the length. Compensation units may alter the longitudinal current profile, shifting the instantaneous maximum current point to an intermediate value lower than the OCP distance. Following up, the electrical two-port model is implemented to calculate the capacitive currents [47]. Later on, with the total current and seabed temperature time series, the TEE model is used to calculate the temperature time series in the given interval, in this way the maximum instantaneous temperature is obtained.

3.2.2 Power-transfer Capability Correction Model

The method for the correction of power-transfer capability curves is shown in Figure 3.3. In addition to the previously required inputs for the DTE model, in this case, other

setting-dependent inputs, such as the resolution for the curve calculation, must be indicated. This includes the initial length, the step to increase the length, and the maximum cable length.

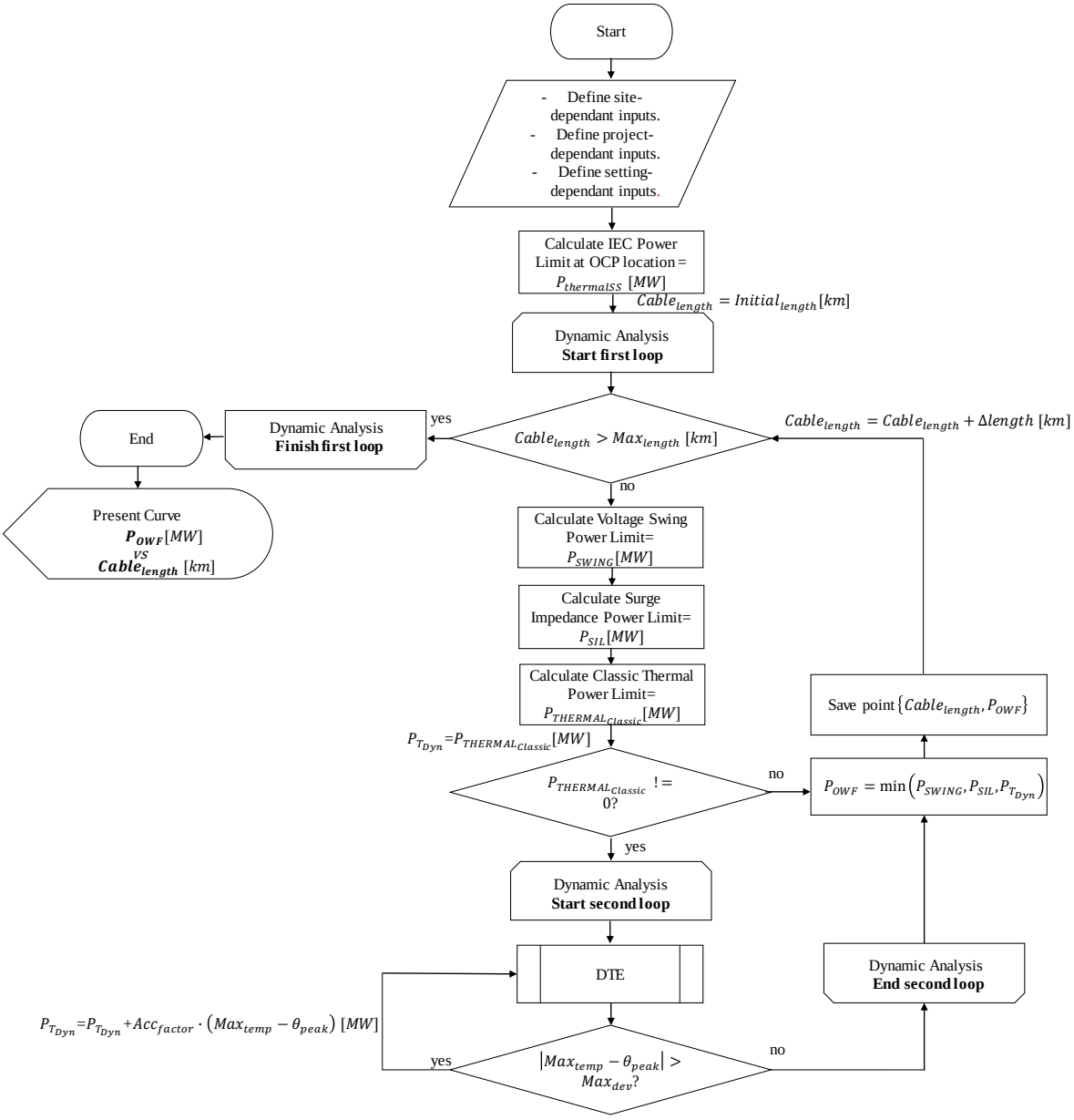

Figure 3.3: Power-transfer capability correction model [C2]

The method consists basically on maximizing the total installed capacity of an OWF. To achieve so, for each point of cable length, the three technical limits are compared: the voltage swing limit (maximum 5%), the surge impedance power limit (the stability

limit), and the thermal limit under dynamic conditions. The minimum value of them is obtained. To calculate the thermal limit under dynamic conditions, the power limit calculated in steady state under constant rated conditions [16], is used as departing point for gradually increasing the OWF installed power. The DTE model is implemented for each annual time series. The maximum installed power under thermal restriction, is thus, that value for which the maximum instantaneous temperature is equal to the standard industrial limit, i.e., 90 °C. At the end, a corrected transmissible power curve is produced, which can be compared with that from the classic method. More details of this method are available in [C2].

3.2.3 Framework for Optimum Sizing of Export Cables

For each of the available annual time series the model presented in Figure 3.4 is applied. The simulation setting inputs include, in addition to the other parameters already explained in the previous models, information related to the cables set lifetime. A cable lifetime is defined by its time-to-failure at a given designed cable length and failure probability. A set of time series for offshore power and seabed temperature are required. This means that the cable providing the best balance between investment, total electrical power losses, and lifetime, for all the temporal sets, is selected for the export system. These three criterion are quantified by means of the LCOE-share of the export cables.

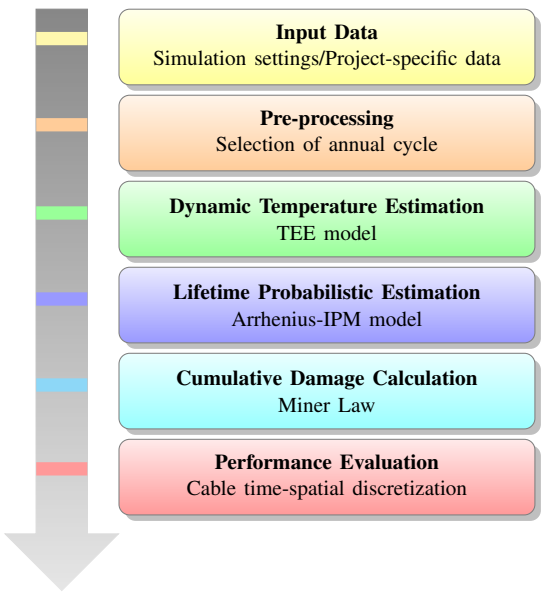

Figure 3.4: Lifetime estimation method for HV AC OWF export cables [J2]

More the availability of data, higher is the confidence on the analysis. In this thesis, 35 years of offshore wind power production time series are used simulated with *CorWind* [15], [48]. Availability of seabed temperature time series is scarce, hence a synthetic

annual time series based on info from the Bornholm Basic area [49] was created. The time series vary between 1 °C-10 °C and takes into account the seasonal fluctuations.

The method in Figure 3.4 allows for calculating the lifetime and total electrical power losses for a given cable type, and annual time series. In the pre-processing stage, it is ensured that the cycle time basis selected is a natural year, because it is the typical time horizon used for calculating DCF, NPV, and the LCOE economic metric. Continuing with the method, at the hot stop, the DTE model is utilized, getting the time series of conductor temperature.

With the temperature time series the cable lifetime is estimated. Many different models can be used for inferring the lifetime of power system components. A review of such models obtained by means of accelerated test experiments is presented in [50]. A benchmarking between different electro-thermal stress models for power cables has been done, such as Zurkov, Crine and Arrhenius-IPM, each within the probabilistic framework needed for associating time-to-failure to reliability. All these models present different analytical expressions and parameter values. However in general they all provide same indications regarding lifetime, being the Arrhenius-IPM model the most conservative for a wide operation range [51]. The parameters of the Arrhenius-IPM, based on accelerated test experiments, are available in the literature [52]. The Arrhenius-IPM combines two single-stress life models and their synergism: the so-called thermal stress model, Arrhenius and for the electric stress, the inverse power model.

The Arrhenius-IPM is unified with the most accepted cumulative probability density function to relate time-to-failure and failure probability for HV equipment, the Weibull pdf [53]. This model is valid for cables specimen used in laboratory tests considering that the probability density function and stress model is representative for the whole range of operation [52]. To extrapolate this result to real-size cables for projects applications, the probabilistic enlargement law is applied [54]. At the end of this procedure, a model for the probabilistic time-to-failure of a real-size cable for a set of operative conditions is analytically deducted.

With the probabilistic lifetime estimation model ready, the Miner's cumulative damage theory is implemented [55]. This law states that summing up the loss-of-life fraction for every time slot, defines the estimated lifetime of the component under analysis when the result is equal to one. The loss-of-life fraction is defined as the inverse of the time-to-failure in a given time fraction. As a result, the number of cycles to fail are estimated, in function of the effects of the electro-thermal cumulative damage.

Finally, the total electrical power losses are calculated in the performance evaluation block. This consists on a spatio-temporal discretization, which allows for a holistic calculation of joule, screen and armouring losses.

The lifetime estimation method of Figure 3.4 is embedded in an optimization framework, ensuring the selection of the export cable to minimize the LCOE-share, subject to the following constraints:

- Only one cable type is selected.
- The calculated lifetime for all the annual cycles is equal or higher than the one provided by the manufacturer.
- The maximum instantaneous temperature for all the annual cycles is equal or lower than the ultimate strength limit.
- The stability power limit is respected.
- The cable is able to support the installed power of the OWF under analysis.

The equations and mathematical formalities of this method are described in detail in [J2].

3.3 Results

The results are presented in this section. They are split into two set of results. The first one is for the power-transfer capability correction model [C2], and the second for the application of the framework to optimally size export cables [J2].

3.3.1 Case Study 1

The histogram of power time series is illustrated in Figure 3.5, where it is appreciable that only 40% of the time, power between 0.9 and 1 p u is produced, according to the simulated OWF power time series. Typical values of 1 Km/W and $2 \cdot 10^6$ J/m^3, for the seabed thermal resistance and thermal specific heat, respectively, are considered. An export system rated at 275 kV using a 800 mm^2 cable, with unity power factor and no compensation unit is subject to study. Other inputs are available in [C2].

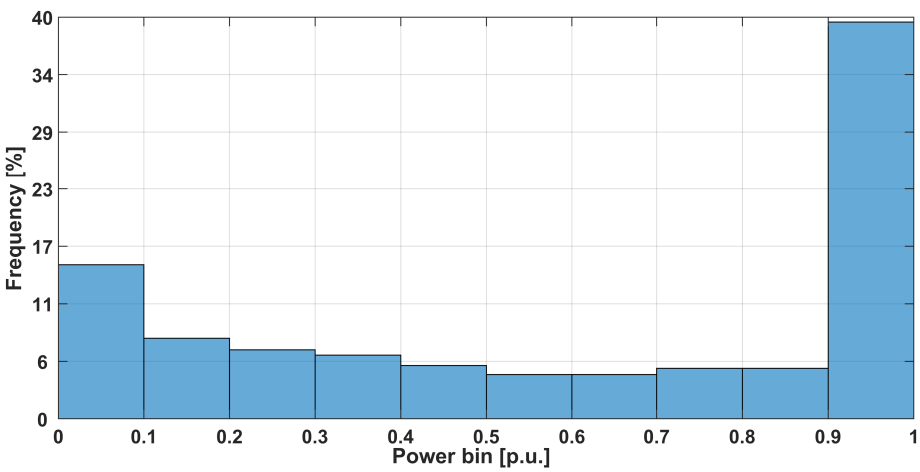

Figure 3.5: Histogram for the OWF power time series [C2]

The comparison between the curves using the traditional and the proposed method is presented in Figure 3.6; the orange line accounts for the power fluctuation, and therefore for each evaluated distance, its magnitude is always higher than the traditional method (blue line), which assumes constant power under rated conditions. The crossing-point with the abscissa is unaffected as expected; in fact, to increase the reach in terms of total length, lower voltage levels or lower nominal frequencies should be evaluated.

The curve obtained through the traditional method was validated against other works as [56] and [57]. Mathematically, the proposed method preserves the exponential trend given the low-degree polynomial relation between P_{OWF} (OWF installed power) and the maximum instantaneous temperature. Both curves are defined by the thermal limit turning this one as the binding constraint; for these values of installed power and total length, the voltage swing is maximum 0.9% for the traditional method, while for the proposed method is 1%, albeit the curve is more steep throughout the distance range (with voltage phase variation lower than 30 °C). Secondly, the surge impedance power limit is always in the order of GW, hence not representing a threat.

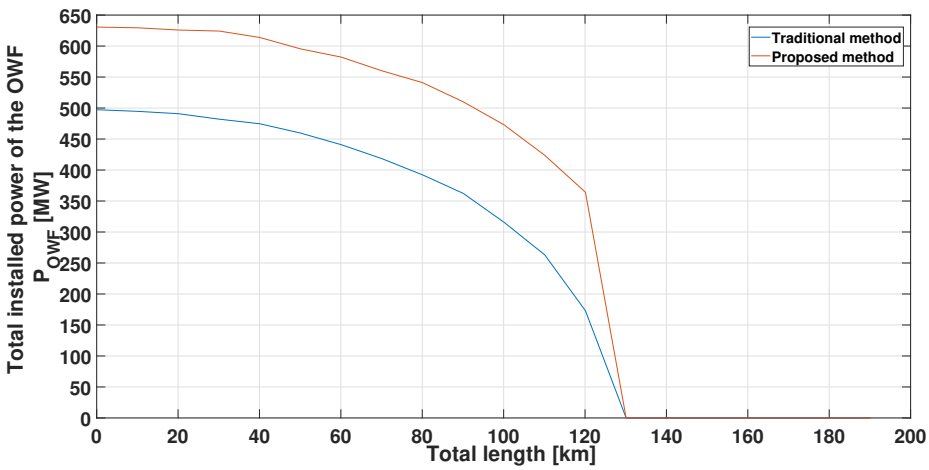

Figure 3.6: Comparison between the traditional method and the proposed method [C2]

The evolution of the gain in power in function of the total length is illustrated in Figure 3.7, the greater the distance the larger the gain. Indeed, for the greatest length (120 km), the installed power of the OWF could be 2.1 times the power calculated using the traditional method. This shows that for very large export route lengths, the under-use of the cable is increasing.

These results also indicates that high voltage AC-based solutions could be more thoroughly assessed in front of the DC counterpart, in benefit of the first one. Further computational experiments point out that the power gain is larger for greater values of soil thermal resistivity, for instance, for a total length of 120 km, an additional increase of OWF installed power of 39% can be achieved, when the soil thermal resistivity is 20% greater than the base value of 1.

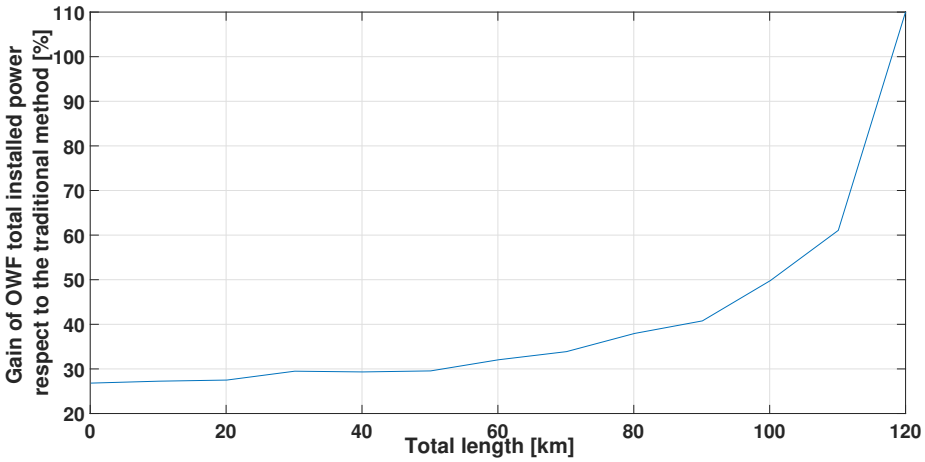

Figure 3.7: Gain of OWF total installed power [C2]

3.3.2 Case Study 2

As a case study the OWF Arcadis Ost 1, foreseen to be constructed in the Baltic Sea in 2030, is considered. Pre-feasibility studies project a total installed capacity of 456 MW (38 Wind Turbines of 12 MW), routing length of the export cables of $d = 89$ km, nominal voltage $V_n = 275$ kV, nominal frequency $f_n = 50$ Hz, unit power factor $pf = 1$, without compensation units. It is assumed that for all the cables the designed lifetime LT_{des} is 30 years, for a failure probability $F_{p_{des}}$ of 5%, and length d_{des} 1 km. As in the previous case study, the nominal values for the thermal resistance and thermal specific heat of the soil are 1 Km/W and $2 \cdot 10^6$ J/m^3, respectively. Likewise, 35 years of offshore wind power production time series, and a seabed synthetic annual time series varying between 1 °C-10 °C are considered. Other inputs are available in [J2].

Employing the full temporal data set according the proposed method, the maximum instantaneous temperature ($\theta_{i_{peak_t}}$) obtained for all years i and available cables t, is given in Figure 3.8.

The results indicate that all cables -except the 500 mm^2 cable- do not exceed the rated temperature limit (indicated by a red dotted line, $\theta_{peak} = 90$ °C). The results also show that the 1,200 mm^2 cable -the size that results when using standard [16]- is significantly underused as expected, exhibiting a maximum $\theta_{i_{peak_t}}$ of 62 °C for all the years. On the other hand, the 630 mm^2 cable -sized according the worst case pattern, [19] (CIGRE: Working Group B1.40)- presents a maximum $\theta_{i_{peak_t}}$ of 88.69 °C, showing that the equivalent step profile is on the conservative side ($\theta_{peak_t} = 88.71$ °C), and achieves to capture a realistic harsh windy scenario; these results confirm the validity of the equivalent cycle for the purpose of facilitating the tendering process. Nevertheless representing an approximation of the real time series, which provide more insight about the power production of the OWF, and in fact, conceptually necessary to perform lifetime studies for cumulative damage.

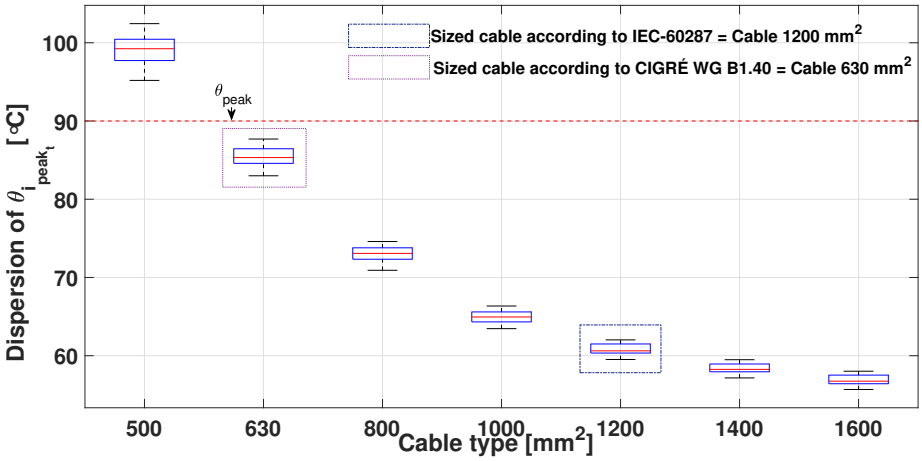

Figure 3.8: Overall thermal simulation results [J2]

Furthermore, the variability of $\theta_{i_{peak_t}}$ for each cable t, in function of the year i, depends strongly on the cable's physical properties.

As shown in the Figure 3.8, the spread of $\theta_{i_{peak_t}}$ decreases with the size of the cables; In fact, from other dispersion perspective, for the 630 mm^2 cable, the mean value is 85.47 °C with a standard deviation of 1.27 °C, while for the type 800 mm^2, these numbers change to 73 °C and 0.96 °C, respectively. This points out that the conductor cable size has a direct relation with the temperature variability due to the power production fluctuations, smaller sizes leading to increased ramping.

Based on the thermal results, the cable size could be either 630 mm^2 or 800 mm^2. The conductor temperature time series for the cables 630 mm^2 (red line) and 800 mm^2 (blue line), at the year with highest $\theta_{i_{peak_t}}$, are given in Figure 3.9.

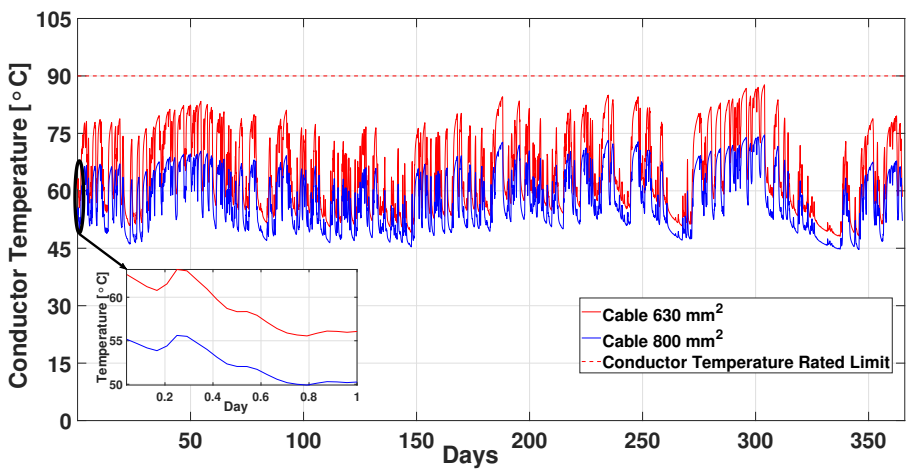

Figure 3.9: Cables conductor temperature time series [J2]

As it is appreciable in Figure 3.9, the instantaneous conductor temperatures between both cables types are considerable different and more critical for smaller cable. For instance, a change in power results in a larger temperature ramping for the smaller cable, which has a lower temperature time constant (see the zoomed-in graph for the first day of operation); the latest is consequence of the growth rate difference among both cable types, and has as a consequence a different conductor temperature frequency distribution as shown in Figure 3.10. It is evident that the conductor temperature distribution resembles a bimodal distribution, showing higher peaks and higher frequency for the 630 mm^2.

The proposed method results in indicating the same cable as the one in [19]. However, the deterministic nature of the latter methods does not allow assessing the reliability of the cable in function of its length. Hence, it is beneficial to move towards a probabilistic approach to avoid too optimistic procedures which may potentially lead to operational failures.

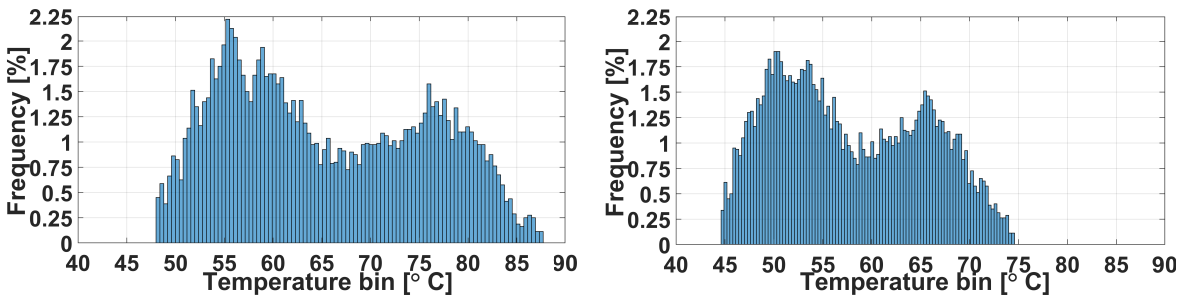

(a) Cable 630 mm^2 **(b)** Cable 800 mm^2

Figure 3.10: Cables conductor temperature histogram [J2]

The different profile of instantaneous temperature yields to different lifetime estimations, due to the different fatigue levels induced by their electro-thermal stresses, as captured in Figure 3.11.

Lifetime estimation is given as a ratio of calculated to design values, as expressed in $(LT_{i_{ratio_t}} = \frac{LT_{des}}{LT_{i_{P_{inc_t}}}}) \leq 1$, in order to minimize uncertainties on the probabilistic lifetime estimation model, where $LT_{i_{P_{inc_t}}}$ is the calculated lifetime for year i and cable type t. As expected, the 630 mm^2 cable exposed to more critical conductor temperature, exhibits a lifetime ratio outside the bounds of the optimization model. In contrast, the 800 mm^2 cable satisfies this constraint for all the simulated annual cycles while satisfying all other constraints.

The mean and standard deviation values of $LT_{i_{ratio_t}}$ for selected 800 mm^2 cable are 0.58 and 0.06, respectively. For $\theta_{i_{peak_t}}$ these values are 73 °C and 0.96 °C, correspondingly, as mentioned before. The standard deviations of these two variables are considered acceptable to show robustness towards different annual generation profiles.

The variability difference for different cables on $LT_{i_{ratio_t}}$ and $\theta_{i_{peak_t}}$, can be explained based on the fact that larger cables have larger time constants (slower dynamic response), hence the reaction speed due to power changes is less pronounced than in smaller cables. This is particularly important condition, since the power production is a stochastic variable difficult to forecast. If the conductor temperature uncertainty can be decreased by the physical properties of the cables itself, it can help to a more reliable operation based on analysis using power production either simulated or measured from a set of years.

Although the proposed framework suggests a cable one size up compared to [19], the decision is based on a more informed and robust evaluation of the operating conditions of the cable, thus, decreasing the likelihood of failures.

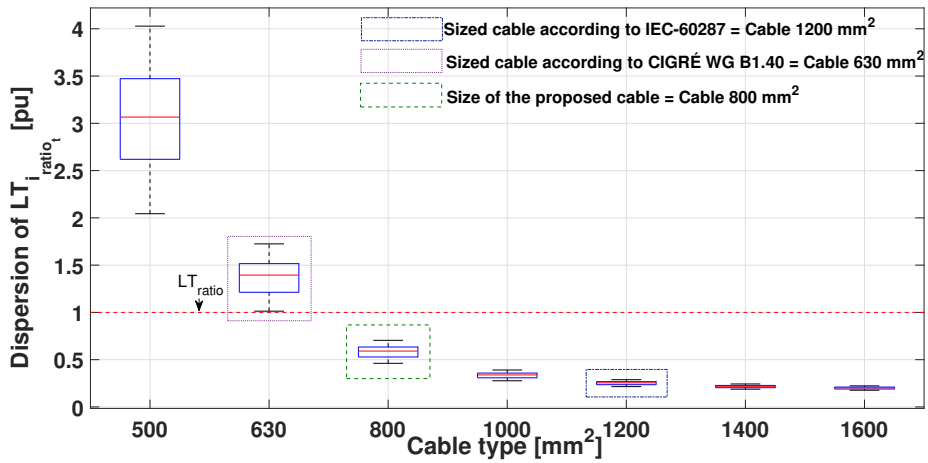

Figure 3.11: Overall lifetime simulation results [J2]

Nonetheless, going from a 1,200 mm^2 (criterion of [16]) to a 800 mm^2 cable has as direct consequence on decrease of initial investment, but also with detriment of larger total power losses. Consequently, the performance evaluation step is applied in order to estimate the total electric losses and to calculate the $LCOE_{es}$ (LCOE-share of export cables).

Overall, the reduction in the cross-section of the export cable provides a reduction of 5% -assuming the most expensive year- in the $LCOE_{es}$ when considering solely the related costs to this component.

Finally, the impact of the export cables length is investigated by means of Figure 3.12 and Figure 3.13. The following simulation considers an increase of the thermal resistance of 0.2 Km/W, an increase of the seabed temperature of 5 °C, and a cable total length of 32.5 km. It is evident according to the Figure 3.12 that all the cables exhibit a $\theta_{i_{peak_t}}$ never higher than 90 °C, with exception of the cable 500 mm^2, which surpasses this value for almost 50% of the cases.

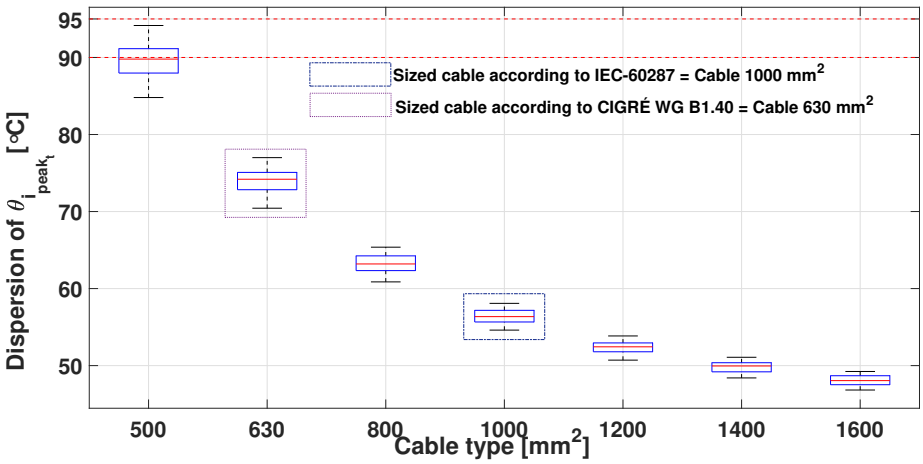

Figure 3.12: Sensitivity of overall thermal simulation results. $d = 32.5\,\text{km}$ [J2]

However, when evaluating the level of exceedance in terms of frequency for that year with the highest $\theta_{i_{peak_t}}$, it is found out that for the temperature range between 90 °C-95 °C, the accumulated probability of occurrence is lower than 1.75%.

This raises the question whether is too conservative to limit the instantaneous conductor temperature to 90 °C, value that is defined as a limit for accumulated stress when operating continuously at this degradation rate in the insulation material [58], but not representing the ultimate strength limit. In fact, in Figure 3.13 is shown that the 500 mm^2 cable satisfies the lifetime constraint for all the generation scenarios, therefore by means of a constraint relaxation of θ_{peak} to 95 °C, this cable type could be choose under these conditions, obtaining a $LCOE_{es}$ reduction of almost 7%. Note that for this case, the cable total length is less restricting from a lifetime estimation probabilistic point of view, therefore improving the size not only compared to [16], but also to [19], with a reduction of roughly 2%.

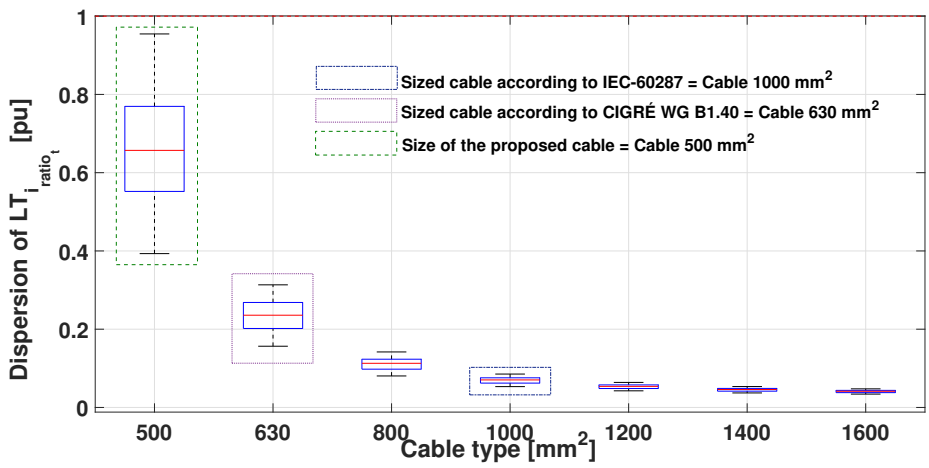

Figure 3.13: Sensitivity of overall lifetime simulation results. $d = 32.5\,\text{km}$ [J2]

3.4 Summary

A set of methods, based on [C1], [C2], and [J2] have been proposed in this chapter. The methods are applied for optimization of the export cables in OWFs.

A model for dynamic temperature estimation (DTE) is designed and calibrated. This model is subsequently implemented in the power-transfer capability correction model, and in the framework for sizing export cables.

The first proposed method provides a realistic and efficient approach for calculating the power-transfer capability of OWF cables, with special interest on export cables, as the effect of technical constraints over transmissible power, in function of the total length, is thoroughly investigated. It has been identified that the binding constraint for submarine cables is the thermal limit, and this restriction can be relaxed if the power fluctuations are taken into account, consequently enlarging the search space, making possible to obtain larger values of installable OWF power for a given cable type, under specific operating conditions. Other techniques to maximize the utilization of AC export cables have been proposed in the literature, including sub-synchronous systems operating between 0 Hz and 50 Hz, however, additional power electronics need to be incorporated, increasing costs and control complexity.

The second proposed method presents a rigorous, and transparent approach for minimizing the $LCOE_{es}$ related to high voltage AC export cables for OWFs. This method supports for lifetime estimation, enabling the transition from a deterministic to a stochastic mindset. The main constraints are the maximum instantaneous conductor temperature (which is related to the ultimate strength of the insulation material), the estimated lifetime of the cable (obtained as an accumulation of stress over the cable operational lifetime), and the electric stability limit. The method is applied systematically and in a cyclic-fashion, for each available annual generation and seabed temperature time series, obtaining as a final output the cable leading to the cheapest $LCOE_{es}$ while evaluating for the whole data set the abiding of security operational constraints.

Bigger cables drive to larger $LCOE_{es}$, however have the advantage of less sensitivity to large generation changes, minimizing the uncertainty introduced by the estimation of the expected power generation levels and variability. The distance from shore also has an impact on the cable sizing; for larger distances the cable lifetime is the limiting factor, while for shorter distances the ultimate thermal strength takes that role. A relaxation of the maximum instantaneous temperature can allow for a further reduction in the cable sizing for shorter distances, providing cost reductions even compared to the most updated industrial practices.

CHAPTER 4
Deterministic Collection System Design

This chapter is a summary of the articles [C3], [C4] and [J3].

4.1 Introduction

The problems of interconnecting WTs in the collection system, and the allocation of WTs to OSSs are studied in this chapter. A deterministic approach for modelling cables failures is adopted considering only radial layouts (with or without branching as depicted in Figure 2.3).

The complexity of designing the radial cable layout of collection systems for large-scale OWFs is well-known, being studied with increased focus in the last ten years [59], [J1]. Finding the global optimum of this problem is generally NP-hard [20]. Four big clusters of methods for approaching this problem can be established: heuristics, metaheuristics, global optimization with mathematical formulations, and hybrids, such as matheuristics [24].

Global optimization encompasses a large set of different alternatives to model the cable layout problem, like BIP [60], MILP [7], [23], [24], [61], [62], MILP with decomposition techniques for stochastic programming [34], [35], MIQP [63], [64], and MINLP [36], [65]. The problem is formulated, and then through an external/commercial solver solutions can be found. Convex formulations bring along strong duality to assess the quality of the best solution.

Addressing different needs, heuristic, metaheuristic and matheuristics methods for designing radial cable layout of collection system for OWFs are presented in this chapter:

- A framework consisting of an unified algorithm for modified versions of the well-known graph theory algorithms, Kruskal, Prim, EW, VAM, and a metaheuristic approach, a GA. Comparisons between all of these methods are performed through two objective functions, NPV and LCOE, taking into consideration the particular constraints treated for OWF practical applications. Results are fully available in [C3] and [C4].
- Development, testing, and application of a MILP mathematical model to quickly find feasible points for large-scale OWF instances, considering the most common engineering constraints in this context. The MILP model is embedded in an

algorithmic framework for obtaining global optimum solution points (or near to it) in reasonable computational time. All together constitute the global optimization model. The linear program supports simultaneous optimization of investment and total electrical power losses. Improvements on the complexity and fidelity for total power losses calculation using time series and capacitive currents are incorporated. Results are fully available in [J3].

4.2 Methods

4.2.1 Heuristics and GA

The framework for designing the radial cable layout by means of heuristics algorithms and a GA is portrayed in Figure 4.1.

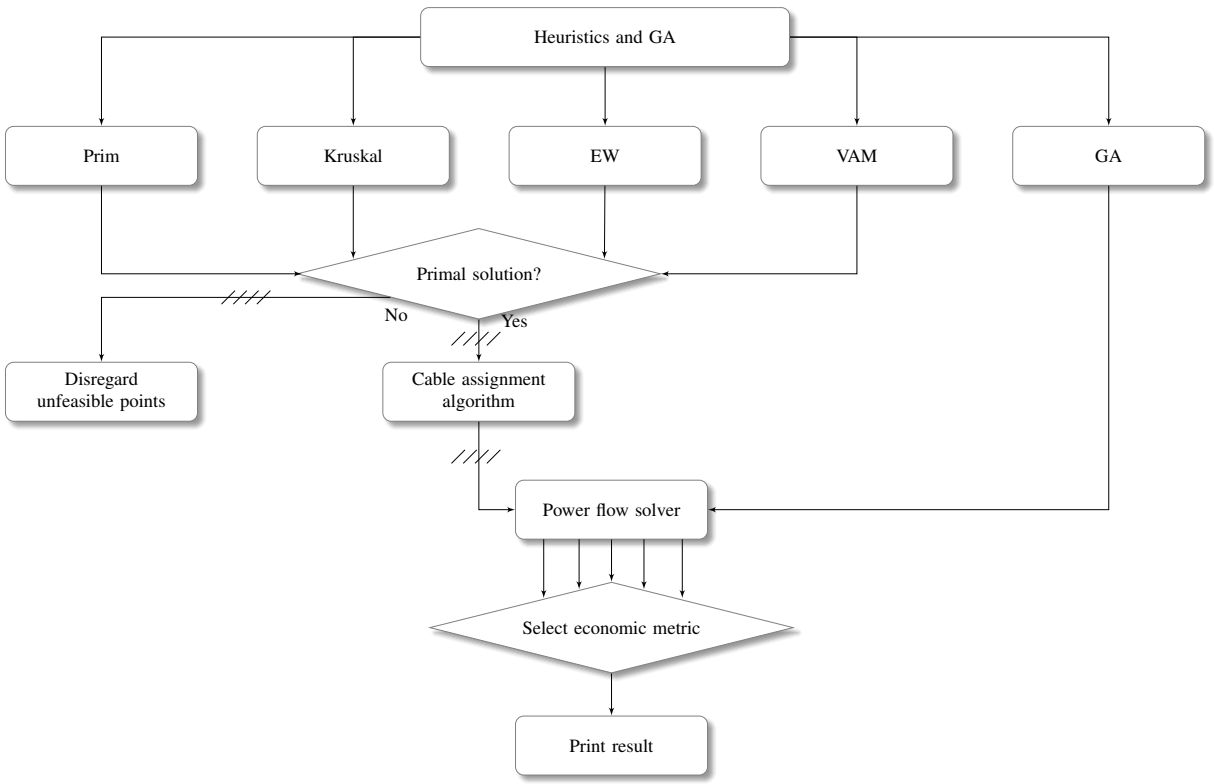

Figure 4.1: Framework for heuristics and the GA [C3]

All methods require the same inputs: WTs and OSS locations, cable database with costs and electrical parameters per unit of length (resistance, capacitance, and inductance), and the offshore wind power production time series. With those inputs, the five methods run in parallel; the four modified heuristics (Prim, Kruskal, EW, and VAM) obtain either

a feasible point (primal) or a unfeasible point; in the first case, an algorithm to assign a cable type to each branch is executed (in order to minimize the total investment), whilst in the second case, those solutions are dispensed, and can be useful to provide a warm start to other solvers (for instance, using a global optimization with repair heuristic). Unfeasible points are due to the cables no-crossing constraint, hence represented as a forest graph; GA provides primals for the considered instances. Finally, all primals (with cables assigned) are evaluated by means of a power flow solver for calculating the electrical power losses. In the end, a single solution is displayed in function of the desired economic metric, which can be: total cables length (L), total initial investment (I), and initial investment plus electrical power losses (IP). The way of computing the objective can vary as well, for instance, metrics similar to the LCOE or NPV can be used.

The heuristic algorithms

The heuristics algorithms are compacted into a single block of coding lines as presented in [C3]. As demonstrated in [22] and [66], the C-MST heuristics Prim, Kruskal, EW, and the VAM, converge to the same paradigm. In fact, if the capacity and no-crossing constraints are not binding, then the result of all the heuristics is the same.

Let the WTs and the OSS be presented as a weighted undirected graph $G(\boldsymbol{V}, \boldsymbol{E}, \boldsymbol{W})$, where in this case, $\boldsymbol{V}$ represents the nodes set (WTs and OSS), $\boldsymbol{E}$ the set of available edges arranged as a pair-set, and $\boldsymbol{W}$ the associated weight for each element $e \in \boldsymbol{E}$. In general, $G(\boldsymbol{V}, \boldsymbol{E}, \boldsymbol{W})$ is a complete graph.

The paradigm consists on associating a singular weight parameter p, $\forall v \in \boldsymbol{V}$. By establishing the parameter set $\boldsymbol{P}$ in function of the heuristic, the effect is equivalent to changing the sequential order with a branch $e \in \boldsymbol{E}$ is selected into the tree, or, what it is the same, the order of integrating each WT node into the OWF collection system. The unified code, for this case, also takes into account the two main constraints (capacity constraint, as given by the largest available cable in number of WTs, and cables no-crossing). One of the main advantages of having a single set of code lines is the possibility to, in theory, have infinite variants, by selecting infinite rules for $\boldsymbol{P}$.

For each branch e_{ij}, two trade-off values are assigned: $t_{ij} = w_{ij} - p_i \wedge t_{ji} = w_{ji} - p_j$, where $w_{ij} = w_{ji}$ is the Euclidean distance between nodes i and j, forming the triple set $\boldsymbol{T}(i, j, t_{ij})$. The nodal weight parameter $p \in \boldsymbol{P}$, $\forall\ v \in \boldsymbol{V}$, must be initialized and updated as the algorithm keeps running, as indicated in [C3].

A generalization of this rule would be: $p_i = a \cdot (b \cdot w_{i1} + (1 - b) \cdot w_{lm})\ \forall\ v \in \boldsymbol{V}$, where a and b are constants with $a \geq 0$ and $0 \leq b \leq 1$, w_{i1} is the distance to the OSS, and w_{lm} the distance difference between the first and the second shortest feasible edges. Thus, if a and b are both equal to one, then the general equation is equivalent to the EW rule; likewise, if a is equal to zero, Kruskal rule is obtained. Other values of a and b lead to Prim and VAM heuristics.

There is certainty about the termination of the algorithm, but primals are not guaranteed.

In the last case, the output graph is a forest, while when a feasible point is found, this is a tree $G_T(\boldsymbol{V_T}, \boldsymbol{E_T}, \boldsymbol{W_T})$, spanning all the vertex-set, $\boldsymbol{V_T} = \boldsymbol{V}$, and using exactly $|\boldsymbol{E_T}| = |\boldsymbol{V}| - 1$ edges. If a feasible point is obtained, then a straight-forward algorithm is run to assign the cheapest cable to each edge of the tree.

More details, formalities, and pseudocodes are presented in [C3].

The GA

The general work flow of the GA can be seen in Figure 4.2.

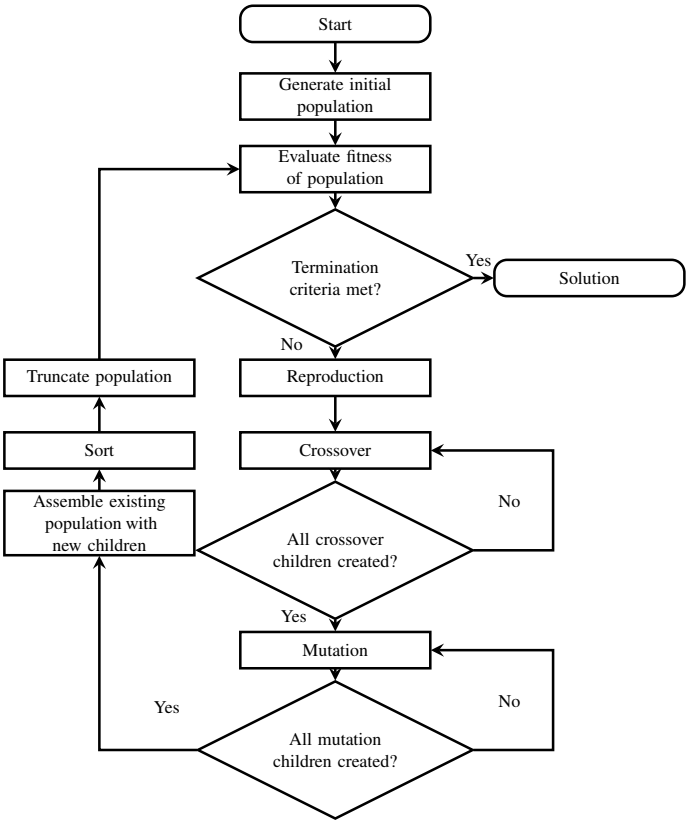

Figure 4.2: The GA flowchart [C4]

The GA is based on an elitist approach, each iteration represents a new population comprised of the individuals from the previous generation (100 parents), and the new children populations, those obtained from crossover (20 children) and from mutation (up to five times the parents number). The individuals are then ranked according to their fitness value. Finally, the population is truncated to the original population size (100 members), eliminating the weakest individuals. This approach allows the algorithm to converge faster as it does not need to re-discover solutions discarded in previous generations.

Each individual goes through a fitness assessment that the determines the cost of the individual. The fitness assessment includes the system capital expenses, and penalizations from the compliance or not of the following restrictions:

- A tree connecting all WTs to the OSS is obtained.
- Only one cable selected per active edge.
- The capacities of the cables are not violated.
- No cables crossings are allowed.

The evaluation of these constraints is carried out in a hierarchical fashion, as depicted in Figure 4.3.

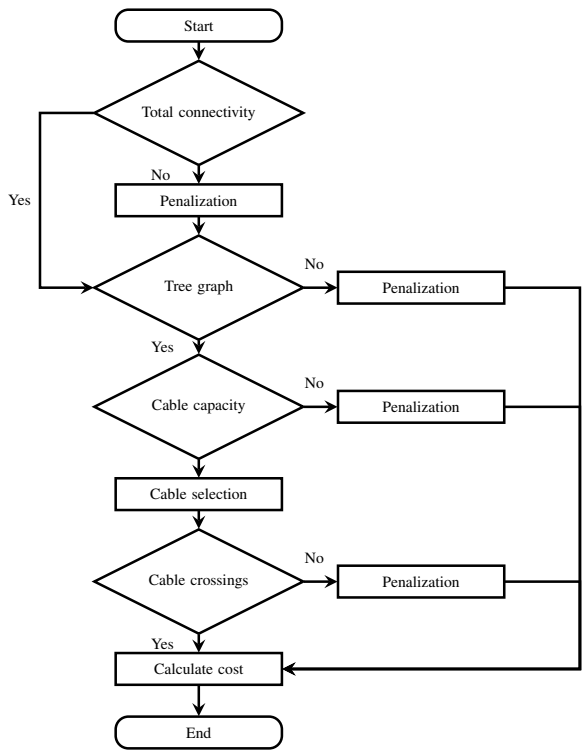

Figure 4.3: The fitness assessment flowchart [C4]

Given the chosen encoding system (binary variables), the selection of only one cable type per active edge is achieved.

Total connectivity evaluates that all WTs are interconnected to the OSS, the implementation is achieved doing a depth-first search and checking the connectivity of all nodes. *Tree graph*, checks that the graph is indeed a tree, the condition is that the number of active edges is equal to the number of WTs. *Cable capacity* checks that the capacity of the largest available cable in number of WTs is not exceeded. First the tree is transformed

into a directional tree rooted at the substation. Then a depth-first search is performed and the number of nodes accessible from each node has to be smaller than the this number. *Cable crossings restriction* is implemented by checking intersections in a set composed of all possible pairs of active edges in the solution.

A hierarchy is established among the penalizations for the constraints through the use of conditional functions and through the cost given to each penalization. The need for a hierarchy is two-fold, the first reason being that in order to calculate the number of nodes per branch the graph needs to be a tree. The second reason is that certain functions used to analyze the cable capacity and cable no-crossings constraints use large amounts of computational power, and it is a unproductive to run them if the solution is already known to be unfeasible.

In terms of the order of the constraint assessment, first both the total connectivity and tree graph constraints are determined. If both constraints are met then capacity constraint is calculated. Again if this constraint is satisfied then the cables no-crossing restriction constrained is analyzed. In this way time is not wasted in computational intensive tasks.

In terms of the penalization cost they are ranked by importance, with the most important constraints having the higher costs. Each penalization is assigned a base cost differentiated by several orders of magnitude from the others, ensuring that, in the case of proportional penalizations the constraints do not interfere with each other. This helps the elitist approach for discarding low quality points.

The total connectivity penalization is assigned the highest cost to ensure that all elements are connected. The tree constraint penalization is proportional to the number of extra edges that impede the formation of a tree graph. The cable constraint penalization is proportional to the number of cables that do not meet the constraint. Finally, the cable no-crossing restriction penalization has the lowest cost and it is proportional to the number of crossings detected.

After each of the constraint analysis the fitness cost is calculated which includes the addition of the corresponding penalizations.

The cable selection process is a method for choosing the appropriate cable from a list for each segment. This method is only done once the cable capacity constraint is met. The process assigns the smallest cross-section possible to each active edge, according to the number of WTs being supported downstream. In doing so the cost is also minimized, as the size of the cross-section is correlated to the cost of the cable.

Finally, The GA, as presented in Figure 4.2, finishes the optimization process and outputs a solution when either of the following conditions are met:

- Iteration number: The process stops after a set number of iterations.
- Stall of the fitness value: The process stops if the fitness value does not change for a fixed amount of iterations.

More details and formalities for the GA are in [C4].

A power flow solver is called for all the obtained primals (with the heuristics and with the GA) to calculate the total electrical power losses; the *Matpower* package [67] is used for these purposes (see Figure 4.1). The OSS is modelled as the slack bus, and the WTs as PV busses. While in the GA the losses may be incorporated to the objective function, this brings a notable increase of the computational burden that would slow down the obtention of feasible points.

4.2.2 The Global Optimization Model

Modelling aspects

Let the OSSs define the set $\boldsymbol{N_o} = \{1, \cdots, n_o\}$. Likewise, for the WTs, let $\boldsymbol{N_w} = \{n_o + 1, \cdots, n_o + n_w\}$. In this way, each one of the OSSs and WTs (modelled as points in the space) have associated a unique identifier i, such as $i \in \boldsymbol{N} = \boldsymbol{N_o} \cup \boldsymbol{N_w}$. The Euclidean norm between the positions of the points i and j, is defined as d_{ij}. The aforementioned inputs are condensed as a weighted directed graph $G(\boldsymbol{N}, \boldsymbol{A}, \boldsymbol{D})$, where $\boldsymbol{N}$ represents the vertex set, $\boldsymbol{A}$ the set of available arcs arranged as a pair-set, and $\boldsymbol{D}$ the set of associated weights for each element $a_{ij} \in \boldsymbol{A}$, where $i \in \boldsymbol{N} \wedge j \in \boldsymbol{N}$. For instance, for $a_{ij} = (i, j)$, $d = d_{ij}$, where $d \in \boldsymbol{D}$. In general, $G(\boldsymbol{N}, \boldsymbol{A}, \boldsymbol{D})$ is a complete directed graph.

Additionally, a predefined list of available cable types is required to interconnect the WTs towards the OSSs. Let the set of cables be $\boldsymbol{T}$ and let the capacity of a cable $t \in \boldsymbol{T}$ be u_t measured in terms of number of supportable WTs connected downstream. Hence, let $\boldsymbol{U}$ be the set of capacities sorted as in $\boldsymbol{T}$.

Furthermore, each cable type t has a cost per unit of length, c_{c_t}, in such a way that u_t and c_{c_t} describe a positive correlation, following an exponential regression model. The set of metric capital expenditures is defined as $\boldsymbol{C_c}$. Similarly the set of metric installation costs is defined by $\boldsymbol{C_p}$.

After defining the graph representation of the problem, the underlying variables associated to the calculation of the desired output, are unequivocally established. Let x_{ij} represent a binary variable that is one if the arc between the vertex i and j is selected in the solution, and zero otherwise. Likewise, the binary variable y_{ij}^k models the k number of WTs connected downstream from j, including the WT at node j (under the condition that $x_{ij} = 1$). Finally, the integer variable σ_i represents the number of WTs connected to the OSS i.

The modelling choices for the calculation of cables capacity, arcs nominal power, and power flow and total power losses are available in [J3]. In general, hyperbolic functions and other non-linear expressions to calculate flow and losses are incorporated.

MILP model

The proposed optimization model is able to cope with an arbitrary number of WTs, n_w, and similarly any reasonable number of OSSs, n_o.

The underlying mathematical formulation is inspired by the formulations and analysis proposed in [60] and [68] with additional constraints stemming from the nature of the problem, and with the objective to improve its tractability.

Previously, the binary variables x_{ij} and y_{ij}^k, and the integer variable σ_i were defined. They refer to an active arc, the number k of WTs connect to that active arc, and the number of WTs connected to OSS i, respectively.

To increase the computational efficiency, the number of variables is reduced as follows. The capacity of the biggest cable is calculated as $U = \max \boldsymbol{U}$, therefore the possible maximum value of k for $i \in \boldsymbol{N_o}$ is equal to $f(i) = U$, while for $i \in \boldsymbol{N_w}$ is $f(i) = U - 1$. This acknowledges that the biggest cable available could be only used at maximum capacity when is connected from a OSS.

Analogously, the set of variables x_{ij}, where $i \in \boldsymbol{N_w}$, and $j \in \boldsymbol{N_o}$ are intrinsically discarded, considering the nature of the power flow, i.e., the OSSs collects the energy from the WTs and not the other way around. Lastly, since the export system is outside the scope at this point, all the arcs between OSSs are disregarded, i.e., $x_{ij} = 0 \; \forall i \in \boldsymbol{N_o} \wedge j \in \boldsymbol{N_o}$.

The graph $G(\boldsymbol{N}, \boldsymbol{A}, \boldsymbol{D})$ is reduced to $G_r(\boldsymbol{N}, \boldsymbol{A_r}, \boldsymbol{D_r})$ after this stage.

Cost coefficients Note that the previously defined decision variables x_{ij} and y_{ij}^k, do not include any information related to the cable type selected in a given arc.

This is because the cable type selection process is handled in a pre-processing stage, given that all the required data is present, and the task is totally independent to any other part of the desired tree(s) [60].

A pre-processing strategy allows integrating more complex power flow and total electrical power losses models, increasing the accuracy without compromising the computational efficiency. In the pre-processing stage, for the case of y_{ij}^k, the length of the arc is known (d_{ij}), and the number of WTs connected by it is also defined (by k). No more inputs are required for this task.

Hence, for each y_{ij}^k, the sub-problem defined by (4.1) to (4.4) is solved beforehand and independently by enumeration.

$$c_{ij}^k = \min \sum_{t \in \boldsymbol{T}} x_{ij,t} \cdot \left((c_{c_t} + c_{p_t}) \cdot d_{ij} + \sum_{\mu=1}^{m} \frac{l_{ij,t}^{\mu,k} \cdot c_e}{(1+r)^\mu} \right) \tag{4.1}$$

$$\text{s.t.} \quad \sum_{t \in \boldsymbol{T}} x_{ij,t} = 1 \tag{4.2}$$

$$x_{ij,t} \cdot (S_{ij,t}^k - S_{r_t}) \leq 0 \quad \forall t \in \boldsymbol{T} \tag{4.3}$$

$$x_{ij,t} \in \{0, 1\} \quad \forall t \in \boldsymbol{T} \tag{4.4}$$

In the objective function (4.1), the first term $((c_{c_t} + c_{p_t}) \cdot d_{ij})$ is for capital expenditure (c_{c_t}) and installation costs (c_{p_t}) of cable t.

The second term in the summation part of (4.1) accounts for the DCF of the economic losses caused by the energy dissipation in the cables, the parameters m, $l_{ij,t}^{\mu,k}$ (see [J3]), c_e, and r, represents the project lifetime (years), total power losses at year μ for cable t (MWh), cost of energy (€/MWh), and discount rate (p.u.) respectively.

The objective function can be simplified by zeroing any of its terms, such as, if only the total length is minimized, the first term in (4.1) has to be replaced uniquely by d_{ij}, while the other term in the same equation is dropped. Similarly, if only the total initial investment is targeted, only the first is kept. Therefore, the set of single objectives available in the model are: length (L), length plus total power losses (LP)—monetizing lengths by assuming the same capital and installation costs for all cable types, initial investment (I), and initial investment plus total power losses (IP).

Likewise, (4.2) ensures that exactly one cable type is selected, while (4.3) guarantees that the capacity of cable t is not exceeded, S_{r_t}; $S_{ij,t}^k$ is the power through arc (i, j) when k turbines are connected in j using cable t. The binary variable for selecting a cable type t for arc (i, j) is defined in (4.4).

The sub-problem from (4.1) to (4.4) seeks to find the cable type t to be used for the arc (i, j), which minimizes the objective (4.1).

Objective function After solving the multiple sub-problems related to cable selection and cost evaluation (maximum $U \cdot |\boldsymbol{N}|^2$ problems) from (4.1), a cost value c_{ij}^k is associated to each y_{ij}^k variable. The linear objective function of the main mathematical model is then

$$\min \sum_{i \in \boldsymbol{N}} \sum_{j \in \boldsymbol{N_w}} \sum_{k=1}^{f(i)} c_{ij}^k \cdot y_{ij}^k \tag{4.5}$$

Constraints In order to present the solution connecting all WTs between each other and to the OSSs, the following constraint is added

$$\sum_{i \in \boldsymbol{N_o}} \sigma_i = n_w \tag{4.6}$$

Constraint (4.6) models the full OWF to be divided into multiple disconnected trees (forest) with σ_i being the number of WTs associated to a OSS i. Hence, the total amount of WTs (n_w) are integrated into the electrical system.
To guarantee full connectivity in OSS i, the next constraint is added

$$\sum_{j \in \boldsymbol{N_w}} \sum_{k=1}^{f(j)} k \cdot y_{ij}^k = \sigma_i \quad \forall i \in \boldsymbol{N_o} \tag{4.7}$$

Note that (4.6) and (4.7) are combined in the case of only one OSS.

To limit the maximum number of feeders per OSS (ϕ), it is used:

$$\sum_{j \in \boldsymbol{N_w}} \sum_{k=1}^{f(j)} y_{ij}^k \leq \phi \quad \forall i \in \boldsymbol{N_o} \tag{4.8}$$

To simultaneously ensure a tree topology, ensure that only one cable type used per arc, and to define the head-tail convention, the next expression is included into the model

$$\sum_{i \in \boldsymbol{N}} \sum_{k=1}^{f(i)} y_{ij}^k = 1 \quad \forall j \in \boldsymbol{N_w} \tag{4.9}$$

The flow conservation, which also avoids disconnected solutions, is considered by means of one linear equality per wind turbine

$$\sum_{i \in \boldsymbol{N}} \sum_{k=1}^{f(i)} k \cdot y_{ij}^k - \sum_{i \in \boldsymbol{N_w}} \sum_{k=1}^{f(i)} k \cdot y_{ji}^k = 1 \quad \forall j \in \boldsymbol{N_w} \tag{4.10}$$

The set $\boldsymbol{\chi}$ stores pairs of arcs $\{(i,j),(u,v)\}$, which are crossing each other. Excluding crossing arcs in the solution is ensured by the simultaneous application of the following linear inequalities

$$x_{ij} + x_{ji} + x_{uv} + x_{vu} \leq 1 \quad \forall \{(i,j),(u,v)\} \in \boldsymbol{\chi} \tag{4.11}$$

$$\sum_{k=1}^{f(i)} y_{ij}^k - x_{ij} \leq 0 \quad \forall (i,j) \in \boldsymbol{A_r} \tag{4.12}$$

The no-crossing cables restriction is a practical requirement in order to avoid hot-spots, and potential single-points of failure caused by overlapping cables [23]. Constraint (4.11) exhaustively lists all combinations of crossings arcs, including also the corresponding inverse elements. The constraints in (4.12) ensure that no active arcs are crossing or overlapping between each other. These constraints thus link the variables y_{ij}^k and x_{ij}.

Cables crossings are detected based on a procedure of slopes evaluation. Two arcs are crossing if the crossing point is inside of the lines, but not if this point is located at the extremes of the lines or beyond in the lines' projections.

$$-\sum_{i \in \boldsymbol{N}} \sum_{k=v+1}^{f(i)} \left\lfloor \frac{k-1}{v} \right\rfloor \cdot y_{ij}^k + \sum_{i \in \boldsymbol{N_w}} \sum_{k=v}^{f(i)} y_{ji}^k \leq 0 \quad \forall v = \{2, \cdots, U-1\} \wedge j \in \boldsymbol{N_w} \tag{4.13}$$

Constraint (4.13) represents a set of valid inequalities, initially proposed in [60], to tighten the mathematical model. Given an active arc y_{ij}^k, the maximum number of active arcs rooted in j and connecting v WTs, is expressed by $\left\lfloor \frac{k-1}{v} \right\rfloor$, hence the constraint restricts the maximum number feasible arcs, reducing the search space without excluding valid solutions to the problem.

$$x_{ij} \in \{0,1\} \quad y_{ij}^k \in \{0,1\} \, \forall (i,j) \in \boldsymbol{A_r} \wedge k \in \{1, \cdots, f(i)\} \tag{4.14}$$

$$0 \leq \sigma_i \leq \eta \cdot \left\lceil \frac{n_w}{n_o} \right\rceil \quad \sigma_i \in \mathbb{Z}_+ \quad \forall i \in \boldsymbol{N_o} \tag{4.15}$$

Constraints (4.14) and (4.15) define the nature of the formulation by the variables definition, a MILP.

Note that variables σ_i are limited in their upper bounds to avoid uneven loading of OSSs (in case $\eta = 1$, otherwise $1 < \eta \leq n_o$). Equally rated OSSs bring benefits like design standardization, and decreasing of the dependency upon a single transformation unit for transporting the generated power.

To summarize, the complete formulation of the main MILP model consists of the objective function (4.5) and the constraints defined in (4.6) - (4.15).

The base formulation presented so far has a maximum number of binary variables equal to $|\boldsymbol{N}|^2 + U \cdot |\boldsymbol{N}|^2$, integer variables number equal to $|\boldsymbol{N_o}|$ (linear in function of n_o), and constraints (excluding the no-crossing constraints and valid inequalities) of $1 + 2 \cdot |\boldsymbol{N_o}| + 2 \cdot |\boldsymbol{N_w}|$. Flow formulations, such as the one proposed in [24], have more variables ($2 \cdot |\boldsymbol{N}|^2 + U \cdot |\boldsymbol{N}|^2$) and constraints ($|\boldsymbol{N}|^2 + 2 \cdot |\boldsymbol{N_w}| + |\boldsymbol{N_o}|$); integer and binary variables are quadratic in function of the problem size. This fact along with the addition of valid inequalities may explain why the model from (4.5) to (4.15) is often more efficient to solve.

Optimization framework

Candidate arcs Given the NP-Hard nature of this problem, which is similar to a C-MST with additional constraints [7], [69], more reductions are required. The limitations for successfully finding feasible points and high quality solutions, using solely mathematical models and commercial solvers, is demonstrated in [24].

For large-scale OWFs (with more than 100 WTs) the computing time for robust global optimization solvers generally becomes notoriously long. Likewise, in general, solution times become unpredictable, while very large memory requirements are demanded to build the branch-and-cut tree. Besides, the constraints generation must be done with special care (the full set of no-crossing constraints has a combinatorial nature) to increase computational efficiency.

To make the formulation more flexible and implementable, a further operation to the graph G_r is proposed. The function $f(i, G_r, \upsilon)$ calculates the set $\boldsymbol{\Upsilon}_i$, defined as the υ-closest WTs to i. In other words, it is intuitively considered that a WT will be connected to one of the WTs in its vicinity. Therefore, by systematically applying $f(i, G_r, \upsilon)$ to each $i \in \boldsymbol{N_w}$, the reduced graph $G_r^{'}$ is found. The set $\boldsymbol{A_r^{'}}$ contains the candidate arcs to the solution of the problem.

With this strategy, the maximum number of variables is reduced to $|\boldsymbol{N_o}| + (U + 1) \cdot |\boldsymbol{N_o}| \cdot |\boldsymbol{N_w}| + U \cdot \upsilon \cdot |\boldsymbol{N_w}|$. Additionally, the number of no-crossing constraints decreases dramatically as well. Overall, the arcs set transformation follows $\boldsymbol{A} \rightarrow \boldsymbol{A_r} \rightarrow \boldsymbol{A_r^{'}}$.

The Algorithm The main algorithm defining the full framework with the mathematical model is presented in Algorithm 1.

---

1. $k_f \leftarrow 1$
2. **for** $(\upsilon_f = \upsilon_{f_{min}} : \upsilon_{f_\delta} : \upsilon_{f_{max}})$ **do**
3. $\quad G_r^{'} \leftarrow f(i, G_r, \upsilon_f) \quad \forall i \in \boldsymbol{N_w}$
4. $\quad c_{ij}^k = 0 \quad \forall (i,j) \in \boldsymbol{A_r^{'}} \wedge k \in \{1, \cdots, f(i)\}$
5. $\quad$ *Formulate and solve MILP model from (4.5) to (4.15)*
6. $\quad$ **if** *(problem is feasible)* **then**
7. $\quad\quad$ *Save initial feasible point:* $\boldsymbol{I} = x_{ij} \cup y_{ij}^k \quad \forall (i,j) \in \boldsymbol{A_r^{'}} \wedge k \in \{1, \cdots, f(i)\}$
8. $\quad\quad$ *Break*
9. $\quad$ **else**
10. $\quad\quad k_f \leftarrow k_f + 1$
11. $\quad$ **end if**
12. **end for**
13. $k_o \leftarrow 1$
14. **for** $(\upsilon_o = \upsilon_{o_{min}} : \upsilon_{o_\delta} : \upsilon_{o_{max}})$ **do**
15. $\quad G_r^{'} \leftarrow f(i, G_r, \upsilon_o) \quad \forall i \in \boldsymbol{N_w}$
16. $\quad \boldsymbol{\Gamma}_{k_o} = \boldsymbol{A_r^{'}}$
17. $\quad$ *Get* c_{ij}^k *through model from (4.1) to (4.4)*
18. $\quad$ *Formulate MILP model from (4.5) to (4.15)*
19. $\quad$ **if** $(k_o == 1)$ **then**
20. $\quad\quad$ *Warm start with initial feasible point* $\boldsymbol{I}$
21. $\quad$ **else**
22. $\quad\quad$ *Warm start with feasible point obtained in* $\boldsymbol{O}_{k_o-1}$
23. $\quad$ **end if**
24. $\quad$ *Solve MILP model from (4.5) to (4.15)*
25. $\quad \boldsymbol{Z}_{k_o} = \{(i,j)\} : x_{ij} = 1 \quad \forall (i,j) \in \boldsymbol{A_r^{'}}$
26. $\quad$ **if** $(k_o > 1)$ **then**
27. $\quad\quad$ **if** $(\boldsymbol{Z}_{k_o} \subset \boldsymbol{\Gamma}_{k_o-1})$ **then**
28. $\quad\quad\quad$ *Save best feasible point:* $\boldsymbol{O}_{k_o} = x_{ij} \cup y_{ij}^k \quad \forall (i,j) \in \boldsymbol{A_r^{'}} \wedge k \in \{1, \cdots, f(i)\}$
29. $\quad\quad\quad$ *Break*
30. $\quad\quad$ **else**
31. $\quad\quad\quad$ *Save feasible point:* $\boldsymbol{O}_{k_o} = x_{ij} \cup y_{ij}^k \quad \forall (i,j) \in \boldsymbol{A_r^{'}} \wedge k \in \{1, \cdots, f(i)\}$
32. $\quad\quad$ **end if**
33. $\quad$ **end if**
34. $\quad k_o \leftarrow k_o + 1$
35. **end for**
36. *Recalculate gaps*

Algorithm 1: The main algorithm [J3]

From line 1 to 12 the task is to efficiently solve a feasibility problem. The idea is to

subsequently increase υ from an initial value $\upsilon = \upsilon_f = \upsilon_{f_{min}}$ to a maximum value $\upsilon = \upsilon_f = \upsilon_{f_{max}}$, with steps υ_{f_δ}, until a feasible point is found. If this is achieved in iteration k_f, the first task is terminated with a feasible point $\boldsymbol{I}$. Conversely, if the model is infeasible, the candidate arcs set is augmented with υ_{f_δ} units, and the process is taken to the iteration $k_f + 1$, where a new trial is attempted.

In order to formulate the MILP model, the cost coefficients calculation from (4.1) to (4.4) is omitted by setting them equal to zero, and the black-box MILP solver terminates when the first feasible point is found.

At this point, the Algorithm 1 requires as parameters $\upsilon_{f_{min}}$, υ_{f_δ}, and $\upsilon_{f_{max}}$. The greater $\upsilon_{f_{min}}$ and υ_{f_δ} the less efficient the feasibility problem becomes, however, increasing the odds to defining a feasible instance of the problem promptly.

Likewise, from line 13 to 35, the global optimization task is performed. The target is to obtain a feasible point with a given relative gap ϵ, expressed as the relative difference of the best feasible point (τ) minus the best achievable value objective (κ), with respect to τ. These values are indexed by iteration number. Similarly to the feasibility task, the iterative process increases the candidate arcs set from $\upsilon = \upsilon_o = \upsilon_{o_{min}}$ to $\upsilon = \upsilon_o = \upsilon_{o_{max}}$, with steps υ_{o_δ}.

The termination criterion is when the set $\boldsymbol{Z}_{k_o}$ of active variables $x_{ij} = 1$ of the problem defined in the iteration k_o, is a subset of the arcs set $\boldsymbol{A}_r^{'}$ defined in the previous iteration $k_o - 1$ ($\boldsymbol{\Gamma}_{k_o-1}$).

In this way, it is inferred that it is not longer necessary to increase υ_o, as the optimum variables have been already provided in the previous iteration.

To guarantee along the process a monotonously decreasing value of the objective function, in iteration k_o, the mathematical model is warm-started with the feasible solution found in $k_o - 1$ ($\boldsymbol{O}_{k_o-1}$). This strategy may help in shortening the convergence time for the sub-instance k_o.

Conceptually, Algorithm 1 intends to determine a reduced search space, where the global minimum point is hopefully included. If only one reduced problem was solved given a υ, it would not be possible to infer about the quality of the solution, and the calculated gap for that particular instance could not represent the global domain of the full problem, potentially leading to an overestimation.

For the global optimization task, Algorithm 1 requires as parameters $\upsilon_{o_{min}}$, υ_{o_δ}, and $\upsilon_{o_{max}}$ for the global optimization task. Naturally, $\upsilon_{o_{min}} \geq \upsilon_{f_{max}}$, and it is reasonable to consider $\upsilon_{o_\delta} > \upsilon_{f_\delta}$. By proper adjustment of the previous parameter, in best case scenario, the full Algorithm is concluded for $k_f = 1$ and $k_o = 2$.

Although for every iteration the maximum required gap ϵ is equally fixed, the equivalent calculated gap, having as reference the full-size domain, varies. Larger values of υ_{k_o} lead to equal or lower values of κ_{k_o}. This causes that in general, τ_{k_o} is also lower, until the ideal reduced search space is found, when equal values of τ_{k_o} should be obtained.

Therefore, after the termination of the algorithm, a gap updating procedure is performed based on the last calculated value of κ_{k_o}, to recalculate the relative difference for all previous iterations respect to this value (line 36). Let the recalculated gap in the global iteration k_g, including the feasibility and global optimization problems, be ϵ_{k_g}. In this sense, an evolution of the gap in function of the iterations is available, providing further insights and the sense of convergence, as the objective value decreases monotonically.

4.3 Results

The first case study is for the application of the framework of Figure 4.1, comparing the heuristics and the GA [C3]. In the second one is used the MILP-based global optimization approach of Section 4.2.2 in several large-scale real-world problems, with benchmarking against a method previously published in the scientific literature [J3].

4.3.1 Case Study 1

An OWF following a randomized micrositing is used to apply the method of Figure 4.1. The OWF consists of 51 WTs, rated each one at 4 MW and nominal voltage 33 kV. Two instances are considered, first, with only one cable type available (500 mm^2 with capacity for nine WTs and price 497 k€/km), and later, with two types available (185 mm^2 with capacity for six WTs and price 327 k€/km, and 300 mm^2 with capacity for seven WTs and price 395 k€/km). Information related to electrical properties of the cables is in [13]. Simulated OWF power time series are utilized for calculating power flow and losses.

The GA has been applied for the OWFs RBN and RBS, part of the Baltic InteGrid Project, in [C4]. Only the case study with multiple cable types is shown here. For more results, the reader is referred to [C3].

Multiple cables type

In the case of multiple cables types, numerous computational experiments indicate that the initial investment results depend strongly on the capacity and unit price difference among the considered cables. In general, the larger the set of available cables and the larger spread between cables' prices, the greater the difference between the GA and the heuristics, in terms of capital investment; this is because, the GA tends to use longer lengths of smaller cables, forming smaller cluster of WTs into feeders groups, giving also higher flexibility to provide feasible solutions, secondly, the heuristics (especially EW algorithm) prioritize forming bigger groups of WTs, requiring longer and bigger cables. As a result of the above, the heuristics provide solutions with lower electrical power losses in their favor.

For the OWF under study, in Table 4.1 results are presented. The GA gives the best solution in terms of initial investment, albeit with higher electrical power losses than all the other methods, due to the reduction of 66.46% of the cable 300 mm^2, and only an increment of 15.15% of the cable 185 mm^2, compared to EW. When using the metric

$LCOE_{cs}$ the effect of the electrical power losses is attenuated because this value is compared to the AEP representing likely only 1% of it.

Table 4.1: Multiple cables results [C3]

	Prim	Kruskal	EW	VAM	GA
Feasible	No	Yes	Yes	Yes	Yes
AEP [GWh]			855.36		
Losses [GWh]	–	7	7.3	7	7.99
Initial Investment [M€]	–	28.42	27.93	28.42	27.90
Diff. with best [%]	–	1.80	0.05	1.80	0
$LCOE_{cs}$ [€/MWh]	–	2.05	2.01	2.05	2.01
Diff. with best [%]	–	1.99	0	1.99	0
NPV_{cs}^{BC} [M€]	–	368.42	368.77	368.42	368.47
NPV_{cs}^{1} [M€]	–	632.98	633.24	632.98	632.73
Δdiff. with best w.r.t BC [%]	–	−25	–	−25	70
NPV_{cs}^{2} [M€]	–	897.54	897.71	897.54	896.99
Δdiff. with best w.r.t BC [%]	–	−51	–	−51	139

However, the NPV_{cs} metric weights out more the electrical power losses, as it can be seen in Table 4.1 for the NPV_{cs}^{BC}, the EW draws as the best option, and the energy unit price increases this differences almost linearly; in fact, in the case of NPV_{cs}^{2}, the Kruskal method cuts out 51% the difference, which indicates that for certain values of discount rate (or weighted average capital costs), price of energy, project lifetime, this one can become the solution with the greatest NPV value.

4.3.2 Case Study 2

The following experiments have been carried out on an Intel Core i7-6600U CPU running at 2.50 GHz and with 16 GB of RAM. The chosen MILP solver is the branch-and-cut solver implemented in IBM ILOG CPLEX Optimization Studio V12.7.1 [70].

The performance of the proposed algorithm is first investigated via sensitivity analysis of the parameters $\upsilon_{o_{min}}$, and υ_{o_δ}, which can be found in [J3].

In the following, the proposed method is benchmarked against results available in literature and acknowledged as best practice in the area today [24]. With this aim, the same testbed is employed, while assuming the same considerations, such as, objective (4.1)-(4.4), and constraints embodied by the equations (4.6)-(4.15).

Benchmarking

A testbed of real-world cases, presented in Table 4.2, is employed. Results for comparison are available in Table 4.3.

Table 4.2: Main inputs parameters for benchmarking [J3]

Ins.	OWF	Obj.	r[%]	c_e[€/MWh]	m	P_n [MW]	n_w	n_o	ϕ	η	V_n [kV]	$\boldsymbol{T}$	$\boldsymbol{U}$	$\boldsymbol{C_c}$+$\boldsymbol{C_p}$ [M€/km]
1	HR1	I	-	-	-	2	80	1	10	1	33	$\{6,7,8\}$	$\{7,11,13\}$	$\{0.37,0.39,0.43\}$
2	HR1	I	-	-	-	2	80	1	10	1	33	$\{9,10\}$	$\{7,12\}$	$\{0.44,0.45\}$
3	HR1	I	-	-	-	2	80	1	10	1	33	$\{4,5\}$	$\{10,14\}$	$\{0.44,0.62\}$
4	O	I	-	-	-	5	30	1	4	1	33	$\{11,12\}$	$\{5,10\}$	$\{0.41,0.61\}$
5	O	I	-	-	-	5	30	1	4	1	33	$\{13,14\}$	$\{4,9\}$	$\{0.38,0.63\}$
6	DT	I	-	-	-	3.6	80	1	10	1	33	$\{6,7,8\}$	$\{4,6,8\}$	$\{0.37,0.39,0.43\}$
7	DT	I	-	-	-	3.6	80	1	10	1	33	$\{4,5\}$	$\{6,8\}$	$\{0.44,0.62\}$
8	TH	I	-	-	-	3	100	1	10	1	33	$\{13,14\}$	$\{7,15\}$	$\{0.38,0.63\}$
9	TH	I	-	-	-	3	100	1	10	1	33	$\{4,5\}$	$\{7,10\}$	$\{0.44,0.62\}$
10	LA	IP	5	40	30	3.6	175	2	10	1	33	$\{1,2,3\}$	$\{7,10,13\}$	$\{0.36,0.58,0.90\}$

Table 4.3: Results for benchmarking [J3]

Ins.	OWF	Obj.[24] [M€]	Obj. [M€]	Diff.[M€]	ϵ_{k_g}[24] [%]	ϵ_{k_g} [%]	Diff.[%]	Time[24] [min]	Time [min]	Diff.[min]
1	HR1	19.44	19.44	0	0.01	0.01	0	30	1.57	28.43
2	HR1	22.61	22.61	0	0.01	0.01	0	30	1	29
3	HR1	23.48	23.48	0	0.17	0.01	0.16	1,440	7.26	1,432.74
4	O	8.05	8.05	0	0	0.01	−0.01	0.42	0.46	−0.04
5	O	8.36	8.36	0	0	0.01	−0.01	1.95	0.45	1.50
6	DT	38.98	38.98	0	4.85	0.01	4.84	30	1.88	28.12
7	DT	50.38	49.83	0.55	7.36	0.01	7.35	10	2.65	7.35
8	TH	22.34	22.31	0.03	3.37	0.7	2.67	5	627.60	−622.60
9	TH	26.64	26.64	0	2.51	0.3	2.21	1,440	107.02	1,332.98
10	LA	-	68.97	-	-	0.5	-	-	748	-

This testbed has been mostly extracted from [24], by selecting the most challenging instances. In [24] a significantly different approach (different mathematical formulation, for instance) from the one proposed in Section 4.2.2, consisting in a matheuristic model, has been designed, implemented, and tested.

The results in [24] where obtained with computational resources similar to those used in these experiments (IX CPU X5550 running at 2.67GHz, CPLEX 12.6).

In order to provide a fair comparison, all practical and technical constraints are conceptually equivalent, while the objective function is the initial investment, as losses are computed differently. Likewise, capacitive currents have been neglected as they are not included in [24].

The comparison results are presented in Table 4.3 (instances 1-9). A small (O), two large (HR1 and DT), and a very large OWFs (TH) are studied. Each instance is defined by a OWF, and a set of cables available $\boldsymbol{T}$.

Three aspects are compared: (i) solution quality, (ii) calculated gap, and (iii) computing time; each of them are directly compared by inspecting the columns Diff.[M€], Diff.[%],

and Diff.[min], respectively. In all metrics, positive value means better performance for the method presented in Section 4.2.2.

Regarding solution quality, it can be seen that, for all instances, the obtained solutions are equal or lower than in the benchmark work. For instance nr. 7, around 550,000 €, representing around 1% of the total cost, are saved. Particularly for this instance, the gap is improved from 7.36% to 0.01%, while simultaneously reducing the computing time.

When the calculated gap in both methods is lower than 0.01%, the objective values are essentially the same. This validates that the dual values between the two models are also equivalent.

In any instance the proposed method provides equally tight or even tighter solutions. The gap values reported in [24] have been recalculated in this method, using the best feasible point as reference (instead of the best dual value obtained in 24 h), to make them comparable with the proposed approach.

Finally, in almost all the instances, the computing time is shorter, with exception of instance nr. 8, where a considerable difference of 622 min is observed.

It is important to clarify that the reported computing times of the proposed method are for the whole running of Algorithm 1, including in all instances the final iteration $k_o = 2$, necessary to confirm finding the global point; in contrast, in the benchmark work, the reported time is when the best feasible point has been found. Similarly, as mentioned before, 24 h is the time limit to obtain the best dual value.

For all the instances, the proposed method calculates feasible points in less than 40 s, with recalculated gap of maximum 41%.

Besides the benchmark cases, an extra instance - not implemented in [24] - is included to show the method's applicability to OWFs with multiple OSSs. LA OWF is the second largest project (measured by installed power) under operation, surpassed only by Walney Extension OWF (although with less number of WTs therefore potentially easier to solve). For this instance, an initial feasible point is obtained in only 3 min, and the best feasible point is calculated in 12 h:28 min, with the gap being improved by 46.87%.

4.4 Summary

A set of methods, based on [C3], [C4], and [J3] have been proposed in this chapter. The methods are applied for optimization of the radial cable layout of collection systems for OWFs.

Standalone algorithms have been firstly proposed. This includes four heuristics and a GA.

Modifications of graph theory based heuristics for the design of C-MST have been proposed. These algorithms present polynomial running time, hence converge very fast for the scale of problems represented by modern OWFs. All the heuristics follow

essentially the same paradigm, in fact, in case the constraints are not binding, the solutions from them are the same. Given the deterministic nature of these algorithms, it is very hard in general the compliance of cable no-crossing constraints; in this case, unfeasible points are obtained in form of a forest graph. If valid solutions are resulted, the results point out their high quality when only a single cable is available. This means that the heuristics provide solutions very close to the global minimum when optimizing solely for length.

Meanwhile, the designed GA allows for overcoming the hard no-crossing constraints, as it is able to evaluate more design alternatives through evolutionary operators, to combine and modify individuals. As a consequence, the required computing time is in the order of hours, and increase dramatically for larger instances. The GA follows a learning procedure, so infeasible points are eliminated progressively in function of the iterations. In comparison to the heuristics, the GA provides cheaper solutions when multiple cables are available, since heuristics can not choice cables in advance. This also results with heuristics, especially EW, to come up with designs with lower electrical losses, as the total length is less.

Metaheuristics support the inclusion of different levels of complexity to model the system, such as power flow and losses calculation. Nevertheless, it is impossible to quantify the solution quality for specific problems.

A MILP-based global optimization model has also been proposed. A black-box solver is required, and the challenge is to provide tight formulations, which can be solved efficiently and effectively by them. Likewise, an algorithm framework is necessitated to further increase the tractability. This gives place to a hybrid method, which combines an exact formulation and heuristic rules, together forming the global optimization model. Linear formulations are noticeably more efficient than quadratic or in general non-linear; therefore, very large problems may be solved more likely with them, but there is also a challenge for adapting complex factors, such as losses and capacitive currents, under the framework of a MILP model.

The proposed matheuristic method has been benchmarked against a state-of-the art method with significantly different approach (different MILP model, and application of up to four distinctive heuristics); with all practical and technical constraints conceptually equivalent.

Ten real-world problem instances have been considered in the benchmark. The numerical results indicate that (i) the proposed algorithm provides, in general, at least equally good solutions, and in some cases, sizeable cheaper ones than the benchmark work, (ii) tighter gaps are calculated, in shorter computing times.

The proposed algorithm also performs satisfactorily for large OWFs with multiple OSSs, where the clustering is intrinsically defined in the mathematical formulation. It does not require predecessor algorithms to group WTs into OSSs, avoiding in this way artificially biased solutions.

CHAPTER 5
Deterministic Collection and Transmission System Design

This chapter is a summary of the article [J4].

5.1 Introduction

In Chapter 3 and Chapter 4 the problems of optimizing the transmission and collection systems cables have been studied, respectively. The economic and technical challenges for addressing these problems have been highlighted individually.

In this chapter, all the problems related to network topology optimization of OWFs are addressed simultaneously, as portrayed in Figure 2.2. This encompasses the optimization of the WTs collection system with WTs allocation to OSSs, while allowing the OSSs to have a set of candidate locations; the export cables are sized as well. A point-to-point connection scheme between OSSs and a OCP is assumed.

For the export cables, the classic technique of [16] is followed in this chapter. However, the probabilistic method proposed in Section 3.2.3 can also be adapted to this method. For the cable layout of the collection systems, only radial layouts are considered, meaning that cables failures are deemed negligible.

In this sense, the deterministic collection and transmission system design is at least as hard as the hardest problem of Chapter 4.

It has been identified that only the following works have studied the full integrated design of the network topology for OWFs using global optimization. A MILP model combined with Benders decomposition is presented in [34], a MILP model [28] solved by branch-and-cut method, a MILP model with progressive contingence incorporation [35], and finally a MIQP model is proposed in [64].

The papers [34], [35], [64] provide remarkable advances on stochastic optimization for problems in this context. Different stochastic scenarios are supported, accounting for wind power variability and cables failure. Distinctive theoretical strategies to accelerate convergence are applied and compared. While in [28] a single MILP model is formulated and later solved by branch-and-cut method. The model optimizes uniquely for initial investment, while also disregards important practical constraints, such as, cables crossings, and forbidden areas.

Nevertheless, the application of those methods did not focus on large-scale OWFs with multiple OSSs, as the case studies were defined by real projects with maximum 30 WTs. Modern OWFs can encompass WTs in the order of hundreds.

Other papers propose the use of metaheuristic for providing feasible points to approach large-scale instances. This includes [32] where PSO is employed and, [71] in which a GA is proposed. Given the intrinsic features of the used metaheuristics, there is no possibility to infer about the quality of the obtained solutions.

In virtue of the above, in this chapter is proposed a MILP model embedded in an efficient algorithmic framework, able to compute global optimum solution points (or near to it) in reasonable computational time, for the full network topology optimization problem in OWFs. Additionally, the model quickly finds feasible points. Likewise, the proposed model supports a combined objective function defined by total system costs, i.e. initial investment and total electrical power losses of both the collection and transmission systems simultaneously. High complex models for losses calculation using time series and capacitive currents are incorporated. Finally, since OWFs are deployed in relatively large areas, forbidden areas due to maritime planning constraints usually appear; hence, they are included also. Results are fully available in [J4].

5.2 Method

5.2.1 Modelling Aspects

The developed model supports any reasonable number of WTs, n_w, and any number of OSSs, n_o. Define the set $\mathcal{N}_o = \{\mathcal{N}_{o1}, \cdots, \mathcal{N}_{on_o}\}$, where an element $\mathcal{N}_{oi}$ is, in turn, an index set representing candidate locations for the ith OSS with $i \leq n_o$. In this way, $\beta_t = \sum_{1 \leq i \leq n_o} |\mathcal{N}_{o_i}|$ defines the total number of potential locations to place OSSs (denoted $\mathcal{N}_{\beta_t} = \{1, \cdots, \beta_t\}$), given a required number n_o, and individual candidate set, $\mathcal{N}_{oi}$, for each $i \in \mathcal{N}_{n_o} = \{1, \cdots, n_o\}$.

Likewise, let $\mathcal{N}_w = \{\beta_t + 1, \cdots, \beta_t + n_w\}$ denote the index set representing the WTs. Hence, the whole set of points including both OSSs candidate locations and WTs locations is given as, $\mathcal{N} = \{0\} \cup \mathcal{N}_{\beta_t} \cup \mathcal{N}_w$, where the node 0 represents the OCP.

As OWFs cover a relatively large area, it is common that they include forbidden zones - defined as spaces where no WTs or cables can be placed - which must be considered as well. The distance between two points i and j, is defined as d_{ij}.

The complete directed graph $G(\mathcal{N}, \mathcal{A}, \mathcal{D})$ comprises the input sets, where $\mathcal{N}$ represents the vertex set, $\mathcal{A}$ the set of available arcs arranged as a pair-set, and $\mathcal{D}$ the set of associated weights for each element $a \in \mathcal{A}$.

The different types of cables being considered are stored in $\mathcal{T}_c$, and $\mathcal{T}_e$, for the collection and export systems, respectively. The set $\mathcal{T}_c$ relates to the attribute sets $\mathcal{U}_c$, and $\mathcal{C}_c$, representing the capacity (in terms of maximum number of supported WTs), and total

capital expenditures per unit of length, respectively. In general, the greater the cable capacity, the greater the capital cost.

The first set of variables in the model are binary: $z_{i,l}$ x_{ij}, and y_{ij}^k. Choosing the candidate location l for the OSS i is done through the variable $z_{i,l}$, which is equal to one if selected. and zero otherwise. If the arc connecting i, and j is active ($i \in \mathcal{N} \setminus \{0\} \wedge j \in \mathcal{N} \setminus \{0\}$), then $x_{ij} = 1$. Finally, in case $x_{ij} = 1$, the number of WTs connected is defined by y_{ij}^k, where k models the number of WTs rooted at i, including the one at j. A set of positive integer variables is required as well; σ_i, and $\sigma_{i,l}$ represents the number of WTs connected to the OSS i, and at the corresponding candidate location l, respectively.

The modelling choices for the calculation of cables capacity, arcs nominal power, and power flow and total power losses are available in [J4]. In general, hyperbolic functions and other non-linear expressions to calculate flow and losses are incorporated.

5.2.2 MILP model

The number of x_{ij}, and y_{ij}^k variables scale quadratically with the number of WTs. Therefore, reduction strategies are important to limit the size of the model in terms of variables and constraints.

The procedure proposed in Section 4.2.2 is used. The largest individual cable capacity is found as $U_c = \max \mathcal{U}_c$; consequently, the maximum attributable value of k for $i \in \mathcal{N}_{\beta_t}$ is equal to $f(i) = U_c$, in contrast, for elements $i \in \mathcal{N}_w$ is $f(i) = U_c - 1$. This is because, intuitively, a cable only can be used at maximum capacity if connected to a OSS. Finally, all redundant arcs are suppressed, along with those interconnecting OSSs, as only the common industry practice of point-to-point connections from offshore to onshore points is considered. Overall, the original graph $G(\mathcal{N}, \mathcal{A}, \mathcal{D})$ is reduced to $G_r(\mathcal{N}, \mathcal{A}_r, \mathcal{D}_r)$.

Cost coefficients

Designing the electrical cables system in OWFs is manifold: not only arcs must be selected while also choosing the cable type to do so, but total electrical power losses must be considered as they may impact the design. Total electrical power losses are function of the selected arc, cable type, and generated power.

Hence, the straight-forward way to include simultaneously all these aspects is to incorporate in the variable y_{ij}^k the cable type, as for instance transforming the variable to $y_{ij}^{k,t}$. Variable $y_{ij}^{k,t}$ would model whether the arc $a_r = (i, j)$ is selected or not, connecting k WTs through cable type t. Secondly, losses would have to be mathematically explicitly expressed in the objective function. This raises two issues: (i) the number of variables increase linearly with the number of cable types $|\mathcal{T}_c|$, and (ii) ohmic losses are non-linear, therefore simplifications must be assumed for expressing it in a linear model.

A body of actions to circumvent these limitations, while being able to solve the defined problem, are implemented. The approach basically decouples the arc selection and losses

minimization from the cable assignment decision-making problem. These techniques are explained as follows for both the collection system (radial cable layout), and transmission system (point-to-point connection).

Collection system cables The reduced graph $G_r(\mathcal{N}, \mathcal{A}_r, \mathcal{D}_r)$ contains all required information for the cable layout. For y_{ij}^k, the length of arc (i, j) is known, along with the number of WTs connected; this makes possible to evaluate the whole set of available cables in polynomial running time for each of the arcs (such as $i \neq 0 \wedge j \neq 0$), to select that which minimizes the objective function. All cost coefficients are non-negative.

Let the term $(c_{c_t} \cdot d_{ij})$ represent the capital expenditures plus installation costs (per metric unit) of cable t, to join points i and j (cost per metric unit). The parameters $c_{c_t} \in \mathcal{C}_c$ are obtained from the exponential regression function given in [72] (excluding installation costs).

To incorporate the cost of total electrical power losses, a DCF metric is considered. The required parameters are $|\mathcal{M}|$, $l_{c_{ij,t}}^{\mu,k}$, c_p, and r, meaning the project lifetime (years), total power losses at year μ for cable t, when k WTs are connected (in MWh), cost of energy (€/MWh), and discount rate (p.u.), respectively.

Bearing this in mind, for each (i, j) such as $i \neq 0 \wedge j \neq 0$, the following optimization model is formulated and solved independently by enumeration as in [J3].

$$c_{ij}^k = \min \quad \sum_{t \in \mathcal{T}_c} x_{c_{ij,t}} \cdot \left(c_{c_t} \cdot d_{ij} + \sum_{\mu=1}^{|\mathcal{M}|} \frac{l_{c_{ij,t}}^{\mu,k} \cdot c_p}{(1+r)^\mu} \right) \tag{5.1}$$

$$\text{s.t.} \quad \sum_{t \in \mathcal{T}_c} x_{c_{ij,t}} = 1 \tag{5.2}$$

$$x_{c_{ij,t}} \cdot (S_{c_{ij,t}}^k - S_{rc_t}) \leq 0 \quad \forall t \in \mathcal{T}_c \tag{5.3}$$

$$x_{c_{ij,t}} \in \{0, 1\} \quad \forall t \in \mathcal{T}_c \tag{5.4}$$

Note that this set of problems are always feasible as k is limited by U_c. Equation (5.2) ensures that exactly one cable type is selected. Equation (5.3) guarantees that the capacity of cable t is not violated; where $S_{c_{ij,t}}^k$ is the power through arc (i, j), when k turbines are connected in j using cable t, and S_{rc_t} is the rated power of t. Lastly, Equation (5.4) defines the nature of the problem's variables.

After solving the model from (5.1) to (5.4) (maximum $U_c \cdot |\mathcal{N}|^2$ times), the cost coefficients c_{ij}^k are calculated, and the corresponding cable type t is unequivocally determined as per $x_{c_{ij,t}}$.

Transmission system cables Arcs (i, j) such as $i \in \{0\} \wedge j \in \mathcal{N}_{\beta_t}$ are also definable beforehand. The cost of the transmission cables is function of the total length and installed power; the former is known, but the latter is also output of the main optimization model. Likewise, in contrast to the collection system cable layout, there are no binary variables explicitly representing whether certain number of WTs are connected to a OSS or not. In this case, the variables $\sigma_{i,l}$ are used to estimate the cost for a specific candidate location $l \in \mathcal{N}_{\beta_t}$, associated to the OSS $i \in \mathcal{N}_{n_o}$.

Let the variable $x_{0j}^{t,n}$ represent if arc $(0, j)$ is active using n cables t in parallel or not (a limit of $n = 3$ is a reasonable practical constraint to ensure feasibility). The method uses the following optimization model, where the target is to obtain a linear cost function in terms of the WTs connected to a OSS:

$$\min \quad \sum_{n=1}^{3} \sum_{t \in \mathcal{T}_e} x_{e_{ij,t,n}} \cdot \left(c_{e_{t,n}} \cdot d_{0j} + \sum_{\mu=1}^{|\mathcal{M}|} \frac{l_{e_{0j,t,n}}^{\mu,k} \cdot c_e}{(1+r)^{\mu}} \right) \tag{5.5}$$

$$\text{s.t.} \quad \sum_{n=1}^{3} \sum_{t \in \mathcal{T}_e} x_{e_{ij,t,n}} = 1 \tag{5.6}$$

$$\sum_{n=1}^{3} x_{e_{ij,t,n}} \cdot \left(S_{e_{0j,t,n}}^{k} - S_{re_t} \right) \leq 0 \quad \forall t \in \mathcal{T}_e \tag{5.7}$$

$$x_{e_{ij,t,n}} \in \{0, 1\} \quad \forall t \in \mathcal{T}_e \wedge n \in \{1, 2, 3\} \tag{5.8}$$

The mathematical program from (5.5) to (5.8) resembles that described from (5.1) to (5.4). In fact, each equation is mirrored by the order of appearance. Nevertheless, in the case of the transmission cables, most of the parameters and variables are re-indexed accounting for n, which is the number of cables per connection. Contrary to collection system cables, in transmission level parallel cables are installed in practice.

Figure 5.1 presents the basic algorithm for calculating the transmission cables linear cost function.

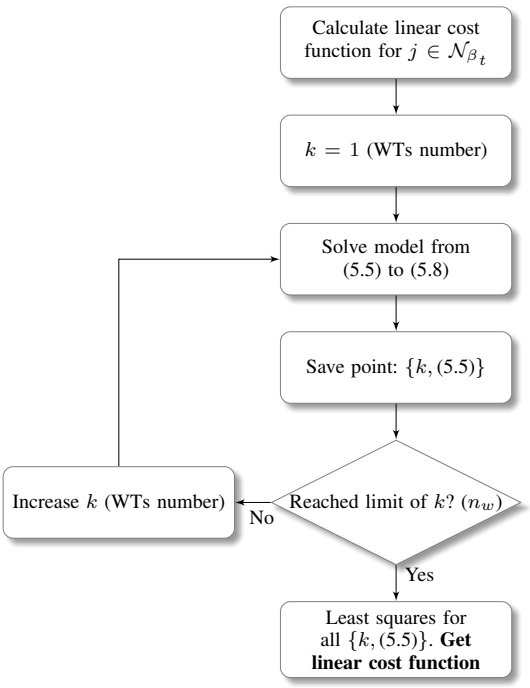

Figure 5.1: Flowchart for calculating the transmission cables linear cost function [J4]

The idea behind this flowchart is to sequentially increase the number k of turbines

connected to a specific OSS location, solving (5.5) to (5.8), and gathering all results to finally obtain the best linear function fitting the data by least squares method.

The procedure is performed for each OSS candidate location. Thus, β_t linear functions are obtained, each characterized by a independent c_l^o, and non-negative linear c_l^ι term, where $l \in \mathcal{N}_{\beta_t}$.

By adaptations on the costs coefficients in (5.1) and (5.5), the following objective functions are supported for the global model: L, LP, I, and IP.

Objective function

After solving the collection and transmission systems sub-problems, the linear objective function of the main mathematical model is formulated as:

$$\min \sum_{i \in \mathcal{N} \setminus \{0\}} \sum_{j \in \mathcal{N}_w} \sum_{k=1}^{f(i)} c_{ij}^k \cdot y_{ij}^k + \sum_{i \in \mathcal{N}_{n_o}} \sum_{l \in \mathcal{N}_{oi}} (c_l^o \cdot z_{i,l} + c_l^\iota \cdot \sigma_{i,l}) \tag{5.9}$$

Constraints

For a given set of candidate locations $\mathcal{N}_{oi}$ for the OSS i, exactly one of them must be chosen. This is modelled through

$$\sum_{l \in \mathcal{N}_{oi}} z_{i,l} = 1 \quad \forall i \in \mathcal{N}_{n_o} \tag{5.10}$$

Note that in constraint (5.10), if an inequality (less than or equal to) replaces the equality, not only multiple locations would be supported, but also multiple number of OSSs.

In order to cluster the WTs (n_w) into n_o OSSs, the following constraint is required:

$$\sum_{i \in \mathcal{N}_{n_o}} \sigma_i = n_w \tag{5.11}$$

In (5.11), σ_i represents the number of WTs associated to the OSS i, its definition is:

$$\sum_{l \in \mathcal{N}_{oi}} \sigma_{i,l} = \sigma_i \quad \forall i \in \mathcal{N}_{n_o} \tag{5.12}$$

Correspondingly, $\sigma_{i,l}$ counts the number of WTs connected to the OSS i at location l and is computed through

$$\sum_{j \in \mathcal{N}_w} \sum_{k=1}^{f(j)} k \cdot y_{lj}^k = \sigma_{i,l} \quad \forall i \in \mathcal{N}_{n_o} \wedge l \in \mathcal{N}_{oi} \tag{5.13}$$

The variables $\sigma_{i,l}$ are for linearization, while σ_i is for the model readability. The following equation, for both selecting an OSS location $z_{i,l}$ and limiting the number of feeders out from them to ϕ, is added:

$$\sum_{j \in \mathcal{N}_w} \sum_{k=1}^{f(j)} y_{lj}^k \leq \phi \cdot z_{i,l} \quad \forall i \in \mathcal{N}_{n_o} \wedge l \in \mathcal{N}_{oi} \tag{5.14}$$

The tree topology, i.e. only one cable type used per arc, and the definition of the head-tail convention, are simultaneously ensured by:

$$\sum_{i \in \mathcal{N} \setminus \{0\}} \sum_{k=1}^{f(i)} y_{ij}^k = 1 \quad \forall j \in \mathcal{N}_w \tag{5.15}$$

The flow conservation, which also avoids the formation of cycles (loops), is considered by means of one linear equality per wind turbine

$$\sum_{i \in \mathcal{N} \setminus \{0\}} \sum_{k=1}^{f(i)} k \cdot y_{ij}^k - \sum_{i \in \mathcal{N}_w} \sum_{k=1}^{f(i)} k \cdot y_{ji}^k = 1 \quad \forall j \in \mathcal{N}_w \tag{5.16}$$

The set $\mathcal{I}$ stores pairs of arcs $\{(i,j),(u,v)\}$, which are crossing each other. Excluding crossing arcs in the solution is ensured by the linear inequalities

$$x_{ij} + x_{ji} + x_{uv} + x_{vu} \leq 1 \quad \forall \{(i,j),(u,v)\} \in \mathcal{I} : \{i,j,u,v\} \neq 0 \tag{5.17}$$

$$\sum_{k=1}^{f(i)} y_{ij}^k - x_{ij} \leq 0 \quad \forall (i,j) \in \mathcal{A}_r : \{i,j\} \neq 0 \tag{5.18}$$

Constraint (5.17) also includes the inverse arcs of those elements.

The following constraints represent a set of valid inequalities to tighten up the mathematical model [68]:

$$-\sum_{i \in \mathcal{N} \setminus \{0\}} \sum_{k=v+1}^{f(i)} \left\lfloor \frac{k-1}{v} \right\rfloor \cdot y_{ij}^k + \sum_{i \in \mathcal{N}_w} \sum_{k=v}^{f(i)} y_{ji}^k \leq 0 \quad \forall v \in \{2, \cdots, U_c - 1\} \wedge j \in \mathcal{N}_w \tag{5.19}$$

$$\begin{gathered} x_{ij} \in \{0,1\} \quad y_{ij}^k \in \{0,1\} \\ \forall (i,j) \in \mathcal{A}_r : \{i,j\} \neq 0 \wedge k \in \{1, \cdots, f(i)\} \end{gathered} \tag{5.20}$$

$$z_{i,l} \in \{0,1\} \quad 0 \leq \sigma_i \leq \eta \cdot \left\lceil \frac{n_w}{n_o} \right\rceil \quad \sigma_i \wedge \sigma_{i,l} \in \mathbb{Z}_+ \forall i \in \mathcal{N}_{n_o} \wedge l \in \mathcal{N}_{oi} \tag{5.21}$$

Constraints (5.20) and (5.21) define the nature of the formulation by the variables definition, a MILP. Note that variables σ_i are limited in their upper bounds to avoid unbalanced OSSs, in terms of connected WTs (in case $\eta = 1$, if unbalancing is permitted then $1 < \eta \leq n_o$), which implicitly also bounds $\sigma_{i,l}$.

To summarize, the complete formulation of the main MILP model consists of the objective function (5.9) and constraints defined in (5.10) - (5.21).

Forbidden areas

A restricted set of regions (inside a OWF) for excavation and cable trenching is supported in this model, as presented in Figure 5.2.

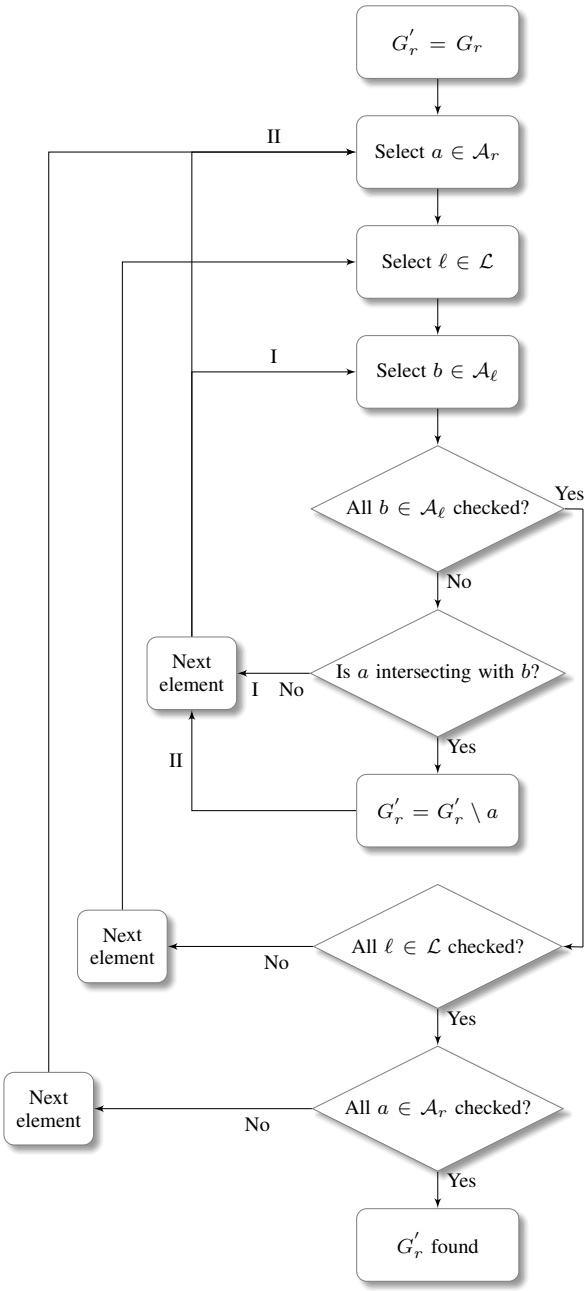

Figure 5.2: Flowchart for incorporating forbidden areas in the model [J4]

Those regions can be modelled as convex polygons [73], non-convex polygons [24], [74], or

closed curves [36]. A convex hull based bypassing algorithm which may incorrectly delimit areas as forbidden, if they are non-convex polygons, is proposed in [73]. Any polygonal shape can be defined using Steiner nodes explicitly in the model as in [74], where the aim is not only to model the area, but also to refine arcs with shortest path. However, bending moments in the cables may be compromised as a result of unrealistic routing. Finally, more accurate computational algorithms to represent more precisely defined shapes is implemented in [36], by means of Delaunay Triangulation Based Navigational Mesh Path-finding. Despite this, unrealistic routing can result as well.

Any polygonal shape is modelled, while simultaneously decreasing the number of variables. By means of this approach, the explicit creation of variables and constraints in the main model to cope with forbidden areas is avoided, while allowing only straight arcs between WTs. On the other hand, the strategy is flexible as any number of shapes are supported.

Let the set of forbidden areas be $\mathcal{L}$. An area $\ell \in \mathcal{L}$, in turn, is defined as a set of arcs $\mathcal{A}_\ell$, where $b \in \mathcal{A}_\ell : b = (i, j)$. The set of arcs $\mathcal{A}_\ell$ defines a sequence of vertices enveloping the points representing a forbidden area l (the sequence $\{i, j, v, i\}$ represents, for example, a triangle with $\mathcal{A}_\ell = \{(i, j), (j, v), (v, i)\}$). The procedure for incorporating these zones into the model is depicted in Figure 5.2, where graph $G_r^{'}$ is obtained from graph G_r, by excluding from the new arcs set $\mathcal{A}_\nabla^{'}$ all the arcs crossing with at least one arc $b \in \mathcal{A}_\ell$.

5.2.3 Optimization Framework

For large OWFs, i.e. in the range of 100s of WTs, the cable layout problem is generally unsolvable for gaps lower than 1% [7]. This is also the computational experience acquired during the experiments. Therefore the graph $G_r^{'}$ needs further reduction to make the model tractable.

The framework proposed in Section 4.2.2 is generalized in this chapter. Let the function $f(i, G_r^{'}, \upsilon)$ obtain the set Υ_i defined as maximum the υ-closest WTs to i; the term *maximum* accounts for vertices which have less than υ arcs available due to prior elimination for crossings with forbidden areas. By systematically applying $f(i, G_r^{'}, \upsilon)$ to each $i \in \mathcal{N}_w$, the reduced graph $G_r^{''}$ is found. The set $\mathcal{A}_\nabla^{''}$ contains the candidate arcs to the solution of the problem. The outcoming arcs from OSSs are also limited to the nearest 50 WTs. An imposed gap of ϵ is an input of the method.

The flowchart is displayed in Figure 5.3; as a first step a feasibility problem is solved, characterized by (i) an objective function equal to zero, (ii) a low υ is set to speed up the process, and (iii) fixed locations of OSSs by choosing arbitrarily one per each i available in $\mathcal{N}_{oi}$.

Following the solution of the feasibility problem, the obtained solution is used to warm start the main model given $G_r^{''}$ for a specific value of υ. The next step is to compare if the best feasible point found so far, is included in the domain of the previously defined problem ($\mathcal{A}_\nabla^{''}$). If this is the case, the process is stopped, since most likely the global minimum has been calculated. Otherwise, the domain is further increased until that

condition is satisfied. In Section 4.3.2, it has been found out that for the feasibility problem $\upsilon = 5$, and for the main problem an initial value of $\upsilon = 15$, and increasing steps equal to 5, represent good parameters to find a proper compromise between computing time, and solution quality.

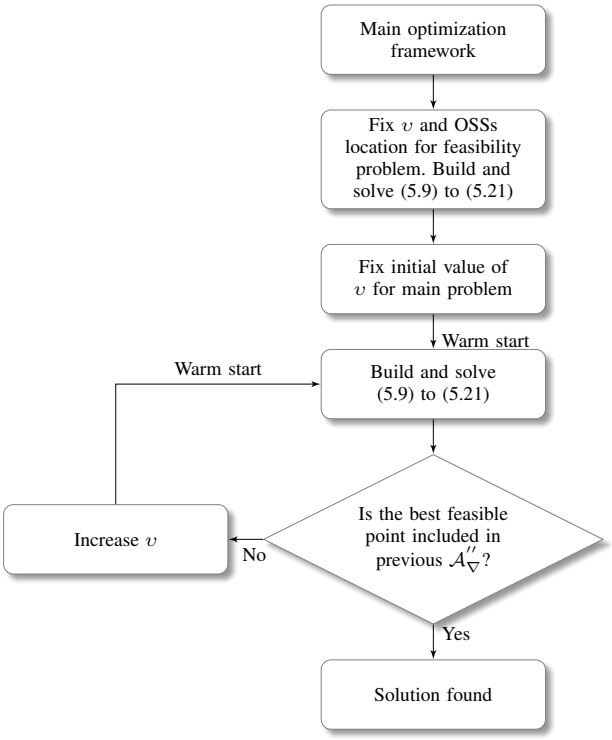

Figure 5.3: Flowchart of the main optimization framework [J4]

5.3 Results

The following case studies have been carried out on an Intel Core i7-6600U CPU running at 2.50 GHz and with 16 GB of RAM. The chosen MILP solver is the branch-and-cut solver implemented in IBM ILOG CPLEX Optimization Studio V12.7.1 [70].

A synthetic OWF (SY) with three forbidden areas is used to test the validity of the model. The real project LA which is the second largest (measured by installed power) project under operation [75], is used to illustrate the ability of the model to solve very large instances. Both cases have more than 100 WTs and several OSSs, representing very challenges instances to solve.

The main high-level parameters for both case studies are given in Table 5.1. The objective function is defined by a combined total economic cost including the initial investment, and the total electrical power losses of the cables systems (see (5.1) and (5.5)). Three forbidden areas are considered in SY, with four candidate locations per OSS, and distance to OCP of roughly 100 km. In LA three possible locations are supported for each OSS,

with length to OCP close to 20 km. In all cases, a maximum number of 10 feeders is allowed per OSS (see (5.14)), in addition to a balanced allocation of WTs to OSSs. Balancing of OSSs is accounted by means of $\eta = 1$, see (5.21).

Table 5.1: Main high-level parameters for the problem instances [J4]

OWF	Objective	r [%]	c_p [€/MWh]	$\lvert\mathcal{M}\rvert$	$\lvert\mathcal{L}\rvert$	η
SY	IP	5	40	30	3	1
LA					0	
OWF	P_n [MW]		$\mathcal{N}_o$	n_w	n_o	ϕ
SY	3.6		$\{\{1,2,3,4\},\{5,6,7,8\}\}$	120	2	10
LA			$\{\{1,2,3\},\{4,5,6\}\}$	175		

The technical and economic parameters for both medium and high voltage cables are presented in Table 5.2. Further technical cable information is available in [13]. For the collection system, the set of cable dimensions is 240 mm^2, 500 mm^2, and 1,000 mm^2, while for transmission, ten different cables types are considered, ranging from 300 mm^2 to 2,000 mm^2. All the cross-sections are commercially standards by manufacturers. Cable capacities and costs are displayed for reproducibility as well in Table 5.2.

Table 5.2: Cables main parameters [J4]

Collection system				
OWF	V_{n_c} [kV]	$\lvert\mathcal{T}_c\rvert$	$\mathcal{U}_c$	$\mathcal{C}_c$ [M€/km]
SY LA	33	3	$\{7,10,13\}$	$\{.36,.58,.90\}$
Transmission system				
OWF	V_{n_e} [kV]	$\lvert\mathcal{T}_e\rvert$	$\mathcal{U}_e$	$\mathcal{C}_e$ [M€/km]
SY	132	10	$\{34,38,42,46,49$ $53,56,59,62,69\}$	$\{.50,.56,.63,.73,.84$ $.96,1.11,1.28,1.51,2.16\}$
LA	150		$\{38,43,47,52,56$ $60,63,67,71,79\}$	$\{.57,.66,.78,.93,1.13$ $1.33,1.59,1.91,2.34,3.60\}$

The graphical result of applying the integrated global optimization model in SY OWF is presented in Figure 5.4. Candidate locations are indicated with red numbers. All hard constraints are satisfied, along with the non crossing of forbidden areas. Only cables with 240 and 500 mm^2 are used in the collection system. For the OSSs, the locations closest to the OCP are chosen, hence minimizing the transmission cable length. Each OSS is being connected with two 500 mm^2 cables.

Numerical results are available in Table 5.3. For SY OWF ($\epsilon = 0.5\%$) an optimality gap of 0.49% is achieved in 3 h, and 31 min. An initial feasible solution is found in 81 s, with

optimality gap equal to 13.42%. In order to assess if the solver is able to take advantage of the problem's structure, an instance of SY, called as SYs, where only one candidate location is fixed per OSS (number 1 and 6 in Figure 5.4), is solved by the model. An equal solution is obtained in 1 h, and 28 min. The total number of combinations in terms of OSSs pairs is 16. If one assumes this an average running time, then a total of 23 h, and 31 min would be required following an enumeration approach. By means of the integrated model a reduction of 85% of running time is obtained.

Finally, the very large instance of LA OWF is studied. The two previously described instances have been solved using the default settings offered by CPLEX. However, out-of-memory problems were faced when evaluating the LA instance. To cope with this limitation, strong variable selection is used. This means that CPLEX invests considerable effort in analyzing potential branches of the nodes tree in the hope of drastically reducing the number of nodes that are explored. The strategy compromises the running time but generally allows for less memory requirements. The LA OWF is solved with a gap of 0.75% in slightly more than 23 h. In this case, the optimal solution results in OSSs located around the center of the OWF. This is intuitively valid, as the shorter length to shore (around 20 km) moves the weight towards minimizing the total length of the collector system cables

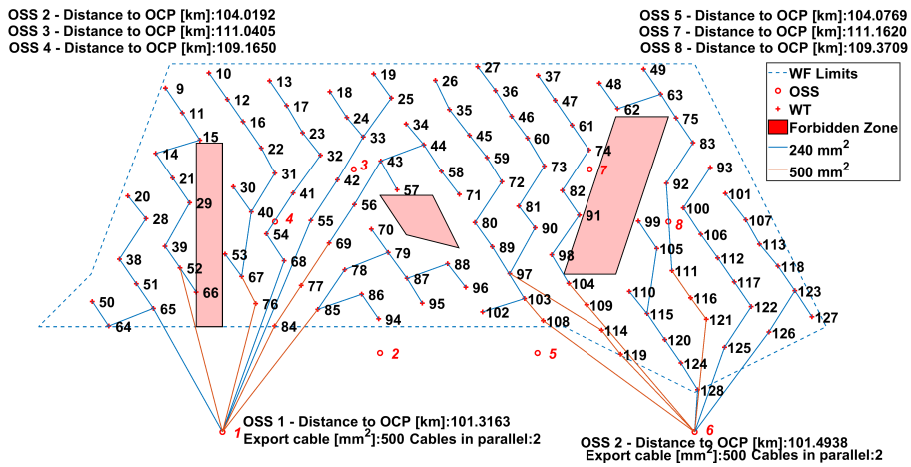

Figure 5.4: SY OWF designed cable layout [J4]

Table 5.3: Main results summary [J4]

Model	Best solution [M€]	Gap [%]	Total computation time [h]
SY	487.47	0.49	3.53
SYs	487.76	0.50	1.48
LA	144	0.75	23.29

5.4 Summary

A method, based on [J4] has been proposed in this chapter. The proposed method provides an integrated global optimization approach to design electrical cable systems of OWFs, particularly the collection and transmission systems. This is the full network topology optimization problem for OWFs.

This method is able to: (i) harmonize and design both systems through a MILP model, (ii) provide fast computing time, and (ii) integrate realistic and high-fidelity physical models for power flow and losses calculation.

The method has been validated against large-scale instances of OWFs projects. Several numerical results prove the validity and accuracy of the approach in terms of abiding hard constraints within reasonable computation time, considering the complexity of the problems. A synthetic OWF (SY), and the second largest project in operation today, the London Array (LA), considering three candidate locations per OSS, have been used as case studies. The SY OWF is solved in around 3.5 h with an optimality gap of 0.49%. The integrated model is roughly 85% faster than an enumeration approach. In the case of LA OWF, strong variable selection is used in the branch-and-cut method, achieving an optimality gap of 0.75% in slightly more than 23 h. The results indicate that the physical optimal locations of the OSSs are strongly affected by the distance to shore, as the export cables total costs start becoming predominant for larger distances.

CHAPTER 6
Stochastic Collection System Design

This chapter is a summary of the articles [C5] and [J5].

6.1 Introduction

In Chapter 4 and Chapter 5 the problems of optimizing the radial cable layout of the collection systems for OWFs, and the full network topology optimization problem are addressed, respectively. In both chapters, a deterministic approach is adopted, meaning that the impact of cable failures is not considered.

However, as explained in Figure 2.3, cable layouts with redundancy may help to include in the minimization the energy curtailment due to random cables failures. In order to do so, such stochasticity must be incorporated into the mathematical program, while forcing the layout to provide alternative path for each WT towards the OSS.

This means that in contrast to Chapter 4, in this chapter a stochastic approach is considered, attributing a failure probability to cables.

Stochastic optimization for OWFs electrical cable optimization has been addressed previously [64], [35], and [34]. Nonetheless, the focus of these articles is the holistic design for small-scale farms, while excluding practical engineering constraints such as no-crossing of cables, among others. The first work in the field [64] proposed a MIQP model using exhaustive uncertainty enumeration. This work is continued in [35] and [34], where the contribution is the development of techniques to accelerate the convergence to obtain solution through decomposition techniques.

In virtue of the above, an algorithmic framework for design collection system with a closed-loop structure, using global optimization, integrated with analytical methods for reliability assessment is presented in this chapter. Additionally, a common framework developed to assess and compare -in economic terms- closed-loop vs radial topology optimization for OWFs is presented. The algorithm is based upon a MILP model solved using a commercial solver, able to account for the three main optimization criteria in electrical network planning: investment, total electrical power losses, and reliability (IRL). For the second point, a recourse problem is solved using the radial design and the same underlying stochastic considerations utilized for the closed-loop design. It is

important to remark that strategies for approaching large instances are quantitatively analyzed and discussed as well.

6.2 Method

6.2.1 Modelling Aspects

The aim of the optimization is to design a closed-loop cable layout of the collection system for an OWF, i.e., to interconnect through power cables the n_{w} WTs to the available OSS, while providing a redundant power evacuation route.

Let $\boldsymbol{N}_{\mathrm{w}} = \{2, \cdots, 1 + n_{\mathrm{w}}\}$. Besides, let the points set be $\boldsymbol{N} = \{1\} \cup \boldsymbol{N}_{\mathrm{w}}$, where the element $i \in \boldsymbol{N}$, such as $i = 1$ is the OSS.

The Euclidean distance between the positions of the points i and j, is denoted by d_{ij}. These inputs are gathered in a weighted undirected graph $G(\boldsymbol{N}, \boldsymbol{E}, \boldsymbol{D})$, where $\boldsymbol{N}$ is the vertex set, $\boldsymbol{E}$ the set of available edges arranged as a pair-set, and $\boldsymbol{D}$ the set of associated euclidean distances for each element $[ij] \in \boldsymbol{E}$, where $i \in \boldsymbol{N} \wedge j \in \boldsymbol{N}$. In general, $G(\boldsymbol{N}, \boldsymbol{E}, \boldsymbol{D})$ is a complete undirected graph. It may be bounded by defining uniquely those edges connecting the $\upsilon < n_{\mathrm{w}}$ closest WTs to each WT, and by the $\sigma < n_{\mathrm{w}}$ edges directly reaching the OSS from the WTs.

Likewise, let $\boldsymbol{T}$ be a predefined list of available cable types, and $\boldsymbol{U}$ be the set of cable capacities sorted in non-decreasing order as in $\boldsymbol{T}$, being measured in Amperes (A), such that u_t is the capacity of cable $t \in \boldsymbol{T}$. Furthermore, each cable type $t \in \boldsymbol{T}$ has a cost per unit of length, c_t (including capital and installation costs), in such a way that $\boldsymbol{U}$ and $\boldsymbol{T}$ are both comonotonic. The set of expenditures per meter is defined as $\boldsymbol{C}$.

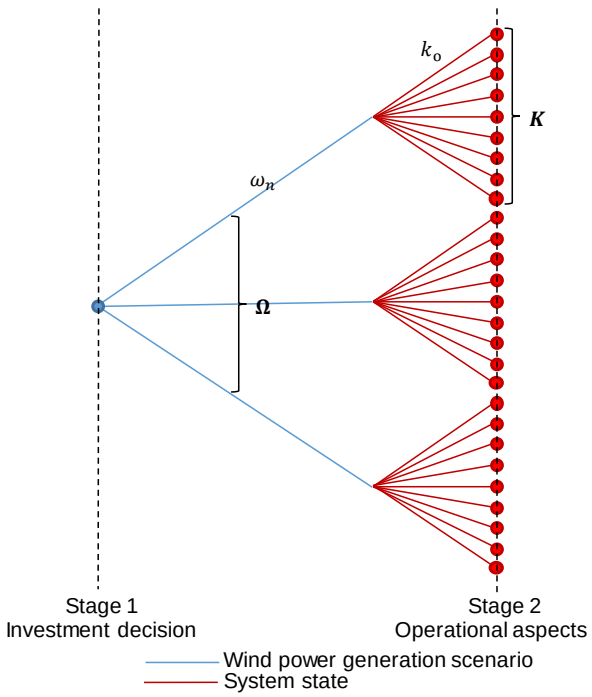

Figure 6.1: Scenario tree, Υ [C5]

The problem is formulated as a stochastic optimization program modelled with two stages: investment (construction) and operation. In Figure 6.1 is presented a graphical representation of the two stages of the model. In this figure it can be seen that uncertainty is represented by means of a scenario tree (Υ), expressing simultaneously how the stochasticity is developing over time (at the moment of the investment decision, uncertainties of the random parameters are present), the different states of the random

parameters (the instances of the random process multiply in function of the generation scenarios and installed cables), and the definition of the non-anticipative decisions in the present (in real-time operation the investment decision can not be changed).

The set of wind power generation scenarios is $\boldsymbol{\Omega}$ (blue lines in Figure 6.1), they represent power states for bins of wind speed, while the representative system states are $\boldsymbol{K}$ (red lines in Figure Figure 6.1). The nominal generation scenario is ω_{n}, and the base system state (k_{o}) represents the case of no failures. The base case is therefore represented by the scenario $\{\omega_{\mathrm{n}}, k_{\mathrm{o}}\}$. A wind power generation scenario ω has associated a duration time τ^{ω} (in hours), and power magnitude ζ^{ω} (in per unit, p.u.), and each system state k, a system probability ψ^{k}.

The system probability ψ^{k} is calculated using a discrete Markov model to define the cables' complementary states: available, and unavailable. Through this, it is possible to calculate ψ^{k} given the failure statistical parameters MTBF and MTTR [76]. In the same way, given the low failure rates of these components a N-1 criterion must be considered in each system state [77]; this means that elements remaining in operation in a contingency are capable of accommodating the new operational situation, and it is very unlikely that other element would fail simultaneously.

The first stage variables are the binary variables $x_{ij,t}$, and y_{ij}; where $x_{ij,t}$ is equal to one if active edge $[ij]$ ($y_{ij} = 1$) uses cable type $t \in \boldsymbol{T}$. The second stage variables are the continuous variables $I_{ij}^{\omega,k}$, $\theta_{i}^{\omega,k}$, and $\delta_{j}^{\omega,k}$. The electrical current in edge $[ij]$ in wind power generation scenario $\omega \in \boldsymbol{\Omega}$, and system state $k \in \boldsymbol{K}$ is represented by $I_{ij}^{\omega,k}$. While the voltage phase at each WT busbar is $\theta_{i}^{\omega,k}$. The curtailed current at wind turbine j in wind power generation scenario $\omega \in \boldsymbol{\Omega}$, and system state $k \in \boldsymbol{K}$ is $\delta_{j}^{\omega,k}$. Note that $\delta_{j}^{\omega,k}$ (in A) is bounded by the current generated at j in the same scenario, I_{j}^{ω}, where $I_{j}^{\omega} = \frac{P_n \cdot \zeta^{\omega} \cdot 1000}{\sqrt{3} \cdot V_n}$, being P_n the nominal power of an individual WT, and V_n the line-to-line nominal voltage of the system.

6.2.2 MILP model and PCI Algorithm

Cost coefficients and objective function

Total electrical power losses are non-linear in function of the current. In that event, two distinctive mathematical expressions to support simultaneous optimization of investment and operation, and simultaneous optimization of investment, operation and losses are deployed. Both objective functions keep the linear structure of the model and must be selected exclusively.

Neglecting total electrical power losses The objective function in this case consists of a simultaneous valuation of the total initial investment plus reliability. The investment is intuitively computed as the sum of cables costs installed in each edge $[ij]$; on the other hand, reliability is quantified through the estimation of the economic losses due to cables failures, as the result of undispatched current (i.e. energy) from each WT. In this way,

the objective function is formalized as:

$$\min \overbrace{\sum_{[ij]\in\boldsymbol{E}} \sum_{t\in\boldsymbol{T}} c_t \cdot d_{ij} \cdot x_{ij,t}}^{\text{Investment}} + \overbrace{c_{\mathrm{e}} \cdot \sum_{i\in\boldsymbol{N}_{\mathrm{w}}} \sum_{\omega\in\boldsymbol{\Omega}} \sum_{k\in\boldsymbol{K}} \tau^{\omega} \cdot \psi^{k} \cdot \delta_i^{\omega,k}}^{\text{Operation/Reliability}} \tag{6.1}$$

Here c_{e} is the cost of energy in €/Ah (equivalent to €/MWh). The sum of system states probabilities must be equal to one, $\sum_{k\in\boldsymbol{K}} \psi^k = 1$, given the mutually exclusive nature of the considered events (at most one cable is subject to failure, N-1 criterion). A system state k represents the failure of a single cable in an active edge $e \in \boldsymbol{E}$, therefore the system probability for the state ψ^k is considered equal to this failure probability. This implies that the availability probability of the other installed cables is considered to be equal to one in this scenario [64], representing a conservative approach as the value of the parameter ψ^k is slightly overestimated (the system probability is the multiplication of each installed cable state probability).

Considering total electrical power losses Total electrical power losses are non-linear in function of the current, cable type, and total length. The designer must try to find a proper balance between modelling fidelity and optimization program complexity. A pre-processing strategy is proposed in order to incorporate this factor into the objective function.

$$f_t = \left\lfloor \frac{\sqrt{3} \cdot V_n \cdot u_t}{P_n \cdot 1000} \right\rfloor \quad \forall t \in \boldsymbol{T} \tag{6.2}$$

The set of cable capacities in terms of number of supportable WTs is defined in Eq. (6.2). Let the new cable type set be:

$$\boldsymbol{T'} = \left\{ \underbrace{1, 2, \cdots, f_1}_{t_1}, \underbrace{f_1 + 1, \cdots, f_2}_{t_2}, f_2 + 1, \cdots, \underbrace{f_{|\boldsymbol{T}|-1} + 1, \cdots, f_{|\boldsymbol{T}|}}_{t_{|\boldsymbol{T}|}} \right\} \tag{6.3}$$

This implies that $\boldsymbol{T'}$ is the discretized form of the maximum capacity $U = \max \boldsymbol{U}$. Note that this is translated into the creation of additional variables $x_{ij,t'} : t' \in \boldsymbol{T'}$. Likewise, if the *floor function* in Eq. (6.2) is replaced by a *decimal round down function*, and $\boldsymbol{T'}$ is also discretized using the same decimal steps, then the number of variables will increase accordingly, to the benefit of gaining in accuracy for the cable capacities.

In $\boldsymbol{T'}$ is contained the non-dominated cable sub-types from $\boldsymbol{T}$; this means that each cable sub-type $t' \in \boldsymbol{T'}$ is related to a cable type $t \in \boldsymbol{T}$, inheriting physical properties such as cost per meter (c_t), electrical resistance per meter (R_t), and electrical reactance per meter (X_t); as shown in Eq. (6.3).

Acknowledging that the investment cost of a cable t exceeds the electrical power losses costs, then the selected cable sub-type to connect n WTs will always be the cheapest (smallest) cable with sufficient capacity, rather than a bigger one with lower electrical

power losses as the electrical resistance decreases with size. As a consequence of the aforementioned, let a new cable capacities set be:

$$\boldsymbol{U'} = \left\{1, 2, \cdots, f_1, f_1+1, \cdots, f_2, f_2+1, \cdots, f_{|\boldsymbol{T}|-1}+1, \cdots, f_{|\boldsymbol{T}|}\right\} \cdot \frac{P_n \cdot 1000}{\sqrt{3} \cdot V_n} \tag{6.4}$$

Let the functions $f(t')$, $g(t')$, and $h(t')$ calculate cost, electrical resistance, and electrical reactance per meter for cable sub-type t', respectively, which are inherited from a cable type t. Whereby, the objective function for simultaneous optimization of investment, electrical losses, and reliability is:

The factor $(3 \cdot 1.5)$ in Eq. (6.5) accounts the joule, screen and armouring losses for the three-phase system. The whole term for total electrical power losses ($h(t')$) is calculated for each $t' \in \boldsymbol{T'}$, before launching the MILP model into the external solver. Therefore, the objective function is a linear weighting of the desired targets: investment, electrical losses, and reliability.

As discussed previously, one of the tasks of the designer is to balance out modelling fidelity and optimization program complexity. The objective function in Eq. (6.5) is a linear function, thus the following simplifications are assumed: (i) integer discretization in Eq. (6.3) which restricts the capacity of cables, and may cause overestimation of electrical losses. This can be diminished by decimal round down, and by increasing discretization steps in Eq. (6.4) at the expense of incrementing the number of variables correspondingly. (ii) Neglection of system states (cables failures) apart of the base state (no failures); however, this is the state with highest probability. (iii) Power flow estimation in a conservative fashion, i.e., overestimating the incoming power flow by neglecting the total power losses downstream. All those simplifications may impact the final layout, however their conservative nature means rather over-designing than impacting the robustness.

$$\overbrace{\min \sum_{[ij]\in\boldsymbol{E}} \sum_{t'\in\boldsymbol{T'}} \left(f(t') + \underbrace{3 \cdot 1.5 \cdot g(t') \cdot \left(\frac{c_{\mathrm{e}}}{\sqrt{3} \cdot V_n \cdot 1000}\right) \cdot \sum_{\omega\in\boldsymbol{\Omega}} \left(u'_{t'} \cdot \zeta^{\omega}\right)^2 \cdot \tau^{\omega}}_{=h(t')\text{. Pre-processing for total electrical power losses}} \right) \cdot d_{ij} \cdot x_{ij,t} +}^{\text{Investment plus total electrical power losses}} \tag{6.5}$$

$$\overbrace{c_{\mathrm{e}} \cdot \sum_{i\in\boldsymbol{N}_{\mathrm{w}}} \sum_{\omega\in\boldsymbol{\Omega}} \sum_{k\in\boldsymbol{K}} \tau^{\omega} \cdot \psi^{k} \cdot \delta_i^{\omega,k}}^{\text{Operation/Reliability}}$$

Constraints

The first stage constraints are first presented. These constraints are only defined by the first stage variables.

In case edge $[ij]$ is active in the solution, then one and only one cable type $t \in \boldsymbol{T}$ or $t' \in \boldsymbol{T'}$ must be chosen as in

$$\sum_{t \in \boldsymbol{T}} x_{ij,t} = y_{ij} \quad \forall [ij] \in \boldsymbol{E} \vee \sum_{t' \in \boldsymbol{T'}} x_{ij,t'} = y_{ij} \quad \forall [ij] \in \boldsymbol{E} \tag{6.6}$$

Note that in case total electrical power losses are considered, then the cable types set is $\boldsymbol{T'}$, otherwise $\boldsymbol{T}$; same logic for $\boldsymbol{U}/\boldsymbol{U'}$, t/t', and $u_t/u'_{t'}$. This applies for the forthcoming mathematical expressions.

A closed-loop (sunflower petals) collection system topology is forced through

$$\sum_{\substack{j \in \boldsymbol{N} \\ j \neq i}} y_{ij} = 2 \quad \forall l \in \boldsymbol{N}_{\mathrm{w}} : l = i \vee l = j \tag{6.7}$$

Limiting the number of feeders (upper limit of ϕ feeders) connected to the OSS is carried out by means of

$$\sum_{i \in \boldsymbol{N}_{\mathrm{w}}} y_{ij} \leq \phi \quad j = 1 \tag{6.8}$$

The set $\boldsymbol{\chi}$ stores pairs of edges $\{[ij], [uv]\}$, which are crossing each other. Excluding crossing edges in the solution is ensured by the simultaneous application of the next linear inequalities along with (6.6)

$$y_{ij} + y_{uv} \leq 1 \quad \forall \{[ij], [uv]\} \in \boldsymbol{\chi} \tag{6.9}$$

The second stage constraints are now deployed. These constraints are only defined by the second stage variables. They are defined by the flow conservation, which also avoids disconnected solutions, as per

$$\sum_{\substack{i \in \boldsymbol{N} \\ j \neq i}} \sum_{\omega \in \boldsymbol{\Omega}} \sum_{k \in \boldsymbol{K}} I_{ji}^{\omega,k} - I_{ij}^{\omega,k} + \delta_j^{\omega,k} = I_j^{\omega} \quad \forall j \in \boldsymbol{N}_{\mathrm{w}} \quad \forall \omega \in \boldsymbol{\Omega} \quad \forall k \in \boldsymbol{K} \tag{6.10}$$

The set of tender constraints, useful to link first and second stage constraints, are lastly presented.

A DC power flow model is applied in order to calculate the power flow distribution along the resultant electrical network. This model assumes no active power losses, nominal voltage at each bar, and no reactive power flow [47]. The DC power flow is forced with the following equations

$$I_{ij}^{\omega,k} - \frac{1000 \cdot V_n \cdot (\theta_i^{\omega,k} - \theta_j^{\omega,k})}{\sqrt{3} \cdot X_t \cdot d_{ij}} - M \cdot (1 - x_{ij,t}) - M \cdot r_{ij}^k \leq 0 \tag{6.11}$$
$$\forall [ij] \in \boldsymbol{E} \quad t \in \boldsymbol{T} \quad \forall \omega \in \boldsymbol{\Omega} \quad \forall k \in \boldsymbol{K}$$

$$-I_{ij}^{\omega,k} + \frac{1000 \cdot V_n \cdot (\theta_i^{\omega,k} - \theta_j^{\omega,k})}{\sqrt{3} \cdot X_t \cdot d_{ij}} - M \cdot (1 - x_{ij,t}) - M \cdot r_{ij}^k \leq 0 \tag{6.12}$$
$$\forall [ij] \in \boldsymbol{E} \quad t \in \boldsymbol{T} \quad \forall \omega \in \boldsymbol{\Omega} \quad \forall k \in \boldsymbol{K}$$

Where r_{ij}^k is a parameter equal to one if edge $[ij]$ is failed, or zero if otherwise, and M is a big enough number to guarantee feasibility for those inactive or failed components.

The cable capacities are not exceeded by including the next bilateral constraints.

$$\sum_{t \in \boldsymbol{T}} u_t \cdot x_{ij,t} \cdot (1 - r_{ij}^k) \geq I_{ij}^{\omega,k} \quad \forall [ij] \in \boldsymbol{E} \quad \forall \omega \in \boldsymbol{\Omega} \quad \forall k \in \boldsymbol{K} \tag{6.13}$$

$$\sum_{t \in \boldsymbol{T}} -u_t \cdot x_{ij,t} \cdot (1 - r_{ij}^k) \leq I_{ij}^{\omega,k} \quad \forall [ij] \in \boldsymbol{E} \quad \forall \omega \in \boldsymbol{\Omega} \quad \forall k \in \boldsymbol{K} \tag{6.14}$$

The current $I_{ij}^{\omega,k}$ may circulate either from i to j or viceversa. In case total electrical power losses are considered, for all scenarios, except the ones linked to k_{o}, the capacity $u'_{t'}$ is inherited from the cable type t. This is to avoid unnecessary energy curtailment. For the base system state, k_{o}, capacity $u'_{t'}$ must be taken from Eq. (6.4).

Finally, constraints in Eq. (6.15) to Eq. (6.19) define the nature of the formulation by the variables definition, a MILP program.

$$x_{ij,t} \in \{0, 1\} \quad \forall t \in \boldsymbol{T} \quad \forall [ij] \in \boldsymbol{E} \tag{6.15}$$

$$y_{ij} \in \{0, 1\} \quad \forall [ij] \in \boldsymbol{E} \tag{6.16}$$

$$-0.1 \leq \theta_i^{\omega,k} \leq 0.1 \quad \forall i \in \boldsymbol{N} \quad \forall \omega \in \boldsymbol{\Omega} \quad \forall k \in \boldsymbol{K} \tag{6.17}$$

$$-U \leq I_{ij}^{\omega,k} \leq U \quad \forall [ij] \in \boldsymbol{E} \quad \forall \omega \in \boldsymbol{\Omega} \quad \forall k \in \boldsymbol{K} \tag{6.18}$$

$$0 \leq \delta_i^{\omega,k} \leq I_i^{\omega,k} \quad \forall i \in \boldsymbol{N}_{\mathrm{w}} \quad \forall \omega \in \boldsymbol{\Omega} \quad \forall k \in \boldsymbol{K} \tag{6.19}$$

Algorithmic framework for the stochastic optimization model: Determining the representative system states

Since the two-stage variables scale-up exponentially as a function of the scenario tree size, the representative systems states must be limited [C5]. The basic version of the stochastic optimization program presented in Section 6.2.2 encompasses the full set $\boldsymbol{E}$; each element $[ij]$ gives place to a system state k to form the system states set $\boldsymbol{K}$.

Nevertheless, the actual selected edges in a solution (i.e. a feasible point satisfying the optimality criteria) is only a subset $\boldsymbol{E'} \subset \boldsymbol{E}$; let the complement set $\boldsymbol{E''}$ contain the unused elements from $\boldsymbol{E}$, and let define the subset $\boldsymbol{E'''} \subset \boldsymbol{E''}$. Hereafter, it is proved that any representative system states set containing at least the scenarios linked to $\boldsymbol{E'}$ ($\boldsymbol{K}_{\boldsymbol{E'}} = \Phi(\boldsymbol{E'})$, using the transformation function Φ which maps from edges set to system states set), is necessary and sufficient to obtain the optimum in $P^{\boldsymbol{\Omega},\boldsymbol{K}}$.

Let the necessary and sufficient set $\boldsymbol{K'}$ encompass:

$$\boldsymbol{K'} = k_{\mathrm{o}} \cup \boldsymbol{K}_{\boldsymbol{E'}} \cup \boldsymbol{K}_{\boldsymbol{E'''}} \tag{6.20}$$

Where $\boldsymbol{K}_{\boldsymbol{E}'''}$ is the system states linked to the subset of unused edges $\boldsymbol{E}'''$.

Axiom 1 *The second stage variables linked to unused elements are equal to the base system state*

$$\forall i \in \boldsymbol{N}_w \quad \forall k \in \boldsymbol{K}_{\boldsymbol{E}'''} \quad \forall \omega \in \boldsymbol{\Omega}, \qquad \delta_i^{\omega,k} = \delta^{\omega,k_o}$$

An intuitive proposition is reflected in Axiom 1: *The curtailed currents in the system state of unused edges are the same than in the base system state.* This basically means that the failures of unused elements will not deteriorate the operation of the system.

From Eq. (6.1) it follows:

$$\sum_{[ij]\in\boldsymbol{E}} \sum_{t\in\boldsymbol{T}} c_t \cdot d_{ij} \cdot x_{ij,t} + c_{\mathrm{e}} \cdot \sum_{i\in\boldsymbol{N}_{\mathrm{w}}} \sum_{\omega\in\boldsymbol{\Omega}} \sum_{k\in\boldsymbol{K}'\setminus\{\boldsymbol{k}_{\mathrm{o}}\}} \tau^{\omega} \cdot \psi^{k} \cdot \delta_i^{\omega,k} + \tag{6.21}$$
$$c_{\mathrm{e}} \cdot \sum_{i\in\boldsymbol{N}_{\mathrm{w}}} \sum_{\omega\in\boldsymbol{\Omega}} \tau^{\omega} \cdot \left(1 - \sum_{k\in\boldsymbol{K}'\setminus\{\boldsymbol{k}_{\mathrm{o}}\}} \psi^{k}\right) \cdot \delta_i^{\omega,k_{\mathrm{o}}}$$

Eq. (6.21) with Eq. (6.20) becomes:

$$\sum_{[ij]\in\boldsymbol{E}} \sum_{t\in\boldsymbol{T}} c_t \cdot d_{ij} \cdot x_{ij,t} + c_{\mathrm{e}} \cdot \sum_{i\in\boldsymbol{N}_{\mathrm{w}}} \sum_{\omega\in\boldsymbol{\Omega}} \sum_{k\in\boldsymbol{K}_{\boldsymbol{E}'}} \tau^{\omega} \cdot \psi^{k} \cdot \delta_i^{\omega,k} + \tag{6.22}$$
$$c_{\mathrm{e}} \cdot \sum_{i\in\boldsymbol{N}_{\mathrm{w}}} \sum_{\omega\in\boldsymbol{\Omega}} \sum_{k\in\boldsymbol{K}_{\boldsymbol{E}'''}} \tau^{\omega} \cdot \psi^{k} \cdot \delta_i^{\omega,k} + c_{\mathrm{e}} \cdot \sum_{i\in\boldsymbol{N}_{\mathrm{w}}} \sum_{\omega\in\boldsymbol{\Omega}} \tau^{\omega} \cdot \left(1 - \sum_{k\in\boldsymbol{K}_{\boldsymbol{E}'}} \psi^{k}\right) \cdot \delta_i^{\omega,k_{\mathrm{o}}} -$$
$$c_p \cdot \sum_{i\in\boldsymbol{N}_{\mathrm{w}}} \sum_{\omega\in\boldsymbol{\Omega}} \sum_{k\in\boldsymbol{K}_{\boldsymbol{E}'''}} \tau^{\omega} \psi^{k} \cdot \delta_i^{\omega,k_{\mathrm{o}}}$$

Eq. (6.22) with Axiom 1 becomes:

$$\sum_{[ij]\in\boldsymbol{E}} \sum_{t\in\boldsymbol{T}} c_t \cdot d_{ij} \cdot x_{ij,t} + c_{\mathrm{e}} \cdot \sum_{i\in\boldsymbol{N}_{\mathrm{w}}} \sum_{\omega\in\boldsymbol{\Omega}} \sum_{k\in\boldsymbol{K}_{\boldsymbol{E}'}} \tau^{\omega} \cdot \psi^{k} \cdot \delta_i^{\omega,k} + \tag{6.23}$$
$$\cancel{c_{\mathrm{e}} \cdot \sum_{i\in\boldsymbol{N}_{\mathrm{w}}} \sum_{\omega\in\boldsymbol{\Omega}} \sum_{k\in\boldsymbol{K}_{\boldsymbol{E}'''}} \tau^{\omega} \cdot \psi^{k} \cdot \delta_i^{\omega,k_{\mathrm{o}}}} + c_{\mathrm{e}} \cdot \sum_{i\in\boldsymbol{N}_{\mathrm{w}}} \sum_{\omega\in\boldsymbol{\Omega}} \tau^{\omega} \cdot \left(1 - \sum_{k\in\boldsymbol{K}_{\boldsymbol{E}'}} \psi^{k}\right) \cdot \delta_i^{\omega,k_{\mathrm{o}}} -$$
$$\cancel{c_p \cdot \sum_{i\in\boldsymbol{N}_{\mathrm{w}}} \sum_{\omega\in\boldsymbol{\Omega}} \sum_{k\in\boldsymbol{K}_{\boldsymbol{E}'''}} \tau^{\omega} \psi^{k} \cdot \delta_i^{\omega,k_{\mathrm{o}}}}$$

Equation (6.23) is analogous to Eq. (6.21) but with $\boldsymbol{K}' \setminus \{\boldsymbol{k}_{\mathrm{o}}\} = \boldsymbol{K}_{\boldsymbol{E}'}$. This proves that *any set $\boldsymbol{K}'$ containing at least the system states associated to all selected edges is sufficient and necessary to find the global optimum of the full problem $P^{\boldsymbol{\Omega},\boldsymbol{K}}$.* Conversely, any instantiation for which $\boldsymbol{K}' \subset \boldsymbol{K}_{\boldsymbol{E}'}$ would lead to an underestimation of operational costs, ultimately causing falling into suboptimal. The proof also applies when including total electrical power losses (6.5).

This contingency structure opens the door for a PCI strategy, aiming to find a proper set $\boldsymbol{K'}$. An improved PCI algorithm based on [35] is proposed in the Algorithm 2.

In the first line of Algorithm 2 a deterministic instance of the full problem is addressed. This means considering uniquely the scenario $\{\omega_{\mathrm{n}}, k_{\mathrm{o}}\}$. For this problem a valid assumption is to consider zero curtailed power. After this, the active edges of interest corresponding to the first stage optimization variables are stored as $\boldsymbol{E'}$, along with the obtained solution variables in $\boldsymbol{X}_{\mathrm{ws}}$ (where $\boldsymbol{X}_{\mathrm{d}}$ and $\boldsymbol{Y}_{\mathrm{d}}$ contains the solution sets corresponding to $x_{ij,t}$, and y_{ij} for the deterministic case, respectively). As no previous iteration has been conducted, cumulative solution variables are unavailable ($\boldsymbol{E}'_{\mathrm{o}}$). Since the second stage variables express contingency scenarios of the components delimited by the first stage variables, the tree Υ uniquely considers the failure states associated to those components. For the case presented in Algorithm 2, solely those feeders which satisfy the reliability level r_{c}, are subject to fail.

Parameter r_{c} defines the degree of connection towards the OSS, so for example, $r_{\mathrm{c}} = 1$ brings along the main feeders (rooted at $i = 1$), and $r_{\mathrm{c}} = 2$ includes the last ones together with the feeders connected to the main ones, and so on for $r_{\mathrm{c}} > 2$, as shown in Figure 6.2. By means of this parameter, the model can be further relaxed for large instances. A reliability level equal to one according to Figure 6.2 would still represent at a large extent the consequences of all cables failures, as those main feeders are the one carrying the vast amount of energy compared to downstream connections. Thus, an important computational burden is avoided, while having a good representation of the system. This is backed up by the fact that cables under higher levels of electro-thermal stress present shorter lifetime [J2].

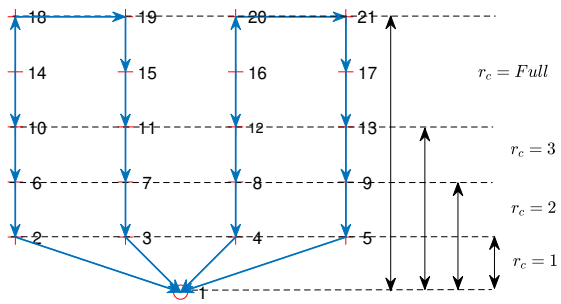

Figure 6.2: Reliabilty level definition [J5]

The PCI routine for stochastic analysis is started at line 4 of Algorithm 2. The opening step is to intersect the current active edges set $\boldsymbol{E'}$, and the cumulative set $\boldsymbol{E}'_{\mathrm{o}}$. If the intersection set is equal to the current active edges $\boldsymbol{E'}$, then the process is terminated, otherwise more iterations are attempted. For the former case, the algorithm is stopped, with solution $[\boldsymbol{X}, \boldsymbol{Y}]$; for the latter case, the iterative process is continued to the subsequent iteration κ. Trivially, for $\kappa = 1$, $\boldsymbol{A} = \emptyset$. Therefore, in line 9 the union set is obtained to update $\boldsymbol{E}'_{\mathrm{o}}$. A new instance of the main problem is solved in line 10, using the initial point $\boldsymbol{X}_{\mathrm{ws}}$ (warm-start point), while considering the full wind power generation

scenarios indicated by the user Ω, and the system states related to edges cumulatively installed in all iterations, ($\boldsymbol{K'} = \Phi(\boldsymbol{E'_o})$).

When the Algorithm 2 converges, the scenario criterion is met: obtention of the proper set $\boldsymbol{K'}$; meaning that all representative systems states have been already considered.

---

1. $[\boldsymbol{X}_d, \boldsymbol{Y}_d] \leftarrow \arg P^{\boldsymbol{\Omega},\boldsymbol{K'}} : \Omega = \omega_n, \boldsymbol{K'} = k_o$ *with gap* ϵ_d
2. $\boldsymbol{E'} \leftarrow \boldsymbol{Y}_d = \{[ij]\} : y_{ij} = 1 \quad \forall [ij] \in \boldsymbol{E} : [ij]$ *satisfies reliability level* r_c
3. $\boldsymbol{E'_o} \leftarrow \emptyset, \boldsymbol{X}_{ws} \leftarrow \boldsymbol{X}_d \cup \boldsymbol{Y}_d$
4. **for** $(\kappa = 1 : 1 : \kappa_{max})$ **do**
5. $\quad \boldsymbol{A} \leftarrow \boldsymbol{E'} \cap \boldsymbol{E'_o}$
6. $\quad$ **if** $(\boldsymbol{E'} == \boldsymbol{A})$ **then**
7. $\quad\quad$ *Break*
8. $\quad$ **end if**
9. $\quad \boldsymbol{E'_o} \leftarrow \boldsymbol{E'} \cup \boldsymbol{E'_o}$
10. $\quad [\boldsymbol{X}, \boldsymbol{Y}] \leftarrow \arg P^{\boldsymbol{\Omega},\boldsymbol{K'}} : \Omega, \boldsymbol{K'} = \Phi(\boldsymbol{E'_o}) \cup k_o$ *with initial point* $\boldsymbol{X}_{ws}$ *and gap* ϵ_s. $\Upsilon = \{\Omega, \boldsymbol{K'}\}$
11. $\quad \boldsymbol{E'} \leftarrow \boldsymbol{Y} = \{[ij]\} : y_{ij} = 1 \quad \forall [ij] \in \boldsymbol{E} : [ij]$ *satisfies reliability level* r_c
12. $\quad \boldsymbol{X}_{ws} \leftarrow \boldsymbol{X} \cup \boldsymbol{Y}$
13. **end for**

Algorithm 2: PCI Algorithm [J5]

6.2.3 Optimization Framework

The full optimization framework is presented in Figure 6.3. The main inputs for the framework can be divided as:

- Project-specific data, such as WTs and OSS location, rated power, wind power generation scenarios, MTBF for cables (in years kilometres per failure), and MTTR for failed cables (in hours).
- Simulation settings, like cables' technical and economic parameters, macroeconomic information, including lifetime and price of energy, and required gap for the deterministic case (ϵ_d) and the stochastic phase (ϵ_s).
- Modelling choices, as reliability level (r_c), total electrical power losses incorporation (1 or 0), and DC power flow model (1 or 0).

A Markov Chain method is applied to calculate the probability for the unavailable state of a cable [76]:

$$\psi^k = \frac{MTTR}{MTTR + MTBT \cdot \frac{8760}{d_{ij}}} \tag{6.24}$$

Where d_{ij} (in kilometres) is the edge length where the component is installed, and k the associated system state.

Continuing with the flowchart of Figure 6.3, two different models are formulated to develop independently the stochastic closed-loop and the deterministic radial designs. As discussed previously, the closed-loop optimization program is based on a flow MILP model, in contrast to the hop-indexed optimization program dedicated for the non-looped layout, chosen such as to enable comparison of topologies for large-scale problems utilizing the state-of-the-art approaches.

The closed-loop stochastic model is formulated in function of the required inputs, especially $Losses$ and DC.

The objective function and constraints are properly adapted to whether losses must be incorporated or not, by means of parameter $Losses$. Similarly, two options for power flow are supported, transportation model ($DC == False$) and a DC power flow ($DC == True$).

A transportation model is fundamentally the simplest of the ways to calculate the distribution of power in an electrical network. It abides the kirchhoff's first law by keeping the current balance at each node. Contrarily, a DC power flow model includes in addition the Kirchhoff's second law, approximating the voltage magnitude to 1 p.u., and ignoring the reactive power flow [47]. The mathematical optimization program is notably relaxed by disregarding the DC power flow, which stress the model by creating additional variables. Finally, after the optimization program is formulated, this is sent to the Algorithm 2, obtaining the layout with linked investment and operation costs.

On the right branch of the flowchart, the radial model is formulated and solved accordingly to [J3]. The obtained solution sets ($\boldsymbol{X_{rd}}$,$\boldsymbol{Y_{rd}}$, conserving the adopted nomenclature as in Section 6.2.2), are used to fix values of the flow model binary variables; simultaneously, Eq. (6.7) are modified as inequalities to allow up to three connections for each WT. With this, a tree topology is converted into a feasible point of the model. Lastly, the flow model is reassembled after all these changes, and sent to the Algorithm 2. In other words, a recourse problem is formulated $Q([\boldsymbol{X_{rd}}, \boldsymbol{Y_{rd}}])$, defined as minimization of the expected costs (operation costs) given the scenario tree (Υ) obtained from the wind power generation scenarios Ω, and the system states linked to $\boldsymbol{Y_{rd}}$. This recourse problem is inexpensive computationally given that the binary values are provided in advance. The recourse problem related to the radial layout is always solved to optimality.

In the last step of the flowchart, the two solutions (closed-loop and radial) are compared in terms of total expenses, investment and operation costs. This flow of tasks guarantee a fair comparison between them, since firstly, the same stochastic reference frame is maintained after the reformulation blocks depicted in Figure 6.3, and, secondly, the PCI algorithm is utilized equally.

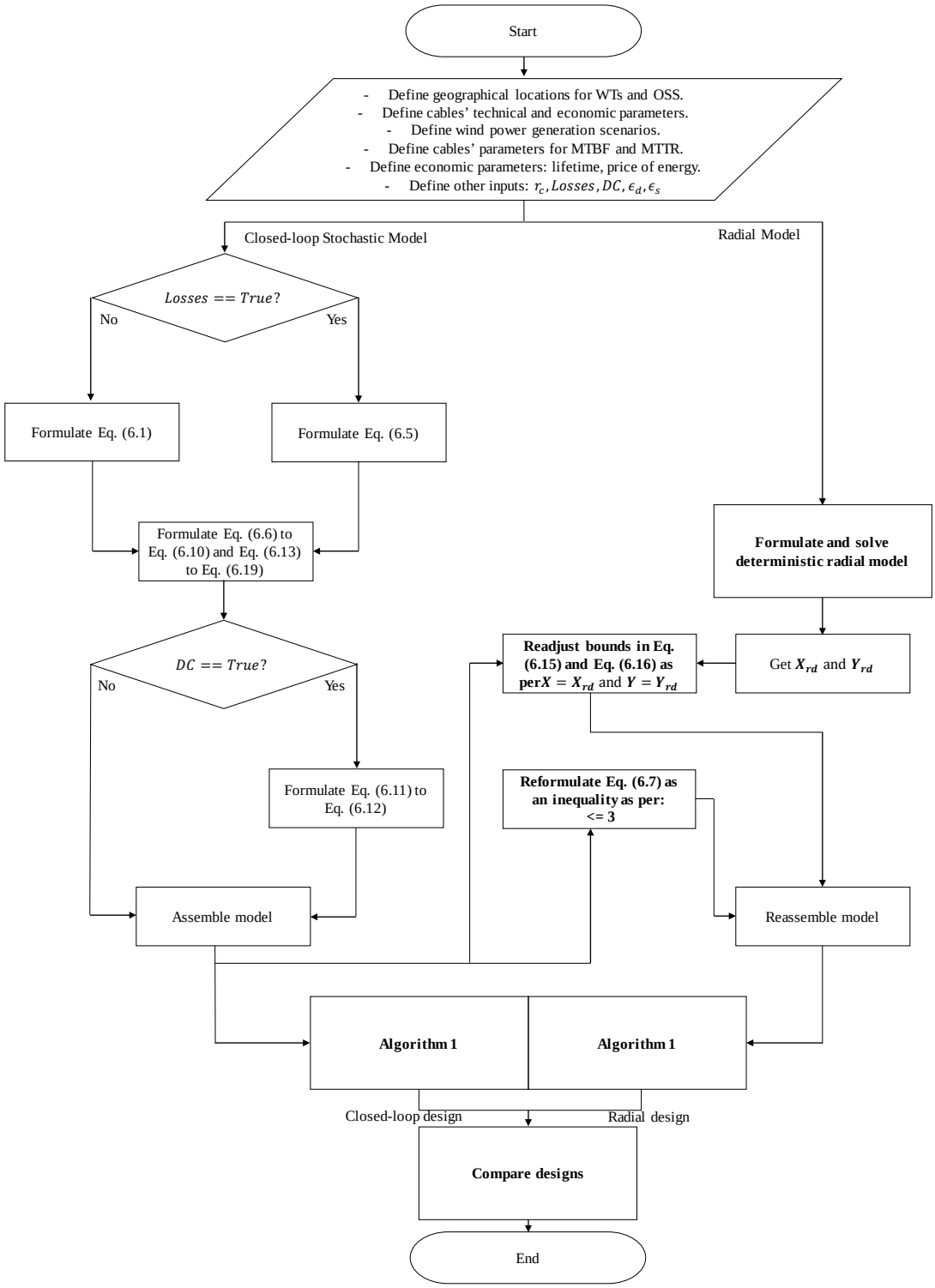

Figure 6.3: Optimization framework for comparing collection system topology [J5]

6.3 Results

The computational experiments presented in this section have been carried out on an Intel Core i7-6600U CPU running at 2.50 GHz and with 16 GB of RAM. The chosen solver is IBM ILOG CPLEX Optimization Studio V12.7.1 [70]. The experiments consist of three real-world cases aiming to test the proposed method for different problem sizes (small, large and very large), and WTs topological distribution (grid-based and coordinate-based).

For all the following studies a MTTR of 30 days (720 h) is considered [78]. The price of energy is assumed to be fixed along the project lifetime with a value of 50 €/MWh (2.86 €/Ah), which is the average price as per [79].

The wind power generation scenarios are also equally fixed as per Table 6.1. Scenario 1 accounts for the nominal power (ω_{n}). The time duration of all the scenarios correspond to a project lifetime of 30 years. The magnitude and duration values lead to a capacity factor of 0.49, which is a reasonable value for modern offshore wind farms.

In general, the simulation results are dependant on several parameters, like the utilization of a discrete Markov model to calculate the failure probabilities given the failure statistical parameters MTBF and MTTR, and the considered price of energy, financial valuation method, project lifetime, cables set, cost functions, among others.

Table 6.1: Wind power generation scenarios [J5]

Scenario	Magnitude [p.u.]	Duration [h]
1	1	65,700
2	0.5	91,980
3	0.2	91,980
4	0	13,140

Other electrical information related to the power cables, such as electrical resistance per meter (R_t) and electrical reactance per meter (X_t), is available in [13].

6.3.1 Small OWF: Ormonde

As a first case study the Ormonde OWF is analyzed [80]. This OWF presents a closed-loop layout in the collection system. Specific inputs for this case study are shown in Table 6.2.

Table 6.2: Data inputs for Ormonde OWF [J5]

P_n	V_n	$\boldsymbol{U}$	$\boldsymbol{C}$	n_{w}	υ	σ	ϕ	ϵ_{d}	ϵ_{s}
5 MW	33 kV	$\{530, 655, 775\}$ A	$\{450, 510, 570\}$ k€/km	30	6	10	4	0.2%	0.2%

To better understand the influence of different modelling choices for the model included Algorithm 2, several simulations and parametric sensitivities are carried out. They target power flow model, reliability level, and total electrical power losses.

Trough these case studies, the complexity of different modules of the model is understood, along with the gains obtained by them.

Power flow model

For this study, only the left branch of Figure 6.3 is executed without considering losses. This means that results focus on closed-loop topology in this section. The objective is to compare a full version of the model (with $DC == True$), and a relaxed version ($DC == False$) employing a simple transportation power flow model. Besides this, the MTBF is varied from 10 to 178 years kilometres per failure, with the latter value being typical for OWFs medium voltage cables under operation today [81], aiming at quantifying the parametric impact of MTBF value. To reduce computational burden when evaluating low values of MTBF, a reliability level of $r_c = 1$ is considered. See Figure 6.2.

Results are presented in Table 6.3. For each MTBF value, the difference of total costs between the DC power flow model and the transportation model is presented. Percentage values are calculated with respect to the power flow relaxation model. Furthermore, total expenses are split into investment and operations costs to analyze their behaviour in function of the MTBF value.

Table 6.3: Power flow models comparison for Ormonde OWF [J5]

MTBF	Total expenses Eq. (6.1)		Investment		Operation	
	Diff.[€]	Diff. [%]	Diff. [€]	Diff. [%]	Diff. [€]	Diff. [%]
10	0	0	0	0	0	0
20	8,000	0.08	32,200	0.37	-24,200	-1.79
30	16,090	0.17	32,200	0.37	-16,110	-1.79
40	23,920	0.25	64,200	0.74	-40,280	-5.52
50	31,970	0.34	64,200	0.74	-32,230	-5.27
178	55,140	0.62	64,200	0.74	-9,060	-5.27

Naturally, the total expenses for the relaxed solutions is lower than the full model (DC power flow), but what it is important to see is the rather limited impact of this relaxation in terms of the objective function value. In the worst case, the DC power flow model provides a solution only 0.62% more expensive than the transportation model. The latter result corresponds for the typical value of MTBF reported for OWFs (MTBF of 178). The cost difference among the power flow models can be explained by inspecting the investment and operation costs. The transportation model results in cheaper designs, but this precisely causes higher operation costs.

When considering a full reliability level, for a MTBF of 178, the solution obtained with a DC power flow model is only 0.25% more expensive than the one from a transportation model. While the difference on investment costs is more or less the same as in Table 6.3 (0.77%), it is observed an increase in the operation costs difference (-7.37%), which balances out the capital investment disparity among both models. The increment of undispatched energy allows for reducing the total expenses difference; this is also expected to happen for lower MTBF values.

The possibility to neglect DC power flow allows for reducing the complexity of the model while still generating dual solutions (by neglecting the DC flow) close to a primal (feasible point for the full model). In closed-loop and meshed topologies the current follows the path with shortest electrical length, i.e., smallest equivalent electrical reactance. Thus, DC power flow requires extra variables modelling voltage phases as in Eq. (6.11) and Eq. (6.12). The strong similarity between radial and closed-loop topologies is due to, in the latter, only a single cable per circuit (interconnected chain of WTs) alters the radiality of the former.

The main benefit behind this relaxation is towards the application of the model for large-scale problem instances, or even for small ones with low optimality gap values ($\epsilon_{\mathrm{d}}, \epsilon_{\mathrm{s}} \leq 0.2\%$). In this work, the comparison between closed-loop and radial designs lies in the relative economic difference, while not in the concrete solutions (construction designs). The dual solutions can be fixed a posteriori by changing a subset of the installed cables. The latter is out of the scope of this work.

Reliability level

The full Algorithm 2 is now implemented. Based on the previous results, the DC power flow model is discarded. In the same manner, total electrical power losses are deactivated and attention is concentrated to a simultaneous minimization of investment plus operation costs. Results for the lowest reliability level ($r_{\mathrm{c}} = 1$), and for full reliability, are displayed in Figure 6.4 and in Figure 6.5, respectively.

A reliability level value equal to $r_{\mathrm{c}} = 1$ is basically a relaxation of the full model. The latest being understood as an instantiation of Algorithm 2 with a large enough value of r_{c}, such as all installed cables of the OWF are included in the system states set, i.e., full reliability. See Figure 6.2 for a graphical description of this concept.

For the reliability relaxation, in Figure 6.4(a) the total cost comparison between the closed-loop and radial designs with increasing MTBF is illustrated. Meanwhile, the Figure 6.4(b) displays the investment and operation costs difference. From Figure 6.4(a), it can be observed that there is break-even point, for a MTBF of around 35, where the total cost of closed-loop and radial designs match.

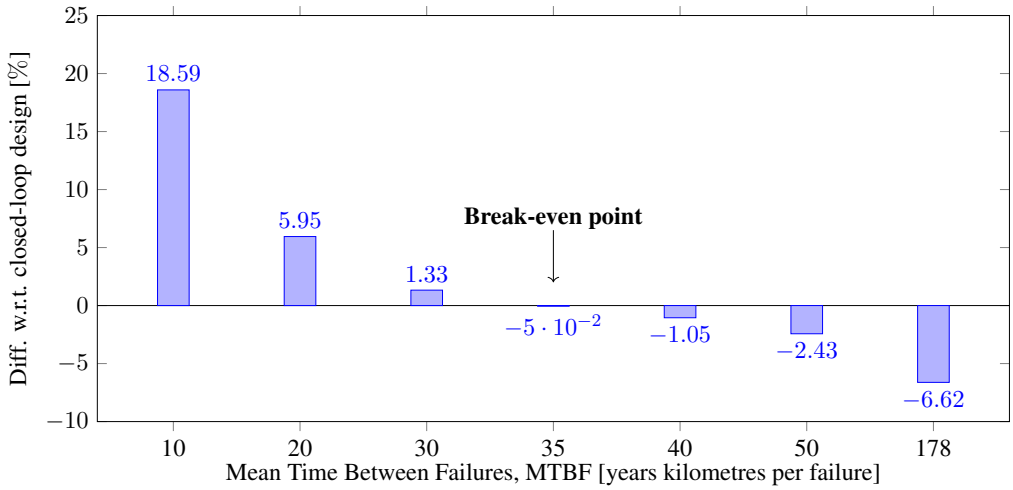

(a) Comparison of objective function (6.1) between closed-loop and radial designs. (Positive percentages mean savings from closed-loop design)

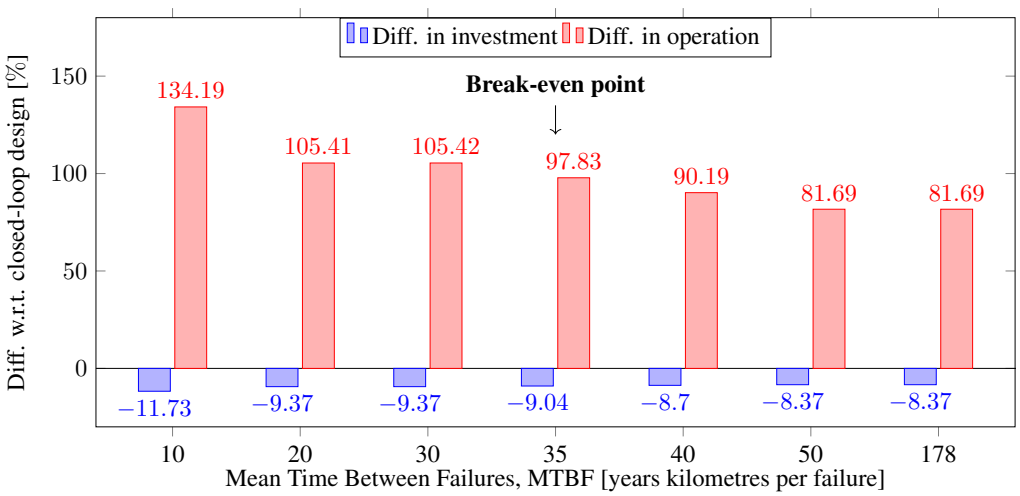

(b) Comparison of investment and operations costs between closed-loop and radial designs. (Positive percentages mean savings from closed-loop design)

Figure 6.4: Sensitivity analysis with reliability level $r_c = 1$ for Ormonde OWF [J5]

To the left of the break-even point in Figure 6.4(a), the closed-loop layout always results as the overall cheapest solution, because despite a higher investment cost- See Figure 6.4(b) (radial design is invariable to MTBF variations)-, it provides a redundant path for each WT, therefore the operation cost savings surpasses that increase (the installed cables for the main feeders are usually bigger as well). Additionally, in Figure 6.4(b) one can see that the non-increasing trend of the investment costs is developed in a discrete manner, as for some consecutive values of MTBF the closed-loop design investment is maintained. The associated percentage difference of operation costs for not modified designs is also kept, as the failures frequency is equally diminished.

On the other hand, for MTBF larger than 35, the radial layout is the best alternative. After a large enough MTBF (in this case at around 50 years kilometres per failure), the failures probabilities drop considerably, meaning that the operation costs become trivial, and hence the focus is merely on the investment costs reduction, which by its part has reached the minimum in the closed-loop alternative. The break-even point may be marginally affected by neglecting the DC power flow in the conservative side, as this value would move to the left. At MTBF of 178, the radial design is 6.62% cheaper than the closed-loop design as shown in Figure 6.4(a).

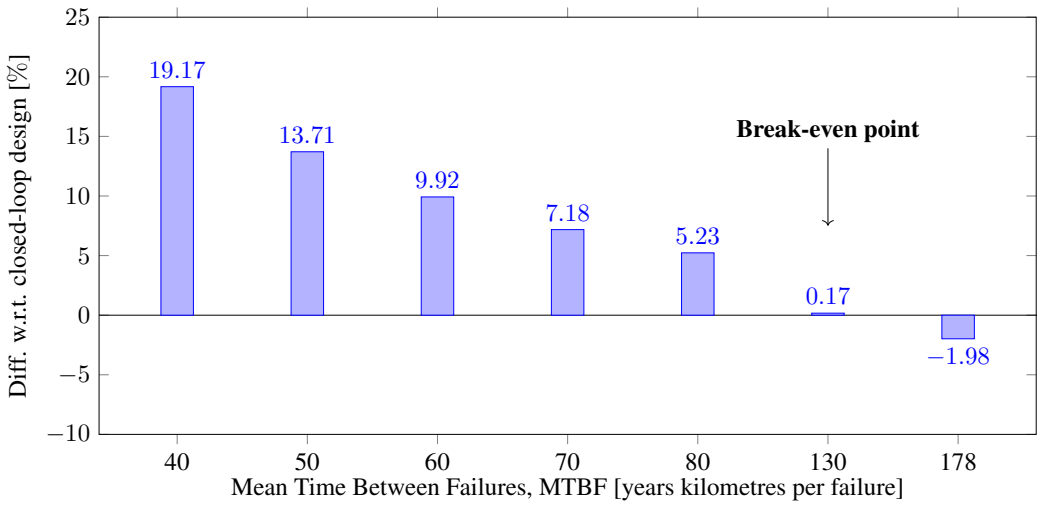

(a) Comparison of objective function (6.1) between closed-loop and radial designs. (Positive percentages mean savings from closed-loop design)

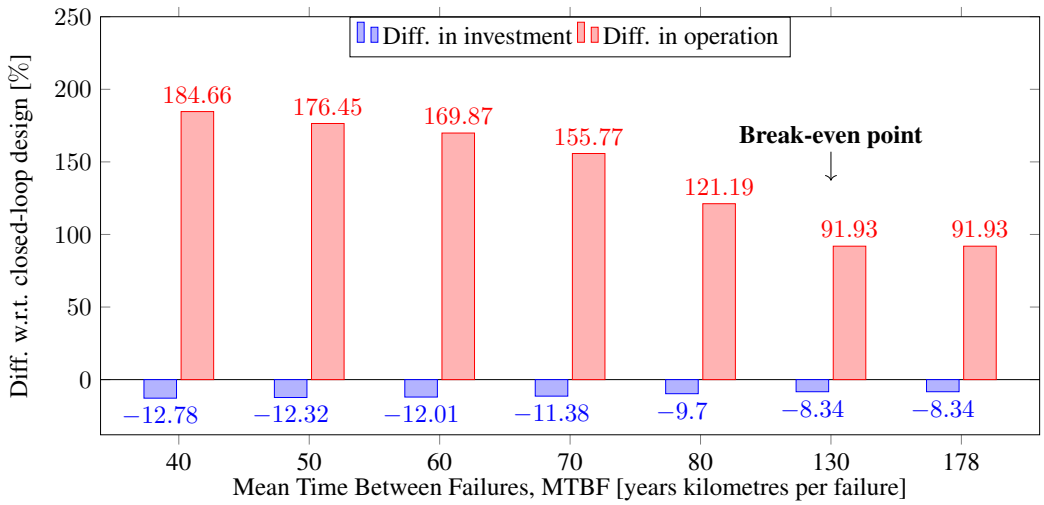

(b) Comparison of investment and operations costs between closed-loop and radial designs. (Positive percentages mean savings from closed-loop design)

Figure 6.5: Computing times for Ormonde OWF stochastic closed-loop design [J5]

A new set of experiments is conducted for full reliability of the Ormonde OWF. The main difference compared to $r_c = 1$ is reflected in Figure 6.5(a), where the break-even point is moved towards the right of the plot to a value roughly equal to 130 years kilometres per failure.

By allowing the whole set of installed cables to fail, the impact over the project economic performance is considerably augmented. In this case, for the worst reported value of MTBF (178 years kilometres per failure), the radial design is only 1.98% cheaper than the closed-loop layout, due to the increase of operation costs with almost the same required investment expense when compared to $r_c = 1$.

The impact of the reliability level on the computing time is presented in Figure 6.6. The difference is of an order of magnitude, moving from seconds for $r_c = 1$ to (tens of) minutes for full reliability. The exponential complexity of the stochastic closed-loop model in function of the parameter MTBF is also noticeable. For MTBF inferior to 40, the computational resources become insufficient to approach the problem for full reliability, as computing time and memory requirements escalate rapidly.

For large values of MTBF, the Algorithm 2 takes advantage of the deterministic solution to feed up the stochastic model with a good starting point. This, together with low failure probability (as MTBF increases), helps conspicuously to accelerate the convergence of the model for optimum gaps. The PCI algorithm takes away a very important share of computational burden by simplifying the full problem. The savings on computing time are more evident for greater values of r_c as the number of candidate edges become larger.

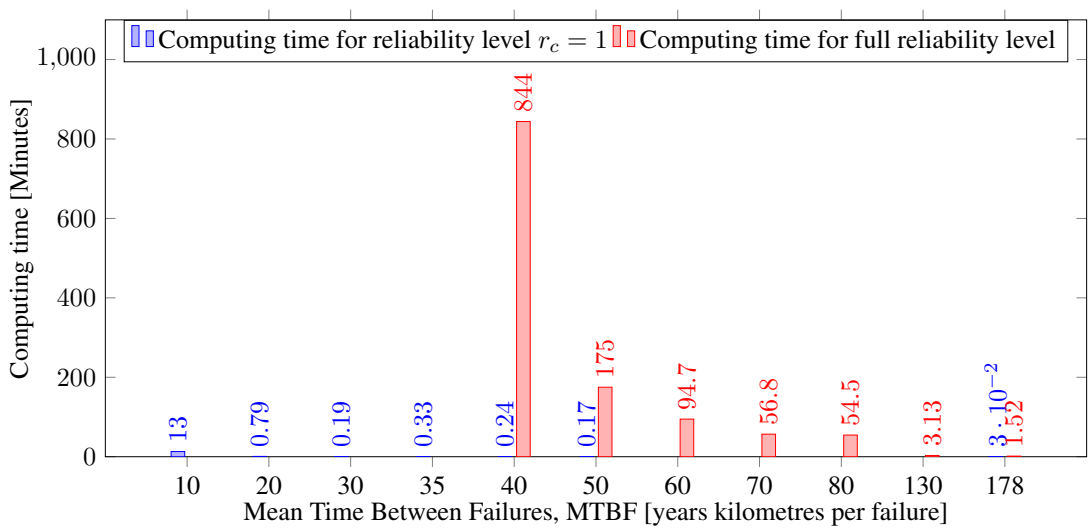

Figure 6.6: Reliabilty level definition [J5]

Total electrical power losses

The left branch of Figure 6.3 is implemented, in this case, activating the total electrical power losses ($Losses == True$) integrated into the objective function Eq. (6.5). A

MTBF of 178 years kilometres per failure is considered, and the transportation power flow mode is enabled ($DC == False$).

Results are displayed in Figure 6.7. Particularly, Figure 6.7(a) is associated to objective function Eq. (6.1) (investment plus reliability, IR), and Figure 6.7(b) to Eq. (6.5) (investment plus reliability plus losses, IRL). There are no significant differences between the two layouts.

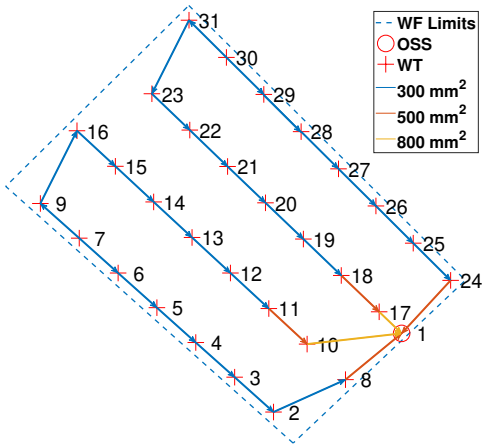

(a) IR objective

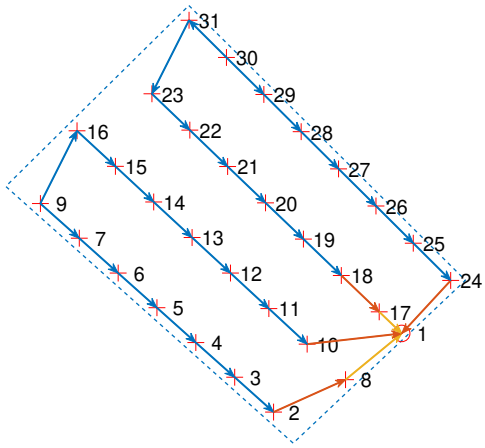

(b) IRL objective

Figure 6.7: Sensitivity analysis for objective function in Ormonde OWF. MTBF=178 [J5]

A visual inspection of the layouts shows that the only difference is the swap of cables connected from WT 1 to WT 11 with those from WT 1 to WT 2. This alteration in the design can be explained given the conservative approach for losses calculation, and simultaneously, the degree of flexibility linked to a transportation model. In Figure 6.7(b), which graph the base case, the current through WTs 9-16 and 30-31 is set to

zero in the solution. This means that the calculated losses are an approximation in the conservative side, compared to a layout with splittable current through a DC power flow.

The main takeaway is that the total expenses of the layout in Figure 6.7(a) (including total electrical power losses) is nearly the same as that from Figure 6.7(b). The required computing time, however, is 16 times higher when including losses compared to a sole optimization of investment and operation costs. The proposed formulation is still more efficient than a MIQP. The demonstration is out of the scope of this work, but computational experiments from the literature validate the efficiency of MILP compared to MIQP [64].

6.3.2 Large OWF: HR1

The second case study is HR1 OWF [82]. Inputs are shown in Table 6.4. The number of WTs for this case is equal to 80. HR1 OWF presents a regular or grid-based layout, since WTs units are uniformly arranged in rows and columns without empty areas inside of the farm; as shown previously in [J3], this type of layouts show a favorable condition in terms of computational complexity when designing the collection system, hence low values $\upsilon = 6$ and $\sigma = 10$ are most likely good enough to cover the global minimum. Larger values of these parameters may compromise the convergence of general purpose solvers. No losses and a transportation power flow mode are used.

Table 6.4: Data inputs for HR1 OWF [J5]

P_n	V_n	$\boldsymbol{U}$	$\boldsymbol{C}$	n_w	υ	σ	ϕ	ϵ_d	ϵ_s
2 MW	33 kV	$\{420, 530\}$ A	$\{410, 450\}$ k€/km	80	6	10	10	0.2%	0.2%/4%

Results for the lowest reliability level, i.e. $r_\mathrm{c} = 1$, are shown in Table 6.5. The optimality gap for both deterministic and stochastic phases of Algorithm 2 are equal $\epsilon_\mathrm{d} = \epsilon_\mathrm{s} = 0.2\%$. Further experiments were done, intending to evaluate lower values of MTBF at these gaps, but computing time increased steeply (note that for MTBF of 90, required time is almost 360 min).

Going back to Figure 6.4, the results of Table 6.5 indicate that the break-even point has been already crossed for MTBF of 90. This is because of the nearly equal percentage of difference in investment for MTBF of 90 in comparison to MTBF of 178. At this point, the radial layout is 0.80% cheaper than the closed-loop design. One can see that for MTBF of 178, the savings difference for HR1 (-2.01%) has decreased substantially when compared to Ormonde, Figure 6.4(a) (-6.62%), and being closer to Ormonde with full reliability, Figure 6.5(a) (-1.98%). Performance cutback of the radial layout is due to the boost of curtailed energy as there are more WTs connected to a single feeder.

Table 6.5: Results with reliability level $r_c = 1$ for HR1 OWF [J5]

MTBF	Diff. in total [%] expenses Eq. (6.1)	Diff. in investment [%]	Diff. in operation [%]	Computing time closed-loop [min]
90	-0.80	-3.34	91.14	359
178	-2.01	-3.31	90.90	43

For full reliability analysis, the value of ϵ_d is fixed to 0.2% while ϵ_s is loose up to 4%. This is necessary as symmetric tight gaps lead to failed convergence due to lack of memory. Providing the optimal solution of the deterministic phase of Algorithm 2 helps to shorten to stochastic phase, taking into account that the base case is the scenario with the largest probability. Results are shown in Table 6.6 where it can be seen that the closed-loop design is a more cost-effective option than the radial layout, even with a rather high optimality gap of up to 4%.

Two important aspects must be highlighted: (i) the transportation model allows for optimizing large OWFs at the expense of an slight underestimation of design costs, but even given this uncertainty, both topologies would be still very close in terms of financial performance. Slightly lower values of MTBF would mean the closed-loop gains more and more value. (ii) A gap of 4% means that the closed-loop layout could be possibly cheaper, increasing then its margin compared to the radial counterpart.

Table 6.6: Results with full reliability level for HR1 OWF [J5]

MTBF	Diff. in total [%] expenses Eq. (6.1)	Diff. in investment [%]	Diff. in operation [%]	Computing time closed-loop [min]
178	1.13	-3.43	83.01	2.47

6.3.3 Very large OWF: WDS

Last real-world case study is WDS OWF [83]. This OWF has an irregular distribution of its 108 WTs (3.6 MW individual power) due to abnormal soil conditions. Given this particular features, larger values of υ and σ are set, as indicated in Table 6.7, in order to cover the global minimum according to the hop-indexed model for radial layout design (right branch of Figure 6.3). The presented optimality gaps (ϵ_d and ϵ_s) represent the technical border considering the lowest reliability level, to obtain solutions within the computational limits. No losses and a transportation power flow mode are used.

Table 6.7: Data inputs for WDS OWF [J5]

P_n	V_n	$\boldsymbol{U}$	$\boldsymbol{C}$	n_w	υ	σ	ϕ	ϵ_d	ϵ_s
3.6 MW	33 kV	$\{875, 1050\}$ A	$\{630, 770\}$ k€/km	108	10	25	10	5%	6%

The numerical results are given in Table 6.8, while graphical results are portrayed in Figure 6.8.

Table 6.8: Results with reliability level $r_c = 1$ for WDS OWF [J5]

MTBF	Diff. in total [%] expenses Eq. (6.1)	Diff. in investment [%]	Diff. in operation [%]	Computing time closed-loop [min]
178	-0.67	-1.65	96.46	0.90

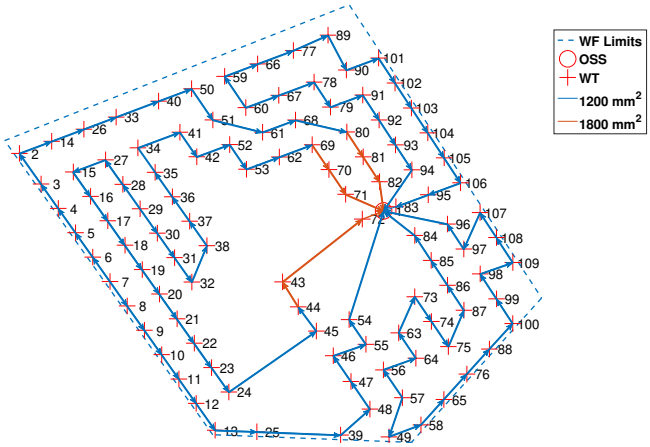

(a) Closed-loop design for WDS with MTBF=178

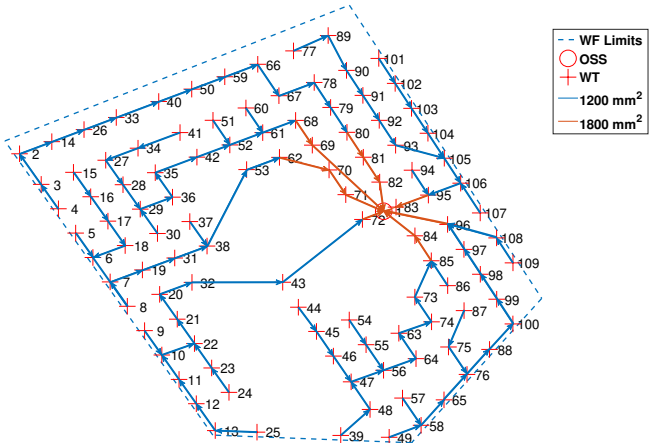

(b) Radial design for WDS

Figure 6.8: Collection system designs for WDS with objective function (6.1) [J5]

Similarly to HR1 (Table 6.5 and Table 6.6), with MTBF of 178, the results in Table 6.8 indicate that a closed-loop design for WDS would most likely pay off under full reliability, since for the lowest redundancy level the radial layout is only 0.67% cheaper. This is understandable based on the greater number of WTs and individual power, leading to more curtailed energy for the same failure. This comparison is upon the condition that

the relative difference between the solutions is maintained, if a zero optimality gap is achieved simultaneously.

The resulted closed-loop and radial layouts are given in Figure 6.8. As aforementioned, this wind farm presents empty areas in between the locations of the generation units, which seems to impact considerably the mathematical complexity of finding a solution for the collection system as studied in Section 4.3.2. This fact is also reflected in this case study, where for the same gap (5%), the flow-based model requires almost double time than the full binary (0.45 h). For Ormonde and HR1 the radial layouts were obtained almost instantaneously.

In addition, the hop-indexed model does not escalate nor with the size of cable set, neither with inclusion of total electrical power losses. However, the flow formulation provides important flexibility to the model such as energy curtailment (used in this case) or other aspects like, e.g. different WTs types (in terms of power rating).

6.4 Summary

A method, based on [C5] and [J4] has been proposed in this chapter. The proposed method provides a global optimization model to solve the OWFs collection system, supporting a simultaneous minimization of investment, operational, and total electrical power costs, including contingencies due to cables failures.

In spite of the currently rather low failure rates of collector cables failures, early stage in offshore projects maturity and the consequent scarcity of available data may mean that future very large OWF projects may face larger level of contingencies.

This method proposes a framework to compare, in economic terms, closed-loop and radial layouts for modern OWFs. Several strategies are incorporated in the algorithmic scheme, in order to be able to study very large real-world problems, such as the use of a transportation power flow model instead of DC power flow or different reliability levels.

Stochastic optimization with scenario numeration brings along a comprehensive consideration of the three main criteria for designing electrical networks; investment, electrical losses, and reliability. However, it also implies a lack a tractability which hardens the applicability for a larger set of problem types. Overall, the impact of medium voltage collector system cables failures is quantified in this chapter, showing the importance of developing methods which enable reliability analysis in the context of computational optimization. A PCI has been proposed in this direction.

The proposed method has been applied to three different real-world OWFs, from small to very large-scale. Results indicate that layouts with single redundancy may bring economic benefits when compared to non-redundant ones, in function of the instance size. For a small OWF the radial topology results as the best option, in contrast to large projects, where the closed-loop is seemingly a better techno-economic solution, when using failures rates available in literature.

CHAPTER 7

Conclusions and Future Research

7.1 Conclusions

Several optimization methods for the electrical network design of OWFs have been proposed in this PhD thesis. The methods can be classified in three topics: (i) Optimum sizing of export power cables, (ii) Deterministic computational optimization of the cable layout of collection systems and the transmission systems, and (iii) Stochastic computational optimization of the cable layout of collection systems.

The optimum sizing of export power cables has been studied in this work by exploiting the high variability and relatively low capacity factor of modern OWFs. While the classic methods consider static rated conditions of generated power and boundary conditions, wind power is a stochastic variable which depends on wind random behaviour. Since detailed information about wind rose are available in the early stages of OWFs development, offshore wind power time series can be simulated in consistent and coherent way accounting for realistic fluctuations.

A deterministic approach for calculating the power-transfer capability of OWF cables has been firstly proposed. The method focuses on the maximum instantaneous temperature limit of 90 °C. The results corroborate the possibility to calculate larger values of installable OWF power for a given cable type, under specific operating conditions.

Nevertheless, reliability assessment applying probabilistic techniques is an essential aspect that is missing in the classic and newer industrial standards, when it comes to sizing the export cables. In trying to obtain the cable which provides the best trade-off between investment, losses and reliability, an optimization framework for sizing has been proposed. These three factors are modelled by means of a LCOE-share metric for export cables.

The reliability requirement is translated into a lifetime estimation value. In the proposed method, loss-of-life fractions in the insulation materials are estimated offline through a probabilistic lifetime model, known as Arrhenius-IPM; the simulated offshore wind power time series are used for this purpose. The lifetime estimation takes into consideration the effects of cable total length: the high capacitive currents and the statistical volume enlargement law. Furthermore, the cable lifetime is inferred based on the accumulated ageing effects previously quantified.

Results show the potential of this method in terms of the LCOE-share reduction. Ac-

cording to the simulations, a reduction up to 5% can be achieved, while guaranteeing all the operational security constraints. An uncertainty analysis of the parameters deemed to be the least available: soil thermal resistivity and seabed temperature, showed that their the impact on cable sizing can be significant.

The distance from shore also has an impact on the cable sizing; for larger distances the cables lifetime is the limiting factor, while for shorter distances the ultimate thermal strength takes that role. A relaxation of the maximum instantaneous temperature can allow for a further reduction in the cable sizing for shorter distances, providing cost reductions even compared to the newer industrial practices.

Regarding the second topic, the deterministic design of the cable layout of collection systems for OWFs appears as a very hard computational problem in this context. Four big clusters of methods exist: heuristics, metaheuristics, global optimization with mathematical formulations, and hybrids.

While heuristics have polynomial running time, the specific characteristics of the problem for offshore wind makes it very hard to obtain high quality solutions. This is accentuated when a large set of available cables is presented, where also a decision of choosing a cable type must be done.

Metaheuristics are a flexible approach which provides a great degree of versatility for modelling the problem, and they are particularly useful for non-convex problems where it is very hard to get feasible points. However, there is barely any theory about running time (generally very resource consuming) and solution quality. An algorithmic framework supporting both well-know modified versions of graph theory heuristics and a GA has been proposed.

The EW shapes itself as the best performer in the set of heuristics. When the EW is able to provide feasible points and there is only a single cable available, it provides strong solutions almost instantaneously for problem sizes in the order of modern OWFs. Contrarily, the designed GA results generally in feasible points, showing its ability to incorporate the planarity constraints. The GA is also able to choose among different cable types with the encoding approach. When electrical power losses have a sizeable weight in the desired objective, heuristics inherently come up with lower losses when compared to the GA (without losses encoded), given that they obtain solutions with shorter length.

An approach combining global optimization (i.e. exact formulation) and heuristics have also been proposed in this PhD thesis. The algorithm is based on a MILP model using a hop-index formulation with pre-processing, in order to manage in advance the inclusion of cable type selection and losses calculation.

The proposed global optimization model has been benchmarked against another available hybrid method. It shows a superiority in terms of: (i) Computing time to obtain feasible points, (ii) Computing time to provide high quality solutions with tight optimality gaps,

and (iii) Capacity to incorporate high fidelity models to calculate total electrical power losses and capacitive currents.

Finally, the algorithmic framework has been generalized for the simultaneous optimization of the radial cable layout of collection systems, with the location of OSSs, and sizing of the export cables. This is an extension of the previous problem. Results indicate the ability to solve very large problem, providing very good solutions with tight optimality certificates in reasonable computing time.

In the last topic, a stochastic model to quantify the economic suitability of building closed-loop collection system for OWFs has been proposed. This is accompanied by an optimization framework where radial layout is compared to the designed closed-loop layout.

The decision of whether design radial or looped layouts for the collection systems lies in the availability of methods to perform computational optimization under uncertainty. The attributed significance to the cables failures frequency may play a role as well. Applying a deterministic optimization model in this work means that cables will operate continuously along the project lifetime. A probabilistic approach implies associating to each cable of the layout a failure probability that will impact the operation performance of the OWF.

In this PhD work, on the one hand, it has been shown that with a deterministic approach, very large problems can be addressed with the proposed method and formulation. An extended version of the collection system problem is studied, including OSSs location, export cables, and forbidden areas. This is achieved by means of the modelling strategy of the problem. On the other hand, stochastic optimization presents a less tractable structure, which causes that the capacity to approach different problems is reduced.

In this regard, in this PhD thesis some strategies to apply the stochastic optimization model for closed-loop designs have been proposed. These strategies include: (i) Reduction of the variables number and system states, (ii) Relaxation of the power flow model, (iii) Relaxation of the optimality gaps, and (iv) Relaxation of the reliability level.

The applicability of the full method is demonstrated by studying three differently sized real-world OWFs. Results show that the profitability of either topology type depends strongly on the project size and WT rating. Closed-loop may be a competitive solution for large scale projects where large amounts of energy are potentially curtailed. The particular geometrical characteristics of the OWF also affect these results, in particular the separation distance between WTs.

Concluding, the research presented in this thesis indicates that, to support the very ambitious targets of offshore wind deployment, the paradigm of the electrical network design of (very large) OWFs needs to become more tailored upon the stochastic nature of wind speed. As optimization is by its own nature moving the design towards the limits, aspects such as lifetime and reliability should be incorporated, resulting in probabilistic approaches. Intrinsic engineering constraints, such as design demands, geometrical and

spatial aspects, and physical modelling of the installation conditions, emerge as the most important parameters in the context of OWFs electrical network design.

7.2 Recommendations for Future Research

Future research efforts could be directed to the following points:

- Elaboration of case studies applying the proposed optimization framework for export cables, comparing DC cables, AC single-core cables, and AC three-core cables.
- Extension of the proposed optimization framework for export cables to other HV power components used in OWFs, such as, transformers and converters.
- Development of heuristics with possibility to choose between cable types and ability to overcome planarity constraints.
- Development of other metaheuristics methods, such as PSO or ACO, with comparison to the GA. Quantitative evaluation using statistical analysis of the solution quality obtained by them.
- Inclusion of dynamic cable rating techniques in the optimization of the collection systems of OWFs.
- Development of algorithmic frameworks based on global optimization methods, to optimize simultaneously the WTs location and the deterministic cable layout of collection systems for large-scale OWFs.
- Development of more complex computational models for the seabed bathymetry and forbidden areas (with non-polygonal shapes). Study the impact of those models on the optimum layout.
- Development of stochastic optimization models for very large OWFs with multiple OSSs, and simultaneous optimization of export cables.
- Extension of the simultaneous optimization model for collection and transmission systems, supporting meshed interconnections between OSSs and OCPs.
- Integration of OWF optimization with other generation technologies, such as solar energy and hydrogen production plants.

Bibliography

[1] GWEC, "Global Wind Report. Annual Market Update 2017", Tech. Rep., 2018, pp. 1–73. [Online]. Available: https://www.researchgate.net/publication/324966225_GLOBAL_WIND_REPORT_-_Annual_Market_Update_2017 (visited on 02/04/2020).

[2] ——, "Global Wind Report 2019", Tech. Rep., 2020, pp. 1–78. [Online]. Available: https://gwec.net/global-wind-report-2019/ (visited on 31/03/2020).

[3] BVG Associates, Recognis, and WindEurope, "Our Energy Our Future", Tech. Rep., 2019, p. 78.

[4] WindEurope, "Offshore Wind in Europe: Key trends and statistics 2018", Brussels, Belgium, Report, Feb. 2019. [Online]. Available: https://windeurope.org/members-area/statistics/offshore-wind-in-europe-2018/ (visited on 08/04/2020).

[5] ——, "Offshore Wind in Europe: Key trends and statistics 2018", Tech. Rep., 2018. [Online]. Available: https://windeurope.org/members-area/wp-content/uploads/files/protected/market-intelligence/reports/WindEurope-Annual-Offshore-Statistics-2018.pdf (visited on 02/04/2020).

[6] Tennet, "North Sea Energy Infrastructure: Status and outlook", Tech. Rep., 2019, pp. 1–29. [Online]. Available: https://www.sintef.no/globalassets/project/eera-deepwind-2019/presentations/opening_piepers_tennet_new.pdf (visited on 02/04/2020).

[7] C. Berzan, K. Veeramachaneni, J. McDermott, and U.-M. O'Reilly, "Algorithms for cable network design on large-scale wind farms", Tech. Rep., 2011, pp. 1–24. [Online]. Available: https://thirld.com/files/msrp_techreport.pdf (visited on 02/04/2020).

[8] T. Kvarts, "Systematic Description of Dynamic Load for Cables for Offshore Wind Farms. Method and Experience", *CIGRÉ*, pp. 1–13, 2016.

[9] ORE Catapult, *Wind farm costs*, 2020. [Online]. Available: https://guidetoanoffshore-windfarm.com/wind-farm-costs (visited on 02/04/2020).

[10] RenewableUK, *RenewableUK - Project Intelligence*, 2018. [Online]. Available: https://www.renewableuk.com/page/ProjectIntelligenceHome (visited on 02/04/2020).

[11] ReNEWS, *Rampion suffers cable fault*, 2017. [Online]. Available: http://renews.biz/105889/rampion-suffers-cable-fault/ (visited on 02/04/2020).

[12] Baltic InteGrid, *The Baltic InteGrid Project*, 2016. [Online]. Available: http://www.baltic-integrid.eu/index.php/home.html (visited on 02/04/2020).

[13] ABB, "XLPE Submarine Cable Systems Attachment to XLPE Land Cable Systems - User's Guide", Tech. Rep., 2018, pp. 1–12. [Online]. Available: new.abb.com/docs/default-source/ewea.../xlpe-submarine-cable-systems-2gm5007.pdf (visited on 29/10/2018).

[14] J. Herbert-Acero, O. Probst, P.-E. Réthoré, G. Larsen, and K. Castillo-Villar, "A Review of Methodological Approaches for the Design and Optimization of Wind Farms", *Energies*, vol. 7, no. 11, pp. 6930–7016, 2014, ISSN: 1996-1073. DOI: 10.3390/en7116930.

[15] M. Koivisto, K. Das, F. Guo, P. Sørensen, E. Nuño Martinez, N. A. Cutululis, and P. Maule, "Using time series simulation tool for assessing the effects of variable renewable energy generation on power and energy systems", *WIREs Energy and Environment*, no. June, pp. 1–15, 2018, ISSN: 2041840X. DOI: 10.1002/wene.329.

[16] IEC, "IEC-60287-1: Electric cables - Calculation of the current rating", Tech. Rep., 2014, p. 136. [Online]. Available: https://www.evs.ee/products/iec-60287-1-1-2006 (visited on 15/04/2019).

[17] ——, "IEC-60853-2: - Calculation of the cyclic and emergency current rating of cables", Tech. Rep., 2008, p. 20.

[18] CIGRÉ, "Current Ratings of Cables for Cyclic and Emergency Loads. Part 1. Cyclic Ratings (Load Factor Less Than 100%) and Response to a Step Function", Tech. Rep. 24, 1976, pp. 63–96.

[19] CIGRÉ: Working Group B1.40, "Offshore Generation Cable Connections", Tech. Rep. 1, 2015, pp. 1–180.

[20] R. Jothi, and B. Raghavachari, "Approximation algorithms for the capacitated minimum spanning tree problem and its variants in network design", *ACM Transactions on Algorithms (TALG)*, vol. 1, no. 5, pp. 265–282, 2005.

[21] E. L. Lawler, "The traveling salesman problem: a guided tour of combinatorial optimization", *Wiley-Interscience Series in Discrete Mathematics*, 1985.

[22] A. Kershenbaum, "Computing capacitated minimal spanning trees efficiently", *Networks*, vol. 4, no. 4, pp. 299–310, 1974, ISSN: 10970037. DOI: 10.1002/net.3230040403.

[23] J. Bauer, and J. Lysgaard, "The offshore wind farm array cable layout problem: A planar open vehicle routing problem", *Journal of the Operational Research Society*, vol. 66, no. 3, pp. 360–368, 2015, ISSN: 14769360. DOI: 10.1057/jors.2013.188.

[24] M. Fischetti, and D. Pisinger, "Optimizing wind farm cable routing considering power losses", *European Journal of Operational Research*, vol. 270, no. 3, pp. 917–930, 2018, ISSN: 03772217. DOI: 10.1016/j.ejor.2017.07.061.

[25] A. M. Jenkins, M. Scutariu, and K. S. Smith, "Offshore wind farm inter-array cable layout", in *IEEE PowerTech at Grenoble*, 2013, pp. 1–6, ISBN: 9781467356695. DOI: 10.1109/PTC.2013.6652477.

[26] R. Ahuja, T. L. Magnanti, and J. B. Orlin, *Encyclopedia of Optimization*. Springer, 2008, pp. 2095–2108.

[27] J. S. Shin, and J. O. Kim, "Optimal Design for Offshore Wind Farm considering Inner Grid Layout and Offshore Substation Location", *IEEE Transactions on Power Systems*, vol. 32, no. 3, pp. 2041–2048, 2017, ISSN: 08858950. DOI: 10.1109/TPWRS.2016.2593501.

[28] P. Fagerfjäll, "Optimizing wind farm layout-more bang for the buck using mixed integer linear programming (MSc. Thesis)", PhD thesis, 2010, p. 111.

[29] M. Sedighi, M. Moradzadeh, O. Kukrer, M. Fahrioglu, and L. Vandevelde, "Optimal Electrical Interconnection Configuration of Off-Shore Wind Farms", *Journal of Clean Energy Technologies*, vol. 4, no. 1, pp. 66–71, 2016, ISSN: 1793821X. DOI: 10.7763/JOCET.2016.V4.255.

[30] H. Ling-ling, C. Ning, Z. Hongyue, and F. Yang, "Optimization of large-scale offshore wind farm electrical collection systems based on improved FCM", in *International Conference on Sustainable Power Generation and Supply (SUPERGEN)*, 2012, pp. 67–67, ISBN: 978-1-84919-673-4. DOI: 10.1049/cp.2012.1785.

[31] D. Li, C. He, and Y. Fu, "Optimization of internal electric connection system of large offshore wind farm with hybrid genetic and immune algorithm", in *3rd International Conference on Deregulation and Restructuring and Power Technologies, (DRPT)*, 2008, pp. 2476–2481, ISBN: 9787900714138. DOI: 10.1109/DRPT.2008.4523827.

[32] P. Hou, W. Hu, Z. Chen, and C. Chen, "Overall Optimization for Offshore Wind Farm Electrical System", *Wind Energy*, vol. 20, no. 2016, pp. 1017–1032, 2017, ISSN: 1099-1824. DOI: 10.1002/we.

[33] S. Wei, L. Zhang, Y. Xu, Y. Fu, and F. Li, "Hierarchical Optimization for the Double-Sided Ring Structure of the Collector System Planning of Large Offshore Wind Farms", *IEEE Transactions on Sustainable Energy*, vol. 8, no. 3, pp. 1029–1040, 2017, ISSN: 19493029. DOI: 10.1109/TSTE.2016.2646061.

[34] S. Lumbreras, and A. Ramos, "Optimal design of the electrical layout of an offshore wind farm applying decomposition strategies", *IEEE Transactions on Power Systems*, vol. 28, no. 2, pp. 1434–1441, 2013, ISSN: 08858950. DOI: 10.1109/TPWRS.2012.2204906.

[35] S. Lumbreras, A. Ramos, and S. Cerisola, "A Progressive Contingency Incorporation Approach for Stochastic Optimization Problems", *IEEE Transactions on Power Systems*, vol. 28, no. 2, pp. 1452–1460, 2013. DOI: 10.1109/TPWRS.2012.2225077.

[36] A. C. Pillai, J. Chick, L. Johanning, M. Khorasanchi, and V. De Laleu, "Offshore wind farm electrical cable layout optimization", *Engineering Optimization*, vol. 47, no. 12, pp. 1689–1708, 2015, ISSN: 10290273. DOI: 10.1080/0305215X.2014.992892.

[37] J. Castro Mora, "Optimización Global de Parques Eólicos Mediante Algoritmos Evolutivos", PhD thesis, Unversidad de Sevilla, 2008, p. 278.

[38] P. Hopewell, F. Castro, and D. Bailey, "Optimising the design of offshore wind farm collection networks", in *Proceedings of the 41st International Universities Power Engineering Conference (UPEC)*, 2006, pp. 84–88.

[39] M. Zhao, Z. Chen, and F. Blaabjerg, "Optimization of Electrical System for a Large DC Offshore Wind Farm by Genetic Algorithm", in *Nordic Workshop on Power and Industrial Electronics*, 2004, p. 8. DOI: 10.1049/iet-rpg.

[40] H. G. Svendsen, "Planning Tool for Clustering and Optimised Grid Connection of Offshore Wind Farms", *Energy Procedia*, vol. 35, pp. 297–306, 2013, ISSN: 18766102. DOI: 10.1016/j.egypro.2013.07.182. [Online]. Available: http://dx.doi.org/10.1016/j.egypro.2013.07.182.

[41] K. Das, and N. A. Cutululis, "Offshore Wind Power Plant Technology Catalogue", Technical University of Denmark, Risø, Tech. Rep., 2017. [Online]. Available: https://backend.orbit.dtu.dk/ws/files/143240154/Technology_Catalogue_final.pdf (visited on 08/04/2020).

[42] R. Olsen, "Dynamic Loadability of Cable Based Transmission Grids", PhD thesis, Technical University of Denmark, 2013. [Online]. Available: https://backend.orbit.dtu.dk/ws/portalfiles/portal/75280125/RasmusOlsen_PhDThesis_2013.pdf (visited on 08/04/2020).

[43] V. K. Agarwal, H. M. Banford, B. S. Bernstein, E. L. Brancato, R. A. Fouracre, G. C. Montanari, J. L. Parpal, J. N. Seguin, D. M. Ryder, and J. Tanaka, "The Mysteries of Multifactor Ageing", *IEEE Electrical Insulation Magazine*, vol. 11, no. 3, pp. 37–43, 1995, ISSN: 08837554. DOI: 10.1109/57.387831.

[44] R. S. Olsen, J. Holboll, and U. S. Gudmundsdottir, "Dynamic Temperature Estimation and Real Time Emergency Rating of Transmission Cables", *IEEE Power and Energy Society General Meeting*, pp. 1–8, 2012, ISSN: 19449925. DOI: 10.1109/PESGM.2012.6345324.

[45] R. S. Olsen, G. J. Anders, J. Holboell, and U. S. Gudmundsdottir, "Modelling of Dynamic Transmission Cable Temperature Considering Soil-Specific Heat, Thermal Resistivity, and Precipitation", *IEEE Transactions on Power Delivery*, vol. 28, no. 3, pp. 1909–1917, 2013, ISSN: 08858977. DOI: 10.1109/TPWRD.2013.2263300.

[46] G. J. Anders, A. Napieralski, and Z. Kulesza, "Calculation of the internal thermal resistance and ampacity of 3-core screened cables with fillers", *IEEE Transactions on Power Delivery*, vol. 14, no. 3, pp. 729–733, 1999, ISSN: 08858977. DOI: 10.1109/61.772307.

[47] J. J. Grainger, and W. D. J. Stevenson, *Power System Analysis*, 2nd editio. McGraw-Hill Education, 1994, ISBN: 978-0-9845438-0-9. DOI: 10.1017/CBO9781107415324.004.

[48] P. Sørensen, N. A. Cutululis, A. Vigueras-Rodríguez, L. E. Jensen, J. Hjerrild, M. H. Donovan, and H. Madsen, "Power Fluctuations From Large Wind Farms", *IEEE Transactions on Power Systems*, vol. 22, no. 3, pp. 958–965, 2007, ISSN: 08858950. DOI: 10.1109/TPWRS.2007.901615.

[49] HELCOM, *Our Baltic Sea*, 2017. [Online]. Available: http://stateofthebalticsea.helcom.fi/in-brief/our-baltic-sea/ (visited on 29/10/2018).

[50] L. A. Escobar, and W. Q. Meeker, "A Review of Accelerated Test Models", *Statistical Science*, vol. 21, no. 4, pp. 552–577, 2006, ISSN: 0883-4237. DOI: 10.1214/088342306000000321. [Online]. Available: http://projecteuclid.org/euclid.ss/1177334529 (visited on 29/10/2018).

[51] G. Mazzanti, "The Combination of Electro-thermal Stress, Load Cycling and Thermal Transients and its Effects on the Life of High Voltage ac Cables", *IEEE Transactions on Dielectrics and Electrical Insulation*, vol. 16, no. 4, pp. 1168–1179, 2009, ISSN: 10709878. DOI: 10.1109/TDEI.2009.5211872.

[52] G. Mazzanti, and G. C. Montanari, "A Comparison between XLPE and EPR as Insulating Materials for HV Cables", *IEEE Transactions on Power Delivery*, vol. 12, no. 1, pp. 15–26, 1997, ISSN: 08858977. DOI: 10.1109/61.568220.

[53] W. Hauschild, and W. Mosch, *Statistical Techniques for High-Voltage Engineering*. 1992.

[54] M. Marzinotto, and G. Mazzanti, "Merging the electro-thermal life model for power cables with the statistical volume enlargement law", *2014 IEEE Conference on Electrical Insulation and Dielectric Phenomena, CEIDP 2014*, no. 3, pp. 502–505, 2014. DOI: 10.1109/CEIDP.2014.6995888.

[55] M. Miner, "Cumulative fatigue damage", *Journal of Applied Mechanics*, vol. 12, no. 3, A159–A164, 1945.

[56] N. B. Negra, J. Todorovic, and T. Ackermann, "Loss evaluation of HVAC and HVDC transmission solutions for large offshore wind farms", *Electric Power Systems Research*, vol. 76, no. 11, pp. 916–927, 2006, ISSN: 03787796. DOI: 10.1016/j.epsr.2005.11.004.

[57] R. Meere, J. Ruddy, P. McNamara, and T. O'Donnell, "Variable AC transmission frequencies for offshore wind farm interconnection", *Renewable Energy*, vol. 103, pp. 321–332, 2017, ISSN: 18790682. DOI: 10.1016/j.renene.2016.11.037.

[58] G. Mazzanti, "Analysis of the Combined Effects of Load Cycling, Thermal Transients, and Electrothermal Stress on Life Expectancy of High-Voltage AC Cables", *IEEE Transactions on Power Delivery*, vol. 22, no. 4, pp. 2000–2009, 2007, ISSN: 08858977. DOI: 10.1109/TPWRD.2007.905547.

[59] S. Lumbreras, and A. Ramos, "Offshore wind farm electrical design: a review", *Wind Energy*, vol. 16, pp. 459–473, 2013, ISSN: 1099-1824. DOI: 10.1002/we.

[60] A. Cerveira, A. F. de Sousa, E. J. Pires, and J. Baptista, "Optimal Cable Design of Wind Farms: The Infrastructure and Losses Cost Minimization Case", *IEEE Transactions on Power Systems*, vol. 31, no. 6, pp. 4319–4329, 2016, ISSN: 08858950. DOI: 10.1109/TPWRS.2016.2521700.

[61] M. Fischetti, and D. Pisinger, "Mixed Integer Linear Programming for new trends in wind farm cable routing", *Electronic Notes in Discrete Mathematics*, vol. 64, pp. 115–124, 2018, ISSN: 15710653. DOI: 10.1016/j.endm.2018.01.013.

[62] A. Wedzik, T. Siewierski, and M. Szypowski, "A new method for simultaneous optimizing of wind farm's network layout and cable cross-sections by MILP optimization", *Applied Energy*, vol. 182, pp. 525–538, 2016, ISSN: 03062619. DOI: 10.1016/j.apenergy.2016.08.094.

[63] A. Hertz, O. Marcotte, A. Mdimagh, M. Carreau, and F. Welt, "Design of a wind farm collection network when several cable types are available", *Journal of the Operational Research Society*, vol. 68, no. 1, pp. 62–73, 2017, ISSN: 0160-5682. DOI: 10.1057/s41274-016-0021-6.

[64] M. Banzo, and A. Ramos, "Stochastic Optimization Model for Electric Power System Planning of Offshore Wind Farms", *IEEE Transactions on Power Systems*, vol. 26, no. 3, pp. 1338–1348, 2011, ISSN: 0885-8950. DOI: 10.1109/TPWRS.2010.2075944.

[65] Y. Chen, Z. Y. Dong, K. Meng, F. Luo, Z. Xu, and K. P. Wong, "Collector System Layout Optimization Framework for Large-Scale Offshore Wind Farms", *IEEE Transactions on Sustainable Energy*, vol. 7, no. 4, pp. 1398–1407, 2016, ISSN: 1949-3029. DOI: 10.1109/TSTE.2016.2549602.

[66] A. Kershenbaum, and W. Chou, "Unified Alporithm for Designing Multidrop Teleprocessing Networks", *IEEE Transactions on Communications*, vol. com-22, no. 11, pp. 1762–1772, 1974.

[67] R. D. Zimmerman, C. E. Murillo-Sánchez, and R. J. Thomas, "MATPOWER: Steady-state operations, planning, and analysis tools for power systems research and education", *IEEE Transactions on Power Systems*, vol. 26, no. 1, pp. 12–19, 2011, ISSN: 08858950. DOI: 10.1109/TPWRS.2010.2051168.

[68] L. Gouveia, and P. Martins, "The capacitated minimum spanning tree problem: revisiting hop-indexed formulations", *Computers & operations research*, vol. 32, no. 9, 2005.

[69] F. M. González-Longatt, P. Wall, P. Regulski, and V. Terzija, "Optimal electric network design for a large offshore wind farm based on a modified genetic algorithm approach", *IEEE Systems Journal*, vol. 6, no. 1, pp. 164–172, 2012.

[70] IBM, "IBM ILOG CPLEX Optimization Studio CPLEX User Manual", Tech. Rep., 2015, pp. 1–564. [Online]. Available: https://www.ibm.com/support/knowledgecenter (visited on 11/04/2019).

[71] O. Dahmani, S. Bourguet, M. MacHmoum, P. Guerin, P. Rhein, and L. Josse, "Optimization of the Connection Topology of an Offshore Wind Farm Network", *IEEE Systems Journal*, vol. 9, no. 4, pp. 1519–1528, 2015, ISSN: 19379234. DOI: 10.1109/JSYST.2014.2330064.

[72] S. Lundberg, "Configuration study of large wind parks", PhD thesis, Chalmers University of Technology, 2003, pp. 1–124.

[73] S. Dutta, and T. Overbye, "A Graph-theoretic Approach for Addressing Trenching Constraints in Wind Farm Collector System Design", in *IEEE Power and Energy Conference at Illinois (PECI)*, 2013, pp. 1–5. DOI: 10.1109/PECI.2013.6506033.

[74] A. Klein, and D. Haugland, "Obstacle-aware optimization of offshore wind farm cable layouts", *Annals of Operations Research*, vol. 272, no. 1-2, pp. 373–388, 2017, ISSN: 15729338. DOI: 10.1007/s10479-017-2581-5.

[75] ESCA, SEAFISH, and RenewableUK, *KIS-ORCA*. [Online]. Available: http://kis-orca.eu/about-us#.XLRI_-gzYuU (visited on 15/04/2019).

[76] E. Calixto, *Gas and Oil Reliability Engineering*, Second. Gulf Professional Publishing, 2016, pp. 269–470. [Online]. Available: https://www.sciencedirect.com/book/9780128054277/gas-and-oil-reliability-engineering#book-info (visited on 05/03/2020).

[77] R. Billinton, and R. N. Allan, *Reliability Evaluation of Engineering Systems: Concepts and Techniques*. 1992, p. 410.

[78] J. Warnock, D. McMillan, J. A. Pilgrim, and S. Shenton, "Review of offshore cable reliability metrics", in *Proceedings of the 13th IET International Conference on AC and DC Power Transmission (ACDC)*, 2017, pp. 1–6. DOI: 10.1049/cp.2017.0071.

[79] Statista, *Monthly average electricity prices in Great Britain (GB) from 2015 to 2019*, 2019. [Online]. Available: https://www.statista.com/statistics/589765/average-electricity-prices-uk/ (visited on 09/03/2020).

[80] Vatenfall, *Ormonde Offshore Wind Farm*. [Online]. Available: https://powerplants.vattenfall.com/ormonde (visited on 05/02/2020).

[81] J. Warnock, D. McMillan, J. Pilgrim, and S. Shenton, "Failure Rates of Offshore Wind Transmission Systems", *Energies*, vol. 12, no. 14, pp. 1–12, 2019, ISSN: 19961073. DOI: 10.3390/en12142682.

[82] Vatenfall, *Horns Rev 1 Offshore Wind Farm*. [Online]. Available: https://powerplants.vattenfall.com/horns-rev (visited on 12/03/2020).

[83] Ørsted, *West of Duddon Sands Offshore Wind Farm*. [Online]. Available: https://westofduddonsands.co.uk/ (visited on 12/03/2020).

Publications

APPENDIX J1

"Electrical Cable Optimization in Offshore Wind Farms - A review"

J.A. Pérez-Rúa, and N. A. Cutululis

in *IEEE Access*, Vol. 7, 85796–85811

July

2019

Electrical Cable Optimization in Offshore Wind Farms - A review

JUAN-ANDRÉS PÉREZ-RÚA[1] and NICOLAOS A. CUTULULIS (SENIOR MEMBER, IEEE) [2]
[1,2]Department of Wind Energy, Technical University of Denmark, Frederiksborgvej 399, 4000 Roskilde, Denmark

Corresponding author: Juan-Andrés Pérez-Rúa (e-mail: juru@dtu.dk).

This research has received funding from the Baltic InteGrid Project http://www.baltic-integrid.eu/

ABSTRACT A state-of-the-art review of the optimization of electrical cables in Offshore Wind Farms (OWFs) is presented in this paper. One of the main contributions of this work is to propose a general classification of this problem, framed in the general context of the Offshore Wind Farms Design and Optimization (OWiFDO). The classification encompasses two complementary aspects. First, the optimum sizing of electrical cables, with the three main approaches used nowadays: static rated sizing, dynamic load cycle profile, and dynamic full time series, being conceptually analyzed and compared. The latest techniques and advances are described, along with the presentation of potential research areas not thoroughly addressed today, such as Dynamic Cable Rating, and cable's lifetime estimation under time-varying conditions. Second, the network optimization of large OWFs is thoroughly presented, dividing the problem with a bottom-top approach: cable layout of collection system, Wind Turbines (WTs) allocation to Offshore Substations (OSSs), number and location of OSSs, and interconnection between OSSs and Onshore Connection Points (OCPs). A comparison among different methods is performed, taking into consideration the main engineering constraints. Global optimization, specifically, Binary Programming (BIP) or Mixed Integer Linear Programming (MILP), is envisaged as the best way to tackle this topic. The full combinatorial problem is found to be better addressed following a Top-Bottom approach, combining exact formulations with high level heuristics, or holistically with evolutionary algorithms.

INDEX TERMS Balance of plant, Cable sizing, Combinatorial optimization, Dynamic rating, Electrical cables, Heuristics, Global optimization, Mathematical programming, Metaheuristics, Offshore Wind Farm, Static rating.

I. INTRODUCTION

OFFSHORE Wind Farms (OWFs) represent one of the fastest and most steadily growing types of renewable energy technologies for electricity generation. The penetration level has increased almost five times in the last seven years, reaching a globally total installed power of nearly 19 GW [1]. This growth is mainly explained by reductions in costs of the technology [2]: the Levelized Cost of Energy (LCOE) has dropped recently from 240 USD/MWh to 170 USD/MWh, accounting for the last five years.

One of the main drivers for cost reduction is the economies of scale, which has been evident in the OWF industry by the accelerated increase of Wind Turbines (WTs) individual power, and consequently, the scaled up of the total installed capacity of state-of-the-start OWFs. The latter brings as side effect the increase of complexity for designing efficient and cost-effective infrastructure, such as the electrical systems, given that: i) the WTs are larger in power and number, being less uniformly scattered around the project area, ii) the Offshore Substations (OSSs) are built farther away from the Onshore Connection Point (OCP), increasing the export systems transmission length, and iii) more stiff, complete and complex requirements from the Transmission Systems Operators (TSOs) to the OWFs for providing auxiliary services are demanded. All added up, means the electrical infrastructure costs can go up to 15% compared to the total capital expenses (CAPEX) [3]. The last point together with the remarkable impact in terms of efficiency and reliability over the operational performance of OWFs (OPEX) [4], turn the electrical infrastructure into a cornerstone matter in designing the full system.

Between 2018 and 2028 more than 19000 km of cables for collection systems are prognosed to be installed worth £5.36bn [5], while longer and bigger cables for export are the trend. Hence, power cables represent an important aspect of the electrical infrastructure to be studied in the design of OWFs; not only because its obvious weight on economic metrics, but also due to its impact in the overall availability of these type of projects.

The OWFs electrical infrastructure design and optimization is a multidisciplinary problem. This fact that has been proved by a comprehensive literature survey performed in the most

important academic sources, detecting a wide variety of definitions, strategies, models, and frameworks to optimize performance metrics related to electrical infrastructure. Additionally, this is a relatively new research area, with no more than 15 years of studies by scientists from different fields, therefore plethora of methodologies and mathematical formulations have been proposed; this is reflected by a relatively large pallet of objectives and requirements identified in the scholar literature.
There is a lack of a comprehensive review articles summarizing, classifying and critically assess the current state of this topic, with only [6] published six years ago being identified. However this manuscript focuses on micrositing, collection systems optimization techniques, transmission systems, and briefly addresses other topics; consequently, improvable by deepening the scope of the cable sizing subject, incorporating new developments, and proposing a general classification of it.
By virtue of the above, a literature review of the latest techniques for optimizing electrical cables in OWFs is performed in this paper, intending to provide a classification of the problem while underlying its most important aspects, highlighting the advancements, and finally identifying the open challenges according to the authors' research.

The current state of offshore wind farms
The earliest OWF venture known as Vindeby, located at the Danish waters of Lolland in the Baltic sea, was decommissioned last September 2017, after 25 years of operation and 243 GWh of energy produced [7]. Vindeby was located at a distance from shore of 2 km, and concrete foundations were installed above seabed with maximum depth of 4 m. The project consisted of 11 WTs of 450 kW (4.95 MW total installed power). By comparing the previous numbers with the largest OWFs under operation nowadays (see Table 1), the accelerated growth of the industry in a rather short time is becoming obvious, with total installed powers in the order of hundreds of MW, export route lengths close to 100 km, and maximum water depths across the projects' area of almost 40 m. The escalation of those parameters means that some factors become more relevant and complex to handle, such as the electrical infrastructure, due to the increased investment, complexity in the designs, and the requirement for new technologies able to withstand such new environmental and operating conditions. For instance, on the one hand, the increase of WTs number causes the collection system design to scale up exponentially in terms of brute force design evaluation; on the other hand, the increase of WTs individual power, challenge the traditional voltage level used currently (33 kV), opening the door for new technologies of cables with higher insulation capacities (66 kV), and in contrast, lower power in WTs would require larger amounts of them, depending upon more sophisticated clustering techniques to allocate them in OSSs groups. See in the Table 1, London Array doubles in WTs number to Walney Extension, but the last one has bigger WTs to compensate such difference. Likewise, export route length is linked to decision-making problems such as choosing between AC and DC technology, voltage level, cables type, converters type, system structure, and so on. These trends are foreseen to remain, as presented in the Table 2, with OWFs projects already reaching the order of GW (both because of bigger WTs and larger amounts of them), distances between OSSs and OCPs of more than a hundred of kilometers, and water depths higher than 40 m. In fact, among the list of OWFs under proposal stage, projects in the order of several thousands of MW are waiting for consents to start construction stage. The previous trends mean that the share of the electrical infrastructure over economic metrics will be higher, putting these concepts in a major role to be taken into account when planning OWFs.

Design and optimization of offshore wind farms
The Offshore Wind Farms Design and Optimization problem (OWiFDO) can be defined as the body of decisions to be made in order to design reliable, secure, and efficient OWFs, while maximizing their performance through the evaluation of a quantifiable target. The definition of the set of modelling options, constraints, objective function, variables and parameters, is up to the OWF developers, according to established and particular practices. The OWiFDO is a non-linear, non-convex problem with integer and continuous variables, laying in the category of NP class [8]. Due to the mathematical complexity of the problem, the full picture of it can be split following a sequential divide-and-conquer approach, such as the one illustrated in the the Fig. 1, where four subsequent sub-problems are defined: i) macrositing, ii) micrositing, iii) infrastructures (including structural, electrical and civil design), iv) and definition of control, protection and operation schemes. The main inputs

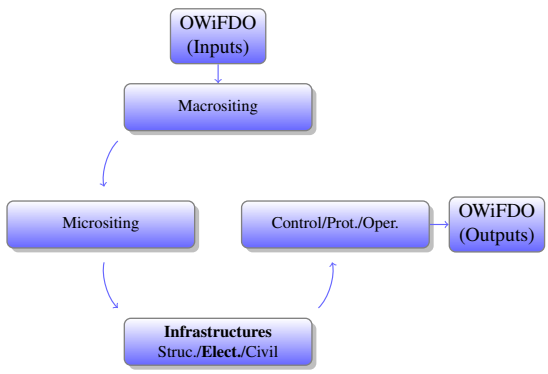

FIGURE 1: Offshore Wind Farms Design and Optimization Problem (OWiFDO): An Overview.

are: minimum and maximum number of WTs, minimum and maximum OWF's total installed power, and definition of the objective, constraints, and other parameters. The macrositing problem encompasses: i) analysis of the available infrastructure (power system capacity at OCP, logistic resources, accessibility, etc), ii) evaluation of the environmental suit-

TABLE 1: Largest OWFs under operation

OWF	Capacity [MW]	Turbines	Export Route Length [km]	Maximum Depth [m]	Commissioning Year
Walney Extension	659	40x8.25MW/47x7 MW	75	23	2018
London Array	630	175x3.6MW	55	25	2013
Gemini	600	150x4MW	110	36	2017

TABLE 2: Largest OWFs under construction

OWF	Capacity [MW]	Turbines	Export Route Length [km]	Maximum Depth [m]	Commissioning Year
Hornsea One	1218	174x7MW	~ 120	37	2020
East Anglia One	714	102x7MW	~ 73	40	2020
Kriegers Flak	604.8	72x8.4MW	~ 45	25	2021

ability (specially relevant in marine spatial planning), iii) wind resource potential assessment, and iv) geographical adequacy (most importantly maximum water depths). The main output of this block is the selection of the OWF site, and the upper bound of project's area; important economic factors such as energy regulatory framework, financing and funding must be taken into consideration in this stage as well, in order to assess the financial sustainability of the project. Micrositing involves the OWF layout design, where the arrangement of the individual WTs is decided; in this sub-problem the number and geographical locations of the WTs along with their sizing are defined. After this, the electrical infrastructure is designed; each of the civil, structural and electrical designs has its own mathematical entity, hence in this paper the electrical infrastructure is studied individually. It is important to note at this point that in order to guarantee an optimum design (or near) of the OWF, the best possible solution in each block should be found, while balancing their effect on following blocks. For instance, when deciding the upper bound of the project's area, care should be taken to harmonize the micrositing and the electrical infrastructure design, because the minimization of the wake losses leads to increased separation between WTs, but at the expense of longer cables required for the collection systems. As an alternative, the loop in the Fig. 1 can be closed to come up with an iterative design process.
With the electrical cables as main target, in the following, a classification of the set of possible actions to optimize its design, according to common practices, innovative solutions, and future actions to be considered in the short panorama, is proposed.

Optimization of electrical cables in offshore wind farms: A classification

The problem classification can be seen in the Fig. 2. In the left branch the topics corresponding to optimum sizing of electrical cables are presented. The definition of a cable's nominal current must take into account the high variability of offshore wind power and its relatively low capacity factor [9]. This implies that a smaller nominal value can be chosen given certain conditions. The three main techniques used in OWFs cable sizing from the perspective of thermo-electrical conditions are presented in the following.
Static rated sizing represents the classic technique recommended in [10], [11], and [12] (industrial technical standards). It a is straight-forward approach, consisting only in a multi-parameter static equation for calculating the continuous current I_t, to be transmitted during infinite time, in order to obtain a continuous conductor temperature equal to 90°C. The smaller cable t with I_t equal or greater than

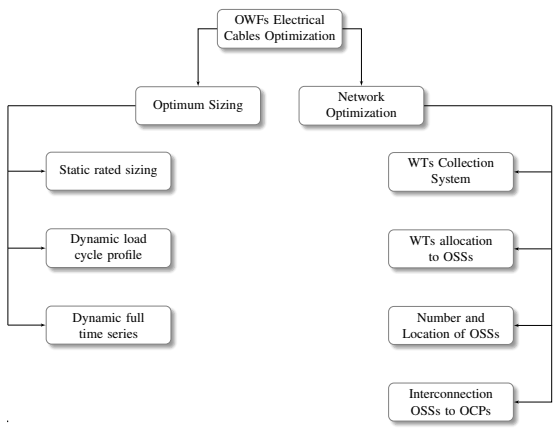

FIGURE 2: OWFs electrical infrastructure problem classification.

the total current (including capacitive currents) at hot spot is selected. The aforementioned IEC and CIGRÉ standards consider static conditions at rated operation, however OWFs are characterized by low capacity factors and high power production variability.
In the last lustrum, an emerging topic in OWFs cable sizing is being studied: Dynamic Rating. The two main approaches using this technique are described in the following.
Dynamic load cycle profile consists in finding the worst case dynamic load profiles, as presented in [13] (CIGRÉ: Working Group B1.40). This approach is taking into account the inherent variability of power production, representing a more sophisticated method that is emerging as industrial practice,

as detailed in [13]. It consists of a four-step signal, calculated using the highest RMS values computed through different periods, sweeping through the yearly data set by means of a rolling RMS filter starting at each singular data point. A pre-processing analysis is needed to be carried out to find the set of periods of interest. In the study presented in [14], it has been concluded that the periods of 7 days, 10 days, 40 days, and 365 days capture reasonably the most representative windy days in a windy year. Thus, in a temporal sequential ordering, the pre-conditioning current is derived calculating the RMS value for the whole data set, lasting 308 days (remaining days after the periods 7, 10, and 40), then the greatest yearly RMS value using a period length of 7 days is obtained, keeping the same procedure for the periods of 10 days and 40 days, while not overlapping the periods between them. With the calculated four-step signal (including capacitive currents), the maximum conductor temperature is calculated, and similarly to the previous method, the smaller cable t with maximum calculated temperate lower than 90°C is chosen. Note that this sequential arrangement represents a conservative criterion itself, because of the assumed steadily increase of current with time. Equivalent step-wise cyclic load profiles, as in [15] and [16], represent other approach to optimally size cables, by obtaining cyclic currents, followed by the application of the standard [11].

Finally, *Dynamic full time series* encompasses the use of full and high resolution time series for performing electro-thermal analysis. The previous two methods exclude reliability analysis, therefore new advances and strategies requiring time series information, such as, generated power, seabed surface temperature, thermal parameters, among others, are required. Related to cables, so far work has been focused on: i) conductor temperature estimation, and ii) cables sizing considering a maximum instantaneous temperature never exceeding 90°C (which also is assumed in the previous two approaches). For conductor temperature estimation, several methods have been developed: Step Response (SR), Finite Method Analysis (FEM) and Thermo-Electrical Equivalent (TEE) model [17]. A TEE (1-D) represents the model with the best computation time-quality performance and is applicable for single-core and three-core type cables, albeit new 2-D models are under study and proposed as per [18]. Limiting the conductor temperature to 90°C is a well-established practice, as presented in [19], however a re-evaluation of the risk of exceeding this constraint in different time horizons becomes relevant and might be a way to avoid underuse of these components.

Important progress has been done in this topic, however there is still room for new advancements, such as the application of lifetime methods and probabilistic techniques for sizing these components.The dynamics of the system must be considered holistically, being able to estimate fatigue factors to which a real operating cable is exposed to. This can be achieved by developing new lifetime models, validating their parameters by real experiments in the frame of accelerated tests, based on historical information and forecast values of produced power, seabed temperature, soil thermal parameters, and so on.

Real time control of OWFs while abiding thermal constraints can be also merged with these concepts. In general, the previous statements can be extrapolated to other power components, like transformers [20], filters, and compensations units. In fact, not much work has been found related to the latter, therefore representing a potentially important research topic in the short to medium term.

The right branch of the Fig. 2 represents the combinatorial optimization problem related to the electrical infrastructure in OWFs. The main objective is to achieve an optimized, in terms of length and/or investment costs, cable layout. Given the mathematical complexity, computational optimization is required; however project-specific particularities must be taken into account. For instance, the number of OSSs can be defined in function of the number of constructing stages of the project, or the WTs clustering can obey to practical reasons such as power balancing or standardization. Special attention is given to this topic as it has been addressed more intensively in the scientific papers; Section II deals with these aspects.

II. NETWORK OPTIMIZATION

The set of activities shaping the problem of the topological network optimization can be seen in the right branch of the Figure 2: i) WTs collection system design, ii) WTs allocation to OSSs, iii) Number and location of OSSs, and finally, iv) the interconnection between OSSs to OCPs. It should be noticed that the selected classification assumes classic OWFs design: large AC OWFs (MV at collection system level and HV at transmission system, operating at $f_n = 50$ Hz), and HVDC connected OWFs (with AC collection system, and the AC/DC station next to the OSS), because those are the types planned, built and under operation nowadays.

A. WTS COLLECTION SYSTEM DESIGN

This problem resembles to historical mathematical problems such as Minimum Spanning Tree (MST) and its constrained version, the Capacitated Minimum Spanning Tree (C-MST), which classifies under the category of NP-hard class [21], and the Travelling Salesman Problem (TSP) with all its variants [22], also NP-hard. Problems from other fields map to this one, like telecommunication networks design back in the 60's and 70's [23], or network planning [21]; however in the case of OWFs, *Ad hoc* methods are necessitated in function of particular spatial (nature reserve or occupied areas, seabed bathymetry, among others), planarity (non-crossing of cables, trenching requirements, and so on), and technical (stochasticity on power generation, cables capacities, topological structure, ancillary services support, etc) constraints.

Based on the literature review, the set of actions used for the collection system design and optimization are represented in the flow chart of the Fig. 3, starting from the data related to variables (binary, integer, continuous, etc), parameters (unitary costs, bounds, etc), objectives, and constraints definition, and continuing with selecting the topological network

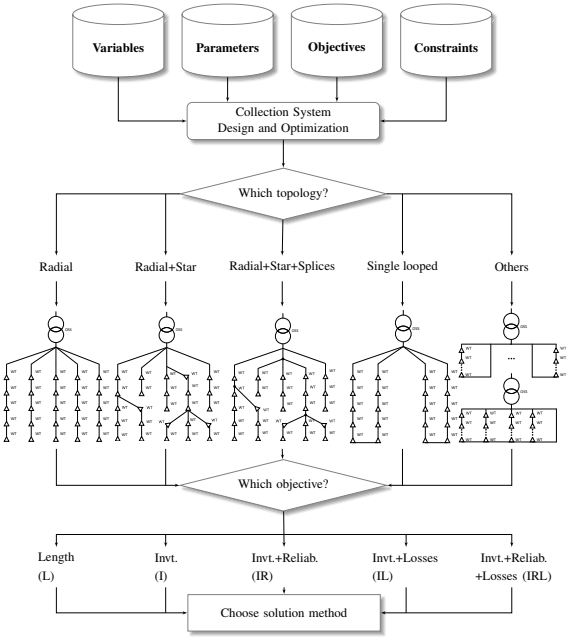

FIGURE 3: OWFs collection systems design and optimization: Decision flowchart.

type. The range of options span networks ensuing different patterns: i) radial, ii) radial plus star, iii) radial plus star plus splices, iv) single looped, and v) others, as illustrated with sample schemes in the same figure. Each topological structure must be defined along with the desired optimization target: i) Length (L), ii) Investment (I), iii) Investment plus Reliability (IR), iv) Investment plus Losses (IL), and iv) Investment plus Reliability plus Losses (IRL). Finally, the solution method must be chosen, for which the modelling choices have to be in accordance with it. The classification of the solution methods is shown in Fig. 4. Clustering

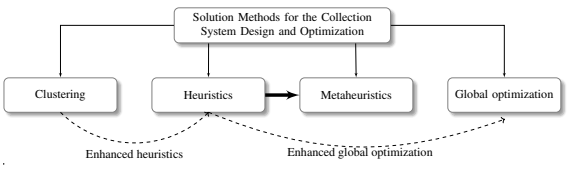

FIGURE 4: OWFs collection systems design and optimization: Solution methods.

techniques split the group of WTs into smaller subgroups, by maximizing the resemblance characteristics among individuals in the same cluster, and minimizing them for two elements belonging to different subgroups; the most used algorithms are [24]: Quality Threshold (QT) (deterministic), K-means, and Fuzzy C-Means (FCM) (both unsupervised machine learning processes). Heuristics are algorithms which sequentially solve a problem by taking decisions in chained steps, such as: Prim [25], Dijkstra [26], Kruskal [27], Esau-Williams (EW) [28], Vogels Approximation Method (VAM) [29], among others, in general following a deterministic manner. Heuristics can be combined with clustering techniques in order to cope with limitations in the former, like cables capacities. Metaheuristics are designed to enhance traditional heuristics for avoiding issues like falling into a local minimals [30], by use of probabilistic criteria for smartly searching the entire design space. Well-acknowledged methods are: Genetic Algorithm (GA) [31], Particle Swarm Optimization (PSO) [32], Simulated Annealing (SA) [33], and Ant Colony Optimization (ACO), Ant Colony System (ACS) [34]. Metaheuristics present a flexible approach and there can be as many formulations as different authors. Lastly, global optimization approaches are more transparent [35], and different formulations have been proposed: Binary Integer Programming (BIP), Mixed Integer Linear Programming (MILP), Mixed Integer Quadratic Programming (MIQP), and Mixed Integer Non-Linear Programming (MINLP); the most efficient formulations are commonly used, since they map to different fields. Global optimization requires external solvers (usually used as black box), which use algorithms such as Branch-and-Cut, or Benders Decomposition [36].

Combining different paradigms lead to new hybrid methods, which mix their strengths in order to palliate the weaknesses. An example of that is merging global optimization with heuristics for accelerating the convergence into global minimum, resulting in new formulations called Matheuristics.

A qualitative comparison between the fundamental versions of the methods is presented in the Table 3. The main functional advantage of heuristics over the other methods is their polynomial running time; this allows for obtaining solution points very quickly. However, typically, those solutions are considerably far away from the global minimum, and robust algorithms proposed so far, optimize mostly for cables total length (L). The stochastic nature of the operators in metaheuristic methods, improve heuristic by offering better quality solutions. Similarly to heuristics, metaheuristics are self-implementable, exluding the need to use external black-box solvers. However, metaheuristics do not quantify the quality of the calculated solutions. In order to cope with the last drawback, global optimization, by means of mathematical programming, provide with a dual value during the computation, which is translated into an assessment of the solution quality. Nonetheless, external solvers are necessitated, and the capacity to model the physics behind is rather limited (inherent to the mathematical program). In function of the priorities established by the developer, any solution method could be categorized as best, hence a clear distinction between brightsides and drawbacks must be delimited prior to the selection of the method.

TABLE 3: OWFs collection systems design and optimization: Qualitative comparison among the methods.

Method	Brightsides	Drawbacks
Heuristics	• Available bound for worst-case behavior. • Polynomial running time. • No need of external solvers.	• Primal bound is mostly weak. • Purpose-built algorithms. • Optimizes mostly for total length.
Metaheuristics	• Frameworks allow high modelling flexibility. • Provides good primal bound. • No need of external solvers.	• No theory on quality and running time. • No worst-case analysis. • Computationally expensive.
Global Optimization	• Dual bound available during computation. • Transparent formulation. • Similar to graph theory problems.	• Uncertainty on computational time and memory. • External solver is required. • Lacks modelling flexibility.

The distribution on the application of these methods in addressing the the OWFs collection systems optimization problem in the scholarly literature (using the web search engine Google Scholar) is presented in Fig. 5. It can be noted that the largest portion of the works apply GA (34%), followed by BIP and MILP global optimization formulations (25%), and heuristics - solely or combined with clustering techniques (19%). Minorities are defined by other metaheuristics and global mathematical modelling types. Different conclusions can be drawn from this illustration. Firstly, GA shapes as the most preferred metaheuristic algorithm, given its flexibility and wide application in different fields [37]. Secondly, due to their fast computation time, heuristics represent a good way of finding initial feasible points. They are also subject to the creativity of the designer to come up with different implementations. Lastly, global optimization represents only the third part of the options spectrum (BIP, MILP, MIQP and MINLP), therefore a significant potential in this area is identified, especially on the proposition of efficient formulations and how to integrate high fidelity models with them. Hybrid methods combining global optimization with heuristics and metaheuristics are scarce (apart of embedded heuristics included in commercial solvers such as [36]), albeit potentially being able to solve large (between 80 and 100 WTs) and very large instances (more than 100 WTs). Consequently, particular focus is directed towards global optimization in this paper.

According to the literature review, the distribution of the objective functions as per the used solution methods is displayed in the Fig. 6. Total length (L), Investment (I), and Investment plus total electrical losses (IL) have been handled using heuristics, metaheuristics, and global optimization methods; on the other hand, when reliability is involved as a target for the system, mathematical formulations emerge as the best approach, due to the flexibility, easiness, and exactness offered by analytical expressions integrated into the framework. Reliability assessment weighted out in the objective function was addressed in [38] through a GA, nevertheless the collection system was based on a grid-based pattern while limiting the possible connections to pre-established alternatives (radial, looped, etc). After selecting the solution method, the modelling choices must be carried out, taking into account the inherent biased caused by the chosen methodology. Mainly five aspects needs to be examined: i) wake effects, ii) wind stochasticity, iii) power flow, iv) electrical losses, and v) reliability, as schematized in Fig. 7. Wake effects are mostly important for micrositing optimization, one of the most used models being the Katic-Jensen, given its linear behaviour and simplicity, as implemented in the pioneer work of; more more advanced and accurate models based on Computational Fluid Dynamics (CFD) are coming up, nonetheless they are expensive computationally and hard to couple with computational optimization techniques. [39]. The impact of wake effect on the collection system optimization has not yet been addressed on the literature, hence assumed to be negligible. Wind stochasticity deals with modelling the wind power production, basically done by applying either discretization of typical probability density functions depending on particular sites [40], or by simulating time series using computational models and historical information

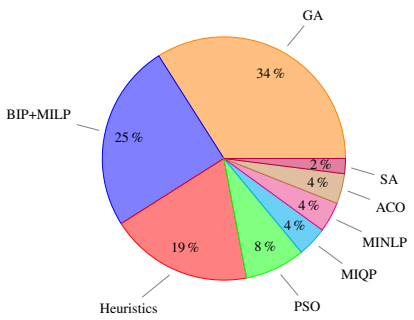

FIGURE 5: OWFs collection systems design and optimization: Distribution of applied methods in the scientific literature.

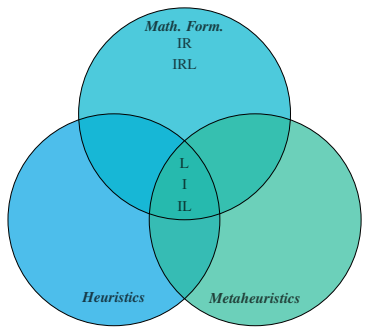

FIGURE 6: OWFs collection systems design and optimization: Applicability of solution methods.

[41]; the main two variables in this matter are wind speed and direction. The effect of change on the wind direction on the collection system optimization has not yet been addressed in the literature. Power flow models, going from low complexity to high complexity are: transportation (Kirchhoff's 2nd law), DCPF (assuming nominal voltages, ignoring losses and reactive power), ACPF (full system of non-linear equations), and Point-to-Point (in-detail transmission line modelling using an infinitesimal lumped model with non-trivial differential equations) [42]. The power flow model drives to different options for modelling the electrical losses, as seen in Fig. 7. In this figure is expressed the interrelation between several blocks. For instance, a DCPF assumes no losses, however they can be computed by doing iterative methods [43]. Likewise, a transportation model can ignore losses or allows integrating it by means of linear or quadratic approximations. AC power flow inherently includes quadratic losses, but can be ignored in the objective function formulation. Point-to-Point flows yield to exact losses calculations [44]. Reliability can be modelled using deterministic and probabilistic approaches [45].

The solution method selection and modelling choice are highly interrelated. Generalizing, mathematical formulations have the enormous advantage of being able to provide certified optimum solutions when the problem is convex; however, their application is subject to the use of commercial solvers, and certain mathematical knowledge of the problem is required for formulating it efficiently and taking advantage of its structure. Therefore, heuristics and metaheuristics can be important because of their easiness in implementation without the need of external solvers using highly efficient programming languages. Additionally, formulations like MILP do not allow explicit (pre-processing techniques can be used as approximation) quadratic modelling of losses (therefore limiting power flow to either DCPF or transportation models), and probabilistic reliability approaches are handled by scenario numeration in a tree fashion, or may be simply ignored. MIQP formulations can include quadratic losses in the objective function, however they are less efficient computationally compared to BIP or MILP. MINLP can capture to a high degree the complexity of the problem, but having the risk of formulating a non-convex problem. On the other hand, heuristics and metaheuristics are more flexible in that sense, due to, in theory, the possibility to consider all the complexity on physical modelling, at expense of not having an optimality guarantee. The proper balance between solution method complexity and model fidelity, represents one of the main challenges for the designer, and compromises have to be adopted within certain assumptions. Each of the different topological network options according to the literature, are discussed in the following, describing the most sound solution methods, modelling choices, and spatial/planarity constraints handling.

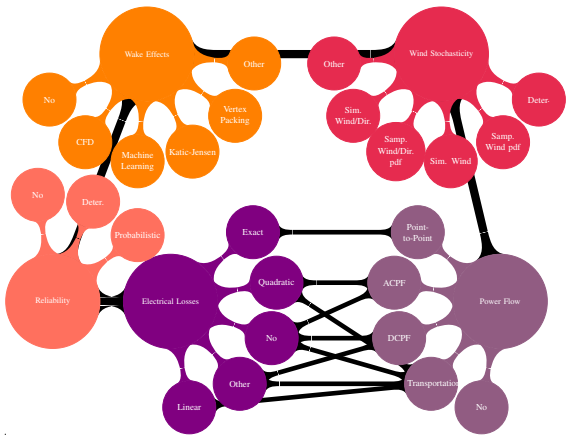

FIGURE 7: OWFs collection systems design and optimization: Modelling choices. The black edges express the relation between different blocks.

1) Radial topology

As presented in Fig. 3, a radial network is that for which branching is not allowed in the nodes corresponding to WTs; mathematically it represents a tree graph with degree equal to 1 or 2 for all vertices belonging to the WTs set. Two publications dealing with this issue are analyzed in the Table 4 and Table 5. Two approaches are developed in [46], one by means of modifications to the probably best-known Vehicle Routing Planning (VRP) heuristic ($\mathcal{O}(|V_c|^2 \log|E| + |E||V_c| + |V_c|C)$), the Clarke and Wright savings, and the other, through the formulation of an BIP model using a straight-forward hop-indexed formulation with planarity constraints (this is very practical for instances where the largest cable capacity C is between 5 and 10 nodes as in OWFs [47]). These two methods were compared in 18 different instances for three OWFs (Barrow with 30 WTs and 1 OSS, Sheringham Shoal with 88 WTs and 2 OSSs, and Walney 1 with 51 WTs and 1 OSS). The BIP model takes up to 20 minutes for solving to optimality all the evaluated instances, while the best heuristic requires less than 0.060 seconds, albeit generating solutions on average 2% more expensive. Those are positive results, however the level of complexity for the models is rather limited, as presented in the Table 4, ignoring wake effects, wind/reliability stochasticity, and power losses. Additionally, the available set of cables is restricted to only 1, and computational experiments point out the escalation on computation time when the capacity C and number of allowed cables are augmented. An important aspect about the heuristics is their inability to optimize the total investment when choosing the cable type, therefore only applying to minimizing total length (L); this limitation is overcome by the BIP formulation. Similar choices are made in [48], but applying a GA algorithm. Comprehensive cost models have been used in this work, encompassing the cost of cables, WTs transformers, and OSSs, however advantages over exact formulations can not be embodied. Nevertheless,

enhancements over heuristics are achieved by including the cable type selection and improving solutions quality. Regarding the spatial and planarity constraints handling, a way to model non-crossing cables for mathematical formulations is by implementing a lazy constraint callback, consisting in stating the corresponding constraints during the construction of the branch-and-cut tree when incumbents are found at any node. By means of this procedure, finding of the maximal cliques in the graph is circumvent. Both works neglect spatial modellings such as seabed bathymetry and restricted zones.

2) Radial plus star topology

A collection system network considering simultaneously radial and star structures is presented in Fig. 3. This problem is equivalent to a C-MST considering the capacitated constraint to be equal to the power capacity of the largest available cable (U), and it is a superset of the radial version. As demonstrated in [31] and [49], branched trees perform better in terms of total trenching length compared to non-branched trees, however the decision of whether permitting branching at WTs or not, from an optimization point of view, depends strongly on the cost models assumed for cables, WTs switchgears, and other electrical components [50]. A comprehensive summary of publications related to this problem is given in Table 6 and Table 7, and based on this survey, it has been identified a lack of consideration about the previous point, meaning papers has not implemented any strategy for accounting these expenses, perhaps due to the scarce information about cost functions of all electrical components involved in the design. Likewise, the impact of wake effects on the electrical collection systems has not yet been addressed applying exact mathematical formulations; this includes the effects of wind direction.

One of the main contributions in [51] is the proposition of heuristics (with proof of admissibility) for optimizing investment of WTs interconnections with multiple cables selection, however being feasible to implement for up to 14 WTs; in this work the exponential time complexity of BIP models is also remarked. Large instances of OWFs collection system design applying heuristic is proposed in [52], taking into consideration cable choices and power losses; nevertheless formalities such as Big $\mathcal{O}$ notation and proofs are dispensed. Metaheuristics have been widely used in the literature, such as the work in [53] where results compared to deterministic heuristics are considerably improved by means of a PSO framework. Exact mathematical formulations encompass basically 4 different types: i) BIP, ii) MILP, iii) MIQP, and iv) MINLP.

BIP and MILP modelling represent the most basic approaches and cover problems instances where is required to optimize length or investment. Many scientists agree on the fact that BIP and MILP present the best balance between solution quality and computation time. The challenge consists on finding efficient strategies for adapting high fidelity models into those programs, for incorporating, for instance, electrical power losses or reliability; pre-processing, decomposition, or heuristics shape up as the way to go to cope with this issue.

The base formulations of BIP and MILP models are presented. These are able to cope with an arbitrary number of WTs, w_n, and considering only one OSS; although with further modifications can be extended for multiple OSSs. Let the OSS define the set $\boldsymbol{N_o}$, such as $\boldsymbol{N_o} = \{1\}$; likewise, for the WTs, $\boldsymbol{N_w} = \{2, \cdots, 1 + w_n\}$. The I^2 norm between points i and j is defined as d_{ij}.

These sets and parameters are condensed as a weighted directed graph $G(\boldsymbol{N}, \boldsymbol{A}, \boldsymbol{D})$, where $\boldsymbol{N}$ represents the vertex set ($\boldsymbol{N} = \boldsymbol{N_o} \cup \boldsymbol{N_w}$), $\boldsymbol{A}$ the set of available arcs arranged as a pair-set, and $\boldsymbol{D}$ the set of associated weights for each element $a_{ij} \in \boldsymbol{A}$, where $i \in \boldsymbol{N} \wedge j \in \boldsymbol{N}$. For instance, for $a_{ij} = (i, j)$, $d = d_{ij}$, where $d \in \boldsymbol{D}$. In general, $G(\boldsymbol{N}, \boldsymbol{A}, \boldsymbol{D})$ is a complete directed graph.

Additionally, a predefined list of available cables types is defined. Let the set of cables be $\boldsymbol{T}$. In this sense, let the capacity of a cable $t \in \boldsymbol{T}$ be u_t (in terms of number of supportable WTs connected downstream). Hence, let $\boldsymbol{U}$ be the set of capacities sorted as in $\boldsymbol{T}$. Furthermore, each cable type t has a cost per unit of length, c_t, in such a way that u_t and c_t describe a perfect positive correlation. The set of metric costs is defined as $\boldsymbol{C}$. In this sense, the parameter c_{ij}^t defines the cost of installing a cable t between i and j. The set $\boldsymbol{\chi}$ stores pairs of arcs $\{(i, j), (u, v)\}$, which are crossing between each other; this constraint also includes the inverse arcs of those elements. This constraint is a practical restriction in order to avoid hot-spots and potential single-points of failure caused by overlapped cables.

BIP

$$\min \sum_{i \in \boldsymbol{N}} \sum_{j \in \boldsymbol{N_w}} \sum_{t=1}^{|\boldsymbol{T}|} \sum_{k=1}^{u_t} c_{ij}^t \cdot y_{ij}^{kt} \tag{1}$$

subject to:

$$\sum_{i \in \boldsymbol{N}} \sum_{t=1}^{|\boldsymbol{T}|} \sum_{k=1}^{u_t} y_{ij}^{kt} = 1 \quad \forall j \in \boldsymbol{N_w} \tag{2}$$

$$\sum_{i \in \boldsymbol{N}} \sum_{t=1}^{|\boldsymbol{T}|} \sum_{k=1}^{u_t} k \cdot y_{ij}^{kt} - \sum_{i \in \boldsymbol{N_w}} \sum_{t=1}^{|\boldsymbol{T}|} \sum_{k=1}^{u_t} k \cdot y_{ji}^{kt} = 1 \quad \forall j \in \boldsymbol{N_w} \tag{3}$$

$$x_{ij} + x_{ji} + x_{uv} + x_{vu} \leq 1 \quad \forall \{(i, j), (u, v)\} \in \boldsymbol{\chi} \tag{4}$$

$$\sum_{t=1}^{|\boldsymbol{T}|} \sum_{k=1}^{u_t} y_{ij}^{kt} - x_{ij} \leq 0 \quad \forall (i, j) \in \boldsymbol{A} \tag{5}$$

$$x_{ij} \in \{0, 1\} \quad y_{ij}^{kt} \in \{0, 1\} \quad \forall (i, j) \in \boldsymbol{A} \wedge t \in \{1, \cdots, |\boldsymbol{T}|\} \wedge k \in \{1, \cdots, u_t\} \tag{6}$$

MILP

$$\min \sum_{i \in \boldsymbol{N}} \sum_{j \in \boldsymbol{N_w}} \sum_{t=1}^{|\boldsymbol{T}|} c_{ij}^t \cdot y_{ij}^t \tag{7}$$

TABLE 4: Radial Collection Systems Papers: Objective, Solution Method, and Modelling Choices

Objective	Solution Method	Wake Effects	Wind Stochasticity	Power Flow	Elect. Losses	Reliability	Paper
L	Heuristics: Modified Clarke and Wright	No	Deterministic	Transportation	No	No	[46]
I	Global optimization: BIP hop-indexed	No	Deterministic	Transportation	No	No	
I	Metaheuristic: GA	No	Deterministic	Transportation	No	No	[48]

TABLE 5: Radial Collection Systems Papers: Spatial and Planarity constraints handling

Seabed bathymetry	Non-crossing cables	Restricted zones	Paper
No	Lazy Constraint Callback	No	[46]
No	No	No	[48]

subject to:

$$\sum_{i \in \boldsymbol{N}} f_{ij} - \sum_{i \in \boldsymbol{N_w}} f_{ji} = 1 \quad \forall j \in \boldsymbol{N_w} \tag{8}$$

$$\sum_{i \in \boldsymbol{N}} \sum_{t=1}^{|\boldsymbol{T}|} y_{ij}^t = 1 \quad \forall j \in \boldsymbol{N_w} \tag{9}$$

$$\sum_{t=1}^{|\boldsymbol{T}|} u_t \cdot y_{ij}^t \geq f_{ij} \quad \forall (i,j) \in \boldsymbol{A} \tag{10}$$

$$x_{ij} + x_{ji} + x_{uv} + x_{vu} \leq 1 \quad \forall \{(i,j),(u,v)\} \in \boldsymbol{\chi} \tag{11}$$

$$\sum_{t=1}^{|\boldsymbol{T}|} y_{ij}^t - x_{ij} \leq 0 \quad \forall (i,j) \in \boldsymbol{A} \tag{12}$$

$$f_{ij} \geq 0 \quad x_{ij} \in \{0,1\} \quad y_{ij}^t \in \{0,1\} \quad \forall (i,j) \in \boldsymbol{A} \wedge t \in \{1, \cdots, |\boldsymbol{T}|\} \tag{13}$$

The main features of the basic BIP formulation are:

- Variables: Two set of binary variables are required. On the one hand, x_{ij} is equal to one if an arc with head in j is selected; on the other hand, y_{ij}^{kt} is one if the arc (i,j) is selected, using the cable type t and connecting k WTs downstream (including the one in j). Thus, the worst-case maximum number of variables is $|\boldsymbol{N}|^2 + U \cdot |\boldsymbol{T}| \cdot |\boldsymbol{N}|^2$.
- Constraints: Constraint (2) permits keeping the topology of the solution, and selecting only one cable type per arc. Constraint (3) is the flow conservation equation, this along with the variables definition, allows for respecting the cables capacity constraints. Constraint (4) and Constraint (5) avoid the use of crossing cables. Finally Constraint (6) defines the variables type. Excluding the crossing constraints which are not fundamental restrictions, the number of constraints is given by $2 \cdot |\boldsymbol{N_w}|$.
- Flexibility: In this context flexibility is defined as the capability to reformulate the objective function without altering the nature of the whole formulation, if total electrical active losses are required to be optimized simultaneously with investment (IL). In this case the following term can be added into the objective (1):

$$\sum_{i \in \boldsymbol{N}} \sum_{j \in \boldsymbol{N_w}} \sum_{t=1}^{|\boldsymbol{T}|} \sum_{k=1}^{u_t} 3 \cdot d_{ij} \cdot R_t \cdot k^2 \cdot I_n^2 \cdot y_{ij}^{kt} \cdot w_f$$

  where R_t is the resistance per unit of length of cable t, I_n is the nominal current of a single WT, and w_f is the weighting factor to quantify the losses in the same domain as the investment.

Correspondingly, the features of the basic MILP formulation are:

- Variables: Three set of variables are required. f_{ij} is linear and models the flow in the arcs, x_{ij} is one if the arc (i,j) is considered in the solution, and y_{ij}^t if a cable t is used in that arc. Thus, the worst-case maximum number of variables is $2 \cdot |\boldsymbol{N}|^2 + |\boldsymbol{T}| \cdot |\boldsymbol{N}|^2$.
- Constraints: The Constraint (8) is the flow conservation equation, and avoids also cycles (loops). Constraint (9) allows keeping the topology of the solution. Constraint (10) ensures not exceeding the cables capacity. Constraint (11) and Constraint (12) avoid the use of crossing cables. Constraint (13) defines the variables type. The number of fundamental constraints is $|\boldsymbol{N}|^2 + 2 \cdot |\boldsymbol{N_w}|$.
- Flexibility: There is no possibility to include total electrical active losses without reformulating the model. By including a quadratic term utilizing the flow variables, a MIQP formulation can be obtained; additionally, a linear loss function can be considered and through the multiplication of y_{ij}^t and f_{ij} a MINLP model is formulated (may be linerizable).

Comparing the basic BIP and MILP formulations, one can conclude that the number of variables are in the same order, whilst the number of constraints are considerable less in BIP than in MILP. Other important advantage of the binary formulation over the mixed one, is its flexibility to be adapted for IL problems. The advantage of modelling explicitly the flow in the arcs in MILP formulations may be useful when trying to optimize taking into account the wake losses in the WTs, when different WTs models are considered, and when including the active power losses in the computation of upstream WTs.

It must be stated that further simplification to both models can be proposed, either by strategies to reduce the number

of variables [54], by means of pre-processing techniques, or by adding valid inequalities or cuts [55]. Particularly, it has been shown in [56] how to include total active losses using a MILP formulation through pre-processing, and how to smartly limit the search space to speed up the termination under certain optimality conditions. These hybrid methods combining classical global optimization with heuristics rules are called Matheuristics.

It is still an open research question to prove analytically in this context which formulation is better than the other. Given a set $X \subseteq R^n$, and two formulations P_1 and P_2 for X, P_1 is a **better formulation** than P_2 if $P_1 \subset P_2$ [57]. This means that if P_1 is a strict subset of P_2, then P_1 is a better formulation than P_2 because the feasible set is smaller. Suppose P_1, P_2 are two formulations for the program: $min\{cx : x \in Z^n\}$ with P_1 a better formulation than P_2. If $z_i^{LP} = min\{cx : x \in P_i\}$ for $i = 1, 2$ are the values of the associated linear programming relaxations, then $z_1^{LP} \geq z_2^{LP}$. Nevertheless the required solution time and memory capacities for both programs may not have any link with this fact, given the unpredictability of combinatorial problems. Further experiments need to be implemented to come up with a representative statistical sample to infer about which formulation solves more efficiently.

Another action to include losses in a linear model is by an iterative method as in [43], where the structure of the problem is exploited by Benders' Decomposition reducing drastically computation time. Wind power stochasticity and reliability can be included in linear formulations with scenario numeration as in [43] and [45], where a Markov model is used to calculate the states probabilities of cables, and finally a tree is formed numbering all possible operating scenarios. The latter opened the door for stochastic optimization in the collection system problem, concepts that is also applied in transmission expansion planning, or unit commitment, for example. The model is formulated as a two-stage stochastic problem, where the first-stage variables represent the set of connections to build, and the second ones power and energy curtailment. The resulting system considers parallel cables installed in the same trench, which is not common in practice.

MIQP formulation permits including quadratic approximation of electrical losses embedded in the optimization model, incorporating probabilistic modelling of the stochasticity of wind and reliability in the same framework, but its computational efficiency is low compared to linear formulations [58], and is dependant on the positive semidefinite nature of the objective function to be a convex problem.

Finally, a MINLP formulation [59] captures the full complexity of wind stochasticity, power flow and electrical losses, and with Benders decomposition solving iteratively a master and subproblems, the feasibility of the final solution may be obtained by adding constraints. The main drawback is the non-convex nature of these problems and the possibility to fall into local minimals.

Modelling the complexity of terrains initially by a WRP in onshore cases (see Table 7) is proposed in [51], where the terrain is modelled as a grid and each cell is attributed with a coefficient to modify the cables' length. This may be the way to go in OWFs. For exact mathematical formulations the most used way to add up cables crossing constraints is by following the explained lazy constraint callback approach, although additional experiments are required to infer about the possibility to exploit these constraints as valid inequalities in small problem instances; concerning metaheuristics, penalization strategies when dectecting the crossings using specialized algorithms such as Bentley-Ottmann [64] are generally applied.

Modelling restricted zones is transparently achieved by adding up fixed edges in order to approximate the areas with polygons as in [56] and [61]. The main disadvantage of the latter is that for complex shapes useful areas can be disconsidered forcing the final solution to be non-optimal, therefore in [62] (linearized MINLP) a more detailed approach with Delaunay triangulation and shortest path algorithms is proposed [65].

3) Radial plus star plus splices topology

Collection systems with optional intermediate nodes (splices for connecting cables outside of WTs switchgears) is illustrated in Fig. 3. An exhaustive handbook of Steiner tree problems is available in [66] for NP-Complete variants. Currently there are no OWFs implementing this approach, not even under planning stage, however it is presented in this paper as a way to show its applicability from an academic perspective. Steiner tree formulation has been used in [67], [68], and [69]. In all these articles, the objective function is the total trenching length of cables, this being the biggest advantage of Steiner tree formulations. However, this does not necessarily means that the total investment cost is optimized. Likewise, all these articles use greedy heuristics for solving the problem, which provide good solutions but without proofs of correctness and optimality. Regarding modelling choices the simplest approaches were chosen: no wakes, deterministic wind speed, transportation power flow, and no reliability considered, since the adopted solution methods were not tailored for OWFs application.

4) Single looped topology

London Array OWF described in Table 1 follows a single looped collection system pattern as the one presented in Fig. 3. Tailored methods for single looped design have been proposed in [70] and [71]. A set of different algorithms combined and nested are used in [70] in a hierarchical fashion, having as most internal block a Multiple Traveling Salesman Problem (MTSP) solver, which is an extension of the classical Travelling Salesman Problem (TSP), but with M salesmen $\{s_1 \cdots s_M\}$ who have to visit each c_i cities $\{c_1 \cdots c_M\}$. There are plenty of heuristics to obtain good quality solutions for the TSP, as Farthest Insertion algorithm and the Chained Lin Kernigan algorithm [72]; the latter presents a gap with the Held-Karp lower bound of 0.2%. The objective function of this particular sub-problem is the

TABLE 6: Radial plus Star Collection Systems Papers: Objective, Solution Method, and Modelling Choices

Objective	Sol. Method	Wake Effects	Wind Stoch.	Power Flow	Elect. Losses	Reliability	Paper
IRL	Global optimization: MILP Benders' Decomposition	No	Sampling Wind pdf	DCPF	Other: Iterative	Probabilistic	[43]
IL	Global optimization: MILP: Matheuristics	No	Sampling Wind pdf	Transportation	Other: Preprocessing	No	[56]
I	Heuristics: Backtracking. Divide-and-Conquer	No	Deterministic	Transportation	No	No	[51]
I	Global optimization: BIP hop-indexed	No	Deterministic	Transportation	No	No	
IL	Heuristics: Modified Prim	Katic-Jensen	Simulation Wind	Transportation	Quadratic	No	[52]
I	Metaheuristics: PSO	No	Deterministic	Transportation	No	No	[53]
I	Global optimization: MILP hop-indexed	No	Deterministic	Transportation	No	No	[60]
I	Global optimization: BIP hop-indexed	No	Deterministic	Transportation	No	No	[49]
I	Global optimization: BIP hop-indexed	No	Deterministic	Transportation	No	No	[61]
IL	Global optimization: MINLP	No	Deterministic	Transportation	Linear	No	[62]
IL	Global optimization: MINLP Benders' Decomposition	No	Simulation Wind	ACPF	Quadratic	No	[59]
L	Heuristics: Enhanced MST.	No	Deterministic	Transportation	No	No	[63]
IL	Global optimization: BIP basic hop-indexed/BIP reformulated hop-indexed	No	Deterministic	Transportation	Other: Preprocessing	No	[54]
IRL	Global optimization: MIQP	No	Sampling Wind pdf	Transportation	Quad.	Probabilistic	[45]

TABLE 7: Radial plus Star Collection Systems Papers: Spatial and Planarity constraints handling

Seabed bathymetry	Non-crossing cables	Restricted zones	Paper
No	No	No	[43]
Weighted Region Problem (WRP)	No	No	[51]
No	Lazy Constraint Callback	Steiner nodes	[56]
No	No	No	[52]
No	No	No	[53]
No	No	No	[60]
No	Lazy Constraint Callback	No	[49]
No	Lazy Constraint Callback	Steiner nodes	[61]
No	Lazy Constraint Callback	Delaunay triangulation/Shortest Path	[62]
No	No	No	[59]
No	No	No	[63]
No	No	No	[54]
No	No	No	[45]

cable's total trenching length and the simplest modelling options are considered. Special attention must be paid to the forbidding of cables crossing, which must be also handled by the strategy for clustering the feeders.

5) Others topologies

The proposition of different types of topologies not mapping to mathematical formulations, but carried out following particular criteria of the OWF developers, has also been adressed in the literature, in articles such as [73], [74], and [75]. Those designs are the result of a case-by-case analysis where limited networks are studied by means of economics, power flow, reliability, and dynamic analyses, applying specialized software. The main output of these studies is the best topology for a particular OWF from a set of finite self-designed networks. Examples of these special designs are: star design, single-sided ring design, combined double-sided half design, single-sided ring design, modified double-sided half ring design, and others.

B. WT ALLOCATION TO OSS

In Section II-A, the assumption is that there is only 1 OSS with a specified geographical location. In this Section, we consider one step up in the complexity layer (bottom-up approach): Given a large OWF with pre-defined number of OSSs (greater than 1) and WTs (typically greater than 100 WTs), with given geographical locations, design the collection systems in such a way, that a WT is allocated unequivocally only to one OSS (i.e., no direct electrical coupling from one WT to more than one OSS), while guaranteeing the OSSs capacities (in terms of nominal power) are not exceeded.

To solve this, there are three alternatives: i) a single approach, where this is solved simultaneously with the collection system problem, ii) a multi-step approach, where as a first step the WTs are clustered, and then each WTs-OSS problem is solved individually by means of one of the methods explained in the previous Section, or iii) a nested approach, which basically consists on an iterative calculation process, where in the outer loop the WTs allocation problem is addressed, and in the inner loop in turn the collection system is tackled.

In the single approach, mathematical formulations can be used transparently to leave the optimization set up to deal with the full problem, as in [46] or [56], however, for large OWFs this may be computationally expensive as presented in [51]. Nevertheless this is the exact way to solve the problem to optimality. Given the flexibility of metaheuristics methods, they can be easily designed to handle this issue, but due to the combinatorial complexity it may be challenging to be adapted as explained in [31]. Using a multi-step approach helps handling the problem complexity, with two ways to split up the WTs in OSSs groups: a) mathematically, by formulating the problem using network theory, for instance as a Minimum Cost Flow Problem (MCFP) [76], or b) by applying clustering algorithms like QT, K-means, FCM, among others. MCFP allows shaping the problem with an BIP mathematical formulation, and the network simplex algorithm can be applied to solve it to optimality by exploiting the problem structure and the duality conditions. Finally, an iterative approach similar to the one used in [63], where using pattern search, the WTs clustering can be updated based on iterative calculations of collection systems searching for a cheaper solutions.

C. NUMBER AND LOCATION OF OSS

In the Section II-B it was considered the number and location of OSSs are defined as inputs, however, when these points are part of the decision-making problem, there are different alternatives to go through it. As a generalization, authors have regarded this problem including the WTs allocation to OSSs, therefore one could consider it as a variant with the added complexity of deciding the OSSs number and geographical location. Three different alternatives of this problem have been found: i) variable OSSs number and variable OSSs location, ii) fixed OSSs number and variable OSSs location, and iii) variable OSSs number and fixed OSSs position.

Variable number and location of OSSs has been coped by means of a multi-step approach in [77] (MILP formulation), [78] (GA), [79] (FCM plus Prim algorithm), and [80] (immune GA). The work of [77] may be the first work dealing with this issue (onshore case) using mathematical models, dividing the full problem into wind farm production optimization model, and wind farm infrastructure optimization model; the potentials of MILP formulations for solving this problem were pointed out, although basic physical modelling choices were selected. The impact of different number and location of OSSs is studied in [78], but the set of potential alternatives were rather limited, and the collection system is assumed to be symmetrically distributed in terms of WTs. A FCM algorithm for clustering WTs into OSSs and finding their location considering the shapes centroid (the maximum number of OSSs must be pre-defined), followed by a FCM algorithm to group the WTs into feeders is used in [79]. Listing heuristically the possible set of OSSs number is carried out in [80], this is accompanied by the subsequent design of the WTs collection system. A nested approach has been applied in [32] and in [70]. An external layer using a PSO algorithm, deciding the number of OSSs and location, is designed with an internal layer clustering the WTs into OSS groups by means of a FCM algorithm in [32]. In every iteration the OSSs number and location are updated and this is followed by an internal recalculation of the WTs division and collection system. Likewise, a nested hierarchical design is proposed in [70].

Fixed OSSs number with variable position is more typically integrated in single approaches using mathematical formulations like in [43], and [81], although of course using metaheuristics is also possible. A multi-step approach is proposed in [62], where a Capacitated Centred Clustering Problem (CCCP) and a heuristic is used to find the OSS location. Lastly, a nested approach can be found in [63].

Variable OSSs number with fixed position is not so common, the work in [82] is considered to follow this procedure, because it is clear the number of OSSs is encoded in the GA but not their positioning, therefore it is assumed they are fixed.

D. INTERCONNECTION OF OSS TO OCP

Let divide this problem into two variants: i) point-to-point interconnection between a single (or few) OSS to a single (or few) OCP, and ii) interconnection between multiple OSSs and multiple OCPs (large OWFs spread out in a large area).

Regarding the first problem, it basically consists on finding the proper balance between the collection system design (including the OSS positioning), and the transmission system design (export system to connect the OSS to the OCP), given that the shorter distance between OSS to OCP, the more expensive the collection system, but the cheaper the transmission system. Most of the authors assume negligible the influence of OSSs location to the transmission system costs inside of a given range. Nevertheless, in works like [83] (onshore case), [84], multi-fidelity and heuristics approaches, respectively, are considered to analyze the trade-off between

these two costs. Other works taking into consideration simultaneously the collection system design (with OSSs location), and the transmission system design are: [43], [32], [85], [70], [82], [86], [87], and others.

When the problem is seen from a broader perspective, the interconnection between multiple OSSs and multiple OCPs gets more interesting. In this case, the OWFs are seen in an aggregated way, disconsidering the collection system design and calculating the total installed power of the OWF. A GA algorithm to support decision-makers about OWF transmission system developing, and long-term offshore grid planning is proposed in [88]; in this work, the objective is to provide a ranking sorted by their total lifetime costs, of different electrical options to interconnect OWFs between each other, and to OCPs, using either HVAC or HVDC technology, and supporting radial, ring, and meshed designs. At the end, decisions of whether new connections or reinforcements in the onshore grid are required are also provided. One of the main disadvantages of this work is that the implementation has to be improved to apply the developed methodology to larger power systems, and also other types of technologies for electricity generation are not considered, which can be very important for a holistic offshore grid planning. The latter aspects has been handled in the series of publications [89], [90], and [91]. A MILP model to solve the transmission expansion problem accounting for fluctuations in wind power generation and load is proposed in [89], where not only offshore energy is considered, but also other types such as hydro, gas, among others. The tool helps to decide about the feasibility to install DC breakers compared to AC breakers in meshed systems. This work was extended in [90] including clustering of OWFs into larger groups in order to reduce computation time, followed by an offshore grid optimization. The tool seeks to find a balance between new OWFs project and the integration with new or reinforced interconnectors between countries, while having present other types of electricity generation connected to OCPs. Lastly, the designed tool was applied to the case study of Baltic Sea in the time horizon 2030 in [91]. Main results indicate that radial connections are preferred when OWFs are highly scattered between each other, in contrast to meshed grids, which are more benefitial for agglomerated OWFs in a given area. The latest works can be improved considering optimal power flow (AC or DC), and integrating more sophisticated platforms to forecast the energy produced in different time horizons.

III. CONCLUSIONS

A detailed review regarding the optimization of electrical cables in Offshore Wind Farms (OWFs) is carried out in this article. As a result, the full picture of the problem is divided in two main branches: optimum sizing of electrical cables, and network optimization.

Regarding the former, the three main techniques available today in the industry practices and scientific literature are presented. They span from a lower to higher level of complexity as follows: static rated sizing, dynamic load cycle profile, and dynamic analysis with full time series. The most commonly used one today is the dynamic load cycle profile, given its simplicity and representability of more realistic power generation scenarios. It intends to exploit the high variability and low capacity factor of the power production (no superior to 50%). Likewise, the third technique embodies an important topic that is shaping up as crucial: Dynamic rating of electrical components; further studies through this technique yields to lifetime estimation, which can be done offline with models calibrated in laboratories, or online by sensing in real time variables such as power, external temperature, or mechanical stresses. In order to do so, novel models encompassing thermal analysis of cables (extendable to other electrical components), including detailed physical components modelling, while not compromising the computation requirements, are necessitated. Development of lifetime models of electrical cables represents an important research area, investigating the impact of real static and dynamic operation conditions, such as total length, and system's dynamics.In general, one can say that the trend is towards combining dynamic sizing with lifetime estimation, ensuring that the chosen solution does not adversely impacts either.

Related to topological network optimization, the cable layout in collection system sub-problem is envisaged to be addressed by applying BIP and/or MILP formulations, given that this approach brings a proper balance between solution quality and computation time, with a physical modelling choices inside of a permitted level of complexity. In the reviewed works applying this methodology, it was not found the inclusion of wake effects, and the power losses are computed either by pre-processing strategies, linearization, or iterative processes. Models with dynamic location of Offshore Substations are required. Details experiments for assessing the efficiency between different mathematical programs are highly encouraged. Given the trend in OWFs towards larger and larger projects, focus must be directed into this aspect, by proposing methodologies able to provide solutions in reasonable computation time.

There is also space for new global optimization formulations including a probabilistic approach for reliability assessment to obtain looped networks, instead of installing parallel cables in the same trench. The effects of the Wind Turbines (WT) fatigue over the cable layout design is becoming increasinglyh important. More elaborated cost models are required as well, including more components: cables, transformers, switchgears, and installation costs. None of the reviewed works deal with modelling the seabed bathymetry, which can have a great impact over final collection systems as this can significantly impact the cables' length. Case studies comparing the new proposed collection system voltage (66 kV) with the classic one (33 kV) can be interesting as well. In the impossibility to use external solvers (hence exact mathematical formulations), metaheuristics seem to be the best choice to solve this problem stage, despite the fact the door is open for designing heuristics with cable choice and

accounting for electrical losses, with time and quality bound proofs. The full picture of the topological network optimization has been addressed until today, by means of multi-step and nested approaches, however evolutionary algorithms mixed with mathematical formulations might be an appealing option.

Finally, the two branches can be combined, for instance, a resultant collection system network can use dynamic rating with probabilistic lifetime models of cables for sizing such elements, in order to provide a more tuned stage after the convergence of combinatorial algorithms.

ACKNOWLEDGMENT

This research has received funding from the Baltic InteGrid Project http://www.baltic-integrid.eu/. Authors thank Prof. Poul Sørensen, Dr. Kaushik Das and Prof. Mathias Stolpe for their contributions to the development of the manuscript.

REFERENCES

[1] GWEC, "Global Wind Report. Annual Market Update 2017," Tech. Rep., 2017. [Online]. Available: http://gwec.net/publications/global-wind-report-2/.[AccessedOct29,2018]

[2] International Renewable Energy Agency, "Innovation Outlook: Offshore Wind, Summary for Policy Makers," p. 16, 2016.

[3] X. Sun, D. Huang, and G. Wu, "The current state of offshore wind energy technology development," Energy, vol. 41, no. 1, pp. 298–312, 2012.

[4] ReNEWS, "Rampion suffers cable fault," 2017. [Online]. Available: http://renews.biz/105889/rampion-suffers-cable-fault/.[AccessedOct29,2018]

[5] RenewableUK, "RenewableUK - Project Intelligence," 2018. [Online]. Available: https://www.renewableuk.com/page/ProjectIntelligenceHome. [AccessedMarch3,2019]

[6] S. Lumbreras and A. Ramos, "Offshore wind farm electrical design: a review," Wind Energy, vol. 16, pp. 459–473, 2013.

[7] W. Offshore, "Decommissioning of world's first offshore site now complete," 2017. [Online]. Available: https://www.windpowermonthly.com/article/1443779/video-decommissioning-worlds-first-offshore-site-complete. [AccessedNov07,2018]

[8] J. Herbert-Acero, O. Probst, P.-E. Réthoré, G. Larsen, and K. Castillo-Villar, "A Review of Methodological Approaches for the Design and Optimization of Wind Farms," Energies, vol. 7, no. 11, pp. 6930–7016, 2014.

[9] M. Koivisto, K. Das, F. Guo, P. Sørensen, E. Nuño Martinez, N. A. Cutululis, and P. Maule, "Using time series simulation tool for assessing the effects of variable renewable energy generation on power and energy systems," WIREs Energy and Environment, no. June, pp. 1–15, 2018.

[10] IEC, "IEC-60287-1: Electric cables - Calculation of the current rating," Tech. Rep., 2014. [Online]. Available: https://www.evs.ee/products/iec-60287-1-1-2006.[AccessedApril15,2019]

[11] ——, "IEC-60853-2: - Calculation of the cyclic and emergency current rating of cables," Tech. Rep., 2008.

[12] CIGRÉ, "Current Ratings of Cables for Cyclic and Emergency Loads. Part 1. Cyclic Ratings (Load Factor Less Than 100%) and Response to a Step Function," Tech. Rep. 24, 1976.

[13] CIGRÉ: Working Group B1.40, "Offshore Generation Cable Connections," Tech. Rep. 1, 2015.

[14] T. Kvarts, "Systematic Description of Dynamic Load for Cables for Offshore Wind Farms. Method and Experience," CIGRÉ, pp. 1–13, 2016.

[15] S. Catmull, R. D. Chippendale, J. A. Pilgrim, G. Hutton, and P. Cangy, "Cyclic Load Profiles for Offshore Wind Farm Cable Rating," IEEE Transactions on Power Delivery, vol. 31, no. 3, pp. 1242–1250, 2016.

[16] R. Chippendale, J. Pilgrim, A. Kazerooni, and D. Ruthven, "Cyclic rating of wind farm cable connections," CIRED - Open Access Proceedings Journal, vol. 2017, no. 1, pp. 91–95, 2017.

[17] R. Olsen, "Dynamic Loadability of Cable Based Transmission Grids," Ph.D. dissertation, Technical University of Denmark, 2013.

[18] D. Chatzipetros and J. A. Pilgrim, "Review of the Accuracy of Single Core Equivalent Thermal Model for Offshore Wind Farm Cables," IEEE Transactions on Power Delivery, vol. 33, no. 4, pp. 1–1, 2017.

[19] M. A. H. Colin and J. A. Pilgrim, "Offshore Cable Optimization by Probabilistic Thermal Risk Estimation," in IEEE International Conference on Probabilistic Methods Applied to Power Systems (PMAPS). IEEE, 2018, pp. 1–6.

[20] T. Zarei, K. Morozovska, T. Laneryd, P. Hilber, M. Wihlén, and O. Hansson, "Reliability considerations and economic benefits of dynamic transformer rating for wind energy integration," International Journal of Electrical Power and Energy Systems, vol. 106, no. December 2017, pp. 598–606, 2019.

[21] R. Jothi and B. Raghavachari, "Approximation algorithms for the capacitated minimum spanning tree problem and its variants in network design," ACM Transactions on Algorithms (TALG), vol. 1, no. 5, pp. 265–282, 2005.

[22] E. L. Lawler, "The traveling salesman problem: a guided tour of combinatorial optimization," Wiley-Interscience Series in Discrete Mathematics, 1985.

[23] A. Kershenbaum, "Computing capacitated minimal spanning trees efficiently," Networks, vol. 4, no. 4, pp. 299–310, 1974.

[24] A. Saxena, M. Prasad, A. Gupta, N. Bharill, O. P. Patel, A. Tiwari, M. J. Er, W. Ding, and C.-T. Lin, "A review of clustering techniques and developments," Neurocomputing, vol. 267, pp. 664–681, 2017.

[25] R. C. Prim, "Shortest Connection Networks And Some Generalizations," Bell System Technical Journal, vol. 36, no. 6, pp. 1389–1401, 1957.

[26] E. W. Dijkstra, "A note on two problems in connexion with graphs," Numerische mathematik, vol. 1, no. 1, pp. 269–271, 1959.

[27] J. B. Kruskal, "On the Shortest Spanning Subtree of a Graph and the Traveling Salesman Problem," Proceedings of the American Mathematical Society, vol. 7, no. 1, pp. 48–50, 1956.

[28] L. R. Esau and K. C. Williams, "On teleprocessing system design, Part II: A method for approximating the optimal network," IBM Systems Journal, vol. 5, no. 3, pp. 142–147, 1966.

[29] K. M. Chandy and R. A. Russell, "The Design or Multipoint Linkages in a Teleprocessing Tree Network," IEEE Transactions on Computers, vol. 100, no. 10, pp. 1062–1066, 1972.

[30] P. R. M. Duailibe, T. T. Borges, A. F. Schiochet, and C. A. P. Soares, "Impact of the Objective Function on the Construction of Internal Grids of Wind Farms Using Genetic Algorithm," Open Journal of Civil Engineering, vol. 06, no. 05, pp. 705–721, 2016.

[31] A. M. Jenkins, M. Scutariu, and K. S. Smith, "Offshore wind farm inter-array cable layout," in IEEE PowerTech at Grenoble, 2013, pp. 1–6.

[32] P. Hou, W. Hu, Z. Chen, and C. Chen, "Overall Optimization for Offshore Wind Farm Electrical System," Wind Energy, vol. 20, no. 2016, pp. 1017–1032, 2017.

[33] S. Lehmann, I. Rutter, D. Wagner, and F. Wegner, "A Simulated-Annealing-Based Approach for Wind Farm Cabling," in Proceedings of the Eighth International Conference on Future Energy Systems, 2017, pp. 203–215.

[34] J. Nedlin, "Ant-based Algorithms for the Wind Farm Cable Layout Problem Bachelor Thesis of," no. January, 2017.

[35] A. Wędzik, T. Siewierski, and M. Szypowski, "A new method for simultaneous optimizing of wind farm's network layout and cable cross-sections by MILP optimization," Applied Energy, vol. 182, pp. 525–538, 2016.

[36] IBM, "IBM ILOG CPLEX Optimization Studio CPLEX User Manual," Tech. Rep., 2015. [Online]. Available: https://www.ibm.com/support/knowledgecenter.[AccessedApril11,2019]

[37] K. Deb, Optimization for engineering design: Algorithms and examples. PHI Learning Pvt. Ltd., 2012.

[38] M. Zhao, Z. Chen, and F. Blaabjerg, "Application of genetic algorithm in electrical system optimization for offshore wind farms," in Proceedings of Third International Conference on Electric Utility Deregulation and Restructuring and Power Technologies (DRPT), 2008, pp. 1–6.

[39] G. Mosetti, C. Poloni, and D. Diviacco, "Optimization of wind turbine positioning in large wind farms by means of a Genetic algorithm. J Wind Eng Ind Aerody 51:105–116," Wind Engineering and Industrial Aerodynamics, vol. 51, no. 51, p. 105–116, 1994.

[40] J. Serrano González, M. Burgos Payán, and J. Riquelme Santos, "Optimum design of transmissions systems for offshore wind farms including decision making under risk," Renewable Energy, vol. 59, pp. 115–127, 2013.

[41] L. Amaral and R. Castro, "Offshore wind farm layout optimization regarding wake effects and electrical losses," Engineering Applications of Artificial Intelligence, vol. 60, no. November 2016, pp. 26–34, 2017.

[42] J. J. Grainger and W. D. J. Stevenson, Power System Analysis, 2nd ed. McGraw-Hill Education, 1994.

[43] S. Lumbreras and A. Ramos, "Optimal design of the electrical layout of an offshore wind farm applying decomposition strategies," IEEE Transactions on Power Systems, vol. 28, no. 2, pp. 1434–1441, 2013.

[44] H. Brakelmann, "Loss Determination for Long Three-Phase High-Voltage Submarine Cables," European Transactions on Electrical Power, vol. 13, no. 3, pp. 193–197, 2003.

[45] M. Banzo and A. Ramos, "Stochastic Optimization Model for Electric Power System Planning of Offshore Wind Farms," IEEE Transactions on Power Systems, vol. 26, no. 3, pp. 1338–1348, 2011.

[46] J. Bauer and J. Lysgaard, "The offshore wind farm array cable layout problem: A planar open vehicle routing problem," Journal of the Operational Research Society, vol. 66, no. 3, pp. 360–368, 2015.

[47] M. T. Godinho, L. Gouveia, and T. L. Magnanti, "Combined route capacity and route length models for unit demand vehicle routing problems," Discrete Optimization, vol. 5, no. 2, pp. 350–372, 2008.

[48] F. M. González-Longatt, P. Wall, P. Regulski, and V. Terzija, "Optimal electric network design for a large offshore wind farm based on a modified genetic algorithm approach," IEEE Systems Journal, vol. 6, no. 1, pp. 164–172, 2012.

[49] A. Klein, D. Haugland, J. Bauer, and M. Mommer, "An integer programming model for branching cable layouts in offshore wind farms," in Modelling, Computation and Optimization in Information Systems and Management Sciences, vol. 1, 2015, pp. 27–36.

[50] M. Fischetti and D. Pisinger, "Mixed Integer Linear Programming for new trends in wind farm cable routing," Electronic Notes in Discrete Mathematics, vol. 64, pp. 115–124, 2018.

[51] C. Berzan, K. Veeramachaneni, J. McDermott, and U.-M. O'Reilly, "Algorithms for cable network design on large-scale wind farms," Tech. Rep., 2011. [Online]. Available: https://thirld.com/files/msrp_techreport.pdf.[AccessedApril15,2019]

[52] P. Hou, W. Hu, C. Chen, and Z. Chen, "Optimisation of offshore wind farm cable connection layout considering levelised production cost using dynamic minimum spanning tree algorithm," IET Renewable Power Generation, vol. 10, no. 2, pp. 175–183, 2016.

[53] P. Hou, W. Hu, and Z. Chen, "Optimisation for offshore wind farm cable connection layout using adaptive particle swarm optimisation minimum spanning tree method," IET Renewable Power Generation, vol. 10, no. 5, pp. 694–702, 2016.

[54] A. Cerveira, A. F. de Sousa, E. J. Pires, and J. Baptista, "Optimal Cable Design of Wind Farms: The Infrastructure and Losses Cost Minimization Case," IEEE Transactions on Power Systems, vol. 31, no. 6, pp. 4319–4329, 2016.

[55] L. Gouveia and P. Martins, "The capacitated minimum spanning tree problem: revisiting hop-indexed formulations," Computers & operations research, vol. 32, no. 9, 2005.

[56] M. Fischetti and D. Pisinger, "Optimizing wind farm cable routing considering power losses," European Journal of Operational Research, vol. 270, no. 3, pp. 917–930, 2018.

[57] L. Wolsey and G. L. Nemhauser, Integer and combinatorial optimization. John Wiley & Sons, 2014.

[58] A. Hertz, O. Marcotte, A. Mdimagh, M. Carreau, and F. Welt, "Design of a wind farm collection network when several cable types are available," Journal of the Operational Research Society, vol. 68, no. 1, pp. 62–73, 2017.

[59] Y. Chen, Z. Y. Dong, K. Meng, F. Luo, Z. Xu, and K. P. Wong, "Collector System Layout Optimization Framework for Large-Scale Offshore Wind Farms," IEEE Transactions on Sustainable Energy, vol. 7, no. 4, pp. 1398–1407, 2016.

[60] A. Cerveira and J. Baptista, "Optimization design in wind farm distribution network," in International Joint Conference SOCO'13-CISIS'13-ICEUTE'13, 2014, pp. 109–119.

[61] A. Klein and D. Haugland, "Obstacle-aware optimization of offshore wind farm cable layouts," Annals of Operations Research, vol. 272, no. 1-2, pp. 373–388, 2017.

[62] A. C. Pillai, J. Chick, L. Johanning, M. Khorasanchi, and V. De Laleu, "Offshore wind farm electrical cable layout optimization," Engineering Optimization, vol. 47, no. 12, pp. 1689–1708, 2015.

[63] J. S. Shin and J. O. Kim, "Optimal Design for Offshore Wind Farm considering Inner Grid Layout and Offshore Substation Location," IEEE Transactions on Power Systems, vol. 32, no. 3, pp. 2041–2048, 2017.

[64] J. L. Bentley and T. A. Ottmann, "Algorithms for reporting and counting geometric intersections," IEEE Transactions on computers, no. 9, pp. 643–647, 1979.

[65] B. Delaunay, "Sur la sphere vide," Izv. Akad. Nauk SSSR, Otdelenie Matematicheskii i Estestvennyka Nauk, vol. 7, no. 1, pp. 793–800, 1934.

[66] M. Hauptmann and M. Karpinski, "A Compendium on Steiner Tree Problems," Tech. Rep., 2015. [Online]. Available: http://theory.informatik.uni-bonn.de/info5/steinerkompendium/netcompendium.pdf.[AccessedNov23,2018]

[67] S. Dutta and T. J. Overbye, "Optimal Wind Farm Collector System Topology Design Considering Total Trenching Length," IEEE Transactions on Sustainable Energy, vol. 3, no. 3, pp. 339–348, 2012.

[68] S. Dutta and T. Overbye, "A Graph-theoretic Approach for Addressing Trenching Constraints in Wind Farm Collector System Design," in IEEE Power and Energy Conference at Illinois (PECI), 2013, pp. 1–5.

[69] B. Neagu and G. Georgescu, "Wind Farm Cable Route Optimization Using a Simple Approach," in Proceedings of the International Conference and Exposition on Electrical and Power Engineering (EPE), 2014, pp. 1004–1009.

[70] S. Wei, L. Zhang, Y. Xu, Y. Fu, and F. Li, "Hierarchical Optimization for the Double-Sided Ring Structure of the Collector System Planning of Large Offshore Wind Farms," IEEE Transactions on Sustainable Energy, vol. 8, no. 3, pp. 1029–1040, 2017.

[71] R. Srikakulapu and U. Vinatha, "Optimal Design of Collector Topology for Offshore Wind Farm Based on Ant Colony Optimization Approach," in IEEE International Conference on Power Electronics, Drives and Energy Systems (PEDES), 2016, pp. 1–6.

[72] D. Applegate, W. Cook, and A. Rohe, "Chained Lin-Kernighan for large traveling salesman problems," INFORMS Journal on Computing, vol. 15, no. 1, pp. 82–92, 2003.

[73] G. Quinonez-Varela, G. Ault, O. Anaya-Lara, and J. McDonald, "Electrical collector system options for large offshore wind farms," IET Renewable power generation, vol. 1, no. 2, pp. 107–114, 2007.

[74] H. J. Bahirat, B. A. Mork, and H. K. Hoidalen, "Comparison of wind farm topologies for offshore applications," in IEEE Power and Energy Society General Meeting (PES), 2012, pp. 1–8.

[75] S. Lundberg, "Configuration study of large wind parks," Ph.D. dissertation, Chalmers University of Technology, 2003.

[76] R. Ahuja, T. L. Magnanti, and J. B. Orlin, Encyclopedia of Optimization. Springer, 2008.

[77] P. Fagerfjäll, Optimizing wind farm layout – more bang for the buck using mixed integer linear programming (MSc. Thesis), 2010.

[78] M. Sedighi, M. Moradzadeh, O. Kukrer, M. Fahrioglu, and L. Vandevelde, "Optimal Electrical Interconnection Configuration of Off-Shore Wind Farms," Journal of Clean Energy Technologies, vol. 4, no. 1, pp. 66–71, 2016.

[79] H. Ling-ling, C. Ning, Z. Hongyue, and F. Yang, "Optimization of large-scale offshore wind farm electrical collection systems based on improved FCM," in International Conference on Sustainable Power Generation and Supply (SUPERGEN), 2012, pp. 67–67.

[80] D. Li, C. He, and Y. Fu, "Optimization of internal electric connection system of large offshore wind farm with hybrid genetic and immune algorithm," in 3rd International Conference on Deregulation and Restructuring and Power Technologies, (DRPT), no. April, 2008, pp. 2476–2481.

[81] S. Lumbreras, A. Ramos, and S. Cerisola, "A Progressive Contingency Incorporation Approach for Stochastic Optimization Problems," IEEE Transactions on Power Systems, vol. 28, no. 2, pp. 1452–1460, 2013.

[82] H. Lingling, F. Yang, and G. Xiaoming, "Optimization of Electric Connection System of Large Offshore Wind Farm with Genetic Algorithm," in International Conference on Sustainable Power Generation and Supply (SUPERGEN). IEEE, 2009, pp. 1–4.

[83] J. Castro Mora, "Optimización Global de Parques Eólicos Mediante Algoritmos Evolutivos," Ph.D. dissertation, Unversidad de Sevilla, 2008.

[84] P. Hopewell, F. Castro, and D. Bailey, "Optimising the design of offshore wind farm collection networks," in Proceedings of the 41st International Universities Power Engineering Conference (UPEC), no. 1, 2006, pp. 84–88.

[85] M. Zhao, Z. Chen, and F. Blaabjerg, "Optimization of Electrical System for a Large DC Offshore Wind Farm by Genetic Algorithm," in Nordic Workshop on Power and Industrial Electronics, 2004, p. 8.

[86] O. Dahmani, S. Bourguet, M. MacHmoum, P. Guerin, P. Rhein, and L. Josse, "Optimization of the Connection Topology of an Offshore Wind Farm Network," IEEE Systems Journal, vol. 9, no. 4, pp. 1519–1528, 2015.

[87] W. S. Moon, J. C. Kim, A. Jo, and J. N. Won, "Grid optimization for offshore wind farm layout and substation location," in Conference Proceedings of IEEE Transportation Electrification Conference and Expo, (ITEC), 2014, pp. 1–6.
[88] H. Ergun, D. Van Hertem, and R. Belmans, "Transmission system topology optimization for large-scale offshore wind integration," IEEE Transactions on Sustainable Energy, vol. 3, no. 4, pp. 908–917, 2012.
[89] T. Trötscher and M. Korpås, "A framework to determine optimal offshore grid structures for wind power integration and power exchange," Wind Energy, vol. 14, p. 977–992, 2011.
[90] H. G. Svendsen, "Planning Tool for Clustering and Optimised Grid Connection of Offshore Wind Farms," Energy Procedia, vol. 35, pp. 297–306, 2013. [Online]. Available: http://dx.doi.org/10.1016/j.egypro.2013.07.182
[91] V. C. Tai and K. Uhlen, "Design and Optimisation of Offshore Grids in Baltic Sea for Scenario Year 2030," Energy Procedia, vol. 53, pp. 124–134, 2014.

JUAN-ANDRÉS PÉREZ-RÚA received the B.Sc. degree in Electrical Engineering, with Summa Cum Laude distinction, from the Technological University of Bolivar, Colombia, in 2012, and the M.Sc. degree in Sustainable Transportation and Electrical Power Systems from the Superior Institute of Engineering from Coimbra, Portugal, the University of Nottinghan, England, and the University of Oviedo, Spain, in 2016. Currently, he is pursuing the Ph.D. degree in the Department of Wind Energy in the Technical University of Denmark. From 2012 to 2014 he worked with HMV Engineers in Colombia as a protection systems design engineer. His present-day areas of interest include integration of renewable energies in power systems, optimization techniques for electrical infrastructure in offshore wind farms, dynamic cables/lines rating, and control.

NICOLAOS A. CUTULULIS received the M.Sc. and Ph.D. degrees, both in Automatic Control in 1998 and 2005, respectively. Currently, he is Professor in the Department of Wind Energy at the Technical University of Denmark. His main research interests are integration of wind power, with a special focus on offshore wind power, and grids, involving a variety of technical disciplines including modeling, optimization, control of wind turbines, and farms, wind power variability, and ancillary services from wind power.

APPENDIX J2

"Optimum Sizing of Offshore Wind Farm Export Cables"

J.A. Pérez-Rúa, K. Das, and N. A. Cutululis

in *International Journal of Electrical Power & Energy Systems*, Vol. 113, 982–990

December

2019

Optimum Sizing of Offshore Wind Farm Export Cables

Juan-Andrés Pérez-Rúa, Kaushik Das, and Nicolaos A. Cutululis

***Abstract*—A methodology for optimum sizing of offshore wind farms high voltage AC export cables is presented. The method uses as main input site-dependent time series of wind power generation and seabed temperature, in order to apply Dynamic Temperature Estimation (DTE) analysis using a Thermo-Electrical Equivalent model (TEE), followed by an estimation of loss-of-life fractions in the insulation materials through a probabilistic lifetime model, known as Arrhenius-IPM. The lifetime estimation takes into consideration the effects of cable total length: the high capacitive currents and the statistical volume enlargement law. Furthermore, the cable lifetime is inferred based on the accumulated ageing effects previously quantified. The methodology is embedded in an optimization framework which provides a transparent, flexible, and scalable formulation. Finally, the applicability of the method is illustrated through a case study, complemented with a sensitivity analysis targeting the main parameters. Results show that a reduction of the objective function of around 5% is achieved when using the proposed methodology.**

***Index Terms*—Offshore wind energy, AC transmission cables, Optimization, Dynamic temperature estimation, Electro-thermal stress, Probabilistic lifetime estimation.**

NOMENCLATURE

α_0	Scale factor of the pdf for lifetime model for $E = E_0$ and $\theta_{i_t} = \theta_0$
$\alpha_t(E, \theta_{i_{j_t}})$	Scale factor of the pdf for lifetime model for a given E and θ_{i_t}
β_t	Shape parameter of the pdf for lifetime model
$\boldsymbol{T_C}$	Set of cables available
$\lambda_1 + \lambda_2$	Ratio of screen and armouring losses respect to joule losses
ρ_{th}	Soil thermal resistivity
θ_0	Room reference temperature for lifetime model
θ_n	Industrial continuous rated temperature
$\theta_{i_{peak_t}}$	Non-negative continuous variable. Models the calculated maximum instantaneous temperature for cable t in the cycle i
θ_{peak}	Allowed maximum instantaneous conductor temperature
A_{p_t}	First cost coefficient of cable t
B	Parameter for lifetime model
b	Parameter linking the synergism between electric and thermal stress for lifetime model
b_d	Length of buried depth
B_{p_t}	Second cost coefficient of cable t
C_{p_t}	Third cost coefficient of cable t
c_{th}	Soil specific heat
C_t	Cost per unit of length of cable t
D	Enlargement factor
d	Export cable total length
d_{des}	Design length
E	Electric field applied to the cable
E_0	Electric field value below which electric aging is negligible
E_n	Industrial continuous rated electric field
$E_{i_{net_t}}$	Net produced energy for year i using cable type t
$F_{p_{des}}$	Design failure probability
h	Number slot-hours in the cycle i
i	Annual cycle
j	Slot-hour belonging to set i
l	A physical section of the cable under analysis
l_D	Real-size cable length
l_f	Specimen cable length
l_{D_T}	Total number of sections to divide the cable under analysis
LT_{des}	Design life
$LT_{i_{P_{inc_t}}}$	Non-negative continous variable. Models the calculated cable lifetime for t in the cycle i
N	Number of sub-layers for dividing the seabed layer of buried depth for thermal model
n_0	Voltage Endurance Coefficient (VEC) for lifetime model
N_y	Project lifetime
P_D	Failure probability for real-size cables
P_f	Failure probability for specimen cables
$P_{i_{inc_t}}$	Non-negative continuous variable. Models power increase respect to P_{IEC_t} for cable t in the cycle i
P_{IEC_t}	Rated power according to IEC standard for cable t
P_{lim_t}	Surge impedance power limit for cable t
P_{owf}	Offshore Wind Farm installed power
pf	Wind farm aggregated power factor
r	Interest rate
r_D	Radius of real-size cable conductor
r_f	Radius of specimen cable conductor
$R_{c_t}(l, j)$	Phase conductor resistance for cable t section l at time j
s	Length of phase spacing
S_{n_t}	Nominal power of cable t
t	Cable type
TL_{i_t}	Total electrical power losses for cable t in year i
V_n	Export system nominal voltage
W_{d_t}	Total phase dielectric losses for cable t
x_{it}	Binary variable. Models whether cable t is selected for cycle i or not

Juan-Andrés Pérez-Rúa, Kaushik Das, and Nicolaos A. Cutululis are with the Department of Wind Energy of the Technical University of Denmark, Frederiksborgvej 399, 4000 Roskilde, Denmark (e-mail: juru@dtu.dk)

Manuscript received XXX, XXX; revised XXX, XXX.

y Number of cycles under consideration
$\boldsymbol{\Theta}_{i_t}$ Set of calculated instantaneous conductor temperature time series for cable t in the cycle i
$\boldsymbol{P}_i$ Set of offshore wind power time series for cycle i
$\boldsymbol{T}_i$ Set of seabed surface temperature time series for cycle i
$\boldsymbol{T}$ Set of seabed surface temperature time series including whole annual dataset
$I_t(l,j)$ Phase current through cable t section l at time j
$L_D(E,\theta_{i_{j_t}},P_D)$ Time-to-failure for a given E, $\theta_{i_{j_t}}$, and P_f for real-size cables
$L_{P_f}(E,\theta_{i_{j_t}},P_f)$ Time-to-failure for a given E, $\theta_{i_{j_t}}$, and P_f for specimen cables

I. Introduction

AMONG the different technologies for power production using renewable resources, offshore wind energy is shaping up as one of the fastest and most steadily growing type. The share of offshore wind has increased almost five times in the last seven year [1], reaching a globally installed power of nearly $19\,\mathrm{GW}$. Offshore Wind Farms (OWFs) projects are capital intensive, having large values of operating leverage; the required electrical infrastructure costs can raise up to 15% compared to the total system costs [2]. The export cables are the power system component in charge of bringing to shore the power produced, it can have a significant impact on the overall wind farm availability being a possible single point of failure [3]. At the same time, the increasingly longer distance from shore means more km of export cables, raising its share in the overall project economy.

Traditionally, the sizing of offshore export cables has been done based on the CIGRÉ [4] and IEC [5]- [6] standards. The standards approach this with a classic point of view, considering steady state conditions under constant rated operation. Recently, a new approach as described in [7], consisting in worst case equivalent step-wise load profiles, is being increasingly used in the industry. This represents a strategy to minimize the cable' cross section, going towards a more refined, realistic, and simplified approach. Cables' most critical element is the insulation layer, which according to manufacturers, has an associated lifetime with failure probability, that is described in terms of rated temperature, $\theta_n = 90\,^\circ\mathrm{C}$, and rated electric field E_n; since this material is in close contact to the conductor external layer, the conductor continuous temperature and electric field, under operation, must be fixed to θ_n and E_n, respectively.

There may be other factors fatiguing the cable, such as mechanical and environmental stress [8]. The former is present during manufacturing, assembling, and laying processes, but their impact is minimized considerably by following state-of-the-art techniques throughout each process. The latter is caused by oxidation, radiation, and moisture; however submarine cables are implicitly protected against these threats, partly due to the buried depth, and partly due to the mechanical protective inner layers of the cable itself. Therefore, the simultaneous electro-thermal stress represents the main ageing factor of the insulation, and consequently, of the whole cable.

To the best of the author's research, offline lifetime estimations of OWFs cables, embedded in a holistic optimization framework, has not yet been addressed in the scientific literature. Most of the works focus on: i) conductor temperature estimation, ii) sizing cables considering a maximum instantaneous temperature never higher than $90\,^\circ\mathrm{C}$, and iii) calculation of conservative step-wise cyclic load profiles. No exploration on this component lifetime, for optimum sizing, under real dynamic operating conditions has been identified. Regarding the first topic, a calculation tool for estimating the conductor temperature time series, using a Single Core Equivalent Thermal Model (SCETM), while analyzing the impact on different cables and installation conditions is presented in [9]. SCETM models with 1-D representation [10] estimates well the conductor temperature, albeit improved versions, using 2-D representations, have been recently proposed [11]. In relation to the second topic, a probabilistic approach for the estimation of cable temperature exceedance in different time horizons, when increasing the installed power in a OWF in real time (similar concept to overplanting [12]), obtaining acceptable risks when compared to test sets is described in [13]; this allows maximizing the produced instantaneous power, but it does not focus on cable sizing. Finally, a method for deriving equivalent load cyclic load curves from wind speed time series is proposed in [14]-[15], and along with the standard [6], the recalculation of the cable rating can be done using the traditional rating calculated by means of [5], and adjustment factor *M*. Nevertheless, due to the statistical analysis used to get the mentioned cycle, the full stochastic nature of the wind is approximated and other strategies such as power curtailment must be considered. A systematic method based on dynamic load from offshore wind farms, to construct a "worst-case dynamic load profile" before using a SCETM model for calculating the varying temperature, is proposed in [16], by again, using approximation techniques to obtain such equivalent load profiles.

The deterministic, constant rated power operation implied in the standards is intuitively too conservative considering that OWFs have a typical capacity factor of 0.4 - 0.5, and the increase of length of export cables.

The main contribution of this paper is to propose a methodology capable of estimating the lifetime of cables for cumulative fatigue. It combines different concepts, considering realistic operation conditions deemed realistic, such as: time varying cyclic power generation, electro-thermal stress, thermal transients, capacity currents, length-dependent failure probability, and variable external temperature. It also accounts for the ultimate strength limit of the insulation material and, proposing a holistic approach for optimizing the export cable utilization.

This paper is structured as follows: The Section II describes the optimization framework, continuing with the methodology depiction in the Section III, and finally, it is reported the application of the model in a case study with respective sensitivity analysis in the Section IV. The potential cross-section reduction from the point of view of electro-thermal stress and lifetime estimation is pointed out. Conclusions extracted after this work close the article in the Section VI.

II. Optimization Framework

A. Cost Model

The cost function to estimate the capital expenses related to the export cables is extracted from [17], where a comprehensive cost survey is provided, and a function is obtained by means of data fitting techniques (1). The cost function is scaled to take into consideration macroeconomics phenomena such as inflation and exchange rate.

$$C_t = A_{p_t} + B_{p_t}\, \mathrm{e}^{\left(\frac{C_{p_t} S_{n_t}}{10^8}\right)^2} \tag{1}$$

Where A_{p_t}, B_{p_t}, and C_{p_t} are coefficients dependant on the nominal voltage of cable type $t \in \boldsymbol{T_C}$ (see Table IV in Appendix), being $\boldsymbol{T_C}$ the set of available cables, S_{n_t} is the rated power of t in VA (also depending of the rated line to line voltage level, V_n), and C_t the cost of t in €/km. Trenching costs are neglected because the installation route is fixed regardless the cable cross-section, and its value is correlated with the capital cost. Power losses cost are included in the objective function.

B. Optimization Model

While the formulation of the objective function and the constraints are general, they are adapted to a specific OWF via the input datasets, such as: an associated offshore wind power production potential $\boldsymbol{P_i}$, a seabed temperature profile $\boldsymbol{T_i}$ (both expressed as i-annual time series data in pu and °C, respectively), specific soil thermal properties, electric operating conditions, and cable installation conditions.

1) Objective Function: The objective function is defined as an index evaluating the share on the Levelized Cost of Energy (LCOE) of the export cable infrastructure ($LCOE_{es}$), with the mathematical formulation given in (2). Let x_{it} represent a binary variable, equal to 1 if a cable type t is selected or 0 if not. Additionally, d is the cable total length (in km), r is the discount rate (assumed as 5%), N_y is the project lifetime (assumed as 30 years), and $E_{i_{net_t}}$ is the produced annual energy accounting for power losses (in MWh) [18].

$$\min \sum_{t \in \boldsymbol{T_C}} \frac{d \cdot C_t \cdot x_{it} \cdot r \cdot (1+r)^{N_y}}{((1+r)^{N_y} - 1) \cdot E_{i_{net_t}}} \tag{2}$$

2) Constraints: Let P_{owf}, P_{lim_t}, θ_{peak}, LT_{des}, $F_{p_{des}}$, d_{des} be parameters representing the OWF installed power (MW), the cable surge impedance power limit for cable t (MW), the allowed maximum instantaneous conductor temperature (°C), cable design lifetime (years), cable design failure probability (%), and cable testing length (km), respectively. Moreover, let $P_{i_{inc_t}}$, $\theta_{i_{peak_t}}$, $LT_{i_{P_{inc_t}}}$ be non-negative continuous variables modelling the power increase respect to P_{IEC_t} calculated with [5] for cable t (pu), the calculated maximum instantaneous conductor temperature for cable t (°C), and the calculated cable lifetime for a given time window i for cable t (years).

$$\sum_{t \in \boldsymbol{T_C}} x_{it} = 1 \tag{3}$$

$$x_{it} \cdot LT_{i_{P_{inc_t}}} \geq x_{it} \cdot LT_{des} \quad \text{At hot spot} \quad \forall t \in \boldsymbol{T_C} \tag{4}$$

$$x_{it} \cdot \theta_{i_{peak_t}} \leq x_{it} \cdot \theta_{peak} \quad \text{At hot spot} \quad \forall t \in \boldsymbol{T_C} \tag{5}$$

$$x_{it} \cdot P_{i_{inc_t}} P_{IEC_t} \leq x_{it} \cdot P_{lim_t} \quad \forall t \in \boldsymbol{T_C} \tag{6}$$

$$x_{it} \cdot P_{i_{inc_t}} P_{IEC_t} \geq x_{it} \cdot P_{owf} \quad \forall t \in \boldsymbol{T_C} \tag{7}$$

$$P_{lim_t} = \frac{|V_S||V_R|}{|B_t|} - \frac{|A_t||V_R^2|}{|B_t|} \cos(\beta_t - \alpha_t) \quad \forall t \in \boldsymbol{T_C} \tag{8}$$

Constraint (3) ensures that the solution has only one cable type. Constraint (4) guarantees that the calculated cable lifetime operating under a given time window and real conditions, is not lower than the one given as design value. Constraint (5) limits the calculated maximum instantaneous conductor temperature, so the material ultimate strength is not met. Constraint (6) permits abiding the cable stability limit. Constraint (7) matches the increase power with the OWF installed power. Constraint (8) calculates the stability or cable surge impedance power limit, where V_S and V_R are line-to-line voltages (assumed to be the rated value), and $|A_t|\angle\alpha_t$ and $|B_t|\angle\beta_t$ represents the cable two-ports model for a cable t [19].

The model presented from (2) to (8) is non-linear. However, the search space is rather small, since only a limited numbers of cable types are available from manufacturers. This allows use of simplistic human-driven or brute-force optimization methods to select proper export cable satisfying (2) to (8). The main challenge, however, is the estimation of lifetime which has not yet been addressed in the field of OWF design. The proposed approach for lifetime calculation is described in the next section.

III. Methodology

The steps of the proposed methodology are presented in the Fig. 1. The main objective of this method is to provide a framework that allows calculating offline the dynamic loadability of export cables for OWF.

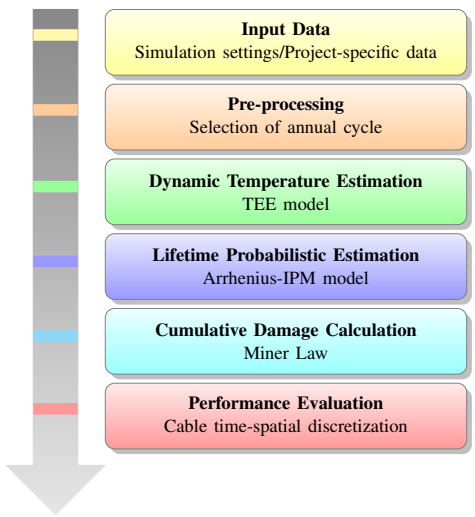

Fig. 1: Lifetime estimation method for OWF's high voltage AC export cables.

A. Input Data

The quality and volume of project-specific datasets has pronounced relevance, influencing a lot the results.

1) Simulation Setting: Defines the main simulation parameters: i) seabed multilayer definition N (as introduced in [20]), ii) cables lifetime design information: LT_{des}, d_{des}, and $F_{p_{des}}$, iii) cables catalogue, and iv) geometrical and thermal information of the cables inner layers.

2) Project-specific data: Gathers OWF electrical information (P_{owf}), (V_n), plus: i) system nominal frequency f_n, ii) wind farm aggregated power factor pf, and iii) series-shunt compensation (indicated as a percentage of the cable total inductance-capacitance). It also defines cable laying conditions: iv) total length d, v) buried depth b_d, and vi) cables spacing s. Finally, it includes: vii) annual power production time series $\boldsymbol{P}_i$, and viii) annual seabed temperature time series $\boldsymbol{T}_i$, along with thermal information of the seabed: ix) thermal resistivity ρ_{th}, and x) specific heat c_{th}. Information related to the seabed is assumed to be spatial-uniform along the cable route.

B. Pre-processing

The cycle time basis selected is a natural year because it is the typical time horizon used for calculating Discounted Cash Flow, and the economic metrics quantifying the project performance for funding plans, such as Net Present Value, LCOE, and Internal Rate of Return. On the other hand, selecting this time frame, represents a conservative approach itself that allows considering the most unfavorable scenario from the point of view of cable stress.

Let $\boldsymbol{P}$ represents the set of available annual time series, so $\boldsymbol{P} = \{\boldsymbol{P}_1, \cdots, \boldsymbol{P}_y\}$, equivalently for the seabed temperature, $\boldsymbol{T} = \{\boldsymbol{T}_1, \cdots, \boldsymbol{T}_y\}$, where $y \in \mathbb{N}^+$ represents the size of the sets. The analysis presented in the Fig. 1 is sequentially and independently repeated for each triple $(\boldsymbol{P}_i, \boldsymbol{T}_i, t)$, where $\boldsymbol{P}_i \in \boldsymbol{P}$, $\boldsymbol{T}_i \in \boldsymbol{T}$, and $t \in \boldsymbol{T_C}$, obtaining in each case a cable lifetime estimation $LT_{i_{P_{inc_t}}}$, and peak temperature $\theta_{i_{peak_t}}$. The optimization procedures consists on finding the cable leading to the minimum objective function, satisfying (3) to (8), for all $i \in \{1, \cdots, y\}$.

C. Dynamic Temperature Estimation

A Thermo-Electrical Equivalent (TEE) model based on the works [21] and [22] have been developed and calibrated as presented in [20]. The theoretical and practical validation of this model can be found in [16] and [10].

For a triple $(\boldsymbol{P}_i, \boldsymbol{T}_i, t)$, where $\boldsymbol{\Theta}_{i_t}$ is the calculated instantaneous conductor temperature in year i for cable t at hot spot (i.e., considering capacitive currents), such as $\boldsymbol{\Theta}_{i_t} = \left\{\theta_{i_{1_t}}, \cdots, \theta_{i_{j_t}}, \cdots, \theta_{i_{h_t}}\right\}$, where h is the number of elements of $\boldsymbol{P}_i$ and $\boldsymbol{T}_i$. As stated in Section II-B, $\max \boldsymbol{\Theta}_{i_t} = \theta_{i_{peak_t}}$.

D. Probabilistic Lifetime Estimation

Many different models can be used for inferring the lifetime of power system components. A review of such models obtained by means of accelerated test experiments is presented in [23]. A benchmarking between different electro-thermal stress models for power cables has been done, such as Zurkov, Crine and Arrhenius-IPM models, each within the probabilistic framework needed for associating time-to-failure to reliability. All these models present different analytical expressions and parameter values, however in general they all provide same indications regarding lifetime, being the Arrhenius-IPM model the most conservative for a wide operation range [24]. The parameters of the Arrhenius-IPM model, based on accelerated test experiments, are available in the literature [25].

According to [24], let (9) represent the mathematical expression for combining two single-stress life models and their synergism: the so-called thermal stress model, Arrhenius and for the electric stress, the Inverse Power Model (IPM). Where $\left(\frac{1}{\theta_0} - \frac{1}{\theta_{i_{j_t}}}\right)$ defines the so-called conventional thermal stress ($\theta_{i_{j_t}}$ is the conductor temperature in Kelvin for a year i, cable type t, and time slot $1 \leq j \leq h$, and θ_0 the room reference temperature), parameter $B = \frac{\Delta W}{k}$ (ΔW is the activation energy of the main thermal degradation reaction, and k is the Boltzmann constant), n_0 is the so-called voltage endurance coefficient (VEC) at θ_0, b is the parameter linking the synergism between electric and thermal stress, E is the electric field of the cable under analysis, E_0 is the value of electric field below which electric aging is considered neglected, and α_0 is the cable's life at θ_0 and E_0.

$$\alpha_t(E, \theta_{i_{j_t}}) = \alpha_0 \cdot \mathrm{e}^{-B \cdot \left(\frac{1}{\theta_0} - \frac{1}{\theta_{i_{j_t}}}\right)} \cdot \left(\frac{E}{E_0}\right)^{-\left(n_0 - b \cdot \left(\frac{1}{\theta_0} - \frac{1}{\theta_{i_{j_t}}}\right)\right)} \tag{9}$$

According to [26] the most accepted cumulative probability density function (pdf) to relate time-to-failure and failure probability for HV equipments is the Weibull pdf, as it is expressed in (10), where t_{P_f} is the life at failure probability P_f, $\alpha_t(E, \theta_{i_{j_t}})$ is the scale factor of the pdf which is function of E and $\theta_{i_{j_t}}$ (time-to-failure for a probability of 0.632), and β_t is the shape parameter of the pdf.

$$P_f(t_{P_f}; E, \theta_{i_{j_t}}) = 1 - \mathrm{e}^{-\left(\frac{t_{P_f}}{\alpha_t(E, \theta_{i_{j_t}})}\right)^{\beta_t}} \tag{10}$$

$$t_{P_f} = [-\ln(1 - P_f)]^{\frac{1}{\beta_t}} \cdot \alpha_t(E, \theta_{i_{j_t}}) \tag{11}$$

$$L_{P_f}(E, \theta_{i_{j_t}}, P_f) = [-\ln(1 - P_f)]^{\frac{1}{\beta_t}} \cdot \alpha_0 \cdot \mathrm{e}^{-B \cdot \left(\frac{1}{\theta_0} - \frac{1}{\theta_{i_{j_t}}}\right)} \cdot \left(\frac{E}{E_0}\right)^{-\left(n_0 - b \cdot \left(\frac{1}{\theta_0} - \frac{1}{\theta_{i_{j_t}}}\right)\right)} \tag{12}$$

Re-arranging (10) with respect to t_{P_f}, it is obtained (11). If one uses the electro-thermal stress model Arrhenius-IPM given in (9), which is valid for failure probability of 0.632, then (12) is found.

Equation (12) models the probabilistic time-to-failure of a cable for a set of operative conditions, E, $\theta_{i_{j_t}}$, and P_f. It is valid for cables specimen used in laboratory tests considering that the pdf and stress model is representative for the whole range of operation [25]. To extrapolate this result to real-size cables for projects applications, the probabilistic enlargement

law is applied [27], see (13). Longer lengths means more potential failure spots, less lifetime.

$$L_D(E,\theta_{i_{j_t}},P_D) = L_{P_f}(E,\theta_{i_{j_t}},P_f)\cdot\left[\frac{\ln(1-P_D)}{D\cdot\ln(1-P_f)}\right]^{\frac{1}{\beta_t}} \tag{13}$$

Where D is the enlargement factor that depends on the ratios of cables length (l_D and l_f) and conductors radius (r_D and r_f) of real-size and cable specimen, respectively, as represented in (14).

$$D = \frac{l_D}{l_f}\cdot\left(\frac{r_D}{r_f}\right)^2 \tag{14}$$

Finally, inserting (12) in (13), the probabilistic lifetime estimation model for real-size cables is obtained:

$$L_D(E,\theta_{i_{j_t}},P_D) = \left[\frac{-\ln(1-P_D)}{D}\right]^{\frac{1}{\beta_t}}\cdot\alpha_0\cdot \mathrm{e}^{-B\cdot\left(\frac{1}{\theta_0}-\frac{1}{\theta_{i_{j_t}}}\right)} \cdot\left(\frac{E}{E_0}\right)^{-\left(n_0-b\cdot\left(\frac{1}{\theta_0}-\frac{1}{\theta_{i_{j_t}}}\right)\right)} \tag{15}$$

The parameters for the model of (15) extracted from [24] are presented in Table I. The probabilistic lifetime model is calibrated to hold for XLPE insulation cables considered in this study. Accelerated life tests done in [25] on cables specimen of $0.4\,\mathrm{m}$ long, with solid copper conductor radius of $0.9\,\mathrm{mm}$, inner semicon thickness of $0.5\,\mathrm{mm}$, and insulation thickness of $1.5\,\mathrm{mm}$ were used to derive the parameters.

TABLE I
PARAMETER VALUES FOR LIFETIME ARRHENIUS-IPM MODEL

$b\left[\mathrm{K}\frac{\mathrm{mm}}{\mathrm{kV}}\right]$	B [K]	n_0	V_n [kV]	$E_0\left[\frac{\mathrm{kV}}{\mathrm{mm}}\right]$	$E_n\left[\frac{\mathrm{kV}}{\mathrm{mm}}\right]$	θ_0 [K]	β_t
4420	12430	15	145	5	7.2	296.5	2

The parameter α_0 has to be calculated to scale the pdf accordingly to the input information, i.e., cable with specific d_{des}, LT_{des}, and $F_{p_{des}}$, operating at rated temperature $\theta_{i_{j_t}} = \theta_n$, for all $j \in \{1,\cdots,h\} \wedge i \in \{1,\cdots,y\}$, and continuous nominal electric field, E_n. Additionally it is assumed to be invariant over the operation range considered in this work. Parameters E_0 and E_n, have to be extrapolated in function of the nominal voltage of the particular cable under analysis. It is assumed these parameters are constant throughout the whole range of stress levels.

E. Cumulative Damage

Let δt be an infinitesimal increment of time within a time slot j in $\boldsymbol{P}_i$, so the infinitesimal loss-of-life fraction of the cable t, is calculated as:

$$\delta LF_j = \left.\frac{\delta t}{L_D(E,\theta_{i_{j_t}},P_D)}\right|_{E=E_n,\theta_{i_{j_t}},P_D=F_{p_{des}}}$$

Integrating the previous expression along j (thermal time constant of cables is slow so it is a reasonable assumption), the loss-of-life fraction in this time slot is obtained in (16):

$$LF_j = \left.\frac{1}{L_D(E,\theta_{i_{j_t}},P_D)}\right|_{E=E_n,\theta_{i_{j_t}},P_D=F_{p_{des}}} \tag{16}$$

According to the Miner's cumulative damage theory [28], summing up the loss-of-life fraction for every time slot, defines the estimated lifetime of the component under analysis when the result is equal to one. Therefore, (17) allows calculating the number of cycles ($LT_{i_{P_{inc_t}}}$ years) of the cable to failure, accounting for the effects of cumulative damage, for the annual time series i and cable type t.

$$LT_{i_{P_{inc_t}}} = \frac{1}{\sum_{j=1}^{h} LF_j} \tag{17}$$

F. Performance Evaluation

The total loss calculation process allows an holistic estimation, taking the variability of current along the cable into consideration [29]. Dynamic temperature estimation includes the effects of conductor resistance variation in function of its temperature. Temperature varies in time resulting in variation of the conductor and other associated losses (screen, armouring, and dielectric). Consequently, the total losses (TL_{i_t}) calculation for a cable t is defined in (18) [20].

$$TL_{i_t} \approx 3\cdot(1+\lambda_1+\lambda_2)\cdot\sum_{l=1}^{l_{D_T}}\sum_{j=1}^{h} R_{c_t}(l,j)\cdot I_t(l,j)^2 + 3\cdot W_{d_t} \tag{18}$$

where l_{D_T}, h, $R_{c_t}(l,j)$, $I_t(l,j)$, and W_{d_t} are the total number of sections that the cable is divided into, total number of hours in the year under analysis, i, as stated in Section III-C, conductor resistance in ohms, current in amperes (being these two last function of distance and time), and total dielectric losses, respectively. The factor $(1+\lambda_1+\lambda_2)$ accounts for the screen and armouring losses, while the constant 3 is for the three-phase system. It is observed that l_{D_T} should be between $10-20$ (depending on cable total length) to achieve a proper computation time-quality balance [20].

IV. CASE STUDY

As a case study the OWF Arcadis Ost 1 (GW1) (see Fig. 2), foreseen to be constructed in the Baltic Sea in 2030, is considered.

Pre-feasibility studies project a total installed capacity of $456\,\mathrm{MW}$ (38 Wind Turbines of $12\,\mathrm{MW}$), routing length of the export cables of $d = 89\,\mathrm{km}$, nominal voltage $V_n = 275\,\mathrm{kV}$, nominal frequency $f_n = 50\,\mathrm{Hz}$, $pf = 1$, without compensation units.

The aim of the analysis is to illustrate how, using the proposed methodology, the sizing of the export cable can be done taking into account the lifetime of the cable. Input data related to cables is extracted from [30]; other inputs are presented in the Table II. Availability of seabed temperature time series is scarce, hence a synthetic time series based on info from

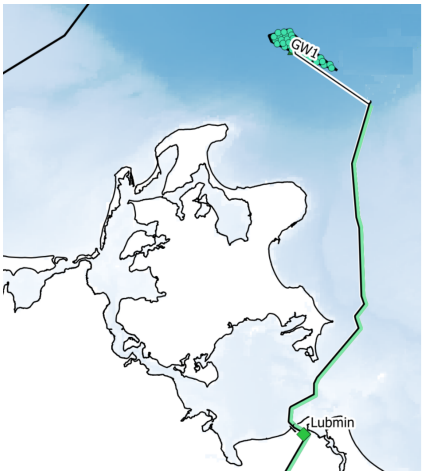

Fig. 2: Map of the project area of the case study.

the Bornholm Basic area [31] was created. The time series vary between 1 °C-10 °C and takes into account the seasonal fluctuations.

TABLE II
CASE STUDY SIMULATION INPUTS

N	ρ_{th} $\left[\frac{\text{Km}}{\text{W}}\right]$	c_{th} $\left[\frac{\text{J}}{\text{m}^3}\right]$	b_d [m]	s [m]	LT_{des} [years]	$F_{p_{des}}$ [%]	d_{des} [km]
10	1	$2 \cdot 10^6$	1	0.4	30	5	1

V. Simulation Results and Sensitivity Analysis

This Section is divided in two parts; Section V-A for the analysis considering the parameters of the Table II and the described time series, benchmarking the proposed method against [5] and [7], and Section V-B for presenting a sensitivity analysis that aims at quantitatively assessing the impact of the uncertainty in the soil thermal resistivity and seabed temperature time series. For both analyses, 35 years of simulated offshore wind power production time series are used simulated with CorWind [32]- [33].

A. Cable Sizing Results

The proposed methodology is benchmarked against two approaches: first, the one recommended in [5], and second, by using the worst case dynamic load profiles, as studied in [7], which actually has been used lately by OWF developers in the tendering process with cable manufacturers.

The method in [5] is straight-forward, consisting only in a multi-parameter static equation for getting the continuous current I_t, to be transmitted during infinite time, in order to obtain a continuous conductor temperature equal to 90 °C. The smaller cable t with I_t equal or greater than the total current (including capacitive currents) at hot spot is selected. The resultant sizing following this approach is a 1,200 mm^2 cable.

Recently, a more sophisticated method is being adapted as industrial practice, as detailed in [7] (CIGRÉ: Working Group B1.40) and [16]; this is represented by a four-step signal, calculated using the highest RMS values computed through different periods, sweeping through the yearly data set by means of a rolling RMS filter starting at each singular data point. A pre-processing analysis is needed to be carried out to find the set of periods of interest. In the study presented in [16], it has been concluded that the periods of 7 days, 10 days, 40 days, and 365 days capture reasonably the most representative windy days in a windy year; this fact has been validated using the data set available in this paper. Thus, in a temporal sequential ordering, the pre-conditioning current is derived calculating the RMS value for the whole data set, lasting 308 days (remanining days after the periods 7, 10, and 40), then the greatest yearly RMS value using a period length of 7 days is obtained, keeping the same procedure for the periods of 10 days and 40 days, while not overlapping the periods between them. Note that this sequential arrangement represents a conservative criterion itself, because of the assumed steadily increase of current with time.

After applying the aforementioned process to this case study, the profile of worst case load pattern is displayed in the Fig. 3. This step-wise pattern is normalized respect to the total current at hot spot, and the main aim is to be provided to cables manufacturers, in order to have a common framework to compare their bids. The smaller cable t with θ_{peak_t} (note the elimination of the subscript i because there is a single pattern representing all the years) inferior than 90 °C is selected.

Using the pattern of the Fig. 3, and considering the synthetic seabed temperature time series, a 630 mm^2 cable is chosen, exhibiting a $\theta_{peak_t} = 88.71$ °C.

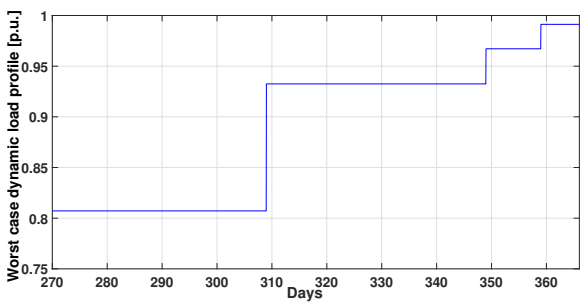

Fig. 3: Profile of worst case dynamic load pattern [7].

Employing the full temporal data set according the proposed methodology, the peak temperature ($\theta_{i_{peak_t}}$) obtained for all points defined by $(\boldsymbol{P}_i, \boldsymbol{T}_i, t)$ is given in Fig. 4. The results indicate that all cables - except the 500 mm^2 cable - satisfy constraint (5), namely do not exceed the rated temperature limit (indicated by a red dotted line, $\theta_{peak} = \theta_n$). The results also show that the 1,200 mm^2 cable -the size that results when using standard [5]- is significantly underused as expected, exhibiting a maximum $\theta_{i_{peak_t}}$ of 62 °C. On the other hand, the 630 mm^2 cable -sized according the worst case pattern- presents a maximum $\theta_{i_{peak_t}}$ of 88.69 °C, showing that the equivalent step profile is on the conservative side ($\theta_{peak_t} = 88.71$ °C), and achieves to capture a realistic harsh windy scenario; these results confirm the validity of the

equivalent cycle for the purpose of facilitating the tendering process, nevertheless representing an approximation of the real time series, which provide more insight about the power production of the OWF, and in fact, conceptually necessary to perform lifetime studies for cumulative damage. Furthermore, the variability of $\theta_{i_{peak_t}}$ for each cable t, in function of the year i, depends strongly on the cable's physical properties.
As shown in Fig. 4, the spread of $\theta_{i_{peak_t}}$ decreases with the size of the cables; In fact, from other dispersion perspective, for the $630\,\mathrm{mm}^2$ cable, the mean value is $85.47\,^\circ\mathrm{C}$ with a standard deviation of $1.27\,^\circ\mathrm{C}$, while for the type $800\,\mathrm{mm}^2$, these numbers change to $73\,^\circ\mathrm{C}$ and $0.96\,^\circ\mathrm{C}$, respectively. This points out that the conductor cable size has a direct relation with the temperature variability due to the power production fluctuations, smaller sizes leading to increased ramping. Based on the thermal results, the cable size could be either $630\,\mathrm{mm}^2$ or $800\,\mathrm{mm}^2$. The conductor temperature time series for the cables $630\,\mathrm{mm}^2$ (red line) and $800\,\mathrm{mm}^2$ (blue line), at the year with highest $\theta_{i_{peak_t}}$, are given in Fig. 5.
As it is appreciable, the instantaneous conductor temperatures between both cables types are considerable different and more critical for smaller cable. For instance, a change in power results in a larger temperature ramping for the smaller cable, which has a lower temperature time constant (see the zoomed-in graph in the Fig. 5 for the first day of operation); the latest is consequence of the growth rate difference among both cable types, and has as a consequence a different conductor temperature frequency distribution as shown in the Fig. 6. It is evident that the conductor temperature distribution resembles a bimodal distribution, showing higher peaks and higher frequency for the $630\,\mathrm{mm}^2$. The proposed method results in indicating the same cable as the one in [7]. However, the deterministic nature of the latter methods does not allow assessing the reliability of the cable in function of its length. Hence, it is beneficial to move towards a probabilistic approach to avoid too optimistic procedures which may potentially lead to operational failures. The different profile of instantaneous

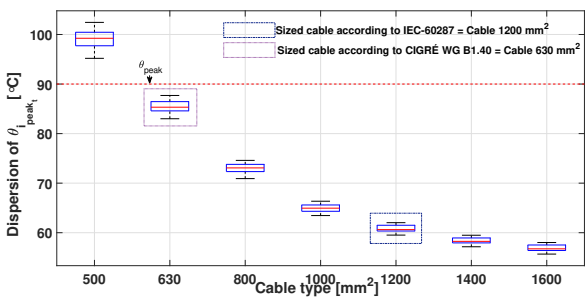

Fig. 4: Overall thermal simulation results.

temperature yields to different lifetime estimations, due to the different fatigue levels induced by their electro-thermal stresses, as captured in the Fig. 7, and with effect on economic metric as displayed in Fig. 8. Lifetime estimation is given as a ratio of calculated to design values, as expressed in $(LT_{i_{ratio_t}} = \frac{LT_{des}}{LT_{i_{P_{inc_t}}}}) \leq 1$, in order to minimize uncertainties on the probabilistic lifetime estimation model.

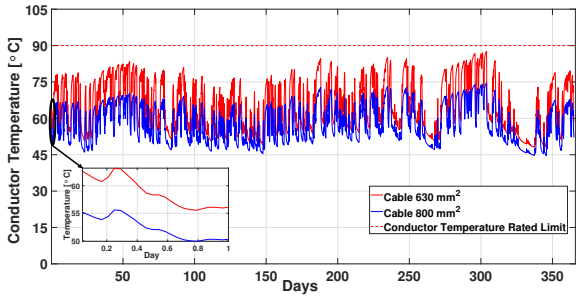

Fig. 5: Cables conductor temperature time series.

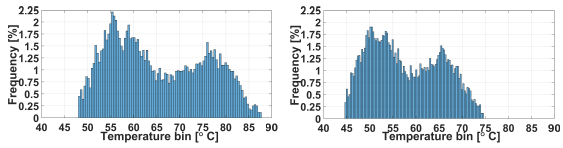

(a) Cable $630\,\mathrm{mm}^2$ (b) Cable $800\,\mathrm{mm}^2$

Fig. 6: Cables conductor temperature histogram.

As expected, the $630\,\mathrm{mm}^2$ cable exposed to more critical conductor temperature, exhibits a lifetime ratio outside the bounds of the optimization model. In contrast, the $800\,\mathrm{mm}^2$ cable satisfies this constraint for all the simulated annual cycles while satisfying all other constraints, resulting to a value of $P_{i_{inc_t}} = 0.99$, which also agrees with the evidence of an underestimating criterion proposed by IEC standard [5] ($P_{i_{inc_t}} = 0.84$ for $1{,}200\,\mathrm{mm}^2$). The mean and standard deviation values of $LT_{i_{ratio_t}}$ for selected $800\,\mathrm{mm}^2$ cable are 0.58 and 0.06, respectively. For $\theta_{i_{peak_t}}$ these values are $73\,^\circ\mathrm{C}$ and $0.96\,^\circ\mathrm{C}$, correspondingly, as mentioned before. The standard deviations of these two variables are considered acceptable to show robustness towards different annual generation profiles. Although the proposed framework suggests a cable one size up compared to [7], the decision is based on a more informed and robust evaluation of the operating conditions of the cable, thus, decreasing the likehood of failures.
The variability difference for different cables on $LT_{i_{ratio_t}}$ and $\theta_{i_{peak_t}}$, can be explained based on the fact that larger cables have larger time constants (slower dynamic response), hence the reaction speed due to power changes is less pronounced than in smaller cables. This is particularly important condition, since the power production is a stochastic variable hard to forecast. If the conductor temperature uncertainty can be decreased by the physical properties of the cables itself, it can help to a more reliable operation based on analysis using power production either simulated or measured from a set of years. Nonetheless, going from a $1{,}200\,\mathrm{mm}^2$ (criterion of [5]) to a $800\,\mathrm{mm}^2$ cable has as direct consequence on decrease of initial investment, but also with detriment of larger total power losses. Consequently, the performance evaluation step introduced in Section III-F, is applied in order to estimate the total electric losses and to calculate the $LCOE_{es}$. Equation (2) is systematically applied for different cables and different

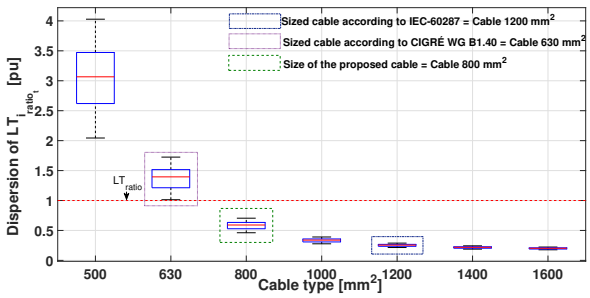

Fig. 7: Overall lifetime simulation results.

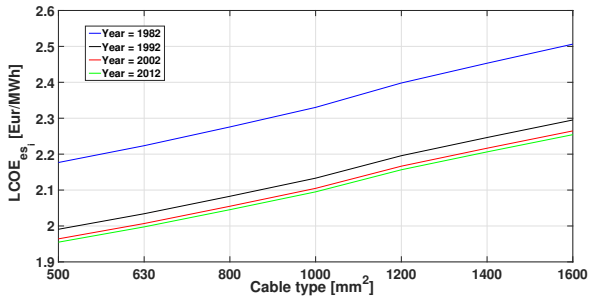

Fig. 8: $LCOE_{es}$ in function of cable type for different years.

years obtaining the plot represented in the Fig. 8. It is evident that regardless the year under analysis, the $LCOE_{es}$ function is increasing monotonically in function of larger cables as presented in Fig. 8; likewise, the curves for different years present no intersections between them, which in combination of the previous point, allows concluding that the objective function is unequivocally minimized for the smallest feasible cable taking into consideration the full data set of annual generation.

Overall, the reduction in the cross-section of the export cable provides a reduction of 5% -assuming the most expensive year- in the $LCOE_{es}$ when considering solely the related costs to this component.

B. Sensitivity Analysis

To assess the impact of the input data uncertainty on the results, a sensitivity analysis is done. Soil thermal resistivity (ρ_{th}) and seabed temperature ($\boldsymbol{T}$) are selected as they are the data with the lower availability.

This analysis consists in combining discrete changes (respect to the base case values) on ρ_{th} and $\boldsymbol{T}$, expressed as $\Delta\rho_{th} = \{0, 0.2\}\ \frac{\mathrm{Km}}{\mathrm{W}}$ and $\Delta T = \{0, 5\}$ °C, respectively. The results are presented in the Table III, where it is clear that an individual increase of 20% on ρ_{th} ($0.2\ \frac{\mathrm{Km}}{\mathrm{W}}$), and 50% of the peak value on $\boldsymbol{T}$ (5°C), causes that for each case, a larger cable would be required, namely $1{,}000\,\mathrm{mm}^2$; furthermore, for the critical condition of a simultaneous deviation of these design values, the impact would be large, resulting in selecting a $1{,}200\,\mathrm{mm}^2$. The effect of the individual and combined change of ρ_{th} and $\boldsymbol{T}$ (using reasonable deviations) is not negligible as the results reveal, since the cable size according to the framework proposed in this paper, should be scaled up one or two steps when compared to the base case conditions. It is recommended therefore to dedicate efforts towards gathering high quality data related to these parameters and their typical fluctuations along the year; as a result, operational failure risks can be minimized while optimally sizing the export cable. A high resolution uncertainty analysis would also help determining with higher accuracy the weight of the parameters leading to better performance of the proposed methodology. The last column in Table III show the final variation of the

TABLE III
RESULTS OF SENSITIVITY ANALYSIS

$\Delta\rho_{th}\ \left[\frac{\mathrm{Km}}{\mathrm{W}}\right]$	$\Delta\boldsymbol{T}$ [°C]	Cable Type $[\mathrm{mm}^2]$	$\Delta LCOE_{es}$ [%]
0	0	800	5
0	5	1000	3
0.2	0	1000	6.8
0.2	5	1200	4

$LCOE_{es}$ savings (respect to [5] criterion). The latest results show that the lowest savings are achieved with a solo variation on $\boldsymbol{T}$, since the IEC standard recommends keeping a constant external temperature which in this cases is still higher than $\boldsymbol{T} + 5$°C, similarly the largest saving is found with a solo variation on ρ_{th}, given the strong dependency of the static equation on this parameter.

Finally, the impact of the export cables length is investigated by means of Fig. 9 and Fig. 10. The following simulation considers the most critical condition for ρ_{th} and $\boldsymbol{T}$, and a cable total length of $32.5\,\mathrm{km}$. It is evident according to the Fig. 9 that all the cables exhibit a $\theta_{i_{peak_t}}$ never higher than $90\,°\mathrm{C}$, with exception of the cable $500\,\mathrm{mm}^2$, which surpasses this value for almost 50% of the cases. However, when evaluating the level of exceedance in terms of frequency for that year with the highest $\theta_{i_{peak_t}}$, it is found out that for the temperature range between $90\,°\mathrm{C}$-$95\,°\mathrm{C}$, the accumulated probability of occurrence is lower than 1.75%.

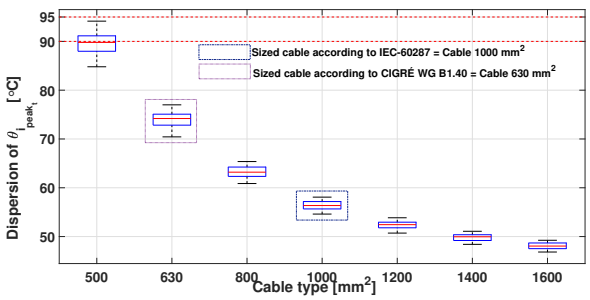

Fig. 9: Sensitivity of overall thermal simulation results. $d = 32.5\,\mathrm{km}$.

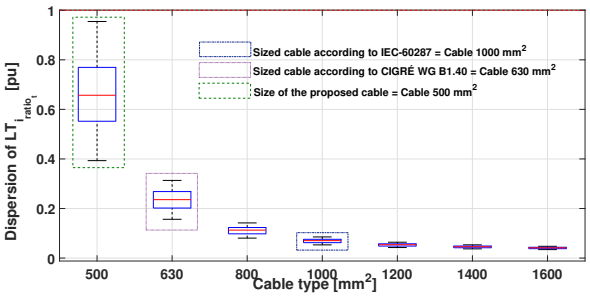

Fig. 10: Sensitivity of overall lifetime simulation results. $d = 32.5\,\mathrm{km}$.

This raises the question whether is too conservative to limit the instantaneous conductor temperature to $90\,^{\circ}\mathrm{C}$, value that is defined as a limit for accumulated stress when operating continuously at this degradation rate in the insulation material [34], but not representing the ultimate strength limit. In fact, in Fig. 10 is shown that the $500\,\mathrm{mm}^2$ cable satisfies the lifetime constraint for all the generation scenarios, therefore by means of a constraint relaxation of θ_{peak} to $95\,^{\circ}\mathrm{C}$, this cable type could be choose under these conditions, obtaining a $LCOE_{es}$ reduction of almost 7%. Note that for this case, the cable total length is less restricting from a lifetime estimation probabilistic point of view, therefore improving the size not only compared to [5], but also to [7], with a reduction of roughly 2%.

VI. Conclusion

The proposed methodology provides a rigorous, and transparent approach for minimizing the $LCOE_{es}$ related to high voltage AC export cables for OWFs.

The main constraints are the maximum instantaneous conductor temperature (which is related to the ultimate strength of the insulation material), the estimated lifetime of the cable (obtained as an accumulation of stress over the cable operational lifetime), and the electric stability limit.

The methodology is applied systematically and in a cyclic-fashion, for each available annual generation and seabed temperature time series, obtaining as a final output the cable leading to the cheapest $LCOE_{es}$ while evaluating for the whole data set the abiding of security operational constraints.

Results show the potential of this methodology in terms of $LCOE_{es}$ reduction. According to the simulations, a reduction up to 5% can be achieved, while guaranteeing all the operational security constraints.

An uncertainty analysis of the parameters deemed to be the least available: soil thermal resistivity and seabed temperature, showed that the impact on cable sizing can be significant.

The analysis highlights the benefits for proper measurement/estimation of these parameters in the planning stage of a OWF project for reducing the risks of failures. Bigger cables drive to larger $LCOE_{es}$, however have the advantage of less sensitivity to large generation changes, minimizing the uncertainty introduced by the estimation of the expected power generation levels and variability. The distance from shore also has an impact on the cable sizing; for larger distances the cables lifetime is the limiting factor, while for shorter distances the ultimate thermal strength takes that role. A relaxation of the maximum instantaneous temperature can allow for a further reduction in the cable sizing for shorter distances, providing cost reductions even compared to the most updated industrial practices.

The proposed methodology depends on the accuracy of several parameters: the values of the lifetime electro-thermal and failure extrapolation models, power generation cycles, seabed soil temperature, and thermal properties of the soil and the cable. To partially mitigate this, the lifetime estimation is normalized, rather than in absolute values. Comprehensive uncertainty analysis is recommended to be performed to quantify accurately this phenomenon, based on real data if possible. Furthermore, availability of real cable failure data will help for further validating the methodology.

Future work direction will move towards adaptation of the methodology to other cables technologies, and identification of hot spots, real-time monitoring, and effective asset management strategies.

Appendix

TABLE IV
Cables cost coefficients

V_n [kV]	A_{p_t}	B_{p_t}	C_{p_t}
22	$0.284 \cdot 10^6$	$0.583 \cdot 10^6$	6.15
33	$0.411 \cdot 10^6$	$0.596 \cdot 10^6$	4.1
45	$0.516 \cdot 10^6$	$0.612 \cdot 10^6$	3
66	$0.688 \cdot 10^6$	$0.625 \cdot 10^6$	2.05
132	$1.971 \cdot 10^6$	$0.209 \cdot 10^6$	1.66
220	$3.181 \cdot 10^6$	$0.11 \cdot 10^6$	1.16
275	$4.181 \cdot 10^6$	$0.07 \cdot 10^6$	0.66

Acknowledgment

This research has received funding from the Baltic InteGrid Project (http://www.baltic-integrid.eu/).

References

[1] GWEC, "Global Wind Report. Annual Market Update 2017," Tech. Rep., 2017. [Online]. Available: http://gwec.net/publications/global-wind-report-2/.[Accessed Oct 29, 2018]

[2] X. Sun, D. Huang, and G. Wu, "The current state of offshore wind energy technology development," *Energy*, vol. 41, no. 1, pp. 298–312, 2012.

[3] ReNEWS, "Rampion suffers cable fault," 2017. [Online]. Available: http://renews.biz/105889/rampion-suffers-cable-fault/.[Accessed Oct 29, 2018]

[4] CIGRÉ, "Current Ratings of Cables for Cyclic and Emergency Loads. Part 1. Cyclic Ratings (Load Factor Less Than 100%) and Response to a Step Function," Tech. Rep. 24, 1976.

[5] IEC, "IEC-60287-1: Electric cables - Calculation of the current rating," Tech. Rep., 2014. [Online]. Available: https://www.evs.ee/products/iec-60287-1-1-2006.[Accessed April 15, 2019]

[6] ——, "IEC-60853-2: - Calculation of the cyclic and emergency current rating of cables," Tech. Rep., 2008.

[7] CIGRÉ: Working Group B1.40, "Offshore Generation Cable Connections," Tech. Rep. 1, 2015.

[8] V. K. Agarwal, H. M. Banford, B. S. Bernstein, E. L. Brancato, R. A. Fouracre, G. C. Montanari, J. L. Parpal, J. N. Seguin, D. M. Ryder, and J. Tanaka, "The Mysteries of Multifactor Ageing," *IEEE Electrical Insulation Magazine*, vol. 11, no. 3, pp. 37–43, 1995.

[9] L. Colla and M. Marelli, "Dynamic Rating of Submarine Cables . Application To Offshore Windfarms," in *European Wind Energy Association (EWEA) Offshore 2013 Conference*, 2013.

[10] G. J. Anders, A. Napieralski, and Z. Kulesza, "Calculation of the internal thermal resistance and ampacity of 3-core screened cables with fillers," *IEEE Transactions on Power Delivery*, vol. 14, no. 3, pp. 729–733, 1999.

[11] D. Chatzipetros and J. A. Pilgrim, "Review of the Accuracy of Single Core Equivalent Thermal Model for Offshore Wind Farm Cables," *IEEE Transactions on Power Delivery*, vol. 33, no. 4, pp. 1–1, 2017.

[12] C. Wolter, H. Klinge Jacobsen, G. Rogdakis, L. Zeni, and N. A. Cutululis, "Overplanting in Offshore Wind Power Plants in Different Regulatory Regimes," *15th Wind Integration Workshop*, pp. 1–9, 2016.

[13] M. A. H. Colin and J. A. Pilgrim, "Offshore Cable Optimization by Probabilistic Thermal Risk Estimation," in *IEEE International Conference on Probabilistic Methods Applied to Power Systems (PMAPS)*. IEEE, 2018, pp. 1–6.

[14] S. Catmull, R. D. Chippendale, J. A. Pilgrim, G. Hutton, and P. Cangy, "Cyclic Load Profiles for Offshore Wind Farm Cable Rating," *IEEE Transactions on Power Delivery*, vol. 31, no. 3, pp. 1242–1250, 2016.

[15] R. Chippendale, J. Pilgrim, A. Kazerooni, and D. Ruthven, "Cyclic rating of wind farm cable connections," *CIRED - Open Access Proceedings Journal*, vol. 2017, no. 1, pp. 91–95, 2017.

[16] T. Kvarts, "Systematic Description of Dynamic Load for Cables for Offshore Wind Farms. Method and Experience," *CIGRÉ*, pp. 1–13, 2016.

[17] S. Lundberg, "Configuration study of large wind parks," Ph.D. dissertation, Chalmers University of Technology, 2003.

[18] P. Hou, W. Hu, C. Chen, and Z. Chen, "Optimisation of offshore wind farm cable connection layout considering levelised production cost using dynamic minimum spanning tree algorithm," *IET Renewable Power Generation*, vol. 10, no. 2, pp. 175–183, 2016.

[19] J. J. Grainger and W. D. J. Stevenson, *Power System Analysis*, 2nd ed. McGraw-Hill Education, 1994.

[20] J.-A. Pérez-Rúa, K. Das, and N. A. Cutululis, "Lifetime estimation and performance evaluation for offshore wind farms transmission cables," in *Paper presented at 15th IET international conference on AC and DC Power Transmission, Coventry, United Kingdom*, 2019, pp. 1–6.

[21] R. S. Olsen, J. Holboll, and U. S. Gudmundsdottir, "Dynamic Temperature Estimation and Real Time Emergency Rating of Transmission Cables," *IEEE Power and Energy Society General Meeting*, pp. 1–8, 2012.

[22] R. S. Olsen, G. J. Anders, J. Holboell, and U. S. Gudmundsdottir, "Modelling of Dynamic Transmission Cable Temperature Considering Soil-Specific Heat, Thermal Resistivity, and Precipitation," *IEEE Transactions on Power Delivery*, vol. 28, no. 3, pp. 1909–1917, 2013.

[23] L. A. Escobar and W. Q. Meeker, "A Review of Accelerated Test Models," *Statistical Science*, vol. 21, no. 4, pp. 552–577, 2006. [Online]. Available: http://projecteuclid.org/euclid.ss/1177334529.[Accessed Oct 29, 2018]

[24] G. Mazzanti, "The Combination of Electro-thermal Stress, Load Cycling and Thermal Transients and its Effects on the Life of High Voltage ac Cables," *IEEE Transactions on Dielectrics and Electrical Insulation*, vol. 16, no. 4, pp. 1168–1179, 2009.

[25] G. Mazzanti and G. C. Montanari, "A Comparison between XLPE and EPR as Insulating Materials for HV Cables," *IEEE Transactions on Power Delivery*, vol. 12, no. 1, pp. 15–26, 1997.

[26] W. Hauschild and W. Mosch, *Statistical Techniques for High-Voltage Engineering*, 1992.

[27] M. Marzinotto and G. Mazzanti, "Merging the electro-thermal life model for power cables with the statistical volume enlargement law," *2014 IEEE Conference on Electrical Insulation and Dielectric Phenomena, CEIDP 2014*, no. 3, pp. 502–505, 2014.

[28] M. Miner, "Cumulative fatigue damage," *Journal of Applied Mechanics*, vol. 12, no. 3, pp. A159–A164, 1945.

[29] H. Brakelmann, "Loss Determination for Long Three-Phase High-Voltage Submarine Cables," *European Transactions on Electrical Power*, vol. 13, no. 3, pp. 193–197, 2003.

[30] ABB, "XLPE Submarine Cable Systems Attachment to XLPE Land Cable Systems - User's Guide," 2018. [Online]. Available: new.abb.com/docs/default-source/ewea.../xlpe-submarine-cable-systems-2gm5007.pdf.[Accessed Oct 29, 2018]

[31] HELCOM, "Our Baltic Sea," 2017. [Online]. Available: http://stateofthebalticsea.helcom.fi/in-brief/our-baltic-sea/. [Accessed Oct 29, 2018]

[32] P. Sørensen, N. A. Cutululis, A. Vigueras-Rodríguez, L. E. Jensen, J. Hjerrild, M. H. Donovan, and H. Madsen, "Power Fluctuations From Large Wind Farms," *IEEE Transactions on Power Systems*, vol. 22, no. 3, pp. 958–965, 2007.

[33] M. Koivisto, K. Das, F. Guo, P. Sørensen, E. Nuño Martinez, N. A. Cutululis, and P. Maule, "Using time series simulation tool for assessing the effects of variable renewable energy generation on power and energy systems," *WIREs Energy and Environment*, no. June, pp. 1–15, 2018.

[34] G. Mazzanti, "Analysis of the Combined Effects of Load Cycling, Thermal Transients, and Electrothermal Stress on Life Expectancy of High-Voltage AC Cables," *IEEE Transactions on Power Delivery*, vol. 22, no. 4, pp. 2000–2009, 2007.

APPENDIX J3

"Global Optimization of Offshore Wind Farm Collection Systems"

J.A. Pérez-Rúa, M. Stolpe,
K. Das, and N. A. Cutululis

in *IEEE Transactions on Power Systems*, Vol. 35, No. 3, 2256–2267

May

2020

Global Optimization of Offshore Wind Farm Collection Systems

Juan-Andrés Pérez-Rúa, Mathias Stolpe, Kaushik Das, *Member, IEEE* and Nicolaos A. Cutululis, *Senior Member, IEEE*

***Abstract*—A mathematical program for global optimization of the cable layout of Offshore Wind Farms (OWFs) is presented. The model consists on a Mixed Integer Linear Program (MILP). Modern branch-and-cut solvers are able to solve large-scale instances, defined by more than hundred Wind Turbines (WTs), and a reasonable number of Offshore Substations (OSSs). In addition to the MILP model to optimize total cable length or initial investment, a pre-processing strategy is proposed in order to incorporate total electrical power losses into the objective function. High fidelity models are adapted to calculate cables current capacities, spatial currents. The MILP model is embedded in an iterative algorithmic framework, solving a sequence of problems with increasing search space size. The search space is defined as a set of underlying candidate arcs. The applicability of the method is illustrated through 10 case studies of real-world large-scale wind farms. Results show that: (i) feasible points are obtained in seconds, (ii) points with an imposed maximum tolerance near the global optimum are calculated in a reasonable computational time in the order of hours, and (iii) the proposed method compares favorably against state-of-the-art method available in literature.**

***Index Terms*—Offshore wind energy, Collection system layout design, Global optimization, Mixed integer linear programming, Medium voltage submarine cables, Heuristics.**

NOMENCLATURE

Acronyms

OWF(s)	Offshore Wind Farm(s).
WT(s)	Wind Turbines(s).
OSS(s)	Offshore Substation(s).
BIP	Binary Integer Programming.
MILP	Mixed Integer Linear Programming.
MIQP	Mixed Integer Quadratic Programming.
MINLP	Mixed Integer Nonlinear Programming.
SCETM	Single-Core Equivalent Thermal Model.
NP	Non-Deterministic Polynomial.
L	Length.
LP	Length plus total Power losses.
I	Initial investment.
IP	Investment plus total Power losses.
WDS	West of Duddon Sands.
TH	Thanet.
LA	London Array.
HR1	Horns Rev 1.
O	Ormonde.
DT	DanTysk.

Juan-Andrés Pérez-Rúa, Mathias Stolpe, Kaushik Das, and Nicolaos A. Cutululis are with the DTU Wind Energy, Technical University of Denmark, Frederiksborgvej 399, 4000 Roskilde, Denmark (e-mail: juru@dtu.dk)

Parameters (non-sets)

n_w	Number of wind turbines.
n_o	Number of offshore substations.
m	Total number of years.
a_{ij}	Arc connecting point i to j (i,j).
d_{ij}	Euclidean norm for arc (i,j).
u_t	Capacity of cable t in number of wind turbines.
c_{c_t}	Metric capital cost of cable t.
c_{p_t}	Metric installation cost of cable t.
I_t	Steady-state rated current of cable t.
V_n	Nominal line-to-line voltage of the system.
P_n	Nominal power of the wind turbines.
S_{r_t}	Nominal power of cable t.
$\vec{\gamma}_t$	Propagation constant of cable t.
$\vec{Z}_{ct}$	Characteristic impedance of cable t.
$\vec{z}_t$	Metric series impedance of cable t.
$\vec{y}_t$	Metric admittance of cable t.
$\vec{I}^k_{ij,t}$	Nominal phasor current of arc (i,j) using cable t, when k wind turbines are connected.
$S^k_{ij,t}$	Nominal power of arc (i,j) using cable t, when k wind turbines are connected.
p^ω	Power produced by a wind turbine at ω hour-slot.
$f^{\omega,k}_{ij}$	Power flow in arc (i,j) at ω hour-slot, when k wind turbines are connected.
$\vec{I}^{\omega,k}_{ij,t}$	Phasor current through arc (i,j) using cable t, at ω hour-slot, when k wind turbines are connected.
λ_1	Screen losses factor.
λ_2	Armouring losses factor.
W_{d_t}	Metric dielectric loss of cable t.
R_t	Metric electrical resistance of cable t.
$l^{\mu,k}_{ij,t}$	Annual total power losses through arc (i,j) using cable t, at year μ, when k wind turbines are connected.
U	Capacity of the biggest cable available given as maximum number of supportable wind turbines.
r	Discount rate.
c^k_{ij}	Metric cost of arc (i,j), when k wind turbines are connected.
ϕ	Maximum number of feeders per offshore substation.
η	Loading symmetry coefficient for offshore substations.
υ	Number of wind turbines arcs set to a wind turbine.
υ_f	Number of wind turbines arcs set to a wind turbine for the feasibility problem.

$\upsilon_{f_{min}}$ $\upsilon_{f_\delta}, \upsilon_{f_{max}}$	Algorithm parameters for the feasibility problem.
υ_o	Number of wind turbines arcs set to a wind turbine for the global optimization problem.
$\upsilon_{o_{min}}$ $\upsilon_{o_\delta}, \upsilon_{o_{max}}$	Algorithm parameters for the global opt. problem.
ϵ	Required relative optimality gap.

Parameters (sets)

$\boldsymbol{N_o}$	Set of offshore substations.
$\boldsymbol{N_w}$	Set of wind turbines.
$\boldsymbol{N}$	Set of offshore substations and wind turbines.
G	Weighted directed graph.
$\boldsymbol{A}$	Set of available arcs.
$\boldsymbol{D}$	Set of arcs weights.
$\boldsymbol{T}$	Set of available cables.
$\boldsymbol{U}$	Set of cables capacities in wind turbines number.
$\boldsymbol{C_c}$	Set of cables capital expenditures costs.
$\boldsymbol{C_p}$	Set of cables installation costs.
$\boldsymbol{\Omega}^\mu$	Set of hours-slot for a year μ.
$\boldsymbol{M}$	Set of operational years.
G_r	First reduced graph.
$\boldsymbol{A_r}$	Set of first reduced arcs.
$\boldsymbol{\chi}$	Set of crossing pairs arcs.
$\boldsymbol{\Upsilon}_i$	Set of wind turbines connected to i.
$G_r^{'}$	Second reduced graph.
$\boldsymbol{A_r^{'}}$	Set of second reduced arcs.

Variables

x_{ij}	Binary variable to activate arc (i, j).
$x_{ij,t}$	Binary variable to select optimum cable type t for arc (i, j).
y_{ij}^k	Binary variable to activate arc (i, j), when k wind turbines are connected.
σ_i	Integer variable of number of wind turbines connected to offshore substation i.

Optimization output (non-sets)

ϵ_{k_f}	Calculated gap at iteration k_f.
ϵ_{k_o}	Calculated gap at iteration k_o.
ϵ_{k_g}	Recalculated gap at iteration k_g.

Optimization output (sets)

$\boldsymbol{I}$	Set of first feasible solution.
$\boldsymbol{O}_{k_o}$	Set of feasible solution at iteration k_o.
$\boldsymbol{\Gamma}_{k_o}$	Set of candidate arcs at iteration k_o.
$\boldsymbol{Z}_{k_o}$	Set of active variables $x_{ij} = 1$ of the problem defined in the iteration k_o.

Subscripts

i	Element in the set $\boldsymbol{N}$.
j	Element in the set $\boldsymbol{N}$.
ij	Arc (i, j) with tail at i and head at j.
k_f	Iteration for the feasibility problem.
k_o	Iteration for the global optimization problem.
k_g	Iteration for the general problem.
t	Cable type in the set $\boldsymbol{T}$.

Superscripts

k	Number of turbines connected in (i, j).
ω	Hour-slot $\in \boldsymbol{\Omega}^\mu$.
μ	Year $\in \boldsymbol{M}$.

I. Introduction

OFFSHORE wind energy represents a backbone technology towards the transition to power systems fully based on renewable energy.

After the invention, and experimentation age during the 1990s, the commercialization and development period is fundamentally focused on turning this technology into not only an environmentally sustainable paradigm, but also financially competitive compared to other classic, and emergent types of energy generation.

The share of Offshore Wind Farms (OWFs) has increased almost five times in the last seven years [1], reaching a globally installed power of nearly $19\,\mathrm{GW}$. OWF projects are capital intensive, having large values of operating leverage where the required electrical infrastructure costs can raise up to 15% compared to the total system costs [2].

The electrical collection system is the set of electrical infrastructure components (AC submarine cables, switchgears, transformers, protection, and control units, etc.). This is required to interconnect the Wind Turbines (WTs) with each other and the Offshore Substation (OSS), guaranteeing an effective, reliable, and efficient collection of energy to the export infrastructure.

Between 2018 and 2028 more than $19{,}000\,\mathrm{km}$ of cables for collection systems are prognosed to be installed in UK only, with an estimated worth of £5.36bn [3]. Economies of scale pushes the development of large-scale OWFs, having more than 80 WTs while increasing their rated power.

The collection system design and optimization problem has been studied with accentuated focus in the last ten years [4], [5]. Finding the global optimum of this problem is generally NP-hard [6]. Four big clusters of methods for tackling this problem can be established: heuristics, metaheuristics, global optimization with mathematical formulations, and hybrids, such as matheuristics.

Global optimization encompasses a large set of different alternatives to model the cable layout problem, like Binary Integer Programming (BIP) [7], Mixed Integer Linear Programming (MILP) [8]–[12], MILP with decomposition techniques for stochastic programming [13], [14], Mixed Integer Quadratic Programming (MIQP) [15], [16], and Mixed Integer Non-Linear Programming (MINLP) [17], [18]. Important advances on mathematical modelling are provided in [7], but disregarding fundamental practical considerations for OWFs, such as cables crossings, multiple OSSs, maximum number of feeders per OSS, wind power stochasticity, among others. The application focuses on global optimization for medium-scale OWFs (with the largest problem instance of 57 units). Similarly, [11] and [12] are tackling small-scale projects (with less than or equal to 30 WTs), without proposing any strategies for scaling the applications to large-scale problems and, as in [7], do not include practical

considerations in their modelling.
Larger instances are designed to optimality in [8], however, following a Planar Open Vehicle Routing Problem approach (no branching), restricting the cables set size, and ignoring power losses. Large-scale OWFs are tackled in [9] and [10], combining a MILP flow-based model with up to four heuristics, considering power losses, and other practical applications.
The works [13], [14], and [16] provide remarkable advances on stochastic optimization for problems in this context. Different stochastic scenarios are supported, accounting for wind power variability, and cables failure. Distinctive theoretical strategies to accelerate convergence are applied and compared. Nonetheless, some simplifications are incorporated, such as iterative processes to calculate total electrical power losses, combined with experts analysis to estimate their impact on the cable layout. Case studies are limited to small-scale applications.
By means of explicit formulation of electrical losses economic costs in the model, a MINLP program is proposed in [18], where, additionally, clustering algorithms are used prior the execution of the program into a commercial solver. Finally, losses can be also computed in the accurate quadratic form as in [15], but at the expense of a decrease in computational efficiency.
Each of these mathematical formulations impose certain limitations about the physics modelling options. For instance, using flow-based MILP makes it more difficult to include the quadratic active power losses explicitly into the objective function. The commonly used power flow equations solved with e.g. the Newton-Raphson method cannot be considered in MILP or MIQP formulations.
The side effects of more flexible modelling formulations are the compromise of solver functionality and performance. The proper balance between solution method and complexity on modelling, represents one of the main challenges for the OWF developer, and trade-offs have to be adopted within certain assumptions. As a generalization, linear-based formulations are computationally more efficient than quadratic or non-linear.
Since the trend in OWFs is to deploy large-scale projects, focus is directed into this aspect. To the best of the authors' knowledge, only [8], [9], [18], and [19] have tackled collection systems for large-scale OWFs with 80 - 100 WTs using global optimization. Only one cable type and no-branching at WTs nodes is considered by Bauer et. al. [8], where heuristics have also been proposed. A matheuristic framework is developed by Fischetti et. al. [9], including the total electrical power losses in the objective function using pre-processing strategies, and flow formulation. A MINLP flow formulation is used in [18], having sets of linear constraints but with explicit linearized losses inclusion in the objective; a fixed neighboring search is implemented, and pre-clustering of WTs to OSS is required, limiting artificially the search space, leading to sub-optimal points. No losses have been included in the optimization in [19], and for large-scale problems, computational experiments point out that feasible solutions may not be found. Additionally, only a single cable is supported.
The main contributions of this work are: (i) development, testing, and application of a mathematical model to quickly find feasible points for large-scale OWF instances (with more than 100 WTs). This is possible by proposing a MILP model with reduced constraints and variables than previously used flow formulations for collection systems in OWFs. (ii) combination of an algorithmic framework with mathematical formulation for obtaining global optimum solution points (or near to it) in reasonable computational time. Additionally, improvements on the complexity and fidelity of modelling aspects for integration with a linear formulation, such as total power losses calculated using time series, and capacitive currents, have been considered. The method does not require pre-clustering of WTs to OSSs, as this is tackled intrinsically in the model.
In Section II, the modelling aspects are explained in details; followed by Section III, where the optimization model is formulated including objective function and constraints definition. The whole framework description is presented in Section IV, where the full mathematical formulation is compacted into a single main iterative algorithm. Computational experiments are performed in Section V, and the work is finalized with the conclusions in Section VI.

II. Modelling aspects

A. Problem graph representation

The aim of the optimization is to design the cable layout of the collection system for OWFs, i.e., to interconnect the n_w WTs to the available OSSs, n_o.
In graph theory, a OWF is represented by a forest with roots at the OSSs. A few OWF developers opt for systems with loops. The inclusion of loops may increase reliability, but raises other technical challenges as cables sizing, and generally these systems are designed following heuristic and experts rules. Radial layouts are the common practice in the industry, since array cables failures are rather rare as they are buried in the seabed [20]. Therefore, the desired result is n_o spanning-trees, which minimize the required objective function, while satisfying the operational and topological constraints.
Let the OSSs define the set $\boldsymbol{N_o} = \{1, \cdots, n_o\}$. Likewise, for the WTs, let $\boldsymbol{N_w} = \{n_o + 1, \cdots, n_o + n_w\}$. In this way, each one of the OSSs and WTs (modelled as points in the space) have associated a unique identifier i, such as $i \in \boldsymbol{N} = \boldsymbol{N_o} \cup \boldsymbol{N_w}$. The Euclidean norm between the positions of the points i and j, is defined as d_{ij}. The aforementioned inputs are condensed as a weighted directed graph $G(\boldsymbol{N}, \boldsymbol{A}, \boldsymbol{D})$, where $\boldsymbol{N}$ represents the vertex set, $\boldsymbol{A}$ the set of available arcs arranged as a pair-set, and $\boldsymbol{D}$ the set of associated weights for each element $a_{ij} \in \boldsymbol{A}$, where $i \in \boldsymbol{N} \wedge j \in \boldsymbol{N}$. For instance, for $a_{ij} = (i, j)$, $d = d_{ij}$, where $d \in \boldsymbol{D}$. In general, $G(\boldsymbol{N}, \boldsymbol{A}, \boldsymbol{D})$ is a complete directed graph.
Additionally, a predefined list of available cables types is required to interconnect the WTs towards the OSSs. Let the set of cables be $\boldsymbol{T}$ and let the capacity of a cable $t \in \boldsymbol{T}$ be u_t measured in terms of number of supportable WTs connected downstream. Hence, let $\boldsymbol{U}$ be the set of capacities sorted as

in $\boldsymbol{T}$ (see the definition in Section II-B).
Furthermore, each cable type t has a cost per unit of length, c_{c_t}, in such a way that u_t and c_{c_t} describe a positive correlation, following an exponential regression model. The set of metric capital expenditures is defined as $\boldsymbol{C_c}$. Similarly the set of metric installation costs is defined by $\boldsymbol{C_p}$.
After defining the graph representation of the problem, the underlying variables associated to the calculation of the desired output, are unequivocally established. Let x_{ij} represent a binary variable that is one if the arc between the vertex i and j is selected in the solution, and zero otherwise. Likewise, the binary variable y_{ij}^k models the k number of WTs connected downstream from j, including the WT at node j (under the condition that $x_{ij} = 1$). Finally, the integer variable σ_i represents the number of WTs connected to the OSS i.

B. Cable capacity

The current capacity I_t of a cable t is calculated using the model given in [21]. This method represents the most common industrial practice, and it is based on a Single-Core Equivalent Thermal Model (SCETM) as generalized in [22] for single-core and three-core cables.

$$u_t = \left\lfloor \frac{S_{r_t} = \sqrt{3} \cdot V_n \cdot I_t}{P_n} \right\rfloor \quad \forall t \in \boldsymbol{T} \tag{1}$$

$$\boldsymbol{U} = \left\{u_1, \cdots, u_{|\boldsymbol{T}|}\right\} \tag{2}$$

The set of cable capacities in terms of number of supportable WTs is defined in (1) and (2), where P_n represents the nominal power of an individual WT, and V_n the line-to-line nominal voltage of the system.
The cables capacity must be assessed in terms of calculated maximum conductor temperature, and the maximum allowable value by design (usually considered $90\,^{\circ}\mathrm{C}$). In this manuscript, the conservative approach described in [21] is followed. This model neglects the slow thermal time constant of submarine cables, and the high variability of offshore wind power, since it assumes nominal steady state conditions. On the other hand, this practical assumption brings along as a result a robust design, while avoiding power curtailment at any instant.

C. Arcs nominal power

The power flow model of a transmission line solving the resultant differential equations considering parameters distributed uniformly throughout the length of the cable [23], is implemented with the expressions:

$$\vec{I}_{ij,t}^k = \frac{k \cdot P_n}{\sqrt{3} \cdot V_n} \cdot \cosh\left(\vec{\gamma}_t \cdot d_{ij}\right) - \frac{V_n}{\vec{Z}_{ct}} \cdot \sinh\left(\vec{\gamma}_t \cdot d_{ij}\right) \tag{3}$$

$$S_{ij,t}^k = \sqrt{3} \cdot V_n \cdot |\vec{I}_{ij,t}^k| \tag{4}$$

The model (3) provides the highest complexity on physics modelling possible to apply given the flexibility of the proposed mathematical formulation (see Section III). This provides more accuracy for securely determining the cable type in an active arc x_{ij}. The characteristic impedance is calculated as $\vec{Z}_{ct} = \sqrt{\vec{z}_t}/\vec{y}_t$, and the propagation constant, $\vec{\gamma}_t = \sqrt{\vec{z}_t} \cdot \vec{y}_t$. The series impedance is represented by $\vec{z}_t$, and the admittance by $\vec{y}_t$. The maximum power flowing through the arc (i, j), given k turbines connected downstream (y_{ij}^k), is calculated as per (4), accounting for the worst-case scenario, as the current in the arc is strictly increasing with length, and the value $\vec{I}_{ij,t}^k$ is calculated at the extreme of it when using cable t.

D. Power flow and total power losses

A transportation model, accurate enough for radial systems, is implemented following [4]. As explained in Section II-B, the set $\boldsymbol{U}$ assumes nominal steady state conditions, describing a practical conservative criterion.

$$\sum_{i \in \boldsymbol{N}} \sum_{k=1}^{f(i)} k \cdot y_{ij}^k \cdot p^\omega - \sum_{i \in \boldsymbol{N_w}} \sum_{k=1}^{f(i)} k \cdot y_{ji}^k \cdot p^\omega = p^\omega \tag{5}$$
$$\forall j \in \boldsymbol{N_w} \wedge \omega \in \boldsymbol{\Omega}^\mu \wedge \mu \in \boldsymbol{M}$$

The transportation model is generalized considering the temporal dimension (5), where $\boldsymbol{M} = \{1, \cdots, m\}$, is the set of operational years with upper limit in the project lifetime, $\boldsymbol{\Omega}^\mu$ is the set of hours-slot for a year μ, and ω a specific hour-slot in $\boldsymbol{\Omega}^\mu$. Let p^w be the power in MW produced by one WT in that hour-slot, simulated with [24].
In this way, let define the auxiliary variable $f_{ij}^{\omega,k} = k \cdot y_{ij}^k \cdot p^\omega$ as the power flow (MW) in arc (i, j) when k WTs are connected downstream (including the one in j), in time instant ω. This ignores wake losses, a reasonable assumption since micrositing optimization techniques are considered already applied [25].

$$\vec{I}_{ij,t}^{\omega,k} = \frac{f_{ij}^{\omega,k}}{\sqrt{3} \cdot V_n} \cdot \cosh\left(\vec{\gamma}_t \cdot d_{ij}\right) - \frac{V_n}{\vec{Z}_{ct}} \cdot \sinh\left(\vec{\gamma}_t \cdot d_{ij}\right) \tag{6}$$

$$l_{ij,t}^{\mu,k} \approx 3 \cdot (1 + \lambda_1 + \lambda_2) \cdot \sum_{\omega \in \boldsymbol{\Omega}^\mu} \omega \cdot R_t \cdot d_{ij} \cdot |\vec{I}_{ij,t}^{\omega,k}|^2 \tag{7}$$
$$+3 \cdot |\boldsymbol{\Omega}^\mu| \cdot \omega \cdot W_{d_t} \cdot d_{ij}$$

Including the capacitive currents, (6) expresses the current at the end of the arc (with respect to i), with magnitude $|\vec{I}_{ij,t}^{\omega,k}|$. The annual total power losses $l_{ij,t}^{\mu,k}$ are calculated with (7). The factor $(1 + \lambda_1 + \lambda_2)$ accounts for the screen and armouring losses and W_{d_t} is the dielectric loss per unit length for the insulation surrounding the conductor in $\mathrm{W/m}$ [21], while the constant 3 is for the three-phase system. This value must be scaled in MWh.

III. Optimization Model

The proposed optimization model described in this Section is able to cope with an arbitrary number of WTs, n_w, and similarly any reasonable number of OSSs, n_o.
The underlying mathematical formulation is inspired by the formulations and analysis proposed in [7] and [26] with additional constraints stemming from the nature of the problem, and with the objective to improve its tractability.
In Section II-A the binary variables x_{ij} and y_{ij}^k, and the integer variable σ_i are defined. They refer to an active arc, the number k of WTs connect to that active arc, and the number of WTs

connected to OSS i, respectively.
To increase the computational efficiency, the number of variables is reduced as follows. The capacity of the biggest cable is calculated as $U = \max \boldsymbol{U}$, therefore the possible maximum value of k for $i \in \boldsymbol{N_o}$ is equal to $f(i) = U$, while for $i \in \boldsymbol{N_w}$ is $f(i) = U - 1$. This acknowledges that the biggest cable available could be only used at maximum capacity when is connected from a OSS.
Analogously, the set of variables x_{ij}, where $i \in \boldsymbol{N_w}$, and $j \in \boldsymbol{N_o}$ are intrinsically discarded, considering the nature of the power flow, i.e., the OSSs collects the energy from the WTs and not the other way around. Lastly, since the export system is outside the scope of this article, all the arcs between OSSs are disregarded, i.e., $x_{ij} = 0 \; \forall i \in \boldsymbol{N_o} \wedge j \in \boldsymbol{N_o}$.
The graph $G(\boldsymbol{N}, \boldsymbol{A}, \boldsymbol{D})$ is reduced to $G_r(\boldsymbol{N}, \boldsymbol{A_r}, \boldsymbol{D_r})$ after this stage. While including the OSSs in the optimization could offer some flexibility, their locations are typically decided already in the development process. Furthermore, their locations are strongly driven by the distance to the onshore connection points, hence is deemed as plausible assumption to consider fixed location of the OSSs.

A. Cost coefficients

Note that the previously defined decision variables x_{ij} and y_{ij}^k, do not include any information related to the cable type selected in a given arc.
This is because the cable type selection process is handled in a pre-processing stage, given that all the required data is present, and the task is totally independent to any other part of the desired tree(s) [7].
A pre-processing strategy allows integrating more complex power flow and total electrical power losses models, increasing the accuracy without compromising the computational efficiency. Along these lines, the distributed model explained in Section II-C is harmonized with the main optimization problem.
At the same time, the aforementioned point allows for a power flow estimation in a conservative fashion, i.e., overestimating the incoming power flow by neglecting the total power losses downstream.
In the pre-processing state, for the case of y_{ij}^k, the length of the arc is known (d_{ij}), and the number of WTs connected by it is also defined (by k). No more inputs are required for this task.
Hence, for each y_{ij}^k, the sub-problem defined by (8) to (11) is solved beforehand and independently by enumeration.

$$c_{ij}^k = \min \sum_{t \in \boldsymbol{T}} x_{ij,t} \cdot \left((c_{c_t} + c_{p_t}) \cdot d_{ij} + \sum_{\mu=1}^{m} \frac{l_{ij,t}^{\mu,k} \cdot c_e}{(1+r)^\mu} \right) \quad (8)$$

$$\text{s.t.} \quad \sum_{t \in \boldsymbol{T}} x_{ij,t} = 1 \quad (9)$$

$$x_{ij,t} \cdot (S_{ij,t}^k - S_{r_t}) \leq 0 \quad \forall t \in \boldsymbol{T} \quad (10)$$

$$x_{ij,t} \in \{0, 1\} \quad \forall t \in \boldsymbol{T} \quad (11)$$

In the objective function (8), the first term $((c_{c_t} + c_{p_t}) \cdot d_{ij})$ is for capital expenditure (c_{c_t}) and installation costs (c_{p_t}) of cable t.
The values for $c_{c_t} \in \boldsymbol{C_c}$ are obtained from the exponential regression function, given as

$$c_{c_t} = a_{p_t} + b_{p_t} \cdot \mathrm{e}^{\left(\frac{c_{p_t} S_{r_t}}{10^8}\right)^2} \quad (12)$$

where a_{p_t}, b_{p_t}, and c_{p_t} are coefficients dependent on the nominal voltage of cable type $t \in \boldsymbol{T}$, S_{r_t} is the rated power of t in VA (also depending on the rated line to line voltage level, V_n, see the definition in Section II-B). The cables capital expenses cost function (12) is extracted from [27], being based on a comprehensive semi-empirical cost survey, applying data fitting techniques.
The second term in the summation part of (8) accounts for the discounted cash flow of the economic losses caused by the energy dissipation in the cables, the parameters m, $l_{ij,t}^{\mu,k}$ (see Section II-D), c_e, and r, represents the project lifetime (years), total power losses at year μ for cable t (MWh), cost of energy (€/MWh), and discount rate (p.u.) respectively.
The objective function can be simplified by zeroing any of its terms, such as, if only the total length is minimized (L), the first term in (8) has to be replaced uniquely by d_{ij}, while the other term in the same equation is dropped. Similarly, if only the total initial investment (I) is targeted, only the first is kept. Therefore, the set of single objectives available in the model are: length (L), length plus total power losses (LP)—monetizing lengths by assuming the same capital and installation costs for all cables types, initial investment (I), and initial investment plus total power losses (IP).
Likewise, (9) ensures that exactly one cable type is selected, while (10) guarantees that the capacity of cable t is not exceeded; $S_{ij,t}^k$ is the power through arc (i, j) when k turbines are connected in j using cable t defined in Section II-C. The binary variable for selecting a cable type t for arc (i, j) is defined in (11).
The sub-problem from (8) to (11) seeks to find the cable type t to be used for the arc (i, j), which minimizes the objective (8).

B. Objective function

After solving the multiple sub-problems related to cable selection and cost evaluation (maximum $U \cdot |\boldsymbol{N}|^2$ problems) from (8), a cost value c_{ij}^k is associated to each y_{ij}^k variable. The linear objective function of the main mathematical model is then

$$\min \sum_{i \in \boldsymbol{N}} \sum_{j \in \boldsymbol{N_w}} \sum_{k=1}^{f(i)} c_{ij}^k \cdot y_{ij}^k \quad (13)$$

C. Constraints

In order to present the solution connecting all WTs between each other and to the OSSs, the following constraint is added

$$\sum_{i \in \boldsymbol{N_o}} \sigma_i = n_w \quad (14)$$

Constraint (14) models the full OWF to be divided into multiple disconnected trees (forest) with σ_i being the number of WTs associated to a OSS i. Hence, the total amount of WTs (n_w) are integrated into the electrical system.

To guarantee full connectivity in OSS i, the next constraint is added

$$\sum_{j \in \boldsymbol{N_w}} \sum_{k=1}^{f(j)} k \cdot y_{ij}^k = \sigma_i \quad \forall i \in \boldsymbol{N_o} \tag{15}$$

Note that (14) and (15) are combined in the case of only one OSS.
To limit the maximum number of feeders per OSS (ϕ), it is used:

$$\sum_{j \in \boldsymbol{N_w}} \sum_{k=1}^{f(j)} y_{ij}^k \leq \phi \quad \forall i \in \boldsymbol{N_o} \tag{16}$$

To simultaneously ensure a tree topology, ensure that only one cable type used per arc, and to define the head-tail convention, the next expression is included into the model

$$\sum_{i \in \boldsymbol{N}} \sum_{k=1}^{f(i)} y_{ij}^k = 1 \quad \forall j \in \boldsymbol{N_w} \tag{17}$$

The flow conservation, which also avoids disconnected solutions, is considered by means of one linear equality per wind turbine

$$\sum_{i \in \boldsymbol{N}} \sum_{k=1}^{f(i)} k \cdot y_{ij}^k - \sum_{i \in \boldsymbol{N_w}} \sum_{k=1}^{f(i)} k \cdot y_{ji}^k = 1 \quad \forall j \in \boldsymbol{N_w} \tag{18}$$

The set $\boldsymbol{\chi}$ stores pairs of arcs $\{(i,j),(u,v)\}$, which are crossing each other. Excluding crossing arcs in the solution is ensured by the simultaneous application of the following linear inequalities

$$x_{ij} + x_{ji} + x_{uv} + x_{vu} \leq 1 \quad \forall \{(i,j),(u,v)\} \in \boldsymbol{\chi} \tag{19}$$

$$\sum_{k=1}^{f(i)} y_{ij}^k - x_{ij} \leq 0 \quad \forall (i,j) \in \boldsymbol{A_r} \tag{20}$$

The no-crossing cables restriction is a practical requirement in order to avoid hot-spots, and potential single-points of failure caused by overlapping cables [8]. Constraint (19) exhaustively lists all combinations of crossings arcs, including also the corresponding inverse elements. The constraints in (20) ensure that no active arcs are crossing or overlapping between each other. These constraints thus link the variables y_{ij}^k and x_{ij}.
Cables crossings are detected based on a procedure of slopes evaluation. Two arcs are crossing if the crossing point is inside of the lines, but not if this point is located at the extremes of the lines or beyond in the lines' projections.

$$-\sum_{i \in \boldsymbol{N}} \sum_{k=v+1}^{f(i)} \left\lfloor \frac{k-1}{v} \right\rfloor \cdot y_{ij}^k + \sum_{i \in \boldsymbol{N_w}} \sum_{k=v}^{f(i)} y_{ji}^k \leq 0 \tag{21}$$
$$\forall v = \{2, \cdots, U-1\} \wedge j \in \boldsymbol{N_w}$$

Constraint (21) represents a set of valid inequalities, initially proposed in [7], to tighten the mathematical model. Given an active arc y_{ij}^k, the maximum number of active arcs rooted in j and connecting v WTs, is expressed by $\left\lfloor \frac{k-1}{v} \right\rfloor$, hence the constraint restricts the maximum number feasible arcs, reducing the search space without excluding valid solutions to the problem.

$$x_{ij} \in \{0,1\} \quad y_{ij}^k \in \{0,1\} \tag{22}$$
$$\forall (i,j) \in \boldsymbol{A_r} \wedge k \in \{1, \cdots, f(i)\}$$

$$0 \leq \sigma_i \leq \eta \cdot \left\lceil \frac{n_w}{n_o} \right\rceil \quad \sigma_i \in \mathbb{Z}_+ \quad \forall i \in \boldsymbol{N_o} \tag{23}$$

Constraints (22) and (23) define the nature of the formulation by the variables definition, a MILP.
Note that variables σ_i are limited in their upper bounds to avoid uneven loading of OSSs (in case $\eta = 1$, otherwise $1 < \eta \leq n_o$). Equally rated OSSs bring benefits like design standardization, and decreasing of the dependency upon a single transformation unit for transporting the generated power.
To summarize, the complete formulation of the main MILP model consists of the objective function (13) and the constraints defined in (14) - (23).
The base formulation presented so far has a maximum number of binary variables equal to $|\boldsymbol{N}|^2 + U \cdot |\boldsymbol{N}|^2$, integer variables number equal to $|\boldsymbol{N_o}|$ (linear in function of n_o), and constraints (excluding the crossing constraints and valid inequalities) of $1 + 2 \cdot |\boldsymbol{N_o}| + 2 \cdot |\boldsymbol{N_w}|$. Flow formulations, such as the one proposed in [9], have more variables ($2 \cdot |\boldsymbol{N}|^2 + U \cdot |\boldsymbol{N}|^2$) and constraints ($|\boldsymbol{N}|^2 + 2 \cdot |\boldsymbol{N_w}| + |\boldsymbol{N_o}|$); integer and binary variables are quadratic in function of the problem size. This fact along with the addition of valid inequalities may explain why the model from (13) to (23) is often more efficient to solve.
Further simplifications to the model are presented in Section IV-A.

IV. Optimization framework

A. Candidate arcs

The reduced graph G_r is obtained after performing the described considerations in the introduction of Section III.
However, given the NP-Hard nature of this problem, which is similar to a Capacitated Minimum Spanning Tree with additional constraints [11], [28], more reductions are required. The limitations for successfully finding feasible points and high quality solutions, using solely mathematical models and commercial solvers, is demonstrated in [9].
For large-scale OWFs (with more than 100 WTs) the computing time for robust global optimization solvers generally becomes notoriously long. Likewise, in general, solution times become unpredictable, while very large memory requirements are demanded to build the branch-and-cut tree. Besides, the constraints generation must be done with special care (the full set of crossing constraints has a combinatorial nature) to increase computational efficiency.
To make the formulation more flexible and implementable, a further operation to the graph G_r is proposed. The function $f(i, G_r, v)$ calculates the set $\boldsymbol{\Upsilon}_i$, defined as the v-closest WTs to i. In other words, it is intuitively considered that a WT will be connected to one of the WTs in its vicinity. Therefore, by systematically applying $f(i, G_r, v)$ to each $i \in \boldsymbol{N_w}$, the

reduced graph $G_r^{'}$ is found. The set $\boldsymbol{A_r^{'}}$ contains the candidate arcs to the solution of the problem.
With this strategy, the maximum number of variables is reduced to $|\boldsymbol{N_o}|+(U+1)\cdot|\boldsymbol{N_o}|\cdot|\boldsymbol{N_w}|+U\cdot\upsilon\cdot|\boldsymbol{N_w}|$. Additionally, the number of crossing constraints decreases dramatically as well.
Overall, the arcs set transformation follows $\boldsymbol{A}\rightarrow\boldsymbol{A_r}\rightarrow\boldsymbol{A_r^{'}}$. All (ij) indexed variables and constraints, presented in the Section III, must be adapted to this reduction process.

B. The Algorithm

The main algorithm defining the full framework with the mathematical model is presented in Algorithm 1.
From line 1 to 12 the task is to efficiently solve a feasibility problem. The idea is to subsequently increase υ from an initial value $\upsilon=\upsilon_f=\upsilon_{f_{min}}$ to a maximum value $\upsilon=\upsilon_f=\upsilon_{f_{max}}$, with steps υ_{f_δ}, until a feasible point is found. If this is achieved in iteration k_f, the first task is terminated with a feasible point $\boldsymbol{I}$. Conversely, if the model is infeasible, the candidate arcs set is augmented with υ_{f_δ} units, and the process is taken to the iteration k_f+1, where a new trial is attempted.

1. $k_f\leftarrow 1$
2. **for** $(\upsilon_f=\upsilon_{f_{min}}:\upsilon_{f_\delta}:\upsilon_{f_{max}})$ **do**
3. $\quad G_r^{'}\leftarrow f(i,G_r,\upsilon_f)\quad\forall i\in\boldsymbol{N_w}$
4. $\quad c_{ij}^k=0\quad\forall(i,j)\in\boldsymbol{A_r^{'}}\wedge k\in\{1,\cdots,f(i)\}$
5. $\quad$ *Formulate and solve MILP model from (13) to (23)*
6. $\quad$ **if** *(problem is feasible)* **then**
7. $\quad\quad$ *Save initial feasible point found:* $\boldsymbol{I}=x_{ij}\cup y_{ij}^k\quad\forall(i,j)\in\boldsymbol{A_r^{'}}\wedge k\in\{1,\cdots,f(i)\}$
8. $\quad\quad$ *Break*
9. $\quad$ **else**
10. $\quad\quad k_f\leftarrow k_f+1$
11. $\quad$ **end if**
12. **end for**
13. $k_o\leftarrow 1$
14. **for** $(\upsilon_o=\upsilon_{o_{min}}:\upsilon_{o_\delta}:\upsilon_{o_{max}})$ **do**
15. $\quad G_r^{'}\leftarrow f(i,G_r,\upsilon_o)\quad\forall i\in\boldsymbol{N_w}$
16. $\quad\boldsymbol{\Gamma}_{k_o}=\boldsymbol{A_r^{'}}$
17. $\quad$ *Get c_{ij}^k through model from (8) to (11)*
18. $\quad$ *Formulate MILP model from (13) to (23)*
19. $\quad$ **if** $(k_o==1)$ **then**
20. $\quad\quad$ *Warm start with initial feasible point $\boldsymbol{I}$*
21. $\quad$ **else**
22. $\quad\quad$ *Warm start with feasible point obtained in $\boldsymbol{O}_{k_o-1}$*
23. $\quad$ **end if**
24. $\quad$ *Solve MILP model from (13) to (23)*
25. $\quad\boldsymbol{Z}_{k_o}=\{(i,j)\}:x_{ij}=1\quad\forall(i,j)\in\boldsymbol{A_r^{'}}$
26. $\quad$ **if** $(k_o>1)$ **then**
27. $\quad\quad$ **if** $(\boldsymbol{Z}_{k_o}\subset\boldsymbol{\Gamma}_{k_o-1})$ **then**
28. $\quad\quad\quad$ *Save best feasible point found:* $\boldsymbol{O}_{k_o}=x_{ij}\cup y_{ij}^k\quad\forall(i,j)\in\boldsymbol{A_r^{'}}\wedge k\in\{1,\cdots,f(i)\}$
29. $\quad\quad\quad$ *Break*
30. $\quad\quad$ **else**
31. $\quad\quad\quad$ *Save feasible point found:* $\boldsymbol{O}_{k_o}=x_{ij}\cup y_{ij}^k\quad\forall(i,j)\in\boldsymbol{A_r^{'}}\wedge k\in\{1,\cdots,f(i)\}$
32. $\quad\quad$ **end if**
33. $\quad$ **end if**
34. $\quad k_o\leftarrow k_o+1$
35. **end for**
36. *Recalculate gaps*

Algorithm 1: The main algorithm

In order to formulate the MILP model, the cost coefficients calculation from (8) to (11) is omitted by setting them equal to zero, and the black-box MILP solver terminates when the first feasible point is found.
At this point, the Algorithm 1 requires as parameters $\upsilon_{f_{min}}$, υ_{f_δ}, and $\upsilon_{f_{max}}$. The greater $\upsilon_{f_{min}}$ and υ_{f_δ} the less efficient the feasibility problem becomes, however, increasing the odds to defining a feasible instance of the problem promptly.
Likewise, from line 13 to 35, the global optimization task is performed. The target is to obtain a feasible point with a given relative gap ϵ, expressed as the relative difference of the best feasible point (τ) minus the best achievable value objective (κ), with respect to τ. These values are indexed by iteration number. Similarly to the feasibility task, the iterative process increases the candidate arcs set from $\upsilon=\upsilon_o=\upsilon_{o_{min}}$ to $\upsilon=\upsilon_o=\upsilon_{o_{max}}$, with steps υ_{o_δ}.
The termination criterion is when the set $\boldsymbol{Z}_{k_o}$ of active variables $x_{ij}=1$ of the problem defined in the iteration k_o, is a subset of the arcs set $\boldsymbol{A_r^{'}}$ defined in the previous iteration k_o-1 $(\boldsymbol{\Gamma}_{k_o-1})$.
In this way, it is inferred that it is not longer necessary to increase υ_o, as the optimum variables have been already provided in the previous iteration.
To guarantee along the process a monotonously decreasing value of the objective function, in iteration k_o, the mathematical model is warm-started with the feasible solution found in k_o-1 $(\boldsymbol{O}_{k_o-1})$. This strategy may help in shortening the convergence time for the sub-instance k_o.
Conceptually, Algorithm 1 intends to determine a reduced search space, where the global minimum point is hopefully included. If only one reduced problem was solved given a υ, it would not be possible to infer about the quality of the solution, and the calculated gap for that particular instance could not represent the global domain of the full problem, potentially leading to an overestimation.
For the global optimization task, Algorithm 1 requires as parameters $\upsilon_{o_{min}}$, υ_{o_δ}, and $\upsilon_{o_{max}}$ for the global optimization task. Naturally, $\upsilon_{o_{min}}\geq\upsilon_{f_{max}}$, and it is reasonable to consider $\upsilon_{o_\delta}>\upsilon_{f_\delta}$. By proper adjustment of the previous parameter, in best case scenario, the full Algorithm is concluded for $k_f=1$ and $k_o=2$.
Although for every iteration the maximum required gap ϵ is equally fixed, the equivalent calculated gap, having as reference the full-size domain, varies. Larger values of υ_{k_o} lead to equal or lower values of κ_{k_o}. This causes that in general, τ_{k_o} is also lower, until the ideal reduced search space is found, when equal values of τ_{k_o} should be obtained.
Therefore, after the termination of the algorithm, a gap updating procedure is performed based on the last calculated value of κ_{k_o}, to recalculate the relative difference for all previous iterations respect to this value (line 36). Let the recalculated gap in the global iteration k_g, including the feasibility and global optimization problems, be ϵ_{k_g}. In this sense, an evolution of the gap in function of the iterations

is available, providing further insights and the sense of convergence, as the objective value decreases monotonically.

V. Computational Experiments

The following experiments have been carried out on an Intel Core i7-6600U CPU running at 2.50 GHz and with 16 GB of RAM. The chosen MILP solver is the branch-and-cut solver implemented in IBM ILOG CPLEX Optimization Studio V12.7.1 [29].

In the Section V-A a sensitivity analysis of the parameters $\upsilon_{o_{min}}$, and υ_{o_δ} is presented. This is achieved by applying the proposed methodology of Section IV, on two OWFs using several sets of parameters.

In Section V-B, the proposed method is benchmarked against the results obtained through a different approach published in the scientific literature [9]. With this aim, the same testbed is employed, while assuming the same considerations, such as, objective (8)-(11), and constraints embodied by the equations (14)-(23).

A. Algorithm's Parameters Sensitivity Analysis

The two real OWFs West of Duddon Sands (WDS) and Thanet (TH) are used for the parameter sensitivity analysis. The information regarding these OWFs is provided in [30].

Table I displays the main parameters for the sensitivity analysis. In the case of WDS, the objective function is defined by a combined total economic cost including the initial investment, and the total electrical power losses of the cable layout (IP). Whilst for TH, the target is to minimize the initial investment of the cable layout, defined as the cables capital expenditures, and installation costs.

The difference between objective functions is not relevant for the purposes of the sensitivity analysis, but rather, to show the capability of the method to support both cases. Economic parameters for the discounted cash flows calculations are also presented.

Both instances are challenging to solve given their large size (equal or more than 100 WTs each), the large number of cables sizes considered (up to three cables types), and maximum capacity $U = \max \boldsymbol{U}$, spanning from 10 to 13 (see Table I). High-level information such as WT power and number (P_n and n_w), OSSs number (n_o), and the maximum number of allowed feeders connected to the OSSs (ϕ) is available. The limit ϕ provides a hard binding constraint. It is fixed to a practical value usually considered by OWFs developers.

Finally, the rest of parameters for the optimization are displayed. The collection systems voltage level (V_n) is the traditionally used, and two different set of cables are considered. The electrical and thermal information of the cables is available in [31].

The capacity set $\boldsymbol{U}$ is determined for each instance, similarly, for the total cost per kilometer, including capital expenditures ($\boldsymbol{C_c}$), and installation costs $\boldsymbol{C_p}$. The cables $\{1, 2, 3\}$ have cross-sections of $240\,\mathrm{mm}^2$, $500\,\mathrm{mm}^2$, and $1{,}000\,\mathrm{mm}^2$, respectively.

The set represented by $\{4, 5\}$ is used for TH, and it has associated electrical and economic parameters matching those considered in the benchmark work [9], while neglecting the capacitive currents (see Section V-B for benchmark analysis).

The whole framework compacted in Algorithm 1 intends to find an approximation of the minimum search space of a given instance. It is presumed the finding the model best feasible point (or near to it) for a given required maximum gap, having as reference the full (global) problem size.

Each problem instance is composed by $k_g = k_f + k_o$ sub-instances (or general iterations), which in turn include those iterations required for solving the feasibility (k_f), and global optimization serial problems (k_o); this implies that, in the best-case scenario, a maximum number of iterations equal to $k_f = 1$ and $k_o = 2$ should be enough to solve any problem instance.

However, factors such as the adequate setting of the algorithm's parameters and the specific spatial characteristics influence the number of global iterations k_g, and the circumvention of local minima.

The avoidance of local minima is crucial, as it has a lifetime impact over a project. Successful implementations depend on the chosen values of $\upsilon_{o_{min}}$, and υ_{o_δ}. The sensitivity analysis elaborates on how the iterative reduction of the search space through Algorithm 1 can lead to sub-optimal solutions.

In pursuance of this, two values associated to the initial value parameter, $\upsilon_{o_{min}}$, are examined: $\{6, 15\}$; while the increase steps parameter, υ_{o_δ}, is set between $\{2, 5, 10\}$. All possible combinations of both parameters are applied to WDS and TH OWFs through the Algorithm 1.

The results are graphically shown in Figure 1 presenting quality of the solution (ordinate) versus computing time (abscissa). Both are normalized to the best corresponding case. Each case is depicted in the legend with [$\upsilon_{o_{min}}$,υ_{o_δ}], i.e. [6,2] and so on.

The results show that for the WDS OWF, the solution for $\upsilon_{o_{min}} = 6$, and $\upsilon_{o_\delta} = 2$ is nearly 2% more expensive than the other cases (see Figure 1a, case [6,2]). For the rest of parameters sets, the obtained solutions are, in practical terms, the same. The costs differences among them are due to the inclusion of total electrical power losses, which are sensitive to small changes of cables lengths. The computing times varies almost in a positively correlated fashion with the values of these parameters, with the fastest case being also the most expensive.

This could be explained by the particular spatial characteristics of WDS, which impact the number of minimum candidate arcs to cover the global minimum. The optimized layout shown in Figure 2a ($\upsilon_{o_{min}} = 15$ and $\upsilon_{o_\delta} = 5$) evidentiate the non-uniform distribution of WTs in the plane, with empty areas around WTs number 43 and number 44, for instance. This can be interpreted as a higher degree of freedom in the design, having the possibility to interconnect WTs located further away from each other.

One should note that the optimized layout has a connection between WTs number 72 and 43, the latter being out of the top-15 closest WTs for the former (in fact, is the 17th closest), hence, making it necessary to increase υ_o to 20, to include this connection.

Returning to the case of $\upsilon_{o_{min}} = 6$, and $\upsilon_{o_\delta} = 2$, the step

TABLE I
MAIN INPUTS PARAMETERS FOR SENSITIVITY ANALYSIS

OWF	Obj.	r[%]	c_e[€/MWh]	m	P_n [MW]	n_w	n_o	ϕ	η	V_n [kV]	$\boldsymbol{T}$	$\boldsymbol{U}$	$\boldsymbol{C_c}+\boldsymbol{C_p}$ [M€/km]
WDS	IP	5	40	30	3.6	108	1	10	1	33	$\{1,2,3\}$	$\{7,10,13\}$	$\{0.36,0.58,0.90\}$
TH	I	-	-	-	3	100	1	10	1	33	$\{4,5\}$	$\{7,10\}$	$\{0.44,0.62\}$

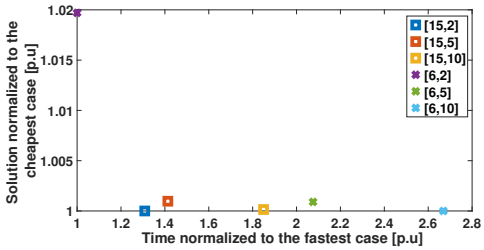

(a) Sensitivity Analysis for West of Duddon Sands (WDS).

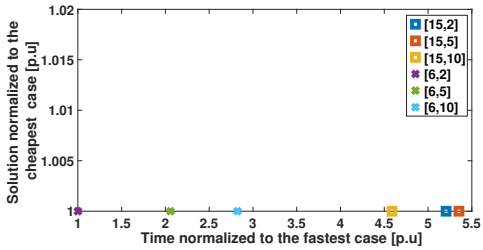

(b) Sensitivity Analysis for Thanet (TH).

Fig. 1: Sensitivity Analysis Results.

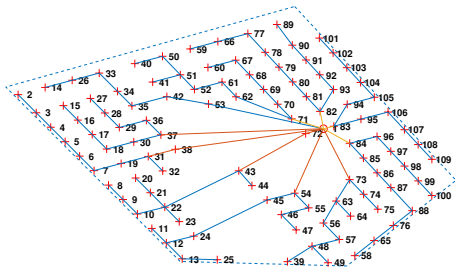

(a) West of Duddon Sands (WDS) Designed Cable Layout. Yellow line: Cable $1{,}000\,\mathrm{mm}^2$, Orange line: Cable $500\,\mathrm{mm}^2$, Blue line: $240\,\mathrm{mm}^2$.

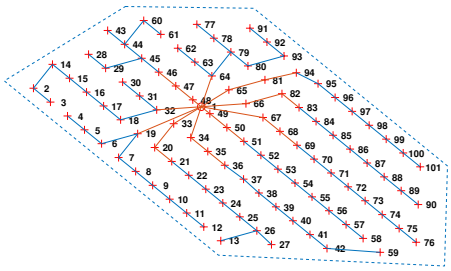

(b) Thanet (TH) Designed Cable Layout. Orange line: Cable supporting up to 10 WTs, Blue line: Cable supporting up to 7 WTs.

Fig. 2: Designed Cable Layouts,

increase value is not enough to provide a significantly broader search space to improve the solution quality.

The results suggest that the values of $\upsilon_{o_\delta}=5$, and $\upsilon_{o_\delta}=10$, result in an improvement of the solution in each iteration, and confirm in the last iteration the covering of minimum candidate arcs set. A value of $\upsilon_{o_\delta}=2$ in this case provides the same output, but evidently with potentially higher chances of falling into suboptimal points for other OWFs.

For the TH OWF, all the cases generate the same result, as shown in Figure 1b. In contrast to WDS OWF, Thanet presents a regular (grid-based) micrositing layout (see Figure 2b), hence, less degree of flexibility, which translates in an optimum point represented by WTs each connected to maximum the 6th closest WT.

In order to increase the likelihood for getting a balance between solution quality, computing time, and memory requirements, a heuristic rule of considering $\upsilon_{o_{min}}=15$, and $\upsilon_{o_\delta}=5$ is implemented in this manuscript.

Certainly, every single OWF should be individually analysed to come up with tailored parameters, but results point out that these settings may lead to adequate terminations in most of the problems.

Table II summarizes in-detail the results of the experiments using the proposed framework with $\upsilon_{f_{min}}=5$, $\upsilon_{f_\delta}=1$, $\upsilon_{f_{max}}=15$, $\upsilon_{o_{min}}=15$, $\upsilon_{o_\delta}=5$, and $\upsilon_{o_{max}}=50$.

For each of the sub-instances, the output CT1 includes the total processing time in order to generate the Constraints (14) to (23), and additionally, the solution of the independent sub-problems as defined in the model from (8) to (11). Note that in the case of the feasibility problems the latest procedure is circumvented by fixing the cost coefficients equal to zero.

Likewise, CT2 is the computing time to solve the main mathematical model (from (13) to (23)) for a given maximum gap, in the case of WDS $\epsilon=0.5\%$, and for TH $\epsilon=0.3\%$. An additional experiment with $\epsilon=0.5\%$ for TH has been run, with a duration of around an hour, finding a solution only 0.07% more expensive than the one presented in Table II, with a calculation time approx. 50% smaller. In principle, any imposed maximum gap is supported, at the potential expense of a very steep increase on computing time. The column Obj presents the objective value of the best feasible point obtained under the explained conditions, after the termination of each

TABLE II
IN-DETAIL RESULTS SUMMARY

	k_f/ k_o	v_f/ v_o	CT1 Time Unit	CT2 Time Unit	Obj [M€]	$\epsilon_{k_f}/\epsilon_{k_o}$ [%]	ϵ_{k_g} [%]
W	$k_f \leftarrow 1$	$v_f \leftarrow 5$	7.89s	36.93s	72.84	0	38.62
D	$k_o \leftarrow 1$	$v_o \leftarrow 15$	0.08h	1.01h	45.70	0.46	2.17
S	$k_o \leftarrow 2$	$v_o \leftarrow 20$	0.11h	0.36h	44.93	0.47	0.50
	$k_o \leftarrow 3$	$v_o \leftarrow 25$	0.14h	0.16h	44.93	0.50	0.50
T	$k_f \leftarrow 1$	$v_f \leftarrow 5$	6.65s	10.37s	40	0	33.60
H	$k_o \leftarrow 1$	$v_o \leftarrow 15$	15.80s	1.02h	26.64	0.30	0.30
	$k_o \leftarrow 2$	$v_o \leftarrow 20$	30.22s	0.75h	26.64	0.30	0.30

sub-instance calculation. Finally, the columns $\epsilon_{k_f}/\epsilon_{k_o}$, and ϵ_{k_g} gather the calculated gap of the best feasible point, and the recalculated gap for each sub-instances, respectively, after the Algorithm 1 terminates as explained in Section IV-B.

By means of this strategy, is surmised the delimitation of a reduced search space representative of the global problem, including the global minimum point.

In the particular case of WDS, the results say that an unnecessary continuation to a fifth cycle, i.e. $k_g = 5$, was avoided due to the warm start strategy. The objective value does not change between $k_o = 2$ and $k_o = 3$, this being a clear (but not mathematically conclusive) signal of the successful convergence of the method.

Furthermore, an overestimation of ϵ_{k_o} is seen for $v_o = 15$ when referenced to the approximated minimum search space, as $\epsilon_{k_g} = 2.17\% > 0.5\%$. It should be noted that the first feasible point is found in almost 45 seconds, and from there, the best feasible point is found in very reasonable computing time. A reduction of the gap from 38.62% to 0.50% is obtained in only 1 h:53 min (one hour and 53 minutes).

In contrast to WDS, only three global iterations are required for TH, mainly due to the more uniform distribution of WTs, as shown in the Figure 2b. For TH OWF, a feasible point is obtained in 17 s, and in 1 h:47 min the gap is improved from 33.60% to 0.30%.

The proposed procedure can be impacted by multiple valid solutions around the required maximum gap. Nevertheless, this would cause only false continuations of the Algorithm 1, rather than affect the solution quality. The previous point is partially palliated by the likely decrease of computing time in subsequent iterations, given the warm start point provided from the previous step. If the objective value was used as criterion to stop the algorithm, a maximum ratio of objective change per subsequent iterations should be set, which would be open to different assessment criteria, and potentially could lead to false terminations.

For both WDS and TH, the values ϵ_{k_g} reported in Table II for the last iteration, are representative of the full problem; fact validated when solving them without reduced search space (full arcs set), provided the best feasible point available.

B. Benchmarking

A testbed of real-world cases, presented in Table III, is employed. The OWFs names are given in the Acronyms definition. Results comparison are available in Table IV.

This testbed has been mostly extracted from [9], by selecting the most challenging instances. In [9] a significantly different approach (different mathematical formulation, for instance) from the one proposed in this article, consisting in a matheuristic model, has been designed, implemented, and tested.

The results in [9] where obtained with computational resources similar to those used in this manuscript (IX CPU X5550 running at 2.67GHz, CPLEX 12.6).

In order to provide a fair comparison, all practical and technical constraints are conceptually equivalent, while the objective function is the initial investment, as losses are computed differently. Likewise, capacitive currents have been neglected as they are not included in [9].

The comparison results are presented in Table IV (instances 1-9). A small (O), two large (HR1 and DT), and a very large OWF (TH) are studied. Each instance is defined by a OWF, and a set of cables available $\boldsymbol{T}$.

Three aspects are compared: (i) solution quality, (ii) calculated gap, and (iii) computing time; each of them are directly compared by inspecting the columns Diff.[M€], Diff.[%], and Diff.[min], respectively. In all metrics, positive value means better performance for the method proposed in this article.

Regarding solution quality, it can be seen that, for all instances, the obtained solutions are equal or lower than in the benchmark work. For instance nr. 7, around €550,000, representing around 1% of the total cost, are saved. Particularly for this instance, the gap is improved from 7.36% to 0.01%, while simultaneously reducing the computing time. When the calculated gap in both methods is lower than 0.01%, the objective values are essentially the same. This validates that the dual values between the two models are also equivalent.

In any instance the proposed method provides equally tight or even tighter solutions. The gap values reported in [9] have been recalculated in this manuscript using the best feasible point as reference (instead of the best dual value obtained in 24 h), to make them comparable with the proposed approach. Finally, in almost all the instances, the computing time is shorter, with exception of instance nr. 8, where a considerable difference of 622 min is observed.

It is important to clarify that the reported computing times of the proposed method are for the whole running of Algorithm 1, including in all instances the final iteration $k_o = 2$, necessary to confirm finding the global point; in contrast, in the benchmark work, the reported time is when the best feasible point has been found. Similarly, as mentioned before, 24 h is the time limit to obtain the best dual value.

For all the instances, the proposed method calculates feasible points in less than 40 s, with recalculated gap of maximum 41%.

Besides the benchmark cases, an extra instance - not implemented in [9] - is included to show the method's applicability to OWFs with multiple OSSs. LA OWF is the second largest project (measured by installed power) under operation, surpassed only by Walney Extension OWF

TABLE III
MAIN INPUTS PARAMETERS FOR BENCHMARKING

Ins.	OWF	Obj.	r[%]	c_e[€/MWh]	m	P_n [MW]	n_w	n_o	ϕ	η	V_n [kV]	$\boldsymbol{T}$	$\boldsymbol{U}$	$\boldsymbol{C_c}$+$\boldsymbol{C_p}$ [M€/km]
1	HR1	I	-	-	-	2	80	1	10	1	33	$\{6,7,8\}$	$\{7,11,13\}$	$\{0.37,0.39,0.43\}$
2	HR1	I	-	-	-	2	80	1	10	1	33	$\{9,10\}$	$\{7,12\}$	$\{0.44,0.45\}$
3	HR1	I	-	-	-	2	80	1	10	1	33	$\{4,5\}$	$\{10,14\}$	$\{0.44,0.62\}$
4	O	I	-	-	-	5	30	1	4	1	33	$\{11,12\}$	$\{5,10\}$	$\{0.41,0.61\}$
5	O	I	-	-	-	5	30	1	4	1	33	$\{13,14\}$	$\{4,9\}$	$\{0.38,0.63\}$
6	DT	I	-	-	-	3.6	80	1	10	1	33	$\{6,7,8\}$	$\{4,6,8\}$	$\{0.37,0.39,0.43\}$
7	DT	I	-	-	-	3.6	80	1	10	1	33	$\{4,5\}$	$\{6,8\}$	$\{0.44,0.62\}$
8	TH	I	-	-	-	3	100	1	10	1	33	$\{13,14\}$	$\{7,15\}$	$\{0.38,0.63\}$
9	TH	I	-	-	-	3	100	1	10	1	33	$\{4,5\}$	$\{7,10\}$	$\{0.44,0.62\}$
10	LA	IP	5	40	30	3.6	175	2	10	1	33	$\{1,2,3\}$	$\{7,10,13\}$	$\{0.36,0.58,0.90\}$

TABLE IV
RESULTS FOR BENCHMARKING

Ins.	OWF	Obj. [9] [M€]	Obj. [M€]	Diff.[M€]	ϵ_{k_g} [9] [%]	ϵ_{k_g} [%]	Diff.[%]	Time [9] [min]	Time [min]	Diff.[min]
1	HR1	19.44	19.44	0	0.01	0.01	0	30	1.57	28.43
2	HR1	22.61	22.61	0	0.01	0.01	0	30	1	29
3	HR1	23.48	23.48	0	0.17	0.01	0.16	1,440	7.26	1,432.74
4	O	8.05	8.05	0	0	0.01	−0.01	0.42	0.46	−0.04
5	O	8.36	8.36	0	0	0.01	−0.01	1.95	0.45	1.50
6	DT	38.98	38.98	0	4.85	0.01	4.84	30	1.88	28.12
7	DT	50.38	49.83	0.55	7.36	0.01	7.35	10	2.65	7.35
8	TH	22.34	22.31	0.03	3.37	0.7	2.67	5	627.60	−622.60
9	TH	26.64	26.64	0	2.51	0.3	2.21	1,440	107.02	1,332.98
10	LA	-	68.97	-	-	0.5	-	-	748	-

(although with less number of WTs therefore potentially easier to solve). For this instance, an initial feasible point is obtained in only 3 min, and the best feasible point is calculated in 12 h:28 min, with the gap being improved by 46.87%.

VI. CONCLUSION

The proposed method provides a global optimization approach to solve the cable layout of OWFs collection systems.

The main novelties of this manuscript are: (i) proposition of a model, able to provide very good solutions in very reasonable computing times, (ii) possibility to provide very tight solution quality certificates, (iii) integration of realistic and high-fidelity models to calculate total electrical power losses, and capacitive currents in the collection systems.

An algorithmic framework for reducing the search space iteratively is the main technique used. The objective function supports the total economic costs, including initial investment, and lost revenues due to total electrical power losses in the project lifetime.

The proposed methodology has been benchmarked against a state-of-the art method with significantly different approach (different MILP model, and application of up to four distinctive heuristics); with all practical and technical constraints conceptually equivalent.

Ten real-world problem instances have been considered in the benchmark. The numerical results indicate that (i) the proposed algorithm provides, in general, at least equally good solutions, and in some cases, sizeable cheaper ones than the benchmark work, (ii) tighter gaps are calculated, in shorter computing times.

The proposed algorithm also performs satisfactorily for large OWFs with multiple OSSs, where the clustering is intrinsically defined in the mathematical formulation. It does not require predecessor algorithms to group WTs into OSSs, avoiding in this way artificially biased solutions.

ACKNOWLEDGMENT

This research has received funding from the Baltic InteGrid Project (www.baltic-integrid.eu/).

The authors thank Daniel Hermosilla Minguijón for his practical inputs throughout the development of the computational experiments, and Martina Fischetti, Lead Engineer - Operational Research in Vattenfall, for providing the data to perform the benchmark analysis.

REFERENCES

[1] GWEC, "Global Wind Report. Annual Market Update 2017," Tech. Rep., 2017. [Online]. Available: http://gwec.net/publications/global-wind-report-2/.[AccessedOct29,2018]

[2] X. Sun, D. Huang, and G. Wu, "The current state of offshore wind energy technology development," *Energy*, vol. 41, no. 1, pp. 298–312, 2012.

[3] RenewableUK, "RenewableUK - Project Intelligence," 2018. [Online]. Available: https://www.renewableuk.com/page/ProjectIntelligenceHome. [AccessedMarch3,2019]

[4] J.-A. Pérez-Rúa and N. A. Cutululis, "Electrical Cable Optimization in Offshore Wind Farms - A review," *IEEE Access*, vol. 7, no. 1, pp. 85 796–85 811, 2019.

[5] S. Lumbreras and A. Ramos, "Offshore wind farm electrical design: a review," *Wind Energy*, vol. 16, pp. 459–473, 2013.

[6] R. Jothi and B. Raghavachari, "Approximation algorithms for the capacitated minimum spanning tree problem and its variants in network design," *ACM Transactions on Algorithms (TALG)*, vol. 1, no. 5, pp. 265–282, 2005.

[7] A. Cerveira, A. F. de Sousa, E. J. Pires, and J. Baptista, "Optimal Cable Design of Wind Farms: The Infrastructure and Losses Cost Minimization Case," *IEEE Transactions on Power Systems*, vol. 31, no. 6, pp. 4319–4329, 2016.

[8] J. Bauer and J. Lysgaard, "The offshore wind farm array cable layout problem: A planar open vehicle routing problem," *Journal of the Operational Research Society*, vol. 66, no. 3, pp. 360–368, 2015.

[9] M. Fischetti and D. Pisinger, "Optimizing wind farm cable routing considering power losses," *European Journal of Operational Research*, vol. 270, no. 3, pp. 917–930, 2018.

[10] M. Fischetti and D. Pisinger, "Mixed Integer Linear Programming for new trends in wind farm cable routing," *Electronic Notes in Discrete Mathematics*, vol. 64, pp. 115–124, 2018.

[11] C. Berzan, K. Veeramachaneni, J. McDermott, and U.-M. O'Reilly, "Algorithms for cable network design on large-scale wind farms," Tech. Rep., 2011. [Online]. Available: https://thirld.com/files/msrp_techreport.pdf.[AccessedSeptember17,2019]

[12] A. Wędzik, T. Siewierski, and M. Szypowski, "A new method for simultaneous optimizing of wind farm's network layout and cable cross-sections by MILP optimization," *Applied Energy*, vol. 182, pp. 525–538, 2016.

[13] S. Lumbreras, A. Ramos, and S. Cerisola, "A Progressive Contingency Incorporation Approach for Stochastic Optimization Problems," *IEEE Transactions on Power Systems*, vol. 28, no. 2, pp. 1452–1460, 2013.

[14] S. Lumbreras and A. Ramos, "Optimal design of the electrical layout of an offshore wind farm applying decomposition strategies," *IEEE Transactions on Power Systems*, vol. 28, no. 2, pp. 1434–1441, 2013.

[15] A. Hertz, O. Marcotte, A. Mdimagh, M. Carreau, and F. Welt, "Design of a wind farm collection network when several cable types are available," *Journal of the Operational Research Society*, vol. 68, no. 1, pp. 62–73, 2017.

[16] M. Banzo and A. Ramos, "Stochastic Optimization Model for Electric Power System Planning of Offshore Wind Farms," *IEEE Transactions on Power Systems*, vol. 26, no. 3, pp. 1338–1348, 2011.

[17] Y. Chen, Z. Y. Dong, K. Meng, F. Luo, Z. Xu, and K. P. Wong, "Collector System Layout Optimization Framework for Large-Scale Offshore Wind Farms," *IEEE Transactions on Sustainable Energy*, vol. 7, no. 4, pp. 1398–1407, 2016.

[18] A. C. Pillai, J. Chick, L. Johanning, M. Khorasanchi, and V. De Laleu, "Offshore wind farm electrical cable layout optimization," *Engineering Optimization*, vol. 47, no. 12, pp. 1689–1708, 2015.

[19] A. Klein and D. Haugland, "Obstacle-aware optimization of offshore wind farm cable layouts," *Annals of Operations Research*, vol. 272, no. 1-2, pp. 373–388, 2017.

[20] J. Warnock, D. McMillan, J. Pilgrim, and S. Shenton, "Failure Rates of Offshore Wind Transmission Systems," *Energies*, vol. 12, no. 14, pp. 1–12, 2019.

[21] IEC, "IEC-60287-1: Electric cables - Calculation of the current rating," Tech. Rep., 2014. [Online]. Available: https://www.evs.ee/products/iec-60287-1-1-2006.[AccessedApril15,2019]

[22] G. J. Anders, A. Napieralski, and Z. Kulesza, "Calculation of the internal thermal resistance and ampacity of 3-core screened cables with fillers," *IEEE Transactions on Power Delivery*, vol. 14, no. 3, pp. 729–733, 1999.

[23] J. J. Grainger and W. D. J. Stevenson, *Power System Analysis*, 2nd ed. McGraw-Hill Education, 1994.

[24] P. Sørensen, N. A. Cutululis, A. Vigueras-Rodríguez, L. E. Jensen, J. Hjerrild, M. H. Donovan, and H. Madsen, "Power Fluctuations From Large Wind Farms," *IEEE Transactions on Power Systems*, vol. 22, no. 3, pp. 958–965, 2007.

[25] J. Herbert-Acero, O. Probst, P.-E. Réthoré, G. Larsen, and K. Castillo-Villar, "A Review of Methodological Approaches for the Design and Optimization of Wind Farms," *Energies*, vol. 7, no. 11, pp. 6930–7016, 2014.

[26] L. Gouveia and P. Martins, "The capacitated minimum spanning tree problem: revisiting hop-indexed formulations," *Computers & operations research*, vol. 32, no. 9, 2005.

[27] S. Lundberg, "Configuration study of large wind parks," Ph.D. dissertation, Chalmers University of Technology, 2003.

[28] F. M. González-Longatt, P. Wall, P. Regulski, and V. Terzija, "Optimal electric network design for a large offshore wind farm based on a modified genetic algorithm approach," *IEEE Systems Journal*, vol. 6, no. 1, pp. 164–172, 2012.

[29] IBM, "IBM ILOG CPLEX Optimization Studio CPLEX User Manual," Tech. Rep., 2015. [Online]. Available: https://www.ibm.com/support/knowledgecenter.[AccessedApril11,2019]

[30] ESCA, SEAFISH, and RenewableUK, "KIS-ORCA." [Online]. Available: http://kis-orca.eu/about-us#.XLRI_-gzYuU. [AccessedApril15,2019]

[31] ABB, "XLPE Submarine Cable Systems Attachment to XLPE Land Cable Systems - User's Guide," 2018. [Online]. Available: new.abb.com/docs/default-source/ewea.../xlpe-submarine-cable-systems-2gm5007.pdf.[AccessedOct29,2018]

Juan-Andrés Pérez-Rúa received the B.Sc. degree in Electrical Engineering, with Summa Cum Laude distinction, from the Technological University of Bolivar, Colombia, in 2012, and the M.Sc. degree in Sustainable Transportation and Electrical Power Systems from the ISEC college, Coimbra, Portugal, the University of Nottinghan, England, and the University of Oviedo, Spain, in 2016. Currently, he is pursuing the Ph.D. degree in the Department of Wind Energy at the Technical University of Denmark (DTU). His present-day areas of interest include grid integration of renewables in power systems, and optimization.

Mathias Stolpe received the Ph.D. degree in Optimization and Systems Theory from the Royal Institute of Technology (KTH), Stockholm, Sweden in 2003. He works as a Professor in the Department of Wind Energy at the Technical University of Denmark (DTU). His areas of research are structural and multidisciplinary optimization with focus on models and methods for global optimization.

Kaushik Das (S'13, M'17) received the M.Tech. degree in Power system engineering from the IIT Kharagpur, India in 2011, and the Ph.D. degree from the Department of Wind Energy, Technical University of Denmark (DTU), Risø, Denmark in 2016. Currently, he is a Researcher in DTU Wind Energy. His research interest lies in hybrid power plants and grid integration of renewables in power systems. He is a member of IEA Wind, IEEE, CIGRÉ and other professional bodies.

Nicolaos A. Cutululis (M'07, SM'18) received the M.Sc. and Ph.D. degrees, both in Automatic Control in 1998 and 2005, respectively. He is Professor in the Department of Wind Energy at the Technical University of Denmark. His main research interest is integration of wind power, with a special focus on offshore wind and grids.

APPENDIX J4

"Integrated Global Optimization Model for Electrical Cables in Offshore Wind Farms"

J.A. Pérez-Rúa, M. Stolpe,
and N. A. Cutululis

accepted
in *IEEE Transactions on Sustainable Energy*

October

2019

Integrated Global Optimization Model for Electrical Cables in Offshore Wind Farms

Juan-Andrés Pérez-Rúa, Mathias Stolpe, and Nicolaos A. Cutululis, *Senior Member, IEEE*

***Abstract*—A MILP program for integrated global optimization of electrical cables systems in Offshore Wind Farms (OWFs) is presented. Electrical cables encompass the cable layout in collection systems to interconnect Wind Turbines (WTs), and transmission systems to couple Offshore Substations (OSSs) to the Onshore Connection Point (OCP). The program is solved through a modern branch-and-cut solver, demonstrating the ability to tackle large-scale instances with hundreds of WTs and several OSSs. The model supports as objective function the initial investment plus economic losses due to total electrical power losses. The importance and functionality of incorporating electrical losses is demonstrated, along with the need to simultaneously optimize the cable layout, OSSs location, and transmission cables. The method is tested for three case studies. The results show that (i) points near the global optimum, with an imposed maximum tolerance, are calculable within reasonable computational time and effort, and (ii) the integrated model can be much more efficient than a benchmark approach based on enumeration, i.e., exhaustive evaluation of all possible optimization problems derived from unique OSSs locations.**

***Index Terms*—Offshore wind energy, Cable layout, Global optimization, Mixed integer linear programming, Medium voltage cables, High voltage cables.**

NOMENCLATURE

Acronyms

OWF(s)	Offshore Wind Farm(s).
WT(s)	Wind Turbines(s).
OSS(s)	Offshore Substation(s).
SCETM	Single-Core Equivalent Thermal Model.
OCP	Onshore Connection Point.
L	Length.
LP	Length plus total Power losses.
I	Initial investment.
IL	Investment plus total Power losses.
SY	Synthetic.
SYs	Single synthetic.
LA	London Array.

Parameters (non-sets)

n_w	Number of wind turbines.
n_o	Number of required offshore substations.
β_t	Number of potential locations for offshore substations.
d_{ij}	Euclidean norm for arc (i,j).
u_{c_t}	Capacity of cable t for collection system in number of wind turbines.
u_{e_t}	Capacity of cable t for transmission system in number of wind turbines.
c_{c_t}	Metric initial investment cost of cable t for collection system.
$c_{e_{t,n}}$	Metric initial investment cost of cable t for transmission system, with n cables per phase.
I_{c_t}	Steady-state rated current of cable t for collection system.
I_{e_t}	Steady-state rated current of cable t for transmission system.
V_{n_c}	Nominal line-to-line voltage of the collection system.
V_{n_e}	Nominal line-to-line voltage of the transmission system.
P_n	Nominal power of the wind turbines.
S_{rc_t}	Nominal power of cable t for collection system.
S_{re_t}	Nominal power of cable t for transmission systems.
$\vec{\gamma_t}$	Propagation constant of cable t.
$\vec{Z_{c_t}}$	Characteristic impedance of cable t.
$\vec{z_t}$	Metric series impedance of cable t.
$\vec{y_t}$	Metric admittance of cable t.
$\vec{I^k_{c_{ij,t}}}$	Nominal phasor current of arc (i,j) using cable t, for collection system, when k wind turbines are connected.
$\vec{I^k_{e_{ij,t,n}}}$	Nominal phasor current of arc (i,j) using cable t, for transmission system, when k wind turbines are connected, with n cables per phase.
$S^k_{c_{ij,t}}$	Nominal power of arc (i,j) using cable t, for collection system, when k wind turbines are connected.
p^ω	Power produced by a wind turbine at ω hour-slot.
$f^{\omega,k}_{ij}$	Power flow in arc (i,j) at ω hour-slot, when k wind turbines are connected.
$\vec{I^{\omega,k}_{c_{ij,t}}}$	Phasor current through arc (i,j) using cable t, for collection system, at ω hour-slot, when k wind turbines are connected.
λ_1	Screen losses factor.
λ_2	Armouring losses factor.
W_{d_t}	Metric dielectric loss of cable t.
R_t	Metric electrical resistance of cable t.
$l^{\mu,k}_{c_{ij,t}}$	Annual total power losses through arc (i,j) using cable t, for collection system, at year μ, when k wind turbines are connected.
$l^{\mu,k}_{e_{ij,t,n}}$	Annual total power losses through arc (i,j) using cable t, for transmission system, at year μ, when

Juan-Andrés Pérez-Rúa, Mathias Stolpe, and Nicolaos A. Cutululis are with the Department of Wind Energy, Technical University of Denmark, Frederiksborgvej 399, 4000 Roskilde, Denmark (e-mail: juru@dtu.dk)

	k wind turbines are connected, with n cables per phase.
U_c	Capacity of the biggest cable available, for collection system, in number of wind turbines.
r	Discount rate.
c_{ij}^k	Metric cost of arc (i,j), when k wind turbines are connected.
c_l^o	Independent term of linear cost function for offshore substation l.
c_l^t	Dependent term of linear cost function for offshore substation l.
ϕ	Maximum number of feeders per offshore substation.
η	Loading factor for offshore substations.
υ	Maximum number of wind turbines arcs set to a wind turbine.
υ_f	Maximum number of wind turbines arcs set to a wind turbine for feasibility problem.
$\upsilon_{f_{min}}$	Algorithm's parameters for feasibility problem.
$\upsilon_{f_\delta}, \upsilon_{f_{max}}$	
υ_o	Maximum number of wind turbines arcs set to a wind turbine for global optimization problem.
$\upsilon_{o_{min}}$	Algorithm's parameters for global optim. problem.
$\upsilon_{o_\delta}, \upsilon_{o_{max}}$	
ϵ	Required relative optimality gap in MILP solver.

Parameters (sets)

$\mathcal{N}_o$	Set of sets of candidate locations for all offshore substations.
$\mathcal{N}_{\beta_t}$	Set of candidate locations for all offshore substations.
$\mathcal{N}_{n_o}$	Set of required offshore substations.
$\mathcal{N}_{oi}$	Set of candidate locations for offshore substation i.
$\mathcal{N}_w$	Set of wind turbines.
$\mathcal{N}$	Set of offshore substations, wind turbines, and onshore connection point.
G	Weighted directed graph.
$\mathcal{A}$	Set of available arcs.
$\mathcal{D}$	Set of arcs' weights.
$\mathcal{T}_c$	Set of available cables for collection system.
$\mathcal{T}_e$	Set of available cables for transmission system.
$\mathcal{U}_c$	Set of cables' capacities for collection system in wind turbines number.
$\mathcal{U}_e$	Set of cables' capacities for transmission system in wind turbines number.
$\mathcal{C}_c$	Set of cables' initial investment costs for collection system.
$\mathcal{C}_e$	Set of cables' initial investment costs for transmission system.
Ω^μ	Set of hours-slot for a year μ.
$\mathcal{M}$	Set of operational years.
G_r	First reduced graph.
$\mathcal{A}_r$	Set of first reduced arcs.
$\mathcal{I}$	Set of crossing pairs arcs.
$\mathcal{L}$	Set of forbidden areas.
$\mathcal{A}_\ell$	Set of arcs defining area ℓ.
Υ_i	Set of wind turbines connected to i.
G_r'	Second reduced graph.
$\mathcal{A}_{\bar{\nabla}}$	Set of second reduced arcs.
$G_{r''}$	Third reduced graph.
$\mathcal{A}_{\nabla}$	Set of third reduced arcs.

Variables

x_{ij}	Binary variable to activate arc (i,j).
y_{ij}^k	Binary variable to activate arc (i,j), when k wind turbines are connected.
$z_{i,l}$	Binary variable to choose candidate location l for OSS i.
$x_{c_{ij,t}}$	Binary variable for arc (i,j) to select optimum cable type t, for collection system.
$x_{e_{ij,t,n}}$	Binary variable for arc (i,j) to select optimum cable type t, for transmission system, with n cables per phase.
σ_i	Integer variable modelling the number of wind turbines connected to offshore substation i.
$\sigma_{i,l}$	Integer variable modelling the number of wind turbines connected to offshore substation i, at candidate location l.

Subscripts

i	Point $\in \mathcal{N}$.
j	Point $\in \mathcal{N}$.
l	Point $\in \mathcal{N}_o$.
ij	Arc (i,j) with tail at i and head at j.
t	Cable type $\in \mathcal{T}_c$ or $\mathcal{T}_e$.
n	Number of cables per phase.
ℓ	Forbidden area $\in \mathcal{L}$.

Superscripts

k	Number of turbines connected in (i,j).
ω	Hour-slot $\in \Omega^\mu$.
μ	Year $\in \mathcal{M}$.

I. Introduction

COST reductions and operational performance enhancement are the main current challenges for designing and running Offshore Wind Farms (OWFs). Europe (mainly), Asia, and recently North America where the first large-scale installations are expected in 2023 [1], have contributed to the rapid proliferation of this technology for electrical power generation. The share of OWFs worldwide, with respect to the total installed power of wind energy (591 GW), is prognosed to increase from the actual 4% to more than 10% in 2025, reaching a global installed capacity of of 100 GW.

Electrical power cables represent a crucial component of the Balance of Plants (BoP) in OWFs, representing roughly 10% of the total capital expenses [2]. Between 2018 and 2028 more than 19,000 km of cables for collection systems are projected to be installed, with an estimated worth of £5.36bn [3]. Likewise, required export cables with lengths in the order of hundreds of kilometers are the trend given the

distancing of Offshore Substations (OSSs) to the Onshore Connection Point (OCP). Similarly, economies of scale pushes the development of large-scale OWFs, having more than 100 Wind Turbines (WTs), while increasing their rated power.

The importance of electrical cables in OWFs lies not only in the evident cost weight, but also in the operational performance of the whole project. Points of single failure due to electro-thermal and mechanical stress, and their mitigation, is one of the most studied topics in the field nowadays. Therefore, special attention must be addressed to designing systems involving electrical cables, such as the collection system, and the export system, while simultaneously accounting for the interrelation among them.

The integrated design of electrical cables in OWFs comprise the following aspects: (i) limited capacity of the cables' thermal rating, (ii) topological design of the cable layout, (iii) capital expense optimization in both the collection and the transmission systems, (iv) diminution of total electrical power losses, (v) clustering of WTs to OSSs, and (vi) geographical location of the OSSs. As demonstrated in [4], an instance of the main problem involving the points (i), (ii), and (iii) falls into the category of NP hard problems [5], mapping to a modified version of a Capacitated Minimum Spanning Tree (C-MST). By deduction, the main problem dealing simultaneously with all six aspects, inherit the complexity with additional design variables, turning this task into a very challenging subject in the context of computational optimization in OWFs.

In order to tackle the electrical cables design in OWFs, available methods can be classified as follows [6]. (i) Heuristics methods are all those algorithms that are bounded in computation time while developing a solution by construction in sequential steps [7]. (ii) Metaheuristics can be defined as improvement heuristics, which find fast initial feasible points (ideally), and by means of iterative processes, intend to improve them using different stochastic operators [8], [9]. (iii) Global optimization offers the enormous advantage to provide mathematical certifications for optimality in case of convex problems. However, for combinatorial problems, the required computational time is unknown and unpredictable, and for the range of modern large-scale OWFs, memory capacities start becoming an issue as well [10]. (iv) Combination of matheuristics, providing frameworks to cope with these challenges by limiting the search space, in combination with mathematical programs providing feasible points or the global optimum [4].

To the best of the authors' knowledge, only the following works have tackled the full integrated design of electrical cables for OWFs using global optimization. A MILP model combined with Benders decomposition is presented in [11], a MILP model [12] solved by branch-and-cut method, a MILP model with progressive contingence incorporation [13], and finally a MIQP model is proposed in [14].

The works [11], [13], [14] provide remarkable advances on stochastic optimization for problems in this context. Different stochastic scenarios are supported, accounting for wind power variability and cables failure. Distinctive theoretical strategies to accelerate convergence are applied and compared. While in [12] a single MILP model is formulated and later solved by branch-and-cut method. The model optimizes uniquely for initial investment, while also disregards important practical constraints, such as, cables crossings, and forbidden areas.

Nevertheless, the application of those methods did not focus on large-scale OWFs with multiple OSSs, as the case studies were defined by real projects with maximum 30 WTs. State-of-the-art OWFs can encompass WTs in the order of hundreds.

Other works propose the use of metaheuristic for providing feasible points to tackle large-scale instances. This includes [15] where Particle Swarm Optimization is employed and, [16] in which a Genetic Algorithm is proposed. Given the intrinsic features of the used metaheuristics, there is no possibility to infer about the quality of the obtained solutions.

In virtue of the above, in this manuscripts is proposed a MILP model embedded in an efficient algorithmic framework, able to compute global optimum solution points (or near to it) in reasonable computational time, for the full integrated design of electrical cables in large-scale OWFs. Additionally, the model quickly finds feasible points. Likewise, the proposed model supports a combined objective function defined by total system costs, i.e. initial investment and total electrical power losses of both the collection and transmission systems simultaneously.

Compared to [17], the authors propose the following generalizations: (i) modelling of transmission systems, (ii) a compact and single mathematical model which can be used to simultaneously optimize the collection and the transmission system, (iii) flexible locations of OSSs locations, and (iv) inclusion of forbidden areas.

In Section II, the main optimization problem is formulated including objective function and constraints definition. Later on in the Section III, the modelling aspects are explained in detail, followed by the whole framework description in Section IV. Computational experiments are performed in Section V and the work is finalized with the conclusions in Section VI.

II. Optimization Model

In this manuscript is developed a model that supports any reasonable number of WTs, n_w, and any number of OSSs, n_o. Define the set $\mathcal{N}_o = \{\mathcal{N}_{o1}, \cdots, \mathcal{N}_{on_o}\}$, where an element $\mathcal{N}_{oi}$ is, in turn, an index set representing candidate locations for the ith OSS with $i \leq n_o$. In this way, $\beta_t = \sum_{1 \leq i \leq n_o} |\mathcal{N}_{oi}|$ defines the total number of potential locations to place OSSs (denoted $\mathcal{N}_{\beta_t} = \{1, \cdots, \beta_t\}$), given a required number n_o, and individual candidate set, $\mathcal{N}_{oi}$, for each $i \in \mathcal{N}_{n_o} = \{1, \cdots, n_o\}$. Likewise, let $\mathcal{N}_w = \{\beta_t + 1, \cdots, \beta_t + n_w\}$ denote the index set representing the WTs. Hence, the whole set of points including both OSSs candidate locations and WTs locations is given as, $\mathcal{N} = \{0\} \cup \mathcal{N}_{\beta_t} \cup \mathcal{N}_w$, where the node 0 represents the OCP.

The aim is to obtain the optimum design of the cable layout for a full OWF, modelled as n_o spanning-trees, connecting the WTs between each other, and towards the desired number

of OSSs, along with the transmission cables from OSSs to the OCP. Furthermore, as OWFs cover a relatively large area, it is common that they include forbidden zones - defined as spaces where no WTs or cables can be placed - which must be considered as well. The geographical location of the WTs is fixed, calculated in the micrositing optimization process in order to maximize the energy produced in the OWF [18]. The distance between two points i and j, is defined as d_{ij}.

The complete directed graph $G(\mathcal{N}, \mathcal{A}, \mathcal{D})$ comprises the input sets, where $\mathcal{N}$ represents the vertex set, $\mathcal{A}$ the set of available arcs arranged as a pair-set, and $\mathcal{D}$ the set of associated weights for each element $a \in \mathcal{A}$.

The different types of cables being considered are stored in $\mathcal{T}_c$, and $\mathcal{T}_e$, for the collection and export systems, respectively. The set $\mathcal{T}_c$ relates to the attribute sets $\mathcal{U}_c$, and $\mathcal{C}_c$, representing the capacity (in terms of maximum number of supported WTs), and total capital expenditures per unit of length, respectively. In general, the greater the cable capacity, the greater the capital cost.

The first set of variables in the model are binary: $z_{i,l}$ x_{ij}, and y_{ij}^k. Choosing the candidate location l for the OSS i is done through the variable $z_{i,l}$, which is equal to one if selected. and zero otherwise. If the arc connecting i, and j is active ($i \in \mathcal{N} \setminus \{0\} \wedge j \in \mathcal{N} \setminus \{0\}$), then $x_{ij} = 1$. Finally, in case $x_{ij} = 1$, the number of WTs connected is defined by y_{ij}^k, where k models the number of WTs rooted at i, including the one at j. A set of positive integer variables is required as well; σ_i, and $\sigma_{i,l}$ represents the number of WTs connected to the OSS i, and at the corresponding candidate location l, respectively.

The number of x_{ij}, and y_{ij}^k variables scale quadratically with the number of WTs. Therefore, reduction strategies are important to limit the size of the model in terms of variables and constraints. A procedure proposed in [19] and [17] is used. The largest individual cable capacity is found as $U_c = \max \mathcal{U}_c$; consequently, the maximum attributable value of k for $i \in \mathcal{N}_{\beta_t}$ is equal to $f(i) = U_c$, in contrast, for elements $i \in \mathcal{N}_w$ is $f(i) = U_c - 1$. This is because, intuitively, a cable only can be used at maximum capacity if connected to a OSS. Finally, all redundant arcs are suppressed, along with those interconnecting OSSs, as only the common industry practice of point-to-point connections from offshore to onshore points is considered. Overall, the original graph $G(\mathcal{N}, \mathcal{A}, \mathcal{D})$ is reduced to $G_r(\mathcal{N}, \mathcal{A}_r, \mathcal{D}_r)$.

A. Cost coefficients

Designing the electrical cables system in OWFs is manifold: not only arcs must be selected while also choosing the cable type to do so, but total electrical power losses must be considered as they may impact the design. Total electrical power losses are function of the selected arc, cable type, and generated power.

Hence, the straight-forward way to include simultaneously all these aspects is to incorporate in the variable y_{ij}^k the cable type, as for instance transforming the variable to $y_{ij}^{k,t}$. Variable $y_{ij}^{k,t}$ would model whether the arc $a_r = (i, j)$ is selected or not, connecting k WTs through cable type t. Secondly, losses would have to be mathematically explicitly expressed in the objective function. This raises two issues: (i) the number of variables increase linearly with the number of cable types $|\mathcal{T}_c|$, and (ii) ohmic losses are non-linear, therefore simplifications must be assumed for expressing it in a linear model.

A body of actions to circumvent these limitations, while being able to solve the defined problem, are implemented. The approach basically decouples the arc selection and losses minimization from the cable assignment decision-making problem. These techniques are explained in the following sections for both the collection system (cable layout), and transmission system (point-to-point connection).

1) Collection system cables: The reduced graph $G_r(\mathcal{N}, \mathcal{A}_r, \mathcal{D}_r)$ contains all required information for the cable layout. For y_{ij}^k, the length of arc (i, j) is known, along with the number of WTs connected; this makes possible to evaluate the whole set of available cables in polynomial running time for each of the arcs (such as $i \neq 0 \wedge j \neq 0$), to select that which minimizes the objective function. All cost coefficients are non-negative.

Let the term $(c_{c_t} \cdot d_{ij})$ represent the capital expenditures plus installation costs (per metric unit) of cable t, to join points i and j (cost per metric unit). The parameters $c_{c_t} \in \mathcal{C}_c$ are obtained from the exponential regression function given in [20] (excluding installation costs).

To incorporate the cost of total electrical power losses, a discounted cash flow metric is considered. The required parameters are $|\mathcal{M}|$, $l_{c_{ij,t}}^{\mu,k}$, c_p, and r, meaning the project lifetime (years), total power losses at year μ for cable t, when k WTs are connected (in MWh, see Section III-C), cost of energy (€/MWh), and discount rate (p.u.), respectively.

Bearing this in mind, for each (i, j) such as $i \neq 0 \wedge j \neq 0$, the following optimization model is formulated and solved independently by enumeration [17].

$$c_{ij}^k = \min \sum_{t \in \mathcal{T}_c} x_{c_{ij,t}} \cdot \left(c_{c_t} \cdot d_{ij} + \sum_{\mu=1}^{|\mathcal{M}|} \frac{l_{c_{ij,t}}^{\mu,k} \cdot c_p}{(1+r)^\mu} \right) \quad (1)$$

$$\text{s.t.} \quad \sum_{t \in \mathcal{T}_c} x_{c_{ij,t}} = 1 \quad (2)$$

$$x_{c_{ij,t}} \cdot (S_{c_{ij,t}}^k - S_{rc_t}) \leq 0 \quad \forall t \in \mathcal{T}_c \quad (3)$$

$$x_{c_{ij,t}} \in \{0, 1\} \quad \forall t \in \mathcal{T}_c \quad (4)$$

Note that this set of problems are always feasible as k is limited by U_c. Equation (2) ensures that exactly one cable type is selected. Equation (3) guarantees that the capacity of cable t is not violated; where $S_{c_{ij,t}}^k$ is the power through arc (i, j), when k turbines are connected in j using cable t, and S_{rc_t} is the rated power of t (see Section III-A, and Section III-B). Lastly, Equation (4) defines the nature of the problem's variables.

After solving the model from (1) to (4) (maximum $U_c \cdot |\mathcal{N}|^2$ times), the cost coefficients c_{ij}^k are calculated, and the corresponding cable type t is unequivocally determined as per $x_{c_{ij,t}}$.

2) Transmission system cables: Arcs (i, j) such as $i \in \{0\}$ $\wedge$ $j \in \mathcal{N}_{\beta_t}$ are also definable beforehand. The cost of the transmission cables is function of the total length and installed

power; the former is known, but the latter is also output of the main optimization model. Likewise, in contrast to the collection system cable layout, there are no binary variables explicitly representing whether certain number of WTs are connected to a OSS or not. In this case, the variables $\sigma_{i,l}$ are used to estimate the cost for a specific candidate location $l \in \mathcal{N}_{\beta_t}$, associated to the OSS $i \in \mathcal{N}_{n_o}$.
Let the variable $x_{0j}^{t,n}$ represent if arc $(0, j)$ is active using n cables t in parallel or not (a limit of $n = 3$ is a reasonable practical constraint to ensure feasibility). The methodology uses the following optimization model, where the target is to obtain a linear cost function in terms of the WTs connected to a OSS:

$$\min \quad \sum_{n=1}^{3} \sum_{t \in \mathcal{T}_e} x_{e_{ij,t,n}} \cdot \left(c_{e_{t,n}} \cdot d_{0j} + \sum_{\mu=1}^{|\mathcal{M}|} \frac{l_{e_{0j,t,n}}^{\mu,k} \cdot c_e}{(1+r)^{\mu}} \right) \tag{5}$$

$$\text{s.t.} \quad \sum_{n=1}^{3} \sum_{t \in \mathcal{T}_e} x_{e_{ij,t,n}} = 1 \tag{6}$$

$$\sum_{n=1}^{3} x_{e_{ij,t,n}} \cdot \left(S_{e_{0j,t,n}}^{k} - S_{re_t} \right) \leq 0 \quad \forall t \in \mathcal{T}_e \tag{7}$$

$$x_{e_{ij,t,n}} \in \{0, 1\} \quad \forall t \in \mathcal{T}_e \wedge n \in \{1, 2, 3\} \tag{8}$$

The mathematical program from (5) to (8) resembles that described from (1) to (4). In fact, each equation is mirrored by the order of appearance. Nevertheless, in the case of the transmission cables, most of the parameters and variables are re-indexed accounting for n, which is the number of cables per connection. Contrary to collection system cables, in transmission level parallel cables are installed in practice.
Figure 1 presents the basic algorithm for calculating the transmission cables linear cost function. The idea behind is to sequentially increase the number k of turbines connected to a specific OSS location, solving (5) to (8), and gathering all results to finally obtain the best linear function fitting the data by least squares method.

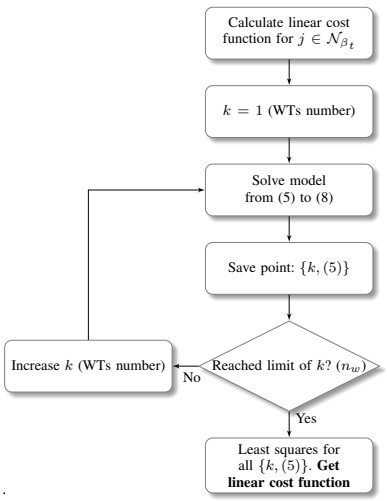

Fig. 1: Flowchart for calculating the transmission cables linear cost function.

The procedure is performed for each OSS candidate location. Thus, β_t linear functions are obtained, each characterized by a independent c_l^o, and non-negative linear c_l^t term, where $l \in \mathcal{N}_{\beta_t}$.
By adaptations on the costs coefficients in (1) and (5), the following objective functions are supported for the global model: length (L), length plus total power losses (LP), initial investment (I), and initial investment plus total power losses (IL)

B. Objective function

After solving the collection and transmission systems sub-problems, the linear objective function of the main mathematical model is formulated as:

$$\min \quad \sum_{i \in \mathcal{N} \setminus \{0\}} \sum_{j \in \mathcal{N}_w} \sum_{k=1}^{f(i)} c_{ij}^k \cdot y_{ij}^k + \sum_{i \in \mathcal{N}_{n_o}} \sum_{l \in \mathcal{N}_{oi}} (c_l^o \cdot z_{i,l} + c_l^t \cdot \sigma_{i,l}) \tag{9}$$

C. Constraints

For a given set of candidate locations $\mathcal{N}_{oi}$ for the OSS i, exactly one of them must be chosen. This is modelled through

$$\sum_{l \in \mathcal{N}_{oi}} z_{i,l} = 1 \quad \forall i \in \mathcal{N}_{n_o} \tag{10}$$

Note that in constraint (10), if an inequality (less than or equal to) replaces the equality, not only multiple locations would be supported, but also multiple number of OSSs.
In order to cluster the WTs (n_w) into n_o OSSs, the following constraint is required:

$$\sum_{i \in \mathcal{N}_{n_o}} \sigma_i = n_w \tag{11}$$

In (11), σ_i represents the number of WTs associated to the OSS i, its definition is:

$$\sum_{l \in \mathcal{N}_{oi}} \sigma_{i,l} = \sigma_i \quad \forall i \in \mathcal{N}_{n_o} \tag{12}$$

Correspondingly, $\sigma_{i,l}$ counts the number of WTs connected to the OSS i at location l and is computed through

$$\sum_{j \in \mathcal{N}_w} \sum_{k=1}^{f(j)} k \cdot y_{lj}^k = \sigma_{i,l} \quad \forall i \in \mathcal{N}_{n_o} \wedge l \in \mathcal{N}_{oi} \tag{13}$$

The variables $\sigma_{i,l}$ are for linearization, while σ_i is for the model readability. The following equation, for both selecting an OSS location $z_{i,l}$ and limiting the number of feeders out from them to ϕ, is added:

$$\sum_{j \in \mathcal{N}_w} \sum_{k=1}^{f(j)} y_{lj}^k \leq \phi \cdot z_{i,l} \quad \forall i \in \mathcal{N}_{n_o} \wedge l \in \mathcal{N}_{oi} \tag{14}$$

The tree topology, i.e. only one cable type used per arc, and the definition of the head-tail convention, are simultaneously ensured by:

$$\sum_{i \in \mathcal{N} \setminus \{0\}} \sum_{k=1}^{f(i)} y_{ij}^k = 1 \quad \forall j \in \mathcal{N}_w \tag{15}$$

The flow conservation, which also avoids the formation of cycles (loops), is considered by means of one linear equality per wind turbine

$$\sum_{i\in\mathcal{N}\setminus\{0\}}\sum_{k=1}^{f(i)} k\cdot y_{ij}^k - \sum_{i\in\mathcal{N}_w}\sum_{k=1}^{f(i)} k\cdot y_{ji}^k = 1 \quad \forall j\in\mathcal{N}_w \tag{16}$$

The set $\mathcal{I}$ stores pairs of arcs $\{(i,j),(u,v)\}$, which are crossing each other. Excluding crossing arcs in the solution is ensured by the linear inequalities

$$x_{ij}+x_{ji}+x_{uv}+x_{vu}\le 1 \tag{17}$$
$$\forall\{(i,j),(u,v)\}\in\mathcal{I}:\{i,j,u,v\}\neq 0$$

$$\sum_{k=1}^{f(i)} y_{ij}^k - x_{ij}\le 0 \quad \forall (i,j)\in\mathcal{A}_r:\{i,j\}\neq 0 \tag{18}$$

Constraint (17) also includes the inverse arcs of those elements. This constraint is a practical restriction in order to avoid hot-spots and potential single-points of failure caused by overlapped cables [21].
The following constraints represent a set of valid inequalities to tighten up the mathematical model [22]:

$$-\sum_{i\in\mathcal{N}\setminus\{0\}}\sum_{k=v+1}^{f(i)}\left\lfloor\frac{k-1}{v}\right\rfloor\cdot y_{ij}^k + \sum_{i\in\mathcal{N}_w}\sum_{k=v}^{f(i)} y_{ji}^k \le 0 \tag{19}$$
$$\forall v\in\{2,\cdots,U_c-1\}\wedge j\in\mathcal{N}_w$$

They can be interpreted as: given an active arc y_{ij}^k, the maximum number of active arcs rooted in j and connecting v WTs is expressed by $\lfloor\frac{k-1}{v}\rfloor$, hence the constraint restricts the maximum number of feasible arcs, reducing the search space without excluding valid solutions to the problem.

$$x_{ij}\in\{0,1\} \quad y_{ij}^k\in\{0,1\} \tag{20}$$
$$\forall (i,j)\in\mathcal{A}_r:\{i,j\}\neq 0\wedge k\in\{1,\cdots,f(i)\}$$

$$z_{i,l}\in\{0,1\} \quad 0\le\sigma_i\le\eta\cdot\left\lceil\frac{n_w}{n_o}\right\rceil \quad \sigma_i\wedge\sigma_{i,l}\in\mathbb{Z}_+ \tag{21}$$
$$\forall i\in\mathcal{N}_{n_o}\wedge l\in\mathcal{N}_{oi}$$

Constraints (20) and (21) define the nature of the formulation by the variables definition, a MILP. Note that variables σ_i are limited in their upper bounds to avoid unbalanced OSSs, in terms of connected WTs (in case $\eta=1$, if unbalancing is permitted then $1<\eta\le n_o$), which implicitly also bounds $\sigma_{i,l}$.
To summarize, the complete formulation of the main MILP model consists of the objective function (9) and constraints defined in (10) - (21).

III. Modelling aspects

The modelling choices presented in the following - with the exception of Section III-D - are based on the ones presented in [17] (particularly Section III-A, Section III-B, and Section III-C).

A. Cable capacity

The current capacity I_{c_t} of a cable t is calculated using the model given in [23]. This method comes from a Single-Core Equivalent Thermal Model (SCETM), as generalized in [24] for single-core and three-core cables. It is conservative when applied for OWFs, hence lifetime of the component is within acceptable intervals [25].

$$u_{c_t} = \left\lfloor\frac{S_{rc_t}=\sqrt{3}\cdot V_{n_c}\cdot I_{c_t}}{P_n}\right\rfloor \quad \forall t\in\mathcal{T}_c \tag{22}$$

$$\mathcal{U}_c = \{u_{c_1},\cdots,u_{c_{|\mathcal{T}_c|}}\} \tag{23}$$

The set of cable capacities in terms of number of supportable WTs is defined in (22) and (23), where P_n represents the nominal power of an individual WT, and V_{n_c} the nominal line-to-line voltage level in the collection system. Regarding the transmission system, the rated power of cables ($S_{re_t}\ \forall t\in\mathcal{T}_e$) is calculated with the voltage level V_{n_e}, such as $S_{re_t}=\sqrt{3}\cdot V_{n_e}\cdot I_{e_t}$.

B. Arcs nominal power

A distributed model is implemented with the next expressions [26]

$$\vec{I_{c_{ij,t}}^k} = \frac{k\cdot P_n}{\sqrt{3}\cdot V_{n_c}}\cdot\cosh(\vec{\gamma_t}\cdot d_{ij}) - \frac{V_{n_c}}{\vec{Z_{c_t}}}\cdot\sinh(\vec{\gamma_t}\cdot d_{ij}) \tag{24}$$

$$S_{c_{ij,t}}^k = \sqrt{3}\cdot V_{n_c}\cdot|\vec{I_{c_{ij,t}}^k}| \tag{25}$$

The characteristic impedance is calculated as $\vec{Z_{c_t}}=\sqrt{\vec{z_t}/\vec{y_t}}$, and the propagation constant, $\vec{\gamma_t}=\sqrt{\vec{z_t}\cdot\vec{y_t}}$. The series impedance is represented by $\vec{z_t}$, and the admittance by $\vec{y_t}$. The maximum power flowing through the arc (i,j), given k turbines connected downstream (y_{ij}^k), is calculated as per (25), accounting for the worst-case scenario, as the current in the arc is strictly increasing with length, and the value $\vec{I_{c_{ij,t}}^k}$ is calculated at the extreme of it when using cable t.
For the transmission cables, (24) and (25) must be calculated per cable ($\frac{k\cdot P_n}{n}$), and considering V_{n_e}, to obtain $S_{e_{ij,t,n}}^k = \sqrt{3}\cdot V_{n_e}\cdot|\vec{I_{e_{ij,t,n}}^k}|$.

C. Power flow and total power losses

A transportation model, accurate enough for radial systems, is implemented through Constraint (16). Time variation can be represented as:

$$\sum_{i\in\mathcal{N}}\sum_{k=1}^{f(i)} k\cdot y_{ij}^k\cdot p^\omega - \sum_{i\in\mathcal{N}_w}\sum_{k=1}^{f(i)} k\cdot y_{ji}^k\cdot p^\omega = p^\omega \tag{26}$$
$$\forall j\in\mathcal{N}_w\wedge\omega\in\Omega^\mu\wedge\mu\in\mathcal{M}$$

Constraint (16) is generalized considering the temporal dimension (26), where $\mathcal{M}=\{1,\cdots,|\mathcal{M}|\}$, is the set of operational years with upper limit in the project lifetime, Ω^μ is the set of hours-slot for a year μ, and ω a specific hour-slot in Ω^μ. By means of the simulation of offshore power time series [27], let p^ω be the power in MW produced by one WT in that hour-slot.

In this way, let define the auxiliary variable $f_{ij}^{\omega,k} = k \cdot y_{ij}^{k} \cdot p^{\omega}$ as the power flow (MW) in arc (i,j) when k WTs are connected downstream (including the one in j), in time instant ω.

$$I_{c_{ij,t}}^{\vec{\omega},k} = \frac{f_{ij}^{\omega,k}}{\sqrt{3} \cdot V_{n_c}} \cdot \cosh\left(\vec{\gamma_t} \cdot d_{ij}\right) - \frac{V_{n_c}}{\vec{Z_{c_t}}} \cdot \sinh\left(\vec{\gamma_t} \cdot d_{ij}\right) \quad (27)$$

$$l_{c_{ij,t}}^{\mu,k} \approx 3 \cdot (1 + \lambda_1 + \lambda_2) \cdot \sum_{\omega \in \Omega^{\mu}} \omega \cdot R_t \cdot d_{ij} \cdot |I_{c_{ij,t}}^{\vec{\omega},k}|^2 + 3 \cdot |\Omega^{\mu}| \cdot \omega \cdot W_{d_t} \quad (28)$$

Including the capacitive currents, (27) expresses the current at the end of the arc (with respect to i), with magnitude $|I_{ij}^{\vec{\omega},k}|$. The annual total power losses $l_{c_{ij,t}}^{\mu,k}$ is calculated with (28). The factor $(1 + \lambda_1 + \lambda_2)$ accounts for the screen and armouring losses (with values from [23]), W_{d_t} is the dielectric loss per unit length for the insulation surrounding the conductor in $\mathrm{W/m}$ (formula given in [23]), while the constant 3 is for the three-phase system. This value must be scaled in MWh.
Losses in transmission cables ($l_{e_{ij,t,n}}^{\mu,k}$) must consider the number of components in paralell per phase.

D. Forbidden areas

A restricted set of regions (inside a OWF) for excavation and cable trenching is supported in this model. Those regions can be modelled as convex polygons [28], non-convex polygons [29], or closed curves [30]. A convex hull based bypassing algorithm which may incorrectly delimit areas as forbidden, if they are non-convex polygons, is proposed in [28]. Any polygonal shape can be defined using Steiner nodes explicitely in the model as in [29], where the aim is not only to model the area, but also to refine arcs with shortest path. However, bending moments in the cables may be compromised as a result of unrealistic routing. Finally, more accurate computational algorithms to represent more precisely defined shapes is implemented in [30], by means of Delaunay Triangulation Based Navigational Mesh Path-finding. Despite this, unrealistic routing can result as well.
A pre-processing strategy schematized in Fig. 2 is proposed in this manuscript. Any polygonal shape is modelled, while simultaneously decreasing the number of variables. By means of this approach, the explicit creation of variables and constraints in the main model to cope with forbidden areas is avoided, while allowing only straight arcs between WTs. On the other hand, the strategy is flexible as any number of shapes are supported.
Let the set of forbidden areas be $\mathcal{L}$. An area $\ell \in \mathcal{L}$, in turn, is defined as a set of arcs $\mathcal{A}_\ell$, where $b \in \mathcal{A}_\ell : b = (i,j)$. The set of arcs $\mathcal{A}_\ell$ defines a sequence of vertices enveloping the points representing a forbidden area l (the sequence $\{i,j,v,i\}$ represents, for example, a triangle with $\mathcal{A}_\ell = \{(i,j),(j,v),(v,i)\}$). The procedure for incorporating these zones into the model is depicted in Fig. 2, where graph $G_r^{'}$ is obtained from graph G_r, by excluding from the new arcs set $\mathcal{A}_{\nabla}^{'}$ all the arcs crossing with at least one arc $b \in \mathcal{A}_\ell$.

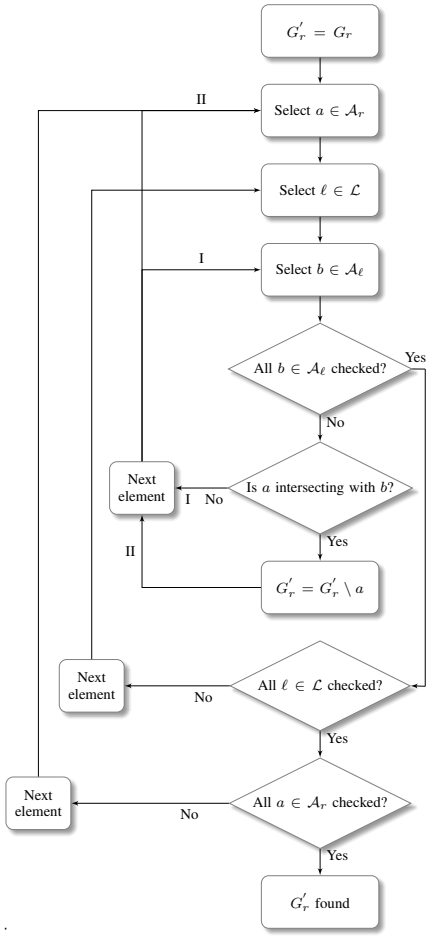

Fig. 2: Flowchart for incorporating forbidden areas in the model.

IV. Optimization framework

For large OWFs, i.e. in the range of 100s of WTs, the cable layout problem is generally unsolvable for gaps lower than 1% [31]. This is also the authors' computational experience. Therefore the graph $G_r^{'}$ needs further reduction to make the model tractable.
The framework proposed in [17] is generalized in this work. Let the function $f(i, G_r^{'}, \upsilon)$ obtain the set Υ_i defined as maximum the υ-closest WTs to i; the term *maximum* accounts for vertices which have less than υ arcs available due to prior elimination for crossings with forbidden areas. In other words, it is considered intuitively that a WT will be connected to one of the WTs in its vicinity. Therefore, by systematically applying $f(i, G_r^{'}, \upsilon)$ to each $i \in \mathcal{N}_w$, the reduced graph $G_r^{''}$ is found. The set $\mathcal{A}_{\nabla}^{''}$ contains the candidate arcs to the solution of the problem. The outcoming arcs from OSSs are also limited to the nearest 50 WTs. An imposed gap of ϵ is an input of the method.
The flowchart is displayed in Fig. 3; as a first step a feasibility problem is solved, characterized by (i) an objective function

equal to zero, (ii) a low υ is set to speed up the process, and (iii) fixed locations of OSSs by choosing arbitrarily one per each i available in $\mathcal{N}_{oi}$. Following the solution of the

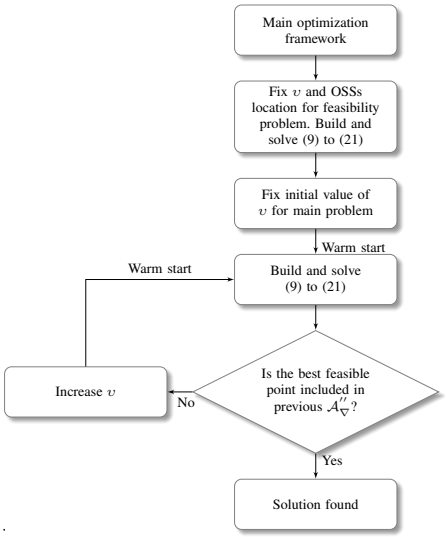

Fig. 3: Flowchart of the main optimization framework.

feasibility problem, the obtained solution is used to warm start the main model given $G_r^{''}$ for a specific value of υ. The next step is to compare if the best feasible point found so far, is included in the domain of the previously defined problem ($\mathcal{A}_{\nabla}^{''}$). If this is the case, the process is stopped, since most likely the global minimum has been calculated. Otherwise, the domain is further increased until that condition is satisfied. In the authors' earlier work [17], it has been found out that for the feasibility problem $\upsilon = 5$, and for the main problem an initial value of $\upsilon = 15$, and increasing steps equal to 5, represent good parameters to find a proper compromise between computing time, and solution quality.

V. Case Study

The following case studies have been carried out on an Intel Core i7-6600U CPU running at 2.50 GHz and with 16 GB of RAM. The chosen MILP solver is the branch-and-cut solver implemented in IBM ILOG CPLEX Optimization Studio V12.7.1 [32].

A synthetic OWF (SY) with three forbidden areas is used to test the validity of the model. The real project London Array (LA) which is the second largest (measured by installed power) project under operation [33], is used to illustrate the ability of the model to solve very large instances. Both cases have more than 100 WTs and several OSSs, representing very challenges instances to solve.

The main high-level parameters for both case studies are given in Table I. The objective function is defined by a combined total economic cost including the initial investment, and the total electrical power losses of the cables systems (see (1) and (5)). Three forbidden areas are considered in SY, with four candidate locations per OSS, and distance to OCP of roughly $100\,\mathrm{km}$. In LA three possible locations are supported for each OSS, with length to OCP close to $20\,\mathrm{km}$. In all cases, a maximum number of 10 feeders is allowed per OSS (see (14)), in addition to a balanced allocation of WTs to OSSs. Balancing of OSSs is accounted by means of $\eta = 1$, see (21). The technical and economic parameters for both medium and

TABLE I
Main high-level parameters for the problem instances

OWF	Objective	r [%]	c_p [€/MWh]	$\lvert\mathcal{M}\rvert$	$\lvert\mathcal{L}\rvert$	η
SY	IL	5	40	30	3	1
LA					0	
OWF	P_n [MW]		$\mathcal{N}_o$	n_w	n_o	ϕ
SY	3.6		$\{\{1,2,3,4\},\{5,6,7,8\}\}$	120	2	10
LA			$\{\{1,2,3\},\{4,5,6\}\}$	175		

high voltage cables are presented in Table II. Further technical cable information is available in [34]. For the collection system, the set of cable dimensions is $240\,\mathrm{mm}^2$, $500\,\mathrm{mm}^2$, and $1{,}000\,\mathrm{mm}^2$, while for transmission, ten different cables types are considered, ranging from $300\,\mathrm{mm}^2$ to $2{,}000\,\mathrm{mm}^2$. All the cross-sections are commercially standards by manufacturers. Cable capacities and costs are displayed for reproducibility as well in Table II. The linear cost function obtained using Fig.

TABLE II
Cables main parameters

Collection system				
OWF	V_{n_c} [kV]	$\lvert\mathcal{T}_c\rvert$	$\mathcal{U}_c$	$\mathcal{C}_c$ [M€/km]
SY	33	3	$\{7,10,13\}$	$\{.36,.58,.90\}$
LA				
Transmission system				
OWF	V_{n_e} [kV]	$\lvert\mathcal{T}_e\rvert$	$\mathcal{U}_e$	$\mathcal{C}_e$ [M€/km]
SY	132	10	$\{34,38,42,46,49$ $53,56,59,62,69\}$	$\{.50,.56,.63,.73,.84$ $.96,1.11,1.28,1.51,2.16\}$
LA	150		$\{38,43,47,52,56$ $60,63,67,71,79\}$	$\{.57,.66,.78,.93,1.13$ $1.33,1.59,1.91,2.34,3.60\}$

1 for the first candidate location of OSS 1 in SY OWF is presented in Fig. 4 with a distance to shore of $101.31\,\mathrm{km}$. In this graph two set of curves are displayed. The first one (blue circles and line) includes the optimization objective function output when (5) - (8) are solved neglecting total electrical power losses (economic losses' discounted cash flow) in (5). The blue circles are the optimum cost of transmission cables from (5), while the blue line is the best linear curve fitting that data. In contrast, the second set of curves is determined by including the total electrical power. The red circles are from the optimization objective function, and the red line is the best linear data fitting.

Three main outcomes can be extracted from Fig. 4. (i) total electrical power losses considerably boost the total costs. For 55 WTs an increase of 50% in costs is estimated. (ii) including electrical losses improves the linear function fit, as the R^2 value of the linear data fitting calculated with losses is higher

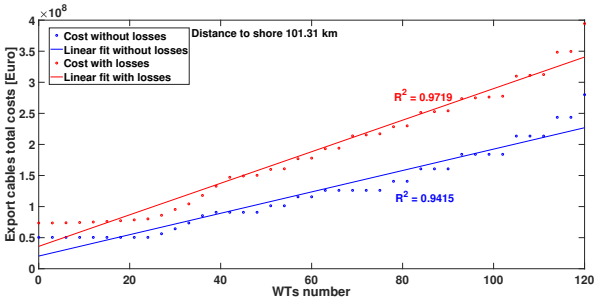

Fig. 4: Linear cost function with and without total electrical power losses.

than that without ($0.9719 > 0.9415$). This is because without taking electric losses into account, a larger number of WTs can be connected to the same cable size. The export route length for different OSSs candidate locations affects mainly the slope of the corresponding linear function, thus, the longer the length the higher the slope. Finally, (iii), it can be seen for both sets that for low WTs numbers, i.e. between 1 and 40, the transmission cables minimum cost is poorly represented by the linear functions. However, it improves visibly at around 40 WTs and higher, which indicates that it can be used for the OWFs target size considered in this manuscript.

Overall, it is possible to infer that by including economic costs of electrical losses, not only a more holistic approach is supported (losses impact the layout as shown in [4], [35]), but also a statistical improvement is achieved, which enhances the accuracy of the model. The graphical result of applying the integrated global optimization model for electrical cables in SY OWF is presented in Fig. 5. Candidate locations are indicated with red numbers. All hard constraints are satisfied, along with the non crossing of forbidden areas. Only cables with 240 and $500\,\mathrm{mm}^2$ are used in the collection system. For the OSSs, the locations closest to the OCP are chosen, hence minimizing the transmission cable length. Each OSS is being connected with two $500\,\mathrm{mm}^2$ cables.

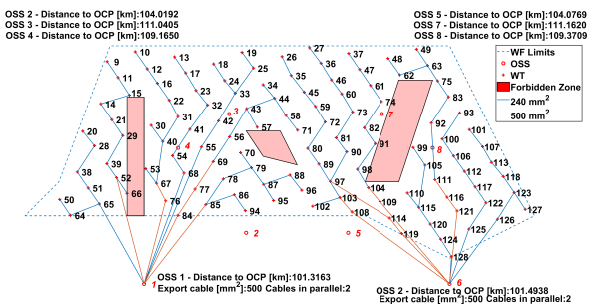

Fig. 5: SY OWF designed cable layout

Numerical results are available in Table III. For SY OWF ($\epsilon = 0.5\%$) an optimality gap of 0.49% is achieved in 3 hours, and 31 minutes. An initial feasible solution is found in 81 seconds, with optimality gap equal to 13.42%. In order to assess if the solver is able to take advantage of the problem's structure, an instance of SY, called as SYs, where only one candidate location is fixed per OSS (number 1 and 6 in Fig. 5), is solved by the model. An equal solution is obtained in 1 hour, and 28 minutes. The total number of combinations in terms of OSSs pairs is 16. If one assumes this an average running time, then a total of 23 hours, and 31 minutes would be required following an enumeration approach. By means of the integrated model a reduction of 85% of running time is obtained.

TABLE III
MAIN RESULTS SUMMARY

Model	Best solution [M€]	Gap [%]	Total computation time [h]
SY	487.47	0.49	3.53
SYs	487.76	0.50	1.48
LA	144	0.75	23.29

Finally, the very large instance of LA OWF is tackled. The two previously described instances have been solved using the default settings offered by CPLEX. However, out-of-memory problems were faced when evaluating the LA instance. To cope with this limitation, strong variable selection is used. This means that CPLEX invests considerable effort in analyzing potential branches of the nodes tree in the hope of drastically reducing the number of nodes that are explored. The strategy compromises the running time but generally allows for less memory requirements. The LA OWF is solved with a gap of 0.75% in slightly more than 23 hours. In this case, the optimal solution results in OSSs located around the center of the OWF. This is intuitively valid, as the shorter length to shore (around $20\,\mathrm{km}$) moves the weight towards minimizing the total length of the collector system cables.

VI. Conclusion

The proposed program provides an integrated global optimization approach to design electrical cable systems of OWFs, particularly the collection and transmission systems. The contributions of this manuscript are manifold: (i) capability to harmonize and design both systems through a MILP model, (ii) fast computing time, and (ii) integration of realistic and high-fidelity physical models. The methodology has been validated against large-scale instances of OWFs projects. Several numerical results prove the validity and accuracy of the approach in terms of abiding hard constraints within reasonable computation time, considering the complexity of the problems. A synthetic OWF (SY), and the second largest project in operation today, the London Array (LA), considering three candidate locations per OSS, have been used as case studies. The SY OWF is solved in around 3.5 hours with an optimality gap of 0.49%. The integrated model is roughly 85% faster than an enumeration approach. In the case of LA OWF, strong variable selection is used in the branch-and-cut method, achieving an optimality gap of 0.75% in slightly more than 23 hours. The results indicate that the physical optimal locations of the OSSs are strongly affected by the distance to shore, as the export cables total costs start becoming predominant for larger distances.

REFERENCES

[1] GWEC, "Global Wind Report 2018," Tech. Rep., 2019. [Online]. Available: https://www.tureb.com.tr/files/bilgi_bankasi/dunya_res_durumu/gwec_global_wind_report_2019.pdf.[AccessedMay27,2019]

[2] X. Sun, D. Huang, and G. Wu, "The current state of offshore wind energy technology development," *Energy*, vol. 41, no. 1, pp. 298–312, 2012.

[3] RenewableUK, "RenewableUK - Project Intelligence," 2018. [Online]. Available: https://www.renewableuk.com/page/ProjectIntelligenceHome. [AccessedMarch3,2019]

[4] M. Fischetti and D. Pisinger, "Optimizing wind farm cable routing considering power losses," *European Journal of Operational Research*, vol. 270, no. 3, pp. 917–930, 2018.

[5] L. Wolsey and G. L. Nemhauser, *Integer and combinatorial optimization*. John Wiley & Sons, 2014.

[6] J.-A. Pérez-Rúa and N. A. Cutululis, "Electrical Cable Optimization in Offshore Wind Farms - A review," *IEEE Access*, vol. 7, no. 1, pp. 85 796–85 811, 2019.

[7] P. Hou, W. Hu, and Z. Chen, "Offshore substation locating in wind farms based on prim algorithm," in *IEEE Power and Energy Society General Meeting*, 2015, pp. 1–5.

[8] F. M. González-Longatt, P. Wall, P. Regulski, and V. Terzija, "Optimal electric network design for a large offshore wind farm based on a modified genetic algorithm approach," *IEEE Systems Journal*, vol. 6, no. 1, pp. 164–172, 2012.

[9] K. Deb, *Optimization for engineering design: Algorithms and examples*. PHI Learning Pvt. Ltd., 2012.

[10] A. Wędzik, T. Siewierski, and M. Szypowski, "A new method for simultaneous optimizing of wind farm's network layout and cable cross-sections by MILP optimization," *Applied Energy*, vol. 182, pp. 525–538, 2016.

[11] S. Lumbreras and A. Ramos, "Optimal design of the electrical layout of an offshore wind farm applying decomposition strategies," *IEEE Transactions on Power Systems*, vol. 28, no. 2, pp. 1434–1441, 2013.

[12] P. Fagerfjäll, "Optimizing wind farm layout-more bang for the buck using mixed integer linear programming (MSc. Thesis)," Ph.D. dissertation, 2010.

[13] S. Lumbreras, A. Ramos, and S. Cerisola, "A Progressive Contingency Incorporation Approach for Stochastic Optimization Problems," *IEEE Transactions on Power Systems*, vol. 28, no. 2, pp. 1452–1460, 2013.

[14] M. Banzo and A. Ramos, "Stochastic Optimization Model for Electric Power System Planning of Offshore Wind Farms," *IEEE Transactions on Power Systems*, vol. 26, no. 3, pp. 1338–1348, 2011.

[15] P. Hou, W. Hu, Z. Chen, and C. Chen, "Overall Optimization for Offshore Wind Farm Electrical System," *Wind Energy*, vol. 20, no. 2016, pp. 1017–1032, 2017.

[16] O. Dahmani, S. Bourguet, M. MacHmoum, P. Guerin, P. Rhein, and L. Josse, "Optimization of the Connection Topology of an Offshore Wind Farm Network," *IEEE Systems Journal*, vol. 9, no. 4, pp. 1519–1528, 2015.

[17] J.-A. Pérez-Rúa, M. Stolpe, K. Das, and N. A. Cutululis, "Global Optimization of Offshore Wind Farm Collection Systems," *IEEE Transactions on Power Systems (Under Review)*, pp. 1–12, 2019. [Online]. Available: http://arxiv.org/abs/1907.02371

[18] J. Herbert-Acero, O. Probst, P.-E. Réthoré, G. Larsen, and K. Castillo-Villar, "A Review of Methodological Approaches for the Design and Optimization of Wind Farms," *Energies*, vol. 7, no. 11, pp. 6930–7016, 2014.

[19] A. Cerveira, A. F. de Sousa, E. J. Pires, and J. Baptista, "Optimal Cable Design of Wind Farms: The Infrastructure and Losses Cost Minimization Case," *IEEE Transactions on Power Systems*, vol. 31, no. 6, pp. 4319–4329, 2016.

[20] S. Lundberg, "Configuration study of large wind parks," Ph.D. dissertation, Chalmers University of Technology, 2003.

[21] J. Bauer and J. Lysgaard, "The offshore wind farm array cable layout problem: A planar open vehicle routing problem," *Journal of the Operational Research Society*, vol. 66, no. 3, pp. 360–368, 2015.

[22] L. Gouveia and P. Martins, "The capacitated minimum spanning tree problem: revisiting hop-indexed formulations," *Computers & operations research*, vol. 32, no. 9, 2005.

[23] IEC, "IEC-60287-1: Electric cables - Calculation of the current rating," Tech. Rep., 2014. [Online]. Available: https://www.evs.ee/products/iec-60287-1-1-2006.[AccessedApril15,2019]

[24] G. J. Anders, A. Napieralski, and Z. Kulesza, "Calculation of the internal thermal resistance and ampacity of 3-core screened cables with fillers," *IEEE Transactions on Power Delivery*, vol. 14, no. 3, pp. 729–733, 1999.

[25] J.-A. Pérez-Rúa, K. Das, and N. A. Cutululis, "Optimum sizing of offshore wind farm export cables," *International Journal of Electrical Power & Energy Systems*, vol. 113, no. December 2019, pp. 982–990, 2019. [Online]. Available: https://doi.org/10.1016/j.ijepes.2019.06.026

[26] J. J. Grainger and W. D. J. Stevenson, *Power System Analysis*, 2nd ed. McGraw-Hill Education, 1994.

[27] P. Sørensen, N. A. Cutululis, A. Vigueras-Rodríguez, L. E. Jensen, J. Hjerrild, M. H. Donovan, and H. Madsen, "Power Fluctuations From Large Wind Farms," *IEEE Transactions on Power Systems*, vol. 22, no. 3, pp. 958–965, 2007.

[28] S. Dutta and T. Overbye, "A Graph-theoretic Approach for Addressing Trenching Constraints in Wind Farm Collector System Design," in *IEEE Power and Energy Conference at Illinois (PECI)*, 2013, pp. 1–5.

[29] A. Klein and D. Haugland, "Obstacle-aware optimization of offshore wind farm cable layouts," *Annals of Operations Research*, vol. 272, no. 1-2, pp. 373–388, 2017.

[30] A. C. Pillai, J. Chick, L. Johanning, M. Khorasanchi, and V. De Laleu, "Offshore wind farm electrical cable layout optimization," *Engineering Optimization*, vol. 47, no. 12, pp. 1689–1708, 2015.

[31] C. Berzan, K. Veeramachaneni, J. McDermott, and U.-M. O'Reilly, "Algorithms for cable network design on large-scale wind farms," Tech. Rep., 2011. [Online]. Available: https://thirld.com/files/msrp_techreport.pdf.[AccessedApril15,2019]

[32] IBM, "IBM ILOG CPLEX Optimization Studio CPLEX User Manual," Tech. Rep., 2015. [Online]. Available: https://www.ibm.com/support/knowledgecenter.[AccessedApril11,2019]

[33] ESCA, SEAFISH, and RenewableUK, "KIS-ORCA." [Online]. Available: http://kis-orca.eu/about-us#.XLRI_-gzYuU. [AccessedApril15,2019]

[34] ABB, "XLPE Submarine Cable Systems Attachment to XLPE Land Cable Systems - User's Guide," 2018. [Online]. Available: new.abb.com/docs/default-source/ewea.../xlpe-submarine-cable-systems-2gm5007.pdf.[AccessedOct29,2018]

[35] A. M. Jenkins, M. Scutariu, and K. S. Smith, "Offshore wind farm inter-array cable layout," in *IEEE PowerTech at Grenoble*, 2013, pp. 1–6.

Juan-Andrés Pérez-Rúa received the B.Sc. degree in Electrical Engineering, with Summa Cum Laude distinction, from the Technological University of Bolivar, Colombia, in 2012, and the M.Sc. degree in Sustainable Transportation and Electrical Power Systems from the ISEC college, Coimbra, Portugal, the University of Nottinghan, England, and the University of Oviedo, Spain, in 2016. Currently, he is pursuing the Ph.D. degree in the Department of Wind Energy at the Technical University of Denmark (DTU). His present-day areas of interest include grid integration of renewables in power systems, and optimization.

Mathias Stolpe received the Ph.D. degree in Optimization and Systems Theory from the Royal Institute of Technology (KTH), Stockholm, Sweden in 2003. He works as a Professor in the Department of Wind Energy at the Technical University of Denmark (DTU). His areas of research are structural and multidisciplinary optimization with focus on models and methods for global optimization.

Nicolaos A. Cutululis received the M.Sc. and Ph.D. degrees, both in Automatic Control in 1998 and 2005, respectively. Currently, he is Professor in the Department of Wind Energy at the Technical University of Denmark. His main research interests are integration of wind power, with a special focus on offshore wind power, and grids.

APPENDIX J5

"Reliability-based Topology Optimization for Offshore Wind Farm Collection System"

J.A. Pérez-Rúa, S. Lumbreras,
A Ramos, and N. A. Cutululis

submitted
to *Wind Energy*

April

2020

Reliability-based Topology Optimization for Offshore Wind Farm Collection System

Juan-Andrés Pérez-Rúa[1], Sara Lumbreras[2], Andrés Ramos[2], and Nicolaos A. Cutululis[1]

[1]DTU Wind Energy, Technical University of Denmark, Frederiksborgvej 399, 4000 Roskilde, Denmark
[2]Institute for Research in Technology, Comillas Pontifical University, Calle de Alberto Aguilera 23, 28015 Madrid, Spain

Correspondence: Juan-Andrés Pérez-Rúa (juru@dtu.dk)

Abstract. An optimization framework for global optimization of the cable layout topology for Offshore Wind Farm (OWF) is presented. The framework designs and compares closed-loop and radial layouts for the collection system of OWFs. For the former, a two-stage stochastic optimization model based on a MILP optimization program is developed, while for the latter, a hop-indexed full binary model is used. The purpose of the framework is to provide a common base for assessing both designs economically, using the same underlying contingency treatment. A discrete Markov model is implemented for calculating the cable failure probability, useful for estimating the time under contingency for multiple power generation scenarios. The objective function supports simultaneous optimization of: (i) initial investment (network topology and cable sizing), (ii) total electrical power losses costs, and (iii) operation costs due to energy curtailment from cables failures. Constraints are added accounting for common engineering aspects. The applicability of the full method is demonstrated by tackling three differently sized real-world OWFs. Results show that: (i) the profitability of either topology type depends strongly on the project size and wind turbine rating. Closed-loop may be a competitive solution for large scale projects where large amounts of energy are potentially curtailed. (ii) The stochastic model presents low tractability to tackle large-scale instances, increasing the required computing time and memory resources. (iii) Strategies must be adopted in order to apply stochastic optimization for modern OWFs, intending analytically or numerically simplification of mathematical models.

1 Introduction

Medium voltage power cables are required for the cable layout of Offshore Wind Farms (OWFs). Cables represent at least 11% of the overall Levelised Cost Of Energy (LCOE), being one of the major cost element along with the wind turbine nacelles, foundations, and Offshore Substation (OSS) (Catapult, 2020). Between 2018 and 2028, a total of 19,702 km of array cables are forecast to be installed, worth 5.36 billions of British pounds, turning power cables into the main component of the Balance of Plant (BoP) (RenewableUK, 2018). However, power cables do not only have a sizeable impact over capital expenses, but also affect greatly the operation and performance of OWFs projects. These electrical components can be single points of failure, leading to strongly undesired contingencies (ReNEWS, 2017). Shallow waters, buried depth, seabed terrain movements (Warnock et al., 2019), electro-thermal stress (Pérez-Rúa et al., 2019a), and harsh accessibility conditions for maintenance and reparation (Besnard et al., 2013), are the differential factors in the context of OWFs. These particular characteristics give rise to

higher failure rates of submarine cables compared to those reported by other offshore industries, such as oil and gas (CIGRE: Working Group B1.10, 2009) (CIGRE: Working Group B1.21, 2009).

In contrast to transmission (with typical rated voltage equal or higher than 110 kV), collection systems (33 kV or 66 kV rated voltage) have been commonly designed in a deterministic fashion, i.e., considering no cable failure during the project´s lifetime. This has resulted in radial topology, i.e., without electrical redundancy - trees according to graph theory (Pérez-Rúa and Cutululis, 2019)- being the most common subject of study in literature in this context, and currently represents the most frequent choice by OWF developers. This is understandable as failure rates tend to increase with the voltage level and the length (Warnock et al., 2019), both higher for the OWF tranmission system. However, this can drive to underestimation of the contingencies occurrence, and their effects due to potential cables failures in collection systems.

Moreover, further insights are gained by applying probabilistic techniques in reliability assessment. The possibility to consider several operation states is fundamental in robust designs. In this sense, cables for collection systems may also be designed to provide increased levels of reliability, generally resulting in closed-loop topologies. With the increase in OWFs installed capacities, the trend of moving towards subsidy-free operating regimes, and more and better data linked to cables failures rates, quantification of economic suitability of closed-loop or radial topology is becoming essential.

Radial topology for OWF collection system, following a deterministic strategy, falls into a standard class of computational problems, being classified in computational complexity as NP-Hard. Thus, scalability is the main challenge, as modern OWFs are in the order of hundreds of Wind Turbines (WTs). State-of-the-arts works have focused on developing new mathematical models solved through global optimization solvers, as per (Chen et al., 2016), (Hertz et al., 2017), (Bauer and Lysgaard, 2015), (Fischetti and Pisinger, 2018b), (Pillai et al., 2015), (Klein and Haugland, 2017), and (Pérez-Rúa et al., 2020b); where the main objective has been to tackle large problems, while incorporating into the models real-world constraints. Mixed Integer Quadratic Programming (MIQP), Mixed Integer Non-Linear Programming (MINLP), and Mixed Integer Linear Programming (MILP) are the most used types of models. Each of these mathematical formulations impose certain limitations on the physics modelling options. For instance, using flow-based MILP makes it more difficult to include the quadratic active power losses explicitly into the objective function. The commonly used power flow equations solved with e.g. the Newton-Raphson method cannot be considered in MILP or MIQP formulations, but with a MINLP. Likewise, linear-based formulations are computationally more efficient than quadratic or non-linear.

Closed-loop designs have been studied in (Fischetti and Pisinger, 2018a) and in (Klein and Haugland, 2020). However, in both, the closed-loop design is done in a deterministic manner. In the former, a MILP model is extended to support this constraint, and in the latter a two-layered optimization process is developed, where the sub-problem uses optimal dual variables of the continuous relaxation of the master problem to increase feasible points diversity. In both articles, the cable sizing is missing, together with very important constraints such as power flow modelling, and cables failures. In this regard, it becomes very hard to assess the economic benefits of designs with increased reliability.

Stochastic optimization for OWFs electrical cable optimization has been addressed previously (Banzo and Ramos, 2011), (Lumbreras et al., 2013), and (Lumbreras and Ramos, 2013). Nonetheless, the focus of these articles is the holistic design for small-scale farms, while excluding practical engineering constraints such as no-crossing of cables, among others. The first

work in the field (Banzo and Ramos, 2011) proposed a MIQP model using exhaustive uncertainty enumeration. This work is continued in (Lumbreras et al., 2013) and (Lumbreras and Ramos, 2013), where the contribution is the development of techniques to accelerate the convergence to obtain solution through decomposition techniques.

The main contributions of this work are: (i) development, testing, and application of an algorithmic framework to design collection system with a closed-loop structure, using global optimization, integrated with analytical methods for reliability assessment. (ii) development of a common framework to assess and compare economically topology optimization for OWFs, namely closed-loop vs radial layouts. In the first point, the algorithm is based upon a MILP model solved using a commercial solver, able to account for the three main optimization criteria in electrical network planning: investment, total electrical power losses, and reliability. For the second point, a recourse problem is solved using the radial design and the same underlying stochastic considerations utilized for the closed-loop design. It is important to remark that strategies for tackling large instances are quantitatively analyzed and discussed as well.

2 Stochastic Optimization Model

2.1 Graph and model representation

In this section the MILP optimization program for the closed-loop stochastic model is deployed (Pérez-Rúa et al., 2020a). The model is formulated using connection decisions (binary) and flow (continuous) variables. The optimization program for the deterministic model used to design radial layouts is not presented as is available in (Pérez-Rúa et al., 2020b). It is fundamentally a hop-indexed model using uniquely binary variables (for the case of single OSS). While the hop-indexed model is more efficiently solved, the flow one brings along more modelling flexibility and versatility.

The aim of the optimization is to design a closed-loop cable layout of the collection system for an OWF, i.e., to interconnect through power cables the n_{w} WTs to the available OSS, while providing a redundant power evacuation route for each turbine. Let $\boldsymbol{N}_{\mathrm{w}} = \{2, \cdots, 1 + n_{\mathrm{w}}\}$. Besides, let the points set be $\boldsymbol{N} = \{1\} \cup \boldsymbol{N}_{\mathrm{w}}$, where the element $i \in \boldsymbol{N}$, such as $i = 1$ is the OSS.

The Euclidean distance between the positions of the points i and j, is denoted by d_{ij}. These inputs are gathered in a weighted undirected graph $G(\boldsymbol{N}, \boldsymbol{E}, \boldsymbol{D})$, with $\boldsymbol{N}$ being the vertex set, $\boldsymbol{E}$ the set of available edges arranged as a pair-set, and $\boldsymbol{D}$ the set of associated euclidean distances for each element $[ij] \in \boldsymbol{E}$, where $i \in \boldsymbol{N} \wedge j \in \boldsymbol{N}$.

In general, $G(\boldsymbol{N}, \boldsymbol{E}, \boldsymbol{D})$ is a complete undirected graph. It may be bounded by defining uniquely those edges connecting the $\upsilon < n_{\mathrm{w}}$ closest WTs to each WT, and by the $\sigma < n_{\mathrm{w}}$ edges directly reaching the OSS from the WTs.

Likewise, let $\boldsymbol{T}$ be a predefined list of available cable types, and $\boldsymbol{U}$ be the set of cable capacities sorted in non-decreasing order as in $\boldsymbol{T}$, being measured in Amperes (A), such that u_t is the capacity of cable $t \in \boldsymbol{T}$. Furthermore, each cable type $t \in \boldsymbol{T}$ has a cost per unit of length, c_t (including capital and installation costs), in such a way that $\boldsymbol{U}$ and $\boldsymbol{T}$ are both comonotonic. The set of expenditures per meter is defined as $\boldsymbol{C}$.

After defining the graph representation of the problem, the designed model and its formulation is deployed. The model captures in the objective function the costs linked to Investment (cables' capital and installation costs), Electrical Losses (in a

conservative and approximated fashion), and Reliability (cost of energy curtailment). The problem is formulated as a stochastic optimization program, modelled with two stages: first, the investment (construction), and second, the operation.

Uncertainty is represented by means of a scenario tree (Υ), expressing simultaneously how the stochasticity is developing over time, the different states of the random parameters, and the definition of the non-anticipative decisions in the present. The set of wind power generation scenarios is $\boldsymbol{\Omega}$, while the representative system states are $\boldsymbol{K}$. The nominal generation scenario is ω_{n}, and the base system state (k_{o}) represents the case of no failures. The base case is therefore represented by the scenario $\{\omega_{\mathrm{n}}, k_{\mathrm{o}}\}$. A wind power generation scenario ω has associated a duration time τ^{ω} (in hours), and power magnitude ζ^{ω} (in p.u.), and each system state k, a system probability ψ^{k}, calculated using a discrete Markov model to define the probability for a cable' complementary states: available, and unavailable (Calixto, 2016). In the same way, given the low failure rates of these components, a N-1 criterion must be considered in each system state (Billinton and Allan, 1992).

The first stage variables are the binary variables $x_{ij,t}$, and y_{ij}; where $x_{ij,t}$ is equal to one if active edge $[ij]$ ($y_{ij} = 1$) uses cable type $t \in \boldsymbol{T}$. The second stage variables are the continuous variables $I_{ij}^{\omega,k}$, $\theta_{i}^{\omega,k}$, and $\delta_{j}^{\omega,k}$. The electrical current in edge $[ij]$ in wind power generation scenario $\omega \in \boldsymbol{\Omega}$, and system state $k \in \boldsymbol{K}$ is represented by $I_{ij}^{\omega,k}$. While the voltage phase at each WT busbar is $\theta_{i}^{\omega,k}$. The curtailed current at wind turbine j in wind power generation scenario $\omega \in \boldsymbol{\Omega}$, and system state $k \in \boldsymbol{K}$ is $\delta_{j}^{\omega,k}$. Note that $\delta_{j}^{\omega,k}$ (in A) is bounded by the current generated at j in the same scenario, I_{j}^{ω}, where $I_{j}^{\omega} = \frac{P_n \cdot \zeta^{\omega} \cdot 1000}{\sqrt{3} \cdot V_n}$, being P_n the nominal power of an individual WT, and V_n the line-to-line nominal voltage of the system.

2.2 Cost coefficients and objective function

Total electrical power losses are non-linear in function of the current. In that event, two distinctive mathematical expressions to support simultaneous optimization of investment and operation, and simultaneous optimization of investment, operation and losses are deployed. Both objective functions keep the linear structure of the model and are be selected exclusively.

2.2.1 Neglecting total electrical power losses

The objective function in this case consists of a simultaneous valuation of the total initial investment plus reliability. The investment is intuitively computed as the sum of cables costs installed in each edge $[ij]$; on the other hand, reliability is quantified through the estimation of the economic losses due to cables failures, as the result of undispatched current (i.e. energy) from each WT. In this way, the objective function is formalized as:

$$\min \overbrace{\sum_{[ij]\in\boldsymbol{E}} \sum_{t\in\boldsymbol{T}} c_t \cdot d_{ij} \cdot x_{ij,t}}^{\text{Investment}} + \overbrace{c_{\mathrm{e}} \cdot \sum_{i\in\boldsymbol{N}_{\mathrm{w}}} \sum_{\omega\in\boldsymbol{\Omega}} \sum_{k\in\boldsymbol{K}} \tau^{\omega} \cdot \psi^{k} \cdot \delta_{i}^{\omega,k}}^{\text{Operation/Reliability}} \tag{1}$$

Here c_{e} is the cost of energy in Euro Ah^{-1} (equivalent to Euro MWh^{-1}). The sum of system states probabilities must be equal to one, $\sum_{k\in\boldsymbol{K}} \psi^{k} = 1$, given the mutually exclusive nature of the considered events (at most one cable is subject to failure, N-1 criterion). A system state k represents the failure of a single cable in an active edge $e \in \boldsymbol{E}$, therefore the system probability for the state ψ^{k} is considered equal to this failure probability. This implies that the availability probability of the other installed cables is considered to be equal to one in this scenario Banzo and Ramos (2011), representing a conservative approach as the

value of the parameter ψ^k is slightly overestimated (the system probability is the multiplication of each installed cable state probability).

2.2.2 Considering total electrical power losses

Total electrical power losses are non-linear in function of the current, cable type, and total length (Pérez-Rúa and Cutululis, 2019). The designer must try to find a proper balance between modelling fidelity and optimization program complexity. A pre-processing strategy is proposed in this manuscript in order to incorporate this factor into the objective function.

$$f_t = \left\lfloor \frac{\sqrt{3} \cdot V_n \cdot u_t}{P_n \cdot 1000} \right\rfloor \quad \forall t \in \boldsymbol{T} \tag{2}$$

The set of cable capacities in terms of number of supportable WTs is defined in Eq. (2). Let the new cable type set be:

$$\boldsymbol{T'} = \left\{ \underbrace{1, 2, \cdots, f_1}_{t_1}, \underbrace{f_1 + 1, \cdots, f_2}_{t_2}, f_2 + 1, \cdots, \underbrace{f_{|\boldsymbol{T}|-1} + 1, \cdots, f_{|\boldsymbol{T}|}}_{t_{|\boldsymbol{T}|}} \right\} \tag{3}$$

This implies that $\boldsymbol{T'}$ is the discretized form of the maximum capacity $U = \max \boldsymbol{U}$. Note that this is translated into the creation of additional variables $x_{ij,t'} : t' \in \boldsymbol{T'}$. Likewise, if the *floor function* in Eq. (2) is replaced by a *decimal round down function*, and $\boldsymbol{T'}$ is also discretized using the same decimal steps, then the number of variables will increase accordingly, to the benefit of gaining in accuracy for the cable capacities. In $\boldsymbol{T'}$ is contained the non-dominated cable sub-types from $\boldsymbol{T}$; this means that each cable sub-type $t' \in \boldsymbol{T'}$ is related to a cable type $t \in \boldsymbol{T}$, inheriting physical properties such as cost per meter (c_t), electrical resistance per meter (R_t), and electrical reactance per meter (X_t); as shown in Eq. (3). Acknowledging that the investment cost of a cable t exceeds the electrical power losses costs, then the selected cable sub-type to connect n WTs will always be the cheapest (smallest) cable with sufficient capacity, rather than a bigger one with lower electrical power losses as the electrical resistance decreases with size. As a consequence of the aforementioned, let a new cable capacities set be:

$$\boldsymbol{U'} = \left\{ 1, 2, \cdots, f_1, f_1 + 1, \cdots, f_2, f_2 + 1, \cdots, f_{|\boldsymbol{T}|-1} + 1, \cdots, f_{|\boldsymbol{T}|} \right\} \cdot \frac{P_n \cdot 1000}{\sqrt{3} \cdot V_n} \tag{4}$$

Let the functions $f(t')$, $g(t')$, and $h(t')$ calculate cost, electrical resistance, and electrical reactance per meter for cable sub-type t', respectively, which are inherited from a cable type t. Whereby, the objective function for simultaneous optimization of investment, electrical losses, and reliability is:

$$\overbrace{\min \sum_{[ij] \in \boldsymbol{E}} \sum_{t' \in \boldsymbol{T'}} \left(f(t') + \underbrace{3 \cdot 1.5 \cdot g(t') \cdot \left(\frac{c_{\mathrm{e}}}{\sqrt{3} \cdot V_n \cdot 1000} \right) \cdot \sum_{\omega \in \boldsymbol{\Omega}} \left(u'_{t'} \cdot \zeta^{\omega} \right)^2 \cdot \tau^{\omega}}_{=h(t')\text{. Pre-processing for total electrical power losses}} \right) \cdot d_{ij} \cdot x_{ij,t} +}^{\text{Investment plus total electrical power losses}} \tag{5}$$

$$\overbrace{c_{\mathrm{e}} \cdot \sum_{i \in \boldsymbol{N}_{\mathrm{w}}} \sum_{\omega \in \boldsymbol{\Omega}} \sum_{k \in \boldsymbol{K}} \tau^{\omega} \cdot \psi^k \cdot \delta_i^{\omega,k}}^{\text{Operation/Reliability}}$$

The factor $(3 \cdot 1.5)$ in Eq. (5) accounts the joule, screen and armouring losses for the three-phase system. The whole term for total electrical power losses ($h(t')$) is calculated for each $t' \in \boldsymbol{T'}$, before launching the MILP model into the external solver. Therefore, the objective function is a linear weighting of the desired targets: investment, electrical losses, and reliability.

As discussed previously, one of the tasks of the designer is to balance out modelling fidelity and optimization program complexity. The objective function in Eq. (5) is a linear function, thus the following simplifications are assumed: (i) integer discretization in Eq. (3) which restricts the capacity of cables, and may cause overestimation of electrical losses. This can be diminished by decimal round down, and by increasing discretization steps in Eq. (4) at the expense of incrementing the number of variables correspondingly. (ii) Neglection of system states (cables failures) apart of the base state (no failures); however, this is the state with highest probability. (iii) Power flow estimation in a conservative fashion, i.e., overestimating the incoming power flow by neglecting the total power losses downstream. All those simplifications may impact the final layout, however their conservative nature means rather over-designing than impacting the robustness.

2.3 Constraints

The first stage constraints are first presented. These constraints are only defined by the first stage variables.

In case edge $[ij]$ is active in the solution, then one and only one cable type $t \in \boldsymbol{T}$ or $t' \in \boldsymbol{T'}$ must be chosen as in

$$\sum_{t \in \boldsymbol{T}} x_{ij,t} = y_{ij} \quad \forall [ij] \in \boldsymbol{E} \vee \sum_{t' \in \boldsymbol{T'}} x_{ij,t'} = y_{ij} \quad \forall [ij] \in \boldsymbol{E} \tag{6}$$

Note that in case total electrical power losses are considered, then the cable types set is $\boldsymbol{T'}$, otherwise $\boldsymbol{T}$; same logic for $\boldsymbol{U}/\boldsymbol{U'}$, t/t', and $u_t/u'_{t'}$. This applies for the forthcoming mathematical expressions.

A closed-loop (sunflower petals) collection system topology is forced through

$$\sum_{\substack{j \in \boldsymbol{N} \\ j \neq i}} y_{ij} = 2 \quad \forall l \in \boldsymbol{N}_{\mathrm{w}} : l = i \vee l = j \tag{7}$$

Limiting the number of feeders (upper limit of ϕ feeders) connected to the OSS is carried out by means of

$$\sum_{i \in \boldsymbol{N}_{\mathrm{w}}} y_{ij} \leq \phi \quad j = 1 \tag{8}$$

The set $\boldsymbol{\chi}$ stores pairs of edges $\{[ij], [uv]\}$, which are crossing each other. Excluding crossing edges in the solution is ensured by the simultaneous application of the next linear inequalities along with (6)

$$y_{ij} + y_{uv} \leq 1 \quad \forall \{[ij], [uv]\} \in \boldsymbol{\chi} \tag{9}$$

The no-crossing cables restriction is a practical requirement in order to avoid hot-spots, and potential single-points of failure caused by overlapping cables Bauer and Lysgaard (2015). Constraint (9) exhaustively lists all combinations of crossings edges. The constraints in (6) ensure that no active edges are crossing or overlapping between each other. These constraints thus link the variables y_{ij} and $x_{ij,t}$.

The second stage constraints are now deployed. These constraints are only defined by the second stage variables. They are defined by the flow conservation, which also avoids disconnected solutions, as per

$$\sum_{\substack{i\in\boldsymbol{N}\\ j\neq i}}\sum_{\omega\in\boldsymbol{\Omega}}\sum_{k\in\boldsymbol{K}} I_{ji}^{\omega,k} - I_{ij}^{\omega,k} + \delta_j^{\omega,k} = I_j^{\omega} \quad \forall j\in\boldsymbol{N}_{\mathrm{w}} \quad \forall\omega\in\boldsymbol{\Omega} \quad \forall k\in\boldsymbol{K} \tag{10}$$

The set of tender constraints, useful to link first and second stage constraints, are lastly presented.

DC power flow is forced with

$$I_{ij}^{\omega,k} - \frac{1000\cdot V_n\cdot(\theta_i^{\omega,k}-\theta_j^{\omega,k})}{\sqrt{3}\cdot X_t\cdot d_{ij}} - M\cdot(1-x_{ij,t}) - M\cdot r_{ij}^k \leq 0 \quad \forall[ij]\in\boldsymbol{E} \quad t\in\boldsymbol{T} \quad \forall\omega\in\boldsymbol{\Omega} \quad \forall k\in\boldsymbol{K} \tag{11}$$

$$-I_{ij}^{\omega,k} + \frac{1000\cdot V_n\cdot(\theta_i^{\omega,k}-\theta_j^{\omega,k})}{\sqrt{3}\cdot X_t\cdot d_{ij}} - M\cdot(1-x_{ij,t}) - M\cdot r_{ij}^k \leq 0 \quad \forall[ij]\in\boldsymbol{E} \quad t\in\boldsymbol{T} \quad \forall\omega\in\boldsymbol{\Omega} \quad \forall k\in\boldsymbol{K} \tag{12}$$

Where r_{ij}^k is a parameter equal to one if edge $[ij]$ is failed, or zero if otherwise, and M is a big enough number to guarantee feasibility for those inactive or failed components.

The cable capacities are not exceeded by including the next bilateral constraints.

$$\sum_{t\in\boldsymbol{T}} u_t\cdot x_{ij,t}\cdot(1-r_{ij}^k) \geq I_{ij}^{\omega,k} \quad \forall[ij]\in\boldsymbol{E} \quad \forall\omega\in\boldsymbol{\Omega} \quad \forall k\in\boldsymbol{K} \tag{13}$$

$$\sum_{t\in\boldsymbol{T}} -u_t\cdot x_{ij,t}\cdot(1-r_{ij}^k) \leq I_{ij}^{\omega,k} \quad \forall[ij]\in\boldsymbol{E} \quad \forall\omega\in\boldsymbol{\Omega} \quad \forall k\in\boldsymbol{K} \tag{14}$$

The current $I_{ij}^{\omega,k}$ may circulate either from i to j or viceversa. In case total electrical power losses are considered, for all scenarios, except the ones linked to k_{o}, the capacity $u'_{t'}$ is inherited from the cable type t. This is to avoid unnecessary energy curtailment. For the base system state, k_{o}, capacity $u'_{t'}$ must be taken from Eq. (4).

Finally, constraints in Eq. (15) to Eq. (19) define the nature of the formulation by the variables definition, a MILP program.

$$x_{ij,t}\in\{0,1\} \quad \forall t\in\boldsymbol{T} \quad \forall[ij]\in\boldsymbol{E} \tag{15}$$

$$y_{ij}\in\{0,1\} \quad \forall[ij]\in\boldsymbol{E} \tag{16}$$

$$-0.1 \leq \theta_i^{\omega,k} \leq 0.1 \quad \forall i\in\boldsymbol{N} \quad \forall\omega\in\boldsymbol{\Omega} \quad \forall k\in\boldsymbol{K} \tag{17}$$

$$-U \leq I_{ij}^{\omega,k} \leq U \quad \forall[ij]\in\boldsymbol{E} \quad \forall\omega\in\boldsymbol{\Omega} \quad \forall k\in\boldsymbol{K} \tag{18}$$

$$0 \leq \delta_i^{\omega,k} \leq I_i^{\omega,k} \quad \forall i\in\boldsymbol{N}_{\mathrm{w}} \quad \forall\omega\in\boldsymbol{\Omega} \quad \forall k\in\boldsymbol{K} \tag{19}$$

3 Algorithmic Framework for the Stochastic Optimization Model: Determining the representative system states

Since the two-stage variables scale-up exponentially as a function of the scenario tree size, the representative systems states must be limited (Pérez-Rúa et al., 2020a). The basic version of the stochastic optimization program presented in Sect. 2 encompasses the full set $\boldsymbol{E}$; each element $[ij]$ gives place to a system state k to form the system states set $\boldsymbol{K}$.

Nevertheless, the actual selected edges in a solution (i.e. a feasible point satisfying the optimality criteria) is only a subset $\boldsymbol{E'} \subset \boldsymbol{E}$; let the complement set $\boldsymbol{E''}$ contain the unused elements from $\boldsymbol{E}$, and let define the subset $\boldsymbol{E'''} \subset \boldsymbol{E''}$. Hereafter, it is proved that any representative system states set containing at least the scenarios linked to $\boldsymbol{E'}$ ($\boldsymbol{K_{E'}} = \Phi(\boldsymbol{E'})$, using the transformation function Φ which maps from edges set to system states set), is necessary and sufficient to obtain the optimum in $P^{\boldsymbol{\Omega},\boldsymbol{K}}$.

Let the necessary and sufficient set $\boldsymbol{K'}$ encompass:

$$\boldsymbol{K'} = k_{\mathrm{o}} \cup \boldsymbol{K_{E'}} \cup \boldsymbol{K_{E'''}} \tag{20}$$

Where $\boldsymbol{K_{E'''}}$ is the system states linked to the subset of unused edges $\boldsymbol{E'''}$.

Axiom 1. *The second stage variables linked to unused elements are equal to the base system state*

$$\forall i \in \boldsymbol{N}_w \quad \forall k \in \boldsymbol{K_{E'''}} \quad \forall \omega \in \boldsymbol{\Omega}, \qquad \delta_i^{\omega,k} = \delta^{\omega,k_o}$$

An intuitive proposition is reflected in Axiom 1: *The curtailed currents in the system state of unused edges are the same than in the base system state*. This basically means that the failures of unused elements will not deteriorate the operation of the system.

From Eq. (1) it follows:

$$\sum_{[ij]\in\boldsymbol{E}} \sum_{t\in\boldsymbol{T}} c_t \cdot d_{ij} \cdot x_{ij,t} + c_{\mathrm{e}} \cdot \sum_{i\in\boldsymbol{N}_{\mathrm{w}}} \sum_{\omega\in\boldsymbol{\Omega}} \sum_{k\in\boldsymbol{K'}\setminus\{\boldsymbol{k}_{\mathrm{o}}\}} \tau^{\omega} \cdot \psi^k \cdot \delta_i^{\omega,k} + \tag{21}$$
$$c_{\mathrm{e}} \cdot \sum_{i\in\boldsymbol{N}_{\mathrm{w}}} \sum_{\omega\in\boldsymbol{\Omega}} \tau^{\omega} \cdot \left(1 - \sum_{k\in\boldsymbol{K'}\setminus\{\boldsymbol{k}_{\mathrm{o}}\}} \psi^k\right) \cdot \delta_i^{\omega,k_{\mathrm{o}}}$$

Eq. (21) with Eq. (20) becomes:

$$\sum_{[ij]\in\boldsymbol{E}} \sum_{t\in\boldsymbol{T}} c_t \cdot d_{ij} \cdot x_{ij,t} + c_{\mathrm{e}} \cdot \sum_{i\in\boldsymbol{N}_{\mathrm{w}}} \sum_{\omega\in\boldsymbol{\Omega}} \sum_{k\in\boldsymbol{K_{E'}}} \tau^{\omega} \cdot \psi^k \cdot \delta_i^{\omega,k} + \tag{22}$$
$$c_{\mathrm{e}} \cdot \sum_{i\in\boldsymbol{N}_{\mathrm{w}}} \sum_{\omega\in\boldsymbol{\Omega}} \sum_{k\in\boldsymbol{K_{E'''}}} \tau^{\omega} \cdot \psi^k \cdot \delta_i^{\omega,k} + c_{\mathrm{e}} \cdot \sum_{i\in\boldsymbol{N}_{\mathrm{w}}} \sum_{\omega\in\boldsymbol{\Omega}} \tau^{\omega} \cdot \left(1 - \sum_{k\in\boldsymbol{K_{E'}}} \psi^k\right) \cdot \delta_i^{\omega,k_{\mathrm{o}}} -$$
$$c_p \cdot \sum_{i\in\boldsymbol{N}_{\mathrm{w}}} \sum_{\omega\in\boldsymbol{\Omega}} \sum_{k\in\boldsymbol{K_{E'''}}} \tau^{\omega} \psi^k \cdot \delta_i^{\omega,k_{\mathrm{o}}}$$

Eq. (22) with Axiom 1 becomes:

$$\sum_{[ij]\in\boldsymbol{E}}\sum_{t\in\boldsymbol{T}} c_t\cdot d_{ij}\cdot x_{ij,t} + c_{\mathrm{e}}\cdot\sum_{i\in\boldsymbol{N}_{\mathrm{w}}}\sum_{\omega\in\boldsymbol{\Omega}}\sum_{k\in\boldsymbol{K}_{\boldsymbol{E}'}}\tau^{\omega}\cdot\psi^{k}\cdot\delta_i^{\omega,k}+ \tag{23}$$

$$c_{\mathrm{e}}\cdot\cancel{\sum_{i\in\boldsymbol{N}_{\mathrm{w}}}\sum_{\omega\in\boldsymbol{\Omega}}\sum_{k\in\boldsymbol{K}_{\boldsymbol{E}'''}}\tau^{\omega}\cdot\psi^{k}\cdot\delta_i^{\omega,k_{\mathrm{o}}}} + c_{\mathrm{e}}\cdot\sum_{i\in\boldsymbol{N}_{\mathrm{w}}}\sum_{\omega\in\boldsymbol{\Omega}}\tau^{\omega}\cdot\left(1-\sum_{k\in\boldsymbol{K}_{\boldsymbol{E}'}}\psi^{k}\right)\cdot\delta_i^{\omega,k_{\mathrm{o}}}-$$

$$c_p\cdot\cancel{\sum_{i\in\boldsymbol{N}_{\mathrm{w}}}\sum_{\omega\in\boldsymbol{\Omega}}\sum_{k\in\boldsymbol{K}_{\boldsymbol{E}'''}}\tau^{\omega}\psi^{k}\cdot\delta_i^{\omega,k_{\mathrm{o}}}}$$

Equation (23) is analogous to Eq. (21) but with $\boldsymbol{K'}\setminus\{\boldsymbol{k}_{\mathrm{o}}\}=\boldsymbol{K}_{\boldsymbol{E}'}$. This proves that *any set $\boldsymbol{K'}$ containing at least the system states associated to all selected edges is sufficient and necessary to find the global optimum of the full problem $P^{\boldsymbol{\Omega},\boldsymbol{K}}$*. Conversely, any instatiation for which $\boldsymbol{K'}\subset\boldsymbol{K}_{\boldsymbol{E}'}$ would lead to an underestimation of operational costs, ultimately causing falling into suboptimal. The proof also applies when including total electrical power losses (5).

This contingency structure opens the door for a Progressive Contingency Incorporation (PCI) strategy, aiming to find a proper set $\boldsymbol{K'}$. An improved PCI algorithm based on (Lumbreras et al., 2013) is proposed in the Algorithm 1.

Algorithm 1 Progressive Contingency Incorporation (PCI) Algorithm

1: $[\boldsymbol{X}_d,\boldsymbol{Y}_d]\leftarrow\arg P^{\boldsymbol{\Omega},\boldsymbol{K'}}:\Omega=\omega_n,\boldsymbol{K'}=k_o$ *with gap* ϵ_d
2: $\boldsymbol{E'}\leftarrow\boldsymbol{Y}_d=\{[ij]\}:y_{ij}=1\quad\forall[ij]\in\boldsymbol{E}:[ij]$ *satisfies reliability level* r_c
3: $\boldsymbol{E}'_o\leftarrow\emptyset,\boldsymbol{X}_{ws}\leftarrow\boldsymbol{X}_d\cup\boldsymbol{Y}_d$
4: **for** $(\kappa=1:1:\kappa_{max})$ **do**
5: $\quad\boldsymbol{A}\leftarrow\boldsymbol{E'}\cap\boldsymbol{E}'_o$
6: $\quad$**if** $(\boldsymbol{E'}==\boldsymbol{A})$ **then**
7: $\quad\quad$*Break*
8: $\quad$**end if**
9: $\quad\boldsymbol{E}'_o\leftarrow\boldsymbol{E'}\cup\boldsymbol{E}'_o$
10: $\quad[\boldsymbol{X},\boldsymbol{Y}]\leftarrow\arg P^{\boldsymbol{\Omega},\boldsymbol{K'}}:\Omega,\boldsymbol{K'}=\Phi(\boldsymbol{E}'_o)\cup k_o$ *with initial point* $\boldsymbol{X}_{ws}$ *and gap* ϵ_s. $\Upsilon=\{\Omega,\boldsymbol{K'}\}$
11: $\quad\boldsymbol{E'}\leftarrow\boldsymbol{Y}=\{[ij]\}:y_{ij}=1\quad\forall[ij]\in\boldsymbol{E}:[ij]$ *satisfies reliability level* r_c
12: $\quad\boldsymbol{X}_{ws}\leftarrow\boldsymbol{X}\cup\boldsymbol{Y}$
13: **end for**

In the first line a deterministic instance of the full problem is tackled. This means considering uniquely the scenario $\{\omega_{\mathrm{n}},k_{\mathrm{o}}\}$. For this problem a valid assumption is to consider zero curtailed power. After this, the active edges of interest corresponding to the first stage optimization variables are stored as $\boldsymbol{E'}$, along with the obtained solution variables in $\boldsymbol{X}_{\mathrm{ws}}$ (where $\boldsymbol{X}_{\mathrm{d}}$ and $\boldsymbol{Y}_{\mathrm{d}}$ contains the solution sets corresponding to $x_{ij,t}$, and y_{ij} for the deterministic case, respectively). As no previous iteration has been conducted, cumulative solution variables are unavailable ($\boldsymbol{E}'_{\mathrm{o}}$). Since the second stage variables express contingency scenarios of the components delimited by the first stage variables, the tree Υ uniquely considers the failure states associated to

those components. For the case presented in Algorithm 1, solely those feeders which satisfy the reliability level r_c, are subject to fail.

Parameter r_c defines the degree of connection towards the OSS, so for example, $r_c = 1$ brings along the main feeders (rooted at $i = 1$), and $r_c = 2$ includes the last ones together with the feeders connected to the main ones, and so on for $r_c > 2$, as shown in Fig. 1. By means of this parameter, the model can be further relaxed for large instances. A reliability level equal to one according to Fig. 1 would still represent at a large extent the consequences of all cables failures, as those main feeders are the one carrying the vast amount of energy compared to downstream connections. Thus, an important computational burden is avoided, while having a good representation of the system. This is backed up by the fact that cables under higher levels of electro-thermal stress present shorter lifetime (Pérez-Rúa et al., 2019b).

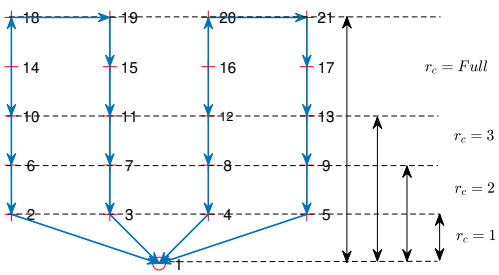

Figure 1. Reliabilty level definition.

The Progressive Contingency Incorporation routine for stochastic analysis is started at line 4. The opening step is to intersect the current active edges set $\boldsymbol{E}'$, and the cumulative set $\boldsymbol{E}'_{\mathrm{o}}$. If the intersection set is equal to the current active edges $\boldsymbol{E}'$, then the process is terminated, otherwise more iterations are attempted. For the former case, the algorithm is stopped, with solution $[\boldsymbol{X}, \boldsymbol{Y}]$; for the latter case, the iterative process is continued to the subsequent iteration κ. Trivially, for $\kappa = 1$, $\boldsymbol{A} = \emptyset$. Therefore, in line 9 the union set is obtained to update $\boldsymbol{E}'_{\mathrm{o}}$. A new instance of the main problem is solved in line 10, using the initial point $\boldsymbol{X}_{\mathrm{ws}}$ (warm-start point), while considering the full wind power generation scenarios indicated by the user Ω, and the system states related to edges cumulatively installed in all iterations, ($\boldsymbol{K}' = \Phi(\boldsymbol{E}'_{\mathrm{o}})$).

When the Algorithm 1 converges, the scenario criterion is met: obtention of the proper set $\boldsymbol{K}'$; meaning that all representative systems states have been already considered.

4 Optimization Framework

The full optimization framework is presented in Fig. 2. The main inputs for the framework can be divided as:

- Project-specific data, such as WTs and OSS location, rated power, wind power generation scenarios, Mean Time Between Failures (MTBF) for cables (in years kilometres per failure), and Mean Time To Repair (MTTR) for failed cables (in hours).

- Simulation settings, like cables' technical and economic parameters, macroeconomic information, including lifetime and price of energy, and required gap for the deterministic case (ϵ_{d}) and the stochastic phase (ϵ_{s}).
- Modelling choices, as reliability level (r_{c}), total electrical power losses incorporation (1 or 0), and DC power flow model (1 or 0).

A Markov Chain methodology is applied to calculate the probability for the unavailable state of a cable (Calixto, 2016):

$$\psi^k = \frac{MTTR}{MTTR + MTBT \cdot \frac{8760}{d_{ij}}} \tag{24}$$

Where d_{ij} (in kilometres) is the edge length where the component is installed, and k the associated system state.

Continuing with the flowchart of Fig. 2, two different models are formulated to tackle independently the stochastic closed-loop and the deterministic radial designs. As discussed previously, the closed-loop optimization program is based on a flow MILP model, in contrast to the hop-indexed optimization program dedicated for the non-looped layout, chosen such as to enable comparison of topologies for large-scale problems utilizing the state-of-the-art approaches.

The closed-loop stochastic model is formulated in function of the required inputs, especially $Losses$ and DC. The objective function and constraints are properly adapted to whether losses must be incorporated or not (See Sect. 2.2).

Similarly, two options for power flow are supported, transportation model ($DC == False$) and a DC power flow ($DC == True$). A transportation model is fundamentally the simplest of the ways to calculate the distribution of power in an electrical network. It abides the kirchhoff's first law by keeping the current balance at each node. Contrarily, a DC power flow model includes in addition the Kirchhoff's second law, approximating the voltage magnitude to 1 p.u., and spurning the reactive power flow (Grainger and Stevenson, 1994). The mathematical optimization program is notably relaxed by disregarding the DC power flow, which stress the model by creating additional variables. Finally, after the optimization program is formulated, this is sent to the Algorithm 1, obtaining the layout with linked investment and operation costs.

On the right branch of the flowchart, the radial model is formulated and solved accordingly to (Pérez-Rúa et al., 2020b). The obtained solution sets ($\boldsymbol{X_{rd}}$,$\boldsymbol{Y_{rd}}$, conserving the adopted nomenclature as in Sect. 3), are used to fix values of the flow model binary variables; simultaneously, Eq. (7) are modified as inequalities to allow up to three connections for each WT. With this, a tree topology is converted into a feasible point of the model. Lastly, the flow model is reassembled after all these changes, and sent to the Algorithm 1. In other words, a recourse problem is tackled $Q([\boldsymbol{X_{rd}}, \boldsymbol{Y_{rd}}])$, defined as minimization of the expected costs (operation costs) given the scenario tree (Υ) obtained from the wind power generation scenarios Ω, and the system states linked to $\boldsymbol{Y_{rd}}$. This recourse problem is inexpensive computationally given that the binary values are provided in advance. The recourse problem related to the radial layout is always solved to optimality.

In the last step of the flowchart, the two solutions (closed-loop and radial) are compared in terms of total expenses, investment and operation costs. This flow of tasks guarantee a fair comparison between them, since firstly, the same stochastic reference frame is maintained after the reformulation blocks depicted in Fig. 2, and, secondly, the PCI algorithm is utilized equally.

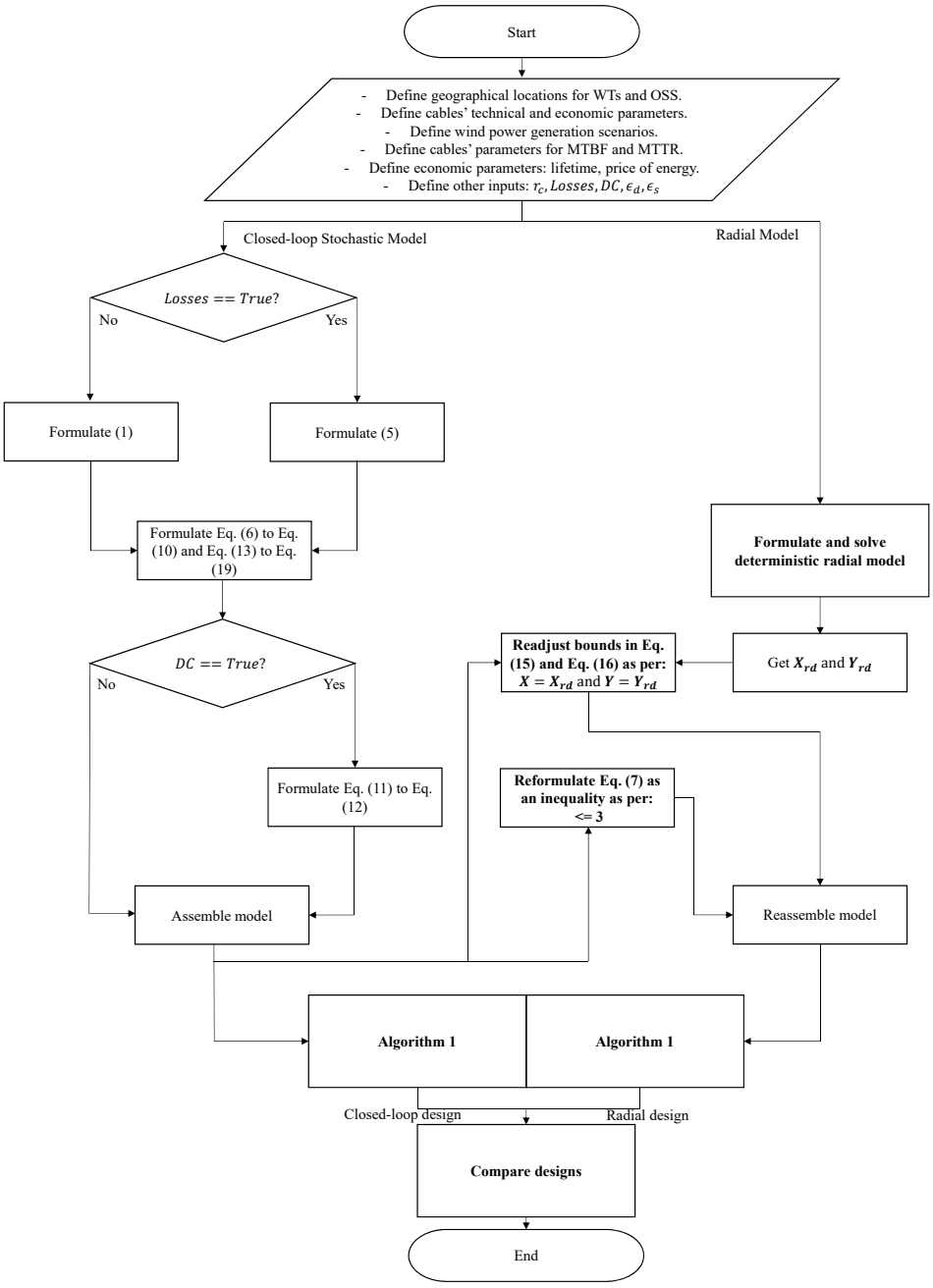

Figure 2. Optimization framework for comparing collection system topology.

5 Results

The computational experiments presented in this section have been carried out on an Intel Core i7-6600U CPU running at 2.50 GHz and with 16 GB of RAM. The chosen solver is IBM ILOG CPLEX Optimization Studio V12.7.1 (IBM, 2015). The experiments consist on three real-world cases aiming to test the proposed method for different problem sizes (small, large and very large), and WTs topological distribution (grid-based and coordinate-based). For all the following studies a MTTR of 30 days (720 h) is considered (Warnock et al., 2017). The price of energy is assumed to be fixed along the project lifetime with a value of 50 Euro MWh^{-1} (2.86 Euro Ah^{-1}), which is the average price as per (Statista, 2019).

The wind power generation scenarios are also equally fixed as per Table 1. Scenario 1 accounts for the nominal power (ω_{n}). The time duration of all the scenarios correspond to a project lifetime of 30 years. The magnitude and duration values lead to a capacity factor of 0.49, which is a reasonable value for modern offshore wind farms.

In general, the simulation results are dependant on several parameters, like the utilization of a discrete Markov model to calculate the failure probabilities given the failure statistical parameters MTBF and MTTR, and the considered price of energy, financial valuation method, project lifetime, cables set, cost functions, among others.

Table 1. Wind power generation scenarios.

Scenario	Magnitude [p.u.]	Duration [h]
1	1	65,700
2	0.5	91,980
3	0.2	91,980
4	0	13,140

Other electrical information related to the power cables, such as electrical resistance per meter (R_t) and electrical reactance per meter (X_t), is available in (ABB, 2018).

5.1 Small OWF: Ormonde

As a first case study the Ormonde (Vatenfall, b) OWF is analyzed. This OWF presents a closed-loop layout in the collection system. Specific inputs for this case study are shown in Table 2.

Table 2. Data inputs for Ormonde OWF.

P_n	V_n	$\boldsymbol{U}$	$\boldsymbol{C}$	n_{w}	υ	σ	ϕ	ϵ_{d}	ϵ_{s}
5 MW	33 kV	$\{530, 655, 775\}$ A	$\{450, 510, 570\}$ kEuro km^{-1}	30	6	10	4	0.2%	0.2%

To better understand the influence of different modelling choices for the model included Algorithm 1, several simulations and parametric sensitivities are carried out. They target power flow model, reliability level, and total electrical power losses.

Trough these case studies, the complexity of different modules of the model is understood, along with the gains obtained by them.

5.1.1 Power flow model

For this study, only the left branch of Fig. 2 is executed without considering losses. This means that results focus on closed-loop topology in this section. The objective is to compare a full version of the model (with $DC == True$), and a relaxed version ($DC == False$) employing a simple transportation power flow model. Besides this, the MTBF is varied from 10 to 178 years kilometres per failure, with the latter value being typical for OWFs medium voltage cables under operation today (Warnock et al., 2019), aiming at quantifying the parametric impact of MTBF value. To reduce computational burden when evaluating low values of MTBF, a reliability level of $r_{\mathrm{c}} = 1$ is considered. See Fig. 1.

Results are presented in Table 3. For each MTBF value, the difference of total costs between the DC power flow model and the transportation model is presented. Percentage values are calculated with respect to the power flow relaxation model. Furthermore, total expenses are split into investment and operations costs to analyze their behaviour in function of the MTBF value.

Naturally, the total expenses for the relaxed solutions is lower than the full model (DC power flow), but what it is important to see is the rather limited impact of this relaxation in terms of the objective function value. In the worst case, the DC power flow model provides a solution only 0.62% more expensive than the transportation model. The latter result corresponds for the typical value of MTBF reported for OWFs (MTBF of 178). The cost difference among the power flow models can be explained by inspecting the investment and operation costs. The transportation model results in cheaper designs, but this precisely causes higher operation costs.

When considering a full reliability level, for a MTBF of 178, the solution obtained with a DC power flow model is only 0.25% more expensive than the one from a transportation model. While the difference on investment costs is more or less the same as in Table 3 (0.77%), it is observed an increase in the operation costs difference (-7.37%), which balances out the capital investment disparity among both models. The increment of undispatched energy allows for reducing the total expenses difference; this is also expected to happen for lower MTBF values.

The possibility to neglect DC power flow allows for reducing the complexity of the model while still generating dual solutions (by neglecting the DC flow) close to a primal (feasible point for the full model). In closed-loop and meshed topologies the current follows the path with shortest electrical length, i.e., smallest equivalent electrical reactance. Thus, DC power flow requires extra variables modelling voltage phases as in Eq. (11) and Eq. (12). The strong similarity between radial and closed-loop topologies is due to, in the latter, only a single cable per circuit (interconnected chain of WTs) alters the radiality of the former.

The main benefit behind this relaxation is towards the application of the model for large-scale problem instances, or even for small ones with low optimality gap values ($\epsilon_{\mathrm{d}}, \epsilon_{\mathrm{s}} \leq 0.2\%$). In this article, the comparison between closed-loop and radial

designs lies in the relative economic difference, while not in the concrete solutions (construction designs). The dual solutions can be fixed a posteriori by changing a subset of the installed cables. The latter is out of the scope of this article.

Table 3. Power flow models comparison for Ormonde OWF.

MTBF	Total expenses Eq. (1)		Investment		Operation	
	Difference [Euro]	Difference [%]	Difference [Euro]	Difference [%]	Difference [Euro]	Difference [%]
10	0	0	0	0	0	0
20	8,000	0.08	32,200	0.37	-24,200	-1.79
30	16,090	0.17	32,200	0.37	-16,110	-1.79
40	23,920	0.25	64,200	0.74	-40,280	-5.52
50	31,970	0.34	64,200	0.74	-32,230	-5.27
178	55,140	0.62	64,200	0.74	-9,060	-5.27

5.1.2 Reliability level

The full Algorithm 1 is now implemented. Based on the results of Sect. 5.1.1, the DC power flow model is discarded. In the same manner, total electrical power losses are deactivated and attention is concentrated to a simultaneous minimization of investment plus operation costs. Results for the lowest reliability level ($r_c = 1$), and for full reliability, are displayed in Fig. 3 and in Fig. 4, respectively.

A reliability level value equal to $r_c = 1$ is basically a relaxation of the full model. The latest being understood as an instantiation of Algorithm 1 with a large enough value of r_c, such as all installed cables of the OWF are included in the system states set, i.e., full reliability. See Fig. 1 for a graphical description of this concept.

For the reliability relaxation, in Fig. 3(a) the total cost comparison between the closed-loop and radial designs with increasing MTBF is illustrated. Meanwhile, the Fig. 3(b) displays the investment and operation costs difference. From Fig. 3(a), it can be observed that there is break-even point, for a MTBF of around 35, where the total cost of closed-loop and radial designs match.

To the left of the break-even point, the closed-loop layout always results as the overall cheapest solution, because despite a higher investment cost- See Fig. 3(b) (radial design is invariable to MTBF variations)-, it provides a redundant path for each WT, therefore the operation cost savings surpasses that increase (the installed cables for the main feeders are usually bigger as well). Additionally, in Fig. 3(b) one can see that the non-increasing trend of the investment costs is developed in a discrete manner, as for some consecutive values of MTBF the closed-loop design investment is maintained. The associated percentage difference of operation costs for not modified designs is also kept, as the failures frequency is equally diminished.

On the other hand, for MTBF larger than 35, the radial layout is the best alternative. After a large enough MTBF (in this case at around 50 years kilometres per failure), the failures probabilities drop considerably, meaning that the operation costs become trivial, and hence the focus is merely on the investment costs reduction, which by its part has reached the minimum in the

closed-loop alternative. The break-even point may be marginally affected by neglecting the DC power flow in the conservative side, as this value would move to the left. At MTBF of 178, the radial design is 6.62% cheaper than the closed-loop design as shown in Fig. 3(a).

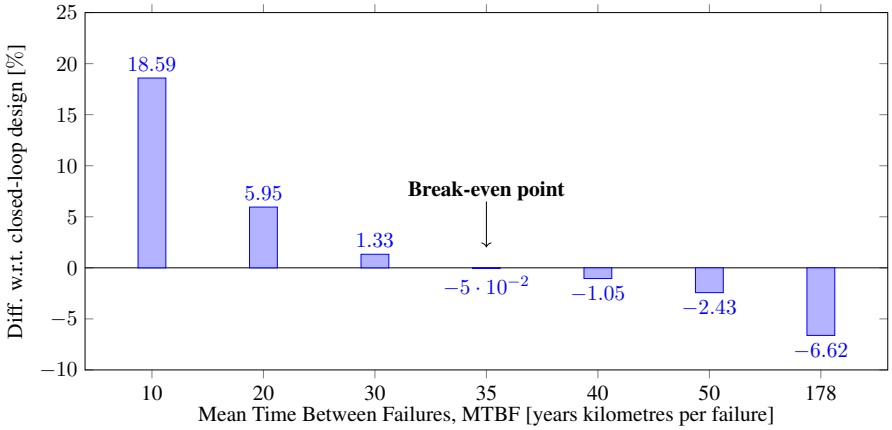

(a) Comparison of objective function (1) between closed-loop and radial designs. (Positive percentages mean savings from closed-loop design)

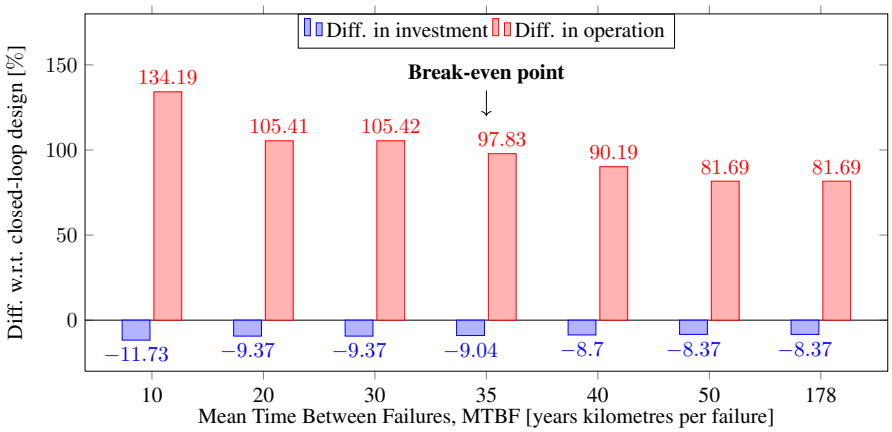

(b) Comparison of investment and operations costs between closed-loop and radial designs. (Positive percentages mean savings from closed-loop design)

Figure 3. Sensitivity analysis with reliability level $r_c = 1$ for Ormonde OWF.

A new set of experiments is conducted for full reliability of the Ormonde OWF. The main difference compared to $r_c = 1$ is reflected in Fig. 4(a), where the break-even point is moved towards the right of the plot to a value roughly equal to 130 years kilometres per failure. By allowing the whole set of installed cables to fail, the impact over the project's economic performance is considerably augmented. In this case, for the worst reported value of MTBF (178 years kilometres per failure), the radial

design is only 1.98% cheaper than the closed-loop layout, due to the increase of operation costs with almost the same required investment expense when compared to $r_c = 1$.

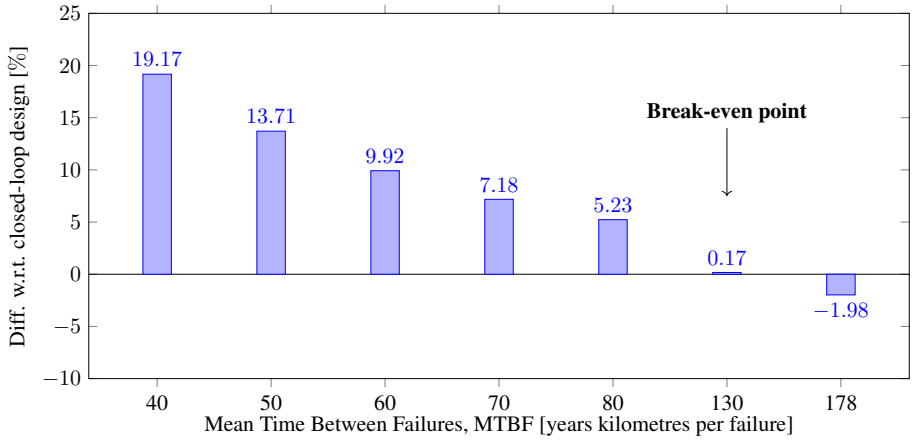

(a) Comparison of objective function (1) between closed-loop and radial designs. (Positive percentages mean savings from closed-loop design)

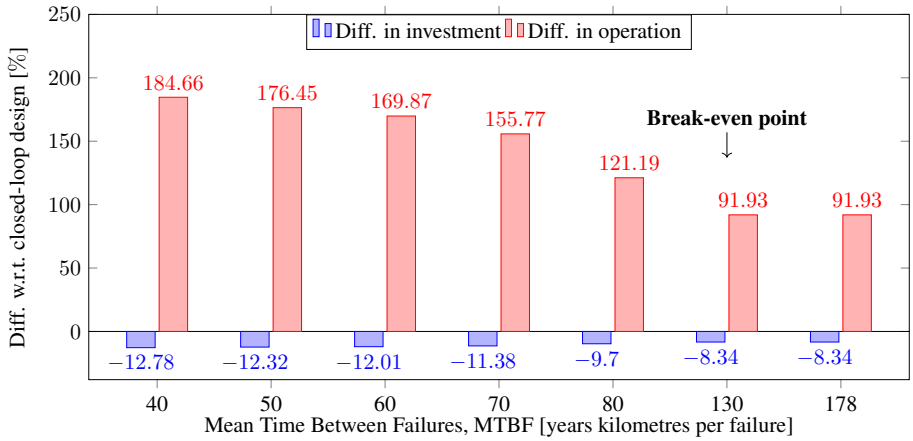

(b) Comparison of investment and operations costs between closed-loop and radial designs. (Positive percentages mean savings from closed-loop design)

Figure 4. Sensitivity analysis with full reliability for Ormonde OWF.

The impact of the reliability level on the computing time is presented in Fig. 5. The difference is of an order of magnitude, moving from seconds for $r_c = 1$ to (tens of) minutes for full reliability. The exponential complexity of the stochastic closed-loop model in function of the parameter MTBF is also noticeable. For MTBF inferior to 40, the computational resources become insufficient to tackle the problem for full reliability, as computing time and memory requirements escalate rapidly.

For large values of MTBF the Algorithm 1 takes advantage of the deterministic solution to feed up the stochastic model with a good starting point. This, together with low failure probability (as MTBF increases), helps conspicuously to accelerate the convergence of the model for optimum gaps. The PCI algorithm takes away a very important share of computational burden by simplifying the full problem. The savings on computing time are more evident for greater values of r_c as the number of candidate edges become larger.

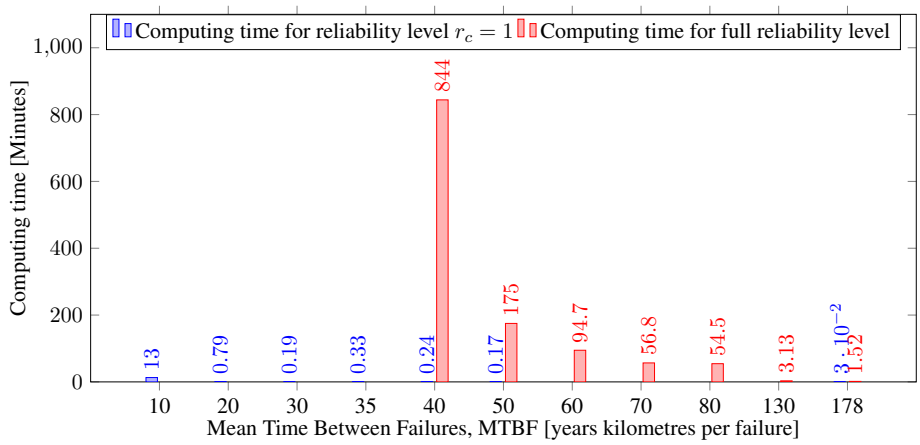

Figure 5. Computing times for Ormonde OWF stochastic closed-loop design.

5.1.3 Total electrical power losses

The left branch of Fig. 2 is implemented, in this case, activating the total electrical power losses ($Losses == True$) integrated into the objective function Eq. (5). A MTBF of 178 years kilometres per failure is considered, and the transportation power flow mode is enabled ($DC == False$).

Results are displayed in Fig. 6. Particularly, Fig. 6(a) is associated to objective function Eq. (1), and Fig. 6(b) to Eq. (5). There are no significant differences between the two layouts.

A visual inspection of the layouts shows that the only difference is the swap of cables connected from WT 1 to WT 11 with those from WT 1 to WT 2. This alteration in the design can be explained given the conservative approach for losses calculation, and simultaneously, the degree of flexibility linked to a transportation model. In Fig. 6(b), which graph the base case, the current through WTs 9-16 and 30-31 is set to zero in the solution. This means that the calculated losses are an approximation in the conservative side, compared to a layout with splittable current through a DC power flow.

The main takeaway is that the total expenses of the layout in Fig. 6(a) (including total electrical power losses) is nearly the same as that from Fig. 6(b). The required computing time, however, is 16 times higher when including losses compared to a sole optimization of investment and operation costs. The proposed formulation is still more efficient than a MIQP. The

demonstration is out of the scope of this work, but computational experiments from the literature validate the efficiency of MILP compared to MIQP (Banzo and Ramos, 2011).

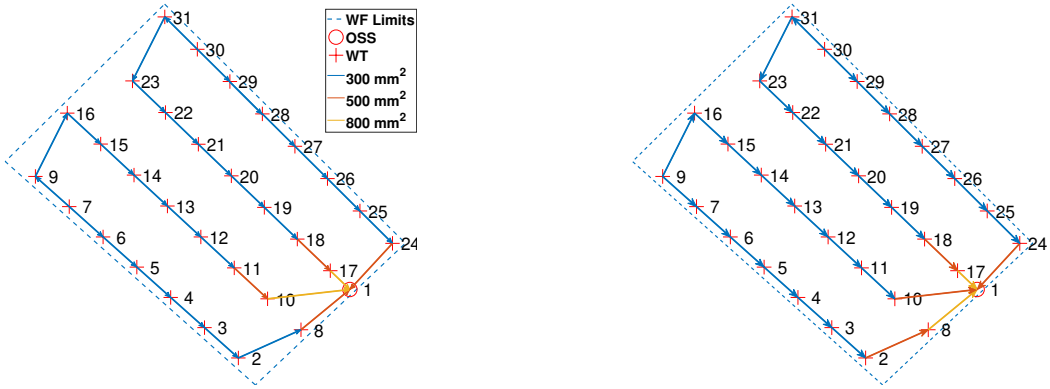

(a) Investment and Operation

(b) Investment, Electrical losses, and Operation

Figure 6. Sensitivity analysis for objective function in Ormonde OWF. MTBF=178.

5.2 Large OWF: Horns Rev 1

The second case study is Horns Rev 1 OWF (Vatenfall, a). Inputs are shown in Table 4. The number of WTs for this case is equal to 80. Horns Rev 1 OWF presents a regular or grid-based layout, since WTs units are uniformly arranged in rows and columns without empty areas inside of the farm; as shown previously in (Pérez-Rúa et al., 2020b), this type of layouts show a favorable condition in terms of computational complexity when designing the collection system, hence low values $\upsilon = 6$ and $\sigma = 10$ are most likely good enough to cover the global minimum. Larger values of these parameters may compromise the convergence of general purpose solvers. No losses and a transportation power flow mode are used.

Table 4. Data inputs for Horns Rev 1 OWF

P_n	V_n	$\boldsymbol{U}$	$\boldsymbol{C}$	n_{w}	υ	σ	ϕ	ϵ_{d}	ϵ_{s}
2 MW	33 kV	$\{420, 530\}$ A	$\{410, 450\}$ kEuro km^{-1}	80	6	10	10	0.2%	0.2%/4%

Results for the lowest reliability level, i.e. $r_{\mathrm{c}} = 1$, are shown in Table 5. The optimality gap for both deterministic and stochastic phases of Algorithm 1 are equal $\epsilon_{\mathrm{d}} = \epsilon_{\mathrm{s}} = 0.2\%$. Further experiments were done, intending to evaluate lower values of MTBF at these gaps, but computing time increased steeply (note that for MTBF of 90, required time is almost 360 min).

Going back to Fig. 3, the results of Table 5 indicate that the break-even point has been already crossed for MTBF of 90. This is because of the nearly equal percentage of difference in investment for MTBF of 90 in comparison to MTBF of 178.

At this point, the radial layout is 0.80% cheaper than the closed-loop design. One can see that for MTBF of 178, the savings difference for Horns Rev 1 (-2.01%) has decreased substantially when compared to Ormonde, Fig. 3(a) (-6.62%), and being closer to Ormonde with full reliability, Fig. 4(a) (-1.98%). Performance cutback of the radial layout is due to the boost of curtailed energy as there are more WTs connected to a single feeder.

Table 5. Results with reliability level $r_c = 1$ for Horns Rev 1 OWF.

MTBF	Diff. in total expenses Eq. (1) [%]	Diff. in investment [%]	Diff. in operation [%]	Computing time closed-loop [min]
90	-0.80	-3.34	91.14	359
178	-2.01	-3.31	90.90	43

For full reliability analysis, the value of ϵ_d is fixed to 0.2% while ϵ_s is loose up to 4%. This is necessary as symmetric tight gaps lead to failed convergence due to lack of memory. Providing the optimal solution of the deterministic phase of Algorithm 1 helps to shorten to stochastic phase, taking into account that the base case is the scenario with the largest probability. Results are shown in Table 6 where it can be seen that the closed-loop design is a more cost-effective option than the radial layout, even with a rather high optimality gap of up to 4%.

Two important aspects must be highlighted: (i) the transportation model allows for optimizing large OWFs at the expense of an slight underestimation of design costs, but even given this uncertainty, both topologies would be still very close in terms of financial performance. Slightly lower values of MTBF would mean the closed-loop gains more and more value. (ii) A gap of 4% means that the closed-loop layout could be possibly cheaper, increasing then its margin compared to the radial counterpart.

Table 6. Results with full reliability level for Horns Rev 1 OWF.

MTBF	Diff. in total expenses Eq. (1) [%]	Diff. in investment [%]	Diff. in operation [%]	Computing time closed-loop [h]
178	1.13	-3.43	83.01	2.47

5.3 Very large OWF: West of Duddon Sands

Last real-world case study is West of Duddon Sands OWF (Ørsted). This OWF has an irregular distribution of its 108 WTs (3.6 MW individual power) due to abnormal soil conditions. Given this particular features, larger values of υ and σ are set, as indicated in Table 7, in order to cover the global minimum according to the hop-indexed model for radial layout design (right branch of Fig. 2). The presented optimality gaps (ϵ_d and ϵ_s) represent the technical border considering the lowest reliability level, to obtain solutions within the computational limits. No losses and a transportation power flow mode are used.

The numerical results are given in Table 8. Similarly to Horns Rev 1 (Table 5 and Table 6), with MTBF of 178, the results indicate that a closed-loop design for West Duddon Sands would most likely pay off under full reliability, since for the lowest

redundancy level the radial layout is only 0.67% cheaper. This is understandable based on the greater number of WTs and individual power, leading to more curtailed energy for the same failure. This comparison is upon the condition that the relative difference between the solutions is maintained, if a zero optimality gap is achieved simultaneously.

Table 7. Data inputs for West of Duddon Sands OWF

P_n	V_n	$\boldsymbol{U}$	$\boldsymbol{C}$	n_{w}	υ	σ	ϕ	ϵ_{d}	ϵ_{s}
3.6 MW	33 kV	$\{875, 1050\}$ A	$\{630, 770\}$ kEuro km^{-1}	108	10	25	10	5%	6%

Table 8. Results with reliability level $r_{\mathrm{c}} = 1$ for West of Duddon Sands OWF.

MTBF	Diff. in total expenses Eq. (1) [%]	Diff. in investment [%]	Diff. in operation [%]	Computing time closed-loop [h]
178	-0.67	-1.65	96.46	0.90

The resulted closed-loop and radial layouts are given in Fig. 7. As aforementioned, this wind farm presents empty areas in between the locations of the generation units, which seems to impact considerably the mathematical complexity of finding a solution for the collection system. Previous studies have shown that the proposed hop-indexed formulation seems to be more compact and therefore more efficiently solved by commercial solvers than a flow formulation (Pérez-Rúa et al., 2020b). This fact is also reflected in this case study, where for the same gap (5%), the flow-based model requires almost double time than the full binary (0.45 h). For Ormonde and Horns Rev 1 the radial layouts were obtained almost instantaneously.

In addition, the hop-indexed model does not escalate nor with the size of cable set, neither with inclusion of total electrical power losses. However, the flow formulation provides important flexibility to the model such as energy curtailment (used in this case) or other aspects like, e.g. different WTs types (in terms of power rating).

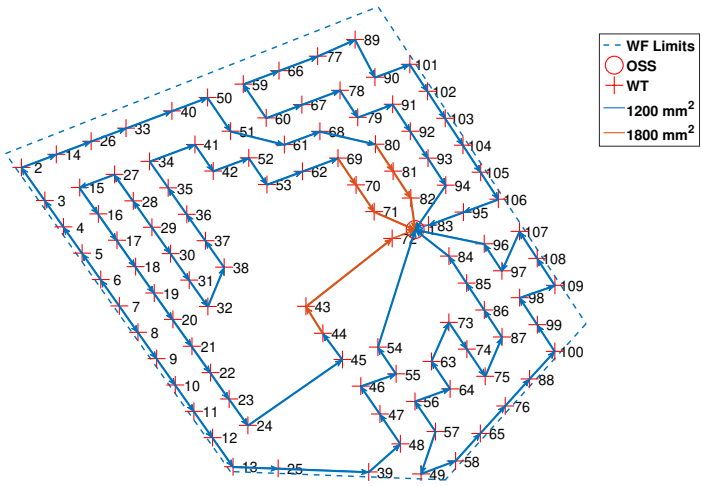

(a) Closed-loop design for West of Duddon Sands with MTBF=178

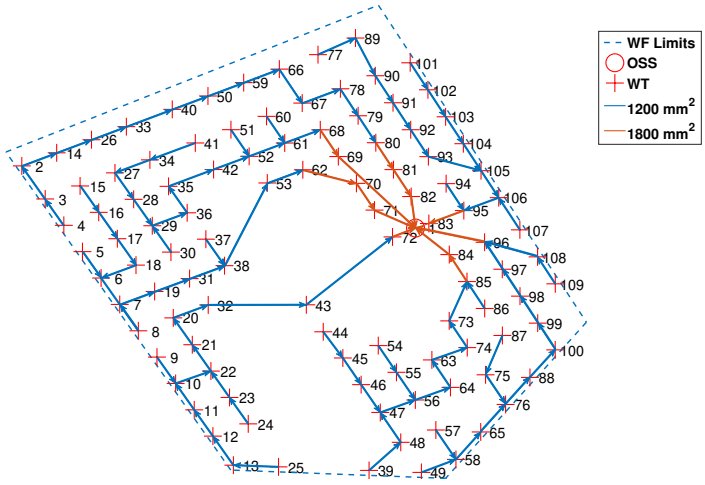

(b) Radial design for West of Duddon Sands

Figure 7. Collection system designs for West of Duddon Sands with objective function (1).

6 Conclusions

The proposed method provides a global optimization model to solve the OWFs collection system, supporting a simultaneous minimization of investment, operational, and total electrical power costs, including contingencies due to cables failures. In spite

of the currently rather low failure rates of collector cables failures, early stage in offshore projects maturity and the consequent scarcity of available data may mean that future very large OWF projects may face larger level of contingencies.

The main contribution of this manuscript is the development of an optimization framework to compare, in economic terms, closed-loop and radial layouts for modern OWFs. Several strategies are incorporated in the algorithmic scheme, in order to be able to study very large real-world problems, such as the use of a transportation power flow model instead of DC power flow or different reliability levels.

The proposed methodology has been applied to three different OWFs, from small to very large-scale. Results indicate that layouts with single redundancy may bring economic benefits when compared to non-redundant ones, in function of the instance size. For a small OWF the radial topology results as the best option, in contrast to large projects, where the closed-loop is seemingly a better techno-economic solution, when using failures rates available in literature.

Stochastic optimization with scenario numeration brings along a comprehensive consideration of the three main criteria for designing electrical networks; investment, electrical losses, and reliability. However, it also implies a lack a tractability which hardens the applicability for a larger set of problem types. Overall, the impact of medium voltage collector system cables failures is quantified in this article, showing the importance of developing methods which enable reliability analysis in the context of computational optimization. A Progressive Contingency Algorithm has been proposed in this direction.

References

ABB: XLPE Submarine Cable Systems Attachment to XLPE Land Cable Systems - User's Guide, new.abb.com/docs/default-source/ewea.../xlpe-submarine-cable-systems-2gm5007.pdf.[AccessedOct29,2018], 2018.

Banzo, M. and Ramos, A.: Stochastic Optimization Model for Electric Power System Planning of Offshore Wind Farms, IEEE Transactions on Power Systems, 26, 1338–1348, https://doi.org/10.1109/TPWRS.2010.2075944, 2011.

Bauer, J. and Lysgaard, J.: The offshore wind farm array cable layout problem: A planar open vehicle routing problem, Journal of the Operational Research Society, 66, 360–368, https://doi.org/10.1057/jors.2013.188, 2015.

Besnard, F., Fischer, K., and Tjernberg, L. B.: A model for the optimization of the maintenance support organization for offshore wind farms, IEEE Transactions on Sustainable Energy, 4, 443–450, https://doi.org/10.1109/TSTE.2012.2225454, 2013.

Billinton, R. and Allan, R. N.: Reliability Evaluation of Engineering Systems: Concepts and Techniques, 1992.

Calixto, E.: Gas and Oil Reliability Engineering, Gulf Professional Publishing, second edn., https://www.sciencedirect.com/book/9780128054277/gas-and-oil-reliability-engineering#book-info[AccessedMarch05,2020], 2016.

Catapult: Wind farm costs, https://guidetoanoffshorewindfarm.com/wind-farm-costs, 2020.

Chen, Y., Dong, Z. Y., Meng, K., Luo, F., Xu, Z., and Wong, K. P.: Collector System Layout Optimization Framework for Large-Scale Offshore Wind Farms, IEEE Transactions on Sustainable Energy, 7, 1398–1407, https://doi.org/10.1109/TSTE.2016.2549602, 2016.

CIGRE: Working Group B1.10: Update of service experience of HV underground and submarine cables, Tech. rep., https://e-cigre.org/publication/ELT_243_3-update-of-service-experience-of-hv-underground-and-submarine-cable-systems.[AccessedMarch30,2020], 2009.

CIGRE: Working Group B1.21: Third-Party Damage to Underground and Submarine Cables, Tech. rep., https://e-cigre.org/publication/398-third-party-damage-to-underground-and-submarine-cables.[AccessedMarch30,2020], 2009.

Fischetti, M. and Pisinger, D.: Mixed Integer Linear Programming for new trends in wind farm cable routing, Electronic Notes in Discrete Mathematics, 64, 115–124, https://doi.org/10.1016/j.endm.2018.01.013, 2018a.

Fischetti, M. and Pisinger, D.: Optimizing wind farm cable routing considering power losses, European Journal of Operational Research, 270, 917–930, https://doi.org/10.1016/j.ejor.2017.07.061, 2018b.

Grainger, J. J. and Stevenson, W. D. J.: Power System Analysis, McGraw-Hill Education, 2nd editio edn., https://doi.org/10.1017/CBO9781107415324.004, 1994.

Hertz, A., Marcotte, O., Mdimagh, A., Carreau, M., and Welt, F.: Design of a wind farm collection network when several cable types are available, Journal of the Operational Research Society, 68, 62–73, https://doi.org/10.1057/s41274-016-0021-6, 2017.

IBM: IBM ILOG CPLEX Optimization Studio CPLEX User Manual, Tech. rep., https://www.ibm.com/support/knowledgecenter.[AccessedApril11,2019], 2015.

Klein, A. and Haugland, D.: Obstacle-aware optimization of offshore wind farm cable layouts, Annals of Operations Research, 272, 373–388, https://doi.org/10.1007/s10479-017-2581-5, 2017.

Klein, A. and Haugland, D.: Optimization of reliable cyclic cable layouts in offshore wind farms, Engineering Optimization, 52, 1–20, https://doi.org/10.1080/0305215X.2020.1717482, https://doi.org/10.1080/0305215X.2020.1717482, 2020.

Lumbreras, S. and Ramos, A.: Optimal design of the electrical layout of an offshore wind farm applying decomposition strategies, IEEE Transactions on Power Systems, 28, 1434–1441, https://doi.org/10.1109/TPWRS.2012.2204906, 2013.

Lumbreras, S., Ramos, A., and Cerisola, S.: A Progressive Contingency Incorporation Approach for Stochastic Optimization Problems, IEEE Transactions on Power Systems, 28, 1452–1460, https://doi.org/10.1109/TPWRS.2012.2225077, 2013.

Ørsted: West of Duddon Sands Offshore Wind Farm, https://westofduddonsands.co.uk/.[AccessedMarch12,2020].

Pérez-Rúa, J.-A. and Cutululis, N. A.: Electrical Cable Optimization in Offshore Wind Farms - A review, IEEE Access, 7, 85 796–85 811, https://doi.org/10.1109/ACCESS.2019.2925873, 2019.

Pérez-Rúa, J.-A., Das, K., and Cutululis, N. A.: Optimum sizing of offshore wind farm export cables, International Journal of Electrical Power & Energy Systems, 113, 982–990, https://doi.org/10.1016/j.ijepes.2019.06.026, https://doi.org/10.1016/j.ijepes.2019.06.026, 2019a.

Pérez-Rúa, J. A., Das, K., and Cutululis, N. A.: Optimum sizing of offshore wind farm export cables, International Journal of Electrical Power and Energy Systems, https://doi.org/10.1016/j.ijepes.2019.06.026, 2019b.

Pérez-Rúa, J.-A., Lumbreras, S., Ramos, A., and Cutululis, N. A.: Closed-Loop Two-Stage Stochastic Optimization of Offshore Wind Farm Collection System, in: Proceedings of Torque Conference (Accepted), pp. 1–10, http://arxiv.org/abs/2003.06598, 2020a.

Pérez-Rúa, J.-A., Stolpe, M., Das, K., and Cutululis, N. A.: Global Optimization of Offshore Wind Farm Collection Systems, IEEE Transactions on Power Systems, 35, 2256–2267, https://doi.org/10.1109/TPWRS.2019.2957312, 2020b.

Pillai, A. C., Chick, J., Johanning, L., Khorasanchi, M., and De Laleu, V.: Offshore wind farm electrical cable layout optimization, Engineering Optimization, 47, 1689–1708, https://doi.org/10.1080/0305215X.2014.992892, 2015.

RenewableUK: RenewableUK - Project Intelligence, https://www.renewableuk.com/page/ProjectIntelligenceHome.[AccessedMarch3, 2019], 2018.

ReNEWS: Rampion suffers cable fault, http://renews.biz/105889/rampion-suffers-cable-fault/.[AccessedOct29,2018], 2017.

Statista: Monthly average electricity prices in Great Britain (GB) from 2015 to 2019, https://www.statista.com/statistics/589765/average-electricity-prices-uk/.[AccessedMarch9,2020], 2019.

Vatenfall: Horns Rev 1 Offshore Wind Farm, https://powerplants.vattenfall.com/horns-rev.[AccessedMarch11,2020], a.

Vatenfall: Ormonde Offshore Wind Farm, https://powerplants.vattenfall.com/ormonde.[AccessedFeb5,2020], b.

Warnock, J., McMillan, D., Pilgrim, J. A., and Shenton, S.: Review of offshore cable reliability metrics, in: Proceedings of the 13th IET International Conference on AC and DC Power Transmission (ACDC), pp. 1–6, https://doi.org/10.1049/cp.2017.0071, 2017.

Warnock, J., McMillan, D., Pilgrim, J., and Shenton, S.: Failure Rates of Offshore Wind Transmission Systems, Energies, 12, 1–12, https://doi.org/10.3390/en12142682, 2019.

APPENDIX C1

"Lifetime estimation and performance evaluation for offshore wind farms transmission cables"

J.A. Pérez-Rúa, K. Das, and N. A. Cutululis

in *Proceedings of the 15th IET International Conference on AC and DC Power Transmission* (*ACDC 2019*)
Coventry, UK

5th–7th February

2019

Lifetime estimation and performance evaluation for offshore wind farms transmission cables

Juan-Andrés Pérez-Rúa*, Kaushik Das*, Nicolaos A. Cutululis*

**Department of Wind Energy, Technical University of Denmark, Frederiksborgvej 399, 4000 Roskilde, Denmark. E-mail: juru@dtu.dk*

Keywords: Offshore wind energy, transmission cables, dynamic temperature prediction, thermo-electrical stress, probabilistic lifetime estimation.

Abstract

A novel methodology for life estimation and performance evaluation of offshore wind farms high voltage AC export cables is presented. The method applies Dynamic Temperature Prediction (DTP) analysis using a Thermo-Electrical Equivalent model (TEE). Furthermore, it is suggested how the cable lifetime might be inferred based on the accumulated ageing effects. Afterwards, a sensitivity analysis of the seabed temperature variations is performed. Finally, a holistic procedure for calculating more accurately the electrical power losses of the cable is presented. Results show that an important increase of the total installed power, or cross-section reduction, can be achieved compared to traditional sizing methods.

1 Introduction

Offshore wind energy represents one of the fastest and most steadily growing renewable technologies. The penetration level has increased almost five times in the last seven years, reaching the impressive globally total installed power of nearly 19 GW [1]. The grid connection for Offshore Wind Farms (OWFs) contributes to around 15 % of the total system costs [2]. The export cable is one of the most important components in this concept, partly because of the increasingly longer distance from shore, and partly because of its direct impact on the overall availability [3].

Currently, the sizing of the offshore export cables is done according to the CIGRE and IEC standards [4]. However, such standards consider steady state conditions under rated operation, i.e., a continuous conductor temperature equal to 90 ℃ and nominal electric field. The limitation of the conductor temperature at this value is due to the close contact with the insulation material, which represents the most critical element in a cable.

In fact, in [5] is proved that other factors such as mechanical stress, and environmental stress, can be neglected thanks to the improvement of manufacturing techniques, and by the installation conditions of the cable itself (which is buried and protected by inner layers). Joints and terminals also deserve attention to maximize the lifetime of the export infrastructure.

Simultaneous electro-thermal stress represents the main ageing factor of the insulation, and consequently, of the whole cable. These standards' criterion may be intuitively too conservative considering that OWFs present a typical capacity factor of around 0.4-0.5. To cope with this issue, different concepts need to be combined in order to develop a methodology capable of estimating the lifetime of cables operating under real conditions, such as: time-varying cyclic power generation, thermal and electrical stress, thermal transients, capacity currents and failure probability.

This paper is divided in the following manner: The Section 2 describes the full model, then the TEE calibration is presented in the Section 3, and finally, it is reported the application of the Dynamic Temperature Prediction (DTP) model to a 245-kV cross-linked polyethylene (XLPE)-insulated cable, operating at realistic time-varying conditions. The potential cross-section reduction from the point of view of electro-thermal is pointed out. Conclusions extracted after this work close the article.

2 Model description

The scheme of the general proposed methodology is presented in the Figure 1. Input data is obtained after simulating offshore power generation, at a particular site, using the software described in [6].

Overall, this methodology is proposed aiming to develop a tool, which provides the first steps towards the offline dynamic loadability of transmission cables for offshore wind farm applications. In the next subsections, a descriptive explanation of each block will be presented. This paper focuses specially in the description, and analysis of the DTP model.

2.1 Pre-processing stage

In this stage is decided the period under which the cable is subject to operate. Different criteria might be defined in order to establish the basis cycle, one of them could be, for instance, the year with highest capacity factor, or that year with highest instantaneous conductor temperature. Studying on detail the best decision for selecting this period is out of scope in this paper, and future publications will deal with this matter.

2.2 Conductor dynamic temperature prediction

Reference [4] provides a set of equations that allow calculating the current to be transmitted in an infinite time period, in order to get a desired constant temperature, under given specific input conditions, such as buried depth, distance between phases, surrounding constant temperature, soil resistivity, etc.

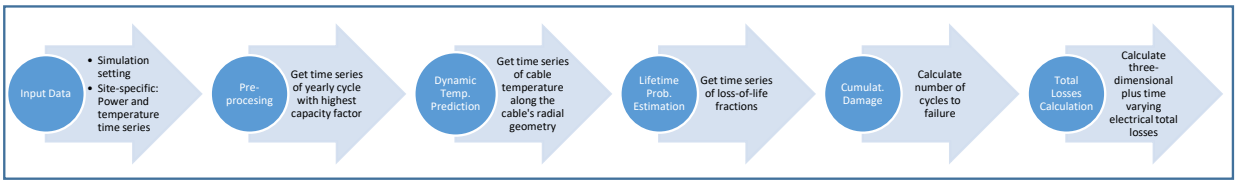

Figure 1: Proposed general methodology.

However, for cases where the load current does not follow a constant profile, but rather a cyclic profile, the standard IEC-60853-2 defines mathematical expressions to correct a cable rating subject to these conditions, but the cycle is limited to some pre-defined discrete patterns, like pulse or triangular trains. On that account, dynamic loadability techniques calculate the current that can be carried for a limited period, without the physical limitations of any part of the cable being exceeded. Dynamic loadability requires the use of Dynamic Thermal Rating (DTR) in order to estimate the cable temperature either for real-time applications or for offline predictions given time series of forecasted load current (DTP). Nowadays, there are mainly three modelling principles for estimation of the cable temperature dynamically: finite elements (FEM), step response (SR) -used by CIGRÉ- and thermoelectric equivalent method (TEE). A comparison between those methods has been done in [7] and [8], where it is remarked that TEE provides results which are within an acceptable range of the FEM simulations (nearly 1°C) with a considerable computation time reduction. TEE models also have proved to exhibit a correct estimation of the temperature as compared to real measured data in experimental tests, with deviations of around 3°C [9].

The TEE method is straightforward from an electrical engineering point of view. It basically consists in a direct translation of thermodynamic variables into electrical variables, i.e., considering the heat flow as electrical current and temperature as nodal voltages. Every layer of the cable is then represented with its thermal resistance T_m and its thermal capacitance C_m, along with the electrical losses; all together form the equivalent circuit presented in the Figure 2. The surrounding, which in the case of submarine cables is defined by the seabed where the cable is buried, can be also divided into multiple layers (N), in order to obtain a more accurate DTP calculation, at cost of a higher computational time required. Equations for calculating the thermal parameters of the cable layers, and surroundings can be found in [8].

The mathematical expression of the system introduced in the Figure 2, under dynamic state applying Kirchhoff laws, is given in the Equation (1). In this equation the matrix A is square and $(N+2)$-dimensional, and its elements are dynamically defined by the total number of sublayers, N. This expression consists of a system of ordinary differential equations (ODE); $\theta_1(t)$ represents the time-varying conductor surface temperature, and $\theta_{N+2}(t)$ correspondingly for the penultimate surrounding layer. It can be appreciated what was mentioned before: the system of equations, once solved, provide information of temperature along different points of radial distance from the cable's center. Additionally, it is inferred the fact that the conductor, screen and armature losses are dependent on the infeed power time series corresponding to the year selected in the pre-processing stage.

$$\begin{bmatrix} \dot{\theta}_{n+2}(t) \\ \dot{\theta}_{n+1}(t) \\ \vdots \\ \dot{\theta}_3(t) \\ \dot{\theta}_2(t) \\ \dot{\theta}_1(t) \end{bmatrix} = A \begin{bmatrix} \theta_{n+2}(t) \\ \theta_{n+1}(t) \\ \vdots \\ \theta_3(t) \\ \theta_2(t) \\ \theta_1(t) \end{bmatrix} + \begin{bmatrix} \frac{\theta_{amb}(t)}{T(n+3)C(n+3)} \\ 0 \\ \vdots \\ 0 \\ \frac{W2+W4(t)+W5(t)}{C3} \\ \frac{W3+W1(t)}{C1} \end{bmatrix} \quad (1)$$

Where the variables shown in the Figure 2 are:

- $W1$, $W2$, $W3$, $W4$, $W5$ = Conductor Joule losses (function of the input power), 50% of dielectric losses, 50% of dielectric losses, screen losses (function of the input power), and armature losses (function of the input power), respectively. All in (W/m).
- $C1 = C_c + 0.5C_i$. Where C_c and C_i are the conductor and insulation thermal capacitances, respectively. All in (J/Km).
- $C3 = C_s + 0.5C_i + C_a + C_j$. Where C_s, C_i, C_a, and C_j are the screen, insulation, armature and jacket thermal capacitances, respectively. All in (J/Km).
- $C(n+3)$= Thermal capacitance of the surrounding sublayer n in (J/Km).
- $T1$, $T3$, $T(n+3)$ = Thermal resistance of the insulation, jacket and the surrounding sublayer n, respectively. All in (Km/W).
- θ_1, θ_2, θ_{n+2}, θ_{amb} = Instantaneous temperature at the surface of the conductor, insulation, surrounding sublayer n, and seabead, respectively. All in (K).

The current along the cable is calculated with Equation (2), where $V_R(z)$, V_S, γ, z, Z_c, $I_R(z)$, and I_s, are voltage vector at z from the Offshore Substation (OSS), voltage vector at OSS, transmission coefficient, current vector at distance z from the OSS, and current vector at OSS, respectively [10].

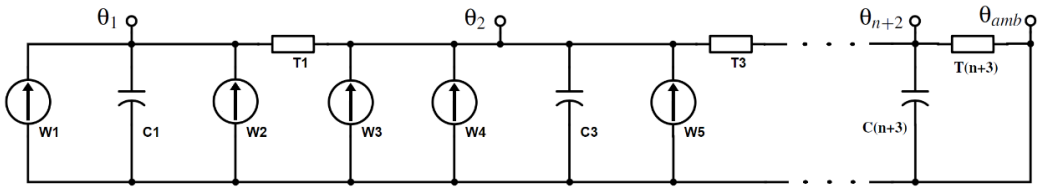

Figure 2: Thermo-Electrical Equivalent (TEE) circuit model for a single-core high voltage submarine cable.

$$V_R(z) = V_s \cosh(\gamma z) - I_s Z_c \sinh(\gamma z)$$
$$I_R(z) = I_s \cosh(\gamma z) - \frac{V_s}{Z_c} \sinh(\gamma z) \quad (2)$$

Where V_s is the nominal or maximum voltage level of the transmission system, and $I_s = f(V_s, P_{series_y})$. Therefore, I_R can be calculated for a given distance z, and the inputs for Equation (1) are obtained: $W1 = f(R_c(\theta_1), I_R(z))$, $W4 = f(R_c(\theta_1), I_R(z))$, $W5 = f(R_c(\theta_1), I_R(z))$. $W2$ and $W3$ are dependent only on the transmission voltage level. The analysis must be carried out for the value of z which brings the most critical thermal performance of the cable; in a AC system without series and parallel compensation, the most critical point is the onshore subestation due to the great capacitive currents typical in submarine cables.

2.3 Lifetime probabilistic estimation

There are several lifetime probabilistic models available in the literature, such as Zurkov, Crine, and Arrhenius-IPM, each within the probabilistic framework needed for associating time-to-failure to reliability. All these models present different analytical expressions and parameter values, however in general they all provide same indications regarding lifetime in function of time-varying electro-thermal stress. The Arrhenius-IPM model seems to be the most conservative over a wide operation range. By means of accelerated test experiments, the parameters of the Arrhenius-IPM model can be calculated accordingly, with subsequent updates considering new manufacturing processes and different cables [11].

2.4 Cumulative damage

One of the simplest models for quantifying cumulative damages for materials, is the one popularized by M.A. Miner in 1945 [12]. See Equation (3), lifetime of a component is obtained when the sum of loss-of-life fractions is equal to one; this model makes use of stress-expected values, ignoring the probabilistic nature of the problem, and considering a linear life-stress relationship [13]. To overcome these limitations, in the framework of modern accelerated tests, and lifetime calculations, Miner's law must be combined with proper failure-time probability density functions. Weibull distributions is usually the most appropriate for performing these studies.

$$\frac{\sum_{i=1}^{k} W_i}{W_{Failure}} = 1 \quad (3)$$

2.5 Total losses calculation

The total losses calculation process allows a holistic estimation, taking into consideration the spatio-temporal variations of current along the cable [14]. The Dynamic Temperature Prediction explained in Section 2.2, includes the effects of conductor resistance variation in function of its temperature, which in turn changes with time and modifies the value of joule losses and other associated (screen and armature losses). Consequently, the total losses (TL) calculation is defined in the Equation (4).

$$TL = \int_l \int_t R_c(l,t) \cdot I(l,k)^2 \approx \sum_{l=1}^{l_{D_T}} \sum_{k=1}^{h} R_c(l.k) \cdot I(l,k)^2 \quad (4)$$

In the Equation (4), l_{D_T}, h, $R_c(l,k)$, and $I(l,k)$ are the total number of sections that the cable is divided, total number of hours in a year, conductor resistance in ohms, and current in amperes, being the two last function of distance and time. The higher l_{D_T} the more accurate the calculation but at the same time, more computational requirements; a proper balance between both parameters must be determined.

3 TEE model calibration

The value of the number of sublayers (N) to divide the seabed is determined by means of a model calibration process, which consists in evaluating the computational time against the solution quality earned when N is increased. To solve the system of equations, a non-stiff differential equations solver using medium order method is applied and performance indices are defined for quantifying the obtained solution quality. Let the Normalized Mean Absolute Error ($NMAE_N$) [15], defined as (5), when using N sublayers in total, and having as a reference the solution N_{max}.

$$NMAE_N = \frac{1}{h} \sum_{k=1}^{h} \left| \frac{\theta_{1k,N} - \theta_{1k,N_{max}}}{\theta_{1k,N_{max}}} \right| \quad (5)$$

To calibrate the TEE model a cable XLPE-245 kV-630 mm², buried at 1 meter, with synthetic hourly input power data for 80 days has been considered. Figure 3 presents both the test current time series (red step line) and the dynamic conductor prediction time series (calculated at sending-end and considering a constant surface seabed temperature of

20°C) for different sublayer numbers N. It can be seen how the temperature becomes smoother when the system of equations increases, however the profile tends to converge when N approaches to a high value. Therefore, in the Figure 4 is displayed how the $NMAE_N$ and computational times vary in function of N, where is noticed that for $N > 10$ the different of slopes between the $NMAE_N$ and computational time curves differs considerable. This is translated into a poor gain in solution quality but a great increase in processing time. Indeed, if one sets $NMAE_N = 1\%$ and computational time equal to 30 seconds, $N = 10$ provides the best balance.

Further experiments have been implemented, augmenting the time-window length from 80 days to a whole year with different time resolutions (5 minutes, 10 minutes, 20 minutes and so on), and a polynomial increase in computing time has been observed in contrast to the exponential impact of the total number of sublayers in the model. Therefore N represents the more binding parameter, and according to the previous results its value is fixed to 10, as the obtained output is accurate enough.

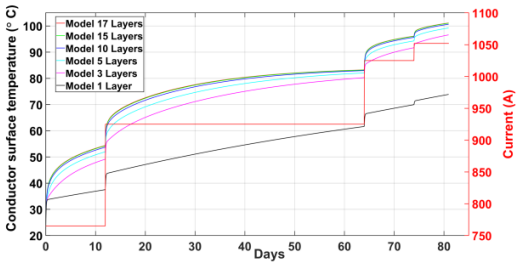

Figure 3: Dynamic temperature prediction of the cable under analysis for synthetic input data.

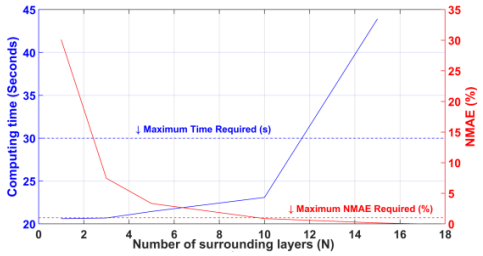

Figure 4: NMAE vs computational time of the cable under analysis.

3 Simulation results

To validate the DTP model built upon a TEE model, a cable XLPE-245 kV-800 mm², with total length of 50 km has been evaluated with the proposed methodology. The input power has been set accordingly to the nominal current calculated by means of the static rating equation found in [4] (450 MW), and fixing the external (or known as well as ambient temperature) temperature to 20°C; both variables constant in time, in order to assess the conductor temperature on steady state conditions.

The results for the dynamic analysis under the aforementioned conditions are presented in the Figure 5. In the Figure 5a, the conductor temperature time series calculated at terminals of the offshore substation (curve red line), is showed along with the input current (blue line). It can be appreciated how the steady state value converges to 90°C after approximately 116 days of operation. Refer to the Figure 5b to see the instantaneous temperature geometrical distribution along the cable cross section in the most critical hour of the year; it is noticeable that for these operating conditions the jacket temperature is around 60°C, value which can be used for recalibrating the model in real-time with on-line measuring, if dynamic temperature control systems should to be implemented.

From these results two main outcomes must be highlighted: First, the dedicated dynamic model is validated under steady state conditions, since the resultant conductor temperature is consistent, and accurate compared to the one calculated by means of the static rating equation of [4] (straight red line). Second, the slow time constant of the system is evident: it requires around 116 days overcoming the thermal transients, and reaching the steady state temperature. This shows that the static equation omits an important part regarding the system settling time, and points out a clear potential for allowing the operation of the cable beyond the nominal power for some periods.

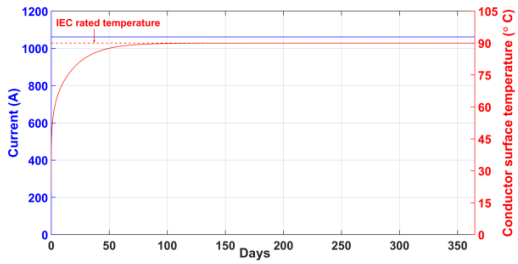

(a) Conductor temperature dynamics

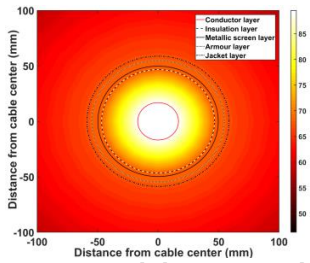

(b) Instantaneous radial temperature distribution at worst time

Figure 5: Dynamic temperature prediction of the cable under analysis for rated conditions evaluated at OSS terminals: 450 MW and $\theta_{amb} = 20$°C.

Other important aspect not included in [4] and other references in the literature, is the effect of the capacitive currents on the cable temperature dynamic analysis and

lifetime. Simulations have been implemented at the onshore connection point terminals to calculate the DTP. The steady state temperature reached by the conductor is around 95℃ after roughly 120 days of operation; the current increase at this physical point causes a greater final temperature, a faster system response and similar settling time than the calculations performed at OSS's terminals. These results reflect a key aspect to take into consideration when sizing a cable, which is the non-uniform degradation of the cable along its longitudinal dimension due to the current distribution. In this case, the terminal at onshore terminals will exhibit a faster degradation rate, and consequently, shorter lifetime expectancy due to accumulation of the capacitive currents.

After the evaluation of the model under rated conditions, the simulation for time-variable inputs is carried out. The main two stochastic variables involved in the analysis are showed in the Figure 6 and Figure 7. The Figure 6 presents the time variation of the external temperature at a particular OWF location (bottom of the seabed); the variable exhibits a considerable temperature spread between -1℃ and 21.5℃. Likewise, for the same OWF location, the power generation time series has been simulated; the power histogram is available in the Figure 7, where it can be appreciated that 39.5% of the time the power generated falls in the $0.9-1.0\ p.u$ bin of power (typical value for offshore sites).

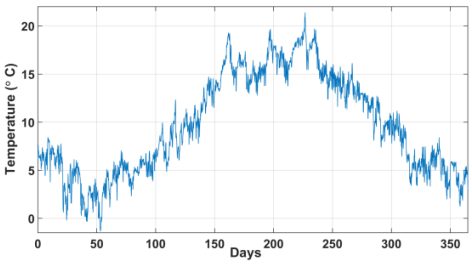

Figure 6: 2-meters above-sea temperature time series.

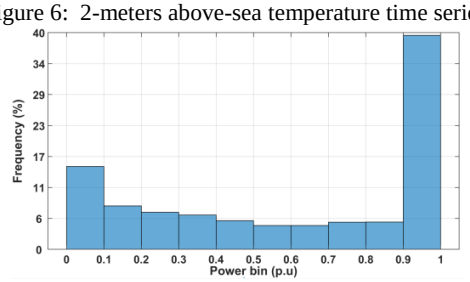

Figure 7: Power generation histogram.

The Figure 8 shows the dynamic state of the conductor temperature, which exhibits a maximum temperature of 80℃. The main outcome is the considerable available margin of cable use exploitation, given that this value is lower than the recommended by manufacturers (90℃). Indeed, it is still a conservative criterion to limit the conductor instantaneous maximum temperature to 90℃, considering that in other time periods the temperature can drop down to 30 ℃. In fact, as it can be seen in the Figure 9, less than 1% of the time the conductor experiences the peak temperature, and a value of 51.5 ℃ represents the mean in a normal pdf function.

Regarding the effect of the external temperature over the dynamic performance of the cable, Figure 10 presents the results when considering a constant average profile (green line), a variable profile with positive 10℃ instantaneous deviation (black line), and variable profile with negative 10℃ instantaneous deviation (blue line), respect to the profile presented in the Figure 6 (base case, red line).

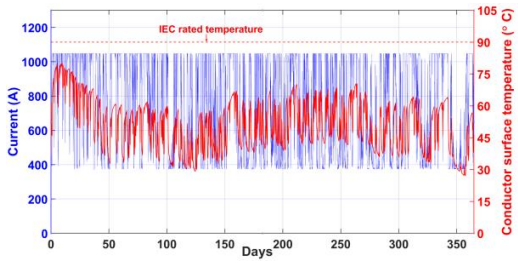

Figure 8: Dynamic temperature prediction of the cable under analysis for time variable conditions evaluated at onshore terminals.

The average-base profile presents a similar behaviour to the base case, however with a slight decrease on mean, and peak magnitudes. On the other hand, the plus-10℃-base profile, causes a greater mean value and lower spread on the temperature distribution, in contrast to the minus-10℃-base profile, which exhibits an opposite behaviour. In terms of temperature magnitude, the effects of the variation seems to cause a linear shift on the conductor temperature, however, it is more interesting to see the non-linear change on the standard deviation, which ultimately will cause a different degradation on the insulation material, and consequently, a pronounced impact over the lifetime of the cable. The effects are more complex when considering the combined changes on magnitude and spread. Lifetime models also demonstrate a considerable impact over the insulation ageing with, in principle, small variations of temperature magnitude.

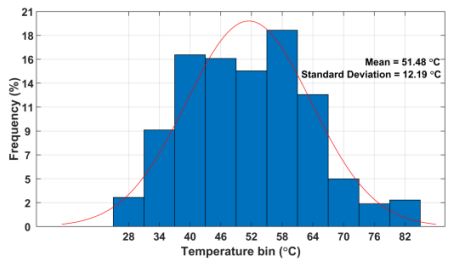

Figure 9: Conductor surface temperature histogram and pdf fitting under base external temperature conditions.

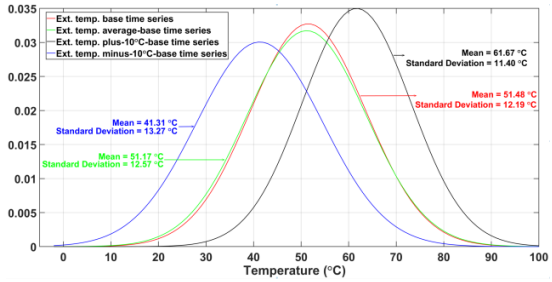

Figure 10: External temperature sensitivity.

Resolution	1	10	100
Total losses (GWh)	20.58	18.29	18.11
Efficiency (%)	99.10	99.20	99.21
Computing time (h)	0.085	0.53	5.76

Table 1: Cable performance evaluation

Table 1 shows the results of the last block of the methodology (Figure 2), which applies the Equation (4), varying the cable sections l_{D_T}, and fixing $h = 8760\ hours$ (carried out for the year with highest capacity factor). As it can be noted, after 10 sections, total losses variation is negligible and unnecessary in terms of the computing time growth, indeed, the efficiency variation is derisory; therefore, a rough approximation of ten sections is more than acceptable. It is important to remark the value of an accurate total electric losses estimation for financial analysis, with more than 0.1% error in the losses calculations.

5 Conclusions

This paper introduced a comprehensive methodology, combining different concepts, to optimally size offshore wind farms AC export cables. The focus of this work has been to describe the basics on the formulated approach, and exploring the application of a TEE model for Dynamic Temperature Prediction (DTP).

The currently used criterion for sizing cables in weather-based systems generations is obsolete and over-conservative, results on this paper point out the over-dimensioning of cables by applying such methodologies, from a point of view of insulation ageing. Additionally, the effects of the variation of seabed temperature have been quantified, and the importance of accurate gathering of data is stressed by performing a sensitivity analysis.

Future work will present the full application of the methodology, in conceptual terms, and by analysing specific case studies.

Acknowledgements

The research leading to these results has received funding from the Baltic InteGrid Project (http://www.baltic-integrid.eu/).

References

[1] GWEC, "Global Wind Report. Annual Market Update 2017," *Glob. Wind Energy Counc.*, p. 72, 2017.

[2] X. Sun, D. Huang, and G. Wu, "The current state of offshore wind energy technology development," *Energy*, vol. 41, no. 1, pp. 298–312, 2012.

[3] ReNEWS, "Rampion suffers cable fault," 2017. [Online]. Available: http://renews.biz/105889/rampion-suffers-cable-fault/.

[4] I. Standard, "IEC-60287-1-1: Electric cables - Calculation of the current rating," 2001.

[5] V. K. Agarwal *et al.*, "The Mysteries of Multifactor Ageing," *IEEE Electr. Insul. Mag.*, vol. 11, no. 3, pp. 37–43, 1995.

[6] P. Sørensen, M. Litong-palima, A. N. Hahman, S. Heunis, M. Ntusi, and J. C. Hansen, "Wind power variability and power system reserves in South Africa," *J. Energy*, vol. 29, no. 1, pp. 59–71, 2018.

[7] R. Olsen, G. J. Anders, J. Holboell, and U. S. Gudmundsdottir, "Modelling of dynamic transmission cable temperature considering soil-specific heat, thermal resistivity, and precipitation," *IEEE Trans. Power Deliv.*, vol. 28, no. 3, pp. 1909–1917, 2013.

[8] R. S. Olsen, J. Holboll, and U. S. Gudmundsdottir, "Dynamic temperature estimation and real time emergency rating of transmission cables," *IEEE Power Energy Soc. Gen. Meet.*, pp. 1–8, 2012.

[9] T. Kvarts, "Systematic Description of Dynamic Load for Cables for Offshore Wind Farms . Method and Experience," no. August 2016, 2018.

[10] J. J. Grainger and W. D. J. Stevenson, *Power System Analysis*. 1994.

[11] G. Mazzanti and G. C. Montanari, "A comparison between XLPE and EPR as insulating materials for HV cables," *IEEE Trans. Power Deliv.*, vol. 12, no. 1, pp. 15–26, 1997.

[12] M. Miner, "Cumulative fatigue damage," *J. Appl. Mech.*, vol. 12, no. 3, pp. A159--A164, 1945.

[13] H. Wire, "Miner's Rule and Cumulative Damage Models," 2018. [Online]. Available: https://www.weibull.com/hotwire/issue116/hottopics116.htm.

[14] H. Brakelmann, "Loss determination for long three-phase high-voltage submarine cables," *Eur. Trans. Electr. Power*, vol. 13, no. 3, pp. 193–197, 2003.

[15] J. L. Aznarte and N. Siebert, "Dynamic Line Rating Using Numerical Weather Predictions and Machine Learning: A Case Study," *IEEE Trans. Power Deliv.*, vol. 32, no. 1, pp. 335–343, 2017.

APPENDIX C2

"Improved Method for Calculating Power-Transfer Capability Curves of Offshore Wind Farms Cables"

J.A. Pérez-Rúa, K. Das, and N. A. Cutululis

in *Proceedings of the*
2019 CIGRÉ International Symposium
Aalborg, Denmark

4th–7th June

2019

Improved Method for Calculating Power-Transfer Capability Curves of Offshore Wind Farms Cables

J.-A. PÉREZ-RÚA, K. DAS, N.A. CUTULULIS
Technical University of Denmark
Department of Wind Energy
Denmark

SUMMARY

The power-transfer capability curve is widely used by Offshore Wind Farms (OWFs) planner when designing their grid connection. An improved method for calculating power-transfer capability curves of OWFs cables is presented in this paper. What differentiates this method compared to the traditional approach, is the consideration of the high power variability and low capacity factors of OWFs, instead of assuming continuous nominal conditions. The method is based on an iterative approach, aiming to determine the maximum total installed power of an OWF, that a cable can support in function of its total length (effective length from the Offshore Substation, OSS, to the Onshore Connection Point, OCP); in order to do so, operational constraints such as: voltage swing limit, Surge Impedance Limit (SIL), and thermal limit are taken into account. By means of this strategy, is possible to estimate more accurately and realistically the power limits and binding constraints, hence exploiting the cables' capacities under particular installation and operating conditions. The translation from rated conditions towards dynamic behaviours, permits the inclusion of more realistic states of the system, for instance, accounting not only for the wind speeds fluctuations, but also the variation of boundary temperatures (seabed), and other thermal parameters which have strong influence over buried cables' thermal performance. The transmission cables are modelled considering a uniform distribution of their electrical parameters, inductance and capacitance, by means of the attenuation constant and characteristic impedance. Likewise, A Thermo-Electrical Equivalent Model (TEE) is applied for the thermal analysis given its good solution quality-computation time balance. The proposed methodology is applied to a 800 mm^2 cable, with the results showing an estimated increase of OWF total installed power of 110% for a total length of 120 km, when compared to the traditional method.

KEYWORDS

Offshore wind energy, transmission cables, power-transfer capability curve, dynamic temperature estimation, operating limits.

juru@dtu.dk

1 INTRODUCTION

Offshore Wind Farms (OWFs) are becoming one of the fastest and most steadily growing type of technologies for electricity generation in Europe. Studies such as [1], survey that the global capacity has increased almost five times in the last seven years, reaching a globally installed power of nearly 19 GW. The location of wind turbines and the Offshore Substations (OSSs), is a matter of accentuated attention nowadays; it is a clear trend that the OSSs are being located farther away from coasts, which causes more scrutiny over classic and new types of transmission technologies, in order to obtain more efficient, effective, reliable, and cheaper systems for exporting power [2]. The impact of transmission systems over OWFs lifetime performance is critical, in terms of single-failure points [3], and economic sustainability [4].

High-Voltage Direct Current (HVDC) emerged as a competitive technology to connect OWFs to shore for large distances and installed power. Nevertheless, the technical maturity of High-Voltage Alternating Current (HVAC) is yet more developed than HVDC, and many OWFs developers still prefer the classical HVAC approach. Therefore, before exploring choices like HVDC transmission, HVAC technology could be further analyzed, taking into consideration the dynamic behaviour of important variables, such as wind power generation, seabed temperature, soil thermal resistivity, etc, instead of steady state approaches as done today following recommendations given by [5], [6], and [7].

Power-transfer capability curves are used substantially when designing the grid connection of OWFs, because they represent a fast way to discern about the required export cable type, while simultaneously choosing the Onshore Connection Point (OCP), given the location of the OSS. To the best of the author's knowledge, those curves have been obtained, so far, by means of static conditions [8–10], assuming operation with constant generated power equal to the OWF installed power. The effect on the curve of the nominal system frequency is studied in [11], but still rated-continuous conditions are assumed. HVAC transmission systems are also subject to study in oil and gas reserves scientific fields as in [12], where analytic calculations and computer simulations are performed to obtain transfer boundary charts of cables, but of course operating conditions compared to OWFs are dissimilar.

To fill the identified gap in the scientific literature, a methodology for calculating power-transfer capability curves of OWFs cables is presented in this work. The impact of cables' thermal and geometrical parameters, site-dependent variables (wind power generation time series, soil temperature time series, soil thermal properties variation, etc), and installation conditions (total length, buried depth, compensation units, among others) over the transmissible OWF installed power offered by cables is quantified. Real operating conditions (thermal transients, capacitive currents, and cyclic generation) are considered. The method consists of an iterative algorithm that includes all important operational constraints in function of the cable's total length: voltage swing limit, Surge Impedance Limit (SIL), and thermal limit. For the Dynamic Thermal Estimation (DTE), a Thermo-Electrical Equivalent (TEE) model is used. The latter has been tested against experimental data in other works like [13], showing its accuracy and correctness. The calibration of the model is presented in [14]. In this case, the calculated maximum instantaneous conductor temperature is limited to 90 °C as industrial practice.

This paper is structured as follows: in the Section 2, the methods are described, on the one hand, in the Section 2.1 the traditional used currently is explained, and on the other hand, in the Section 2.2 the proposed approach is presented. A specific case study is developed in the Section 3, and finally conclusions close this work in the Section 4.

2 METHODOLOGY

In this Section both the traditional and the proposed method are presented. In essence, for more precision, the two methods require the model of a long transmission line, which implies solving the resultant differential equations after the consideration of not-lumped parameters, but rather distributed uniformly throughout the length of the lines (cables) [15]. Formulating the set of differential equations and solving them, after expressing the solution in terms of hyperbolic functions, the following equations are obtained:

$$\vec{V_R} = \vec{V_S} \cdot \cosh(\vec{\gamma} \cdot l) - \vec{I_S} \cdot \vec{Z_c} \cdot \sinh(\vec{\gamma} \cdot l) \tag{1}$$

$$\vec{I_R} = \vec{I_S} \cdot \cosh(\vec{\gamma} \cdot l) - \frac{\vec{V_S}}{\vec{Z_c}} \cdot \sinh(\vec{\gamma} \cdot l) \tag{2}$$

where $\vec{V_S}$ and $\vec{V_R}$, are the line-to-neutral voltages at sending-end (OSS) and receiving-end (OCP), respectively, measured at length l from the OSS; likewise, $\vec{I_S}$ and $\vec{I_R}$, are the line currents at OSS and OCP, respectively. The characteristic impedance ($\vec{Z_c}$) is calculated as $\vec{Z_c} = \sqrt{\vec{z}/\vec{y}}$, and the propagation constant, $\vec{\gamma} = \sqrt{\vec{z} \cdot \vec{y}}$. The series impedance is represented by $\vec{z}$, and the admittance by $\vec{y}$. The two-port cable model is gotten by inspection of Equation 1 and Equation 2: $\vec{A} = \cosh(\vec{\gamma} \cdot l)$, $\vec{B} = \vec{Z_c} \cdot \sinh(\vec{\gamma} \cdot l)$, $\vec{C} = \sinh(\vec{\gamma} \cdot l)/\vec{Z_c}$, and $\vec{D} = \cosh(\vec{\gamma} \cdot l)$. Therefore, the new system of Equations is the following [15]:

$$\vec{V_R} = \vec{V_S} \cdot \vec{A} - \vec{I_S} \cdot \vec{B} \tag{3}$$

$$\vec{I_R} = \vec{I_S} \cdot \vec{D} - \vec{V_S} \cdot \vec{C} \tag{4}$$

Equations 3 and 4 model the balanced three-phase lines systems at highest physics complexity using the two-port model.

2.1 The traditional method

The traditional method is represented in the Algorithm 1. This method requires (5) for the permissible current rating given by [5], as follows:

$$I = \left[\frac{Max_{temp} - T_{amb} - W_d \cdot [0.5 \cdot T_1 + n \cdot (T_2 + T_3 + T_4)]}{R \cdot T_1 + n \cdot R \cdot (1 + \lambda_1) \cdot T_2 + n \cdot R \cdot (1 + \lambda_1 + \lambda_2) \cdot (T_3 + T_4)} \right]^{0.5} \tag{5}$$

where Max_{temp} is the maximum allowed continuous conductor temperature (90 °C is the industrial common practice), T_{amb} is the temperature of the surrounding medium under normal conditions (20 °C is generally considered), W_d is the dielectric loss per unit length for the insulation surrounding the conductor in W/m (formula given in [5]), T_1 is the thermal resistance between the external layers of the conductor and the metal sheath (including semiconductors layers like shields) in Km/W, T_2 is the thermal resistance between the external layers of the metal sheath and armour in Km/W, T_3 is the thermal resistance between the external layers of the armour and the jacket in Km/W, T_4 the soil thermal resistance in Km/W, R is the alternating current resistance per unit length of the conductor at Max_{temp} in Ω/m, λ_1 and λ_2 are the ratio of losses in the metal sheath and armouring to total losses in the cable, respectively.
Finally, n is the number of load-carrying conductors in the cable ($n = 1$ for single-core cables, and $n = 3$ for three-core cables). The model in Equation (5) is based on a Single-Core Equivalent Thermal Model (SCETM), and when $n = 1$, then $T_2 = 0$. Corrections of this model to increase accuracy for large cables is being under study in [16], however for the purposes of this

paper, the SCETM representation is considered satisfactory, as validated in [13] and [17].
The SCETM model is applied and the result is used to fix the value of the current magnitude at OCP, i.e. $|\vec{I_R}|$. The values of R, T_1, T_2, T_3, T_4 depend on the cable's geometrical and thermal properties, and along with mathematical expressions given in [18] and [19], they can be estimated for single-core and three-core cables, respectively. Ratio of losses λ_1 and λ_2 are assumed to be 5% each.
The traditional method also evaluates the voltage swing limit (6) and the SIL (7). The maximum voltage swing (Max_{swing}) between open-circuit and full-load conditions at the receiving-end, is considered to be 0.05 in (6). Meanwhile, the angles of $\vec{A}$ and $\vec{B}$ are α and β, respectively, in (7).

$$P_{SWING} = \left\{ P \in \mathbb{R}^+ : |\vec{V_S} \cdot \vec{A} - \left(\frac{P}{\sqrt{3} \cdot |\vec{V_S}| \cdot pf} \right) \angle \arccos(fp) \cdot \vec{B}| = |\vec{V_S} \cdot \vec{A}| \cdot (1 - Max_{swing}) \right\} \tag{6}$$

$$P_{SIL} = \frac{|\vec{V_S}| \cdot |\vec{V_R}|}{|\vec{B}|} - \frac{|\vec{A}| \cdot |\vec{V_R}|^2}{|\vec{B}|} \cdot \cos(\beta - \alpha) \tag{7}$$

Input: $\vec{V_S}$,$|\vec{I_R}|$,pf, $Initial_{length}$,$\Delta length$,Max_{length}, $Cable_{type}$
Output: $\boldsymbol{P_{OWF}}$,$\boldsymbol{Cable_{length}}$

1. **for** *($Cable_{length} = Initial_{length} : \Delta length : Max_{length}$)* **do**
2. *Get $\vec{A}$,$\vec{B}$,$\vec{C}$,and $\vec{D}$ for given $Cable_{type}$ and $Cable_{length}$.*
3. *Get $\vec{I_S}$ with $\vec{V_S}$,$|\vec{I_R}|$,pf,$\vec{A}$,$\vec{B}$,$\vec{C}$,and $\vec{D}$ in (2).*
4. **if** *($\vec{I_S}$ is feasible)* **then**
   $P_{THERMAL_{Classic}} = \sqrt{3} \cdot |\vec{V_S}| \cdot |\vec{I_S}| \cdot pf$
5. **else**
   $P_{THERMAL_{Classic}} = 0$
6. **end if**
7. *Get P_{SWING} with (6).*
8. *Get P_{SIL} with (7).*
9. *Get $P_{OWF} = \min(P_{THERMAL_{Classic}}, P_{SWING}, P_{SIL})$.*
10. *Save point $\{Cable_{length}, P_{OWF}\}$.*
11. **end for**

Algorithm 1: The traditional power-transfer capability curve method

Algorithm 1 requires as main inputs the voltage at OSS ($\vec{V_S}$), the static thermal limit ($|\vec{I_R}|$), power factor at OSS (pf), and resolution for total length sweeping ($\Delta length$, Max_{length}, and $Initial_{length}$). The output is the the power-transfer capability curve using the traditional method represented by the pair-set ($\boldsymbol{Cable_{length}}, \boldsymbol{P_{OWF}}$). After certain value of length, the two-port model parameters $\vec{C}$ and $\vec{D}$ turn Equation (2) into infeasible for $\vec{I_S}$, under the pre-set conditions $\vec{V_S}$, $|\vec{I_R}|$, and pf (power factor at OSS).
The disadvantage regarding this method is the impossibility to include the natural power fluctuation inherent to OWFs. Equation 5 allows getting the continuous current I to be transmitted during infinite time, in order to obtain a continuous conductor temperature equal to 90 °C. The latest value is considered as the rated limit to not compromise the cable's lifetime following a deterministic approach [20].

2.2 The proposed method

The following methodology is able to cover up the limitations of the traditional approach: power fluctuations of OWFs, and their impact over cables' power-transfer capability curves, are taken into consideration. The general flowchart of the proposed method is presented in the fig. 1.

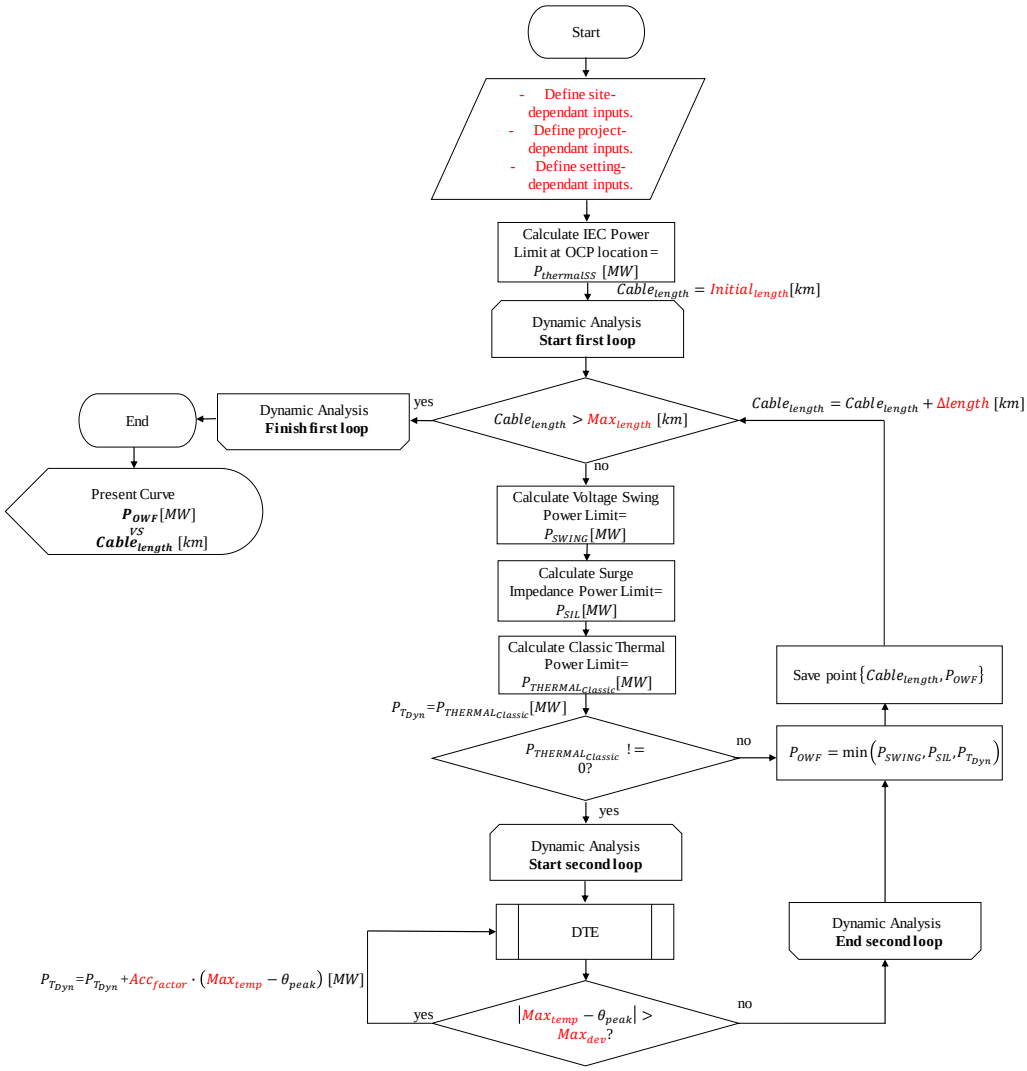

Figure 1: The flowchart of the proposed method.

To initialize the process of the fig. 1, the following inputs (sorted by a top-down approach and marked in red in Figure 1) are required:

- Site-dependant inputs: OWF power time series, seabed temperature time series, and seabed thermal parameters (thermal resistivity and thermal specific heat). The seabed-related parameters are considered to be spatially-uniform for simplicity reasons but the method can be extended to account for spatial variations throughout the cable's trajectory.
- Project-dependant inputs: In this input set is encompassed: project's electrical system data (nominal frequency, nominal voltage at OSS, power factor at OSS, compensation units, export cable type with all its geometrical, thermal, and electrical information, and cable installation conditions, like buried depth and phase spacing).
- Simulation setting-dependant inputs: Inputs conceiving the total length calculation resolution, such as, $Initial_{length}$, $\Delta length$, and Max_{length}; additionally, inputs for the DTE model, like seabed sub-layers number N, as described in [14], number of samples per

hour, the temperature resolution Max_{dev}, and Max_{temp}.

After getting the aforementioned inputs, (5) is applied, providing input ($P_{thermal_{SS}}$) for calculating $P_{THERMAL_{Classic}}$ (see Algorithm 1). After this, the outer loop is started, changing the total length value. In the inner loop, for a particular distance $Cable_{length}$, the power limits are computed: P_{SWING} (6), P_{SIL} (7), and $P_{THERMAL_{Classic}}$. The value of $P_{THERMAL_{Classic}}$ is used to start up the variable $P_{T_{Dyn}}$, that scales-up the power time series representing the total installed power of the OWF; this is followed by the call of the DTE model (see fig. 2), in order to estimate the maximum instantaneous conductor temperature θ_{peak}, value that is compared to Max_{temp} to get the calculated temperature deviation. In case this deviation is higher than Max_{dev}, the process is repeated using the recursive function $P_{T_{Dyn}} = P_{T_{Dyn}} + Acc_{factor} \cdot (Max_{temp} - \theta_{peak})$ to update the value of the OWF installed power. It should be noticed that an important key in this process is Acc_{factor}; this parameter, if too low, makes impossible to force θ_{peak} close to 90 °C, and if too high, causes oscillations around the desired point. This parameter has been calibrated in this work using different sizes of test sets, concluding $Acc_{factor} = 5$ when the temperatures are in °C and the power in MW.

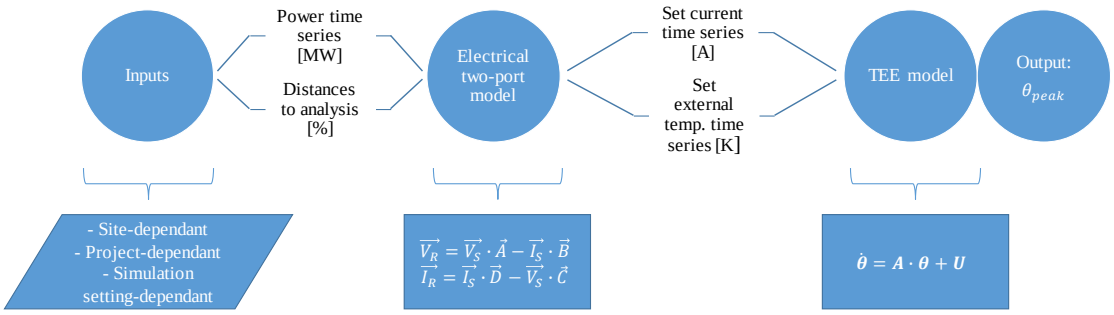

Figure 2: The dynamic temperature estimation method.

Focusing on the DTE model (fig. 2), along with the inputs definition, the parameter $\boldsymbol{Distances\ to\ analysis}$ must be selected in function of the power time series at OSS, and the compensation units. In case no shunt-series compensation units are installed, it is enough to consider a single point $\boldsymbol{Distances\ to\ analysis} = \{100\%\}$ for any instantaneous value of power, because the current strictly increases with the total length; nevertheless, compensation units may alter the longitudinal current profile, shifting the maximum current point to an intermediate value lower than the OCP, i.e., $\boldsymbol{Distances\ to\ analysis} < 100\%$, consequently $\boldsymbol{Distances\ to\ analysis} = f(t)$.

If shunt-series compensation units are installed, in the worst-case scenario the number of instances to run the TEE model are $|\boldsymbol{Distances\ to\ analysis}| = 8760$ (if a resolution of one hour and a normal year are chosen). At the end, the output of this model is the calculated maximum instantaneous conductor temperature θ_{peak} for all the instances.

When θ_{peak} is close enough to 90 °C, the dynamic analysis is terminated, and the corresponding power is compared to P_{SWING} and P_{SIL}, saving the point $\{Cable_{length}, \min(P_{SWING}, P_{SIL}, P_{T_{Dyn}})\}$.

3 CASE STUDY

3.1 Inputs definition

An OWF to be constructed in the Baltic Sea is considered as a case study. The site-dependant inputs are presented in the Table 1; the histogram of power time series is also illustrated in the fig. 3, where it is appreciable that only 40% of the time, power between 0.9 and 1 pu is produced, according to the OWF power time series (in p.u.) simulated by means of the model

described in [21]. For the cable's surrounding temperature, a synthetic time series based on info from the Bornholm Basic area [22] was created, due to the scarcity on real information; the temperature profile ranges between 1 °C to 10 °C, including seasonal variations. Likewise, project-dependant and simulation setting-dependant inputs are presented in the table 2, and table 3, respectively.

Table 1
Site-dependant inputs.

Power time series [MW]	Seabed temp. time series [°C]	Seabed thermal resist. $\left[\frac{\text{Km}}{\text{W}}\right]$	Seabed thermal sp. heat $\left[\frac{\text{J}}{\text{m}^3}\right]$
fig. 3	[1 10]	1	$2 \cdot 10^6$

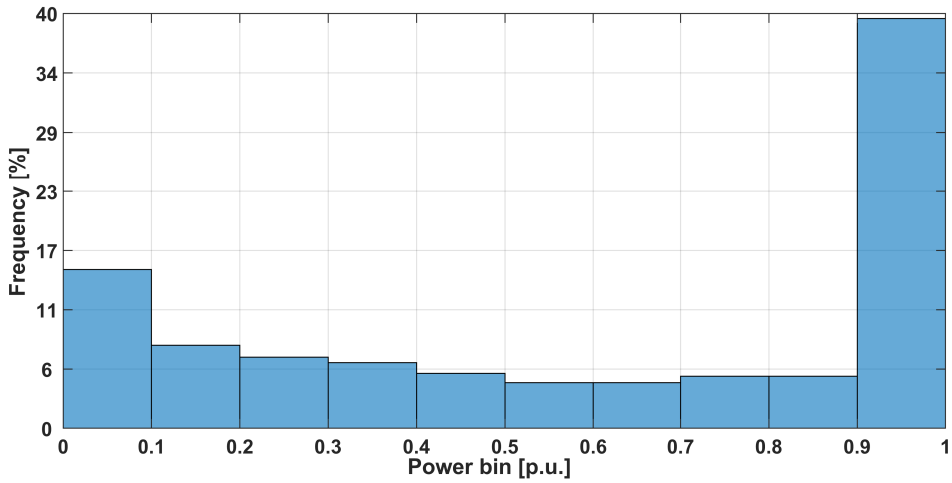

Figure 3: Histogram of power time series.

Table 2
Project-dependant inputs.

Frequency [Hz]	Voltage [kV]	pf	Series-shunt compensation	Cable	Buried depth [m]	Spacing [m]
50	275	1	*No*	800 mm^2	1	0.4

Table 3
Simulation setting-dependant inputs.

$Initial_{length}$ [km]	Δ_{length} [km]	Max_{length} [km]	N	Max_{dev} [°C]	Max_{temp} [°C]	$Samples/hour$
0.1	10	200	10	1	90	1

3.2 Results

The comparison between the curves using the traditional and the proposed method is presented in fig. 4; the orange line accounts for the power fluctuation, and therefore for each evaluated distance its magnitude is always higher than the traditional method (blue line), which assumes constant power. The crossing-point with the abscissa is unaffected as expected; in fact, to increase the reach in terms of total length, lower voltage levels or lower nominal frequencies should be evaluated. The curve obtained through the traditional method was validated against other works as [10] and [11]. Mathematically, the proposed method preserves the exponential trend given the low-degree polynomial relation between P_{OWF} and θ_{peak}. Both curves are defined by the thermal limit turning this one as the binding constraint; for these values of installed

power and total length, the voltage swing is maximum 0.9% for the traditional method, while for the proposed method is 1%, albeit the curve is more steep throughout the distance range (with voltage phase variation lower than 30 °C). Secondly, the SIL limit is always in the order of GW, hence not representing a threat. The traditional method requires only a couple of seconds to be calculated, whilst the proposed method lapses up to 5 hours; however, this computation time is negligible with respect to OWF planning time.

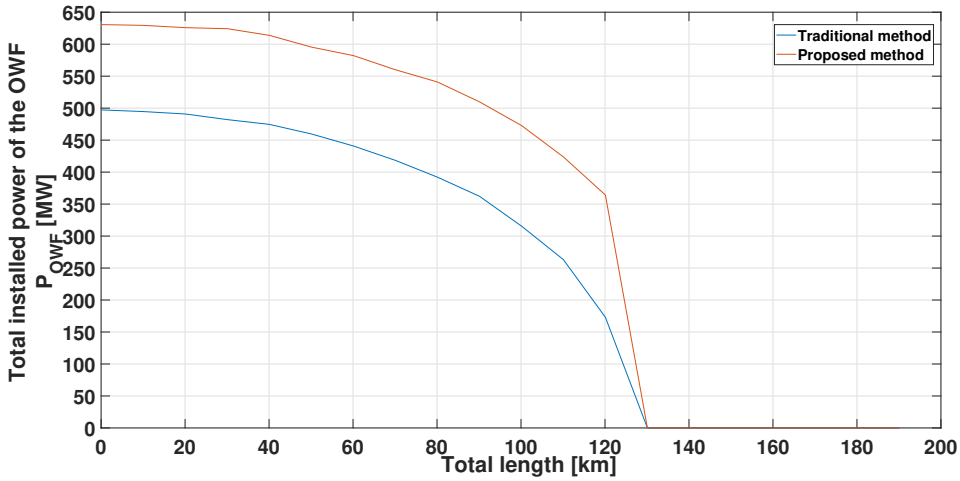

Figure 4: Comparison between the traditional curve method and the proposed curve method.

The evolution of the gain in power in function of the total length is illustrated in the fig. 5, the greater the distance the larger the gain. Indeed, for the greatest length (120 km), the installed power of the OWF could be 2.1 times the power calculated using the traditional method. This shows that for very large export route lengths, the under-use of the cable is increasing. It also indicates that HVAC-based solutions could be more thoroughly assessed in front of the HVDC counterpart, in benefit of the first one. Further computational experiments point out that the power gain is larger for greater values of soil thermal resistivity, for instance, for a total length of 120 km, an additional increase of OWF installed power of 39% can be achieved, when the soil thermal resistivity is 20% greater than the base value shown in table 1.

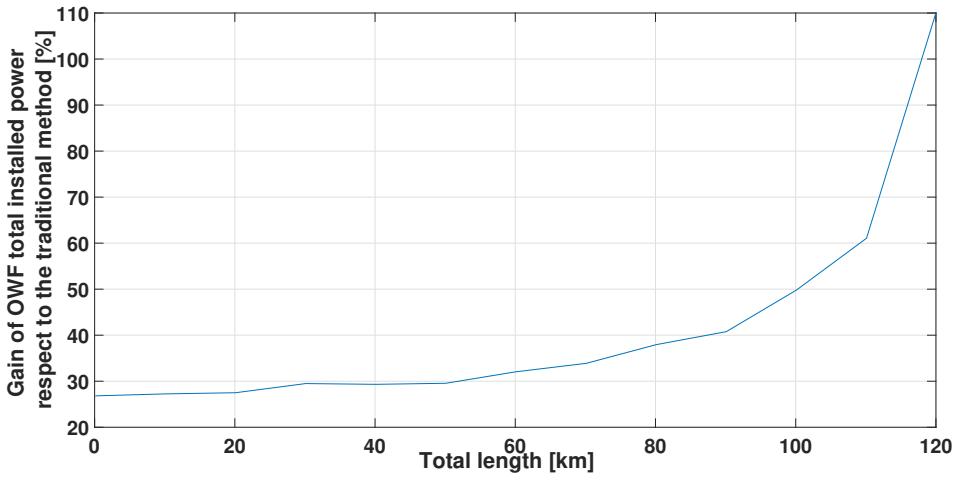

Figure 5: Gain of OWF total installed power.

4 CONCLUSIONS

The proposed method provides a realistic and efficient approach for calculating the power-transfer capability curve of OWF cables, with special interest on export cables, as the effect of technical constraints over transmissible power, in function of the total length, is thoroughly investigated. Technical constraints encompass thermal limit, voltage swing limit, and SIL limit. It has been identified that the binding constraint for submarine cables is the thermal limit, and this restriction can be relaxed if the power fluctuations are taken into account, consequently enlarging the search space, making possible to obtain larger values of installable OWF power for a given cable type, under specific operating conditions. The case study results show an increase of OWF total installed power of 110% for a total length of 120 km, when a cable 800 mm^2 is used. Additional simulation results project further increases on this value for larger values of thermal resistivity. The computational expenses must be considered, the proposed method converges on approximately 5 hours, and larger memory resources are needed, nevertheless, they do not represent any challenge at any extent using a normal PC.
The proposed methodology is dependent on the accuracy of the inputs, as the power generation cycle, seabed soil temperature, and thermal properties of the soil and the cable. Future work includes uncertainty analysis of these parameters, and the inclusion of several power production case scenarios.

ACKNOWLEDGMENTS

This research has received funding from the Baltic InteGrid Project (http://www.baltic-integrid.eu/).

BIBLIOGRAPHY

[1] GWEC, "Global Wind Report. Annual Market Update 2017," Tech. Rep., 2017. [Online]. Available: http://gwec.net/publications/global-wind-report-2/.[AccessedOct29,2018]
[2] I. M. De Alegría, J. L. Martín, I. Kortabarria, J. Andreu, and P. I. Ereño, "Transmission alternatives for offshore electrical power," *Renewable and Sustainable Energy Reviews*, vol. 13, no. 5, pp. 1027–1038, 2009.
[3] ReNEWS, "Rampion suffers cable fault," 2017. [Online]. Available: http://renews.biz/105889/rampion-suffers-cable-fault/.[AccessedOct29,2018]
[4] X. Sun, D. Huang, and G. Wu, "The current state of offshore wind energy technology development," *Energy*, vol. 41, no. 1, pp. 298–312, 2012.
[5] IEC, "IEC-60287-1: Electric cables - Calculation of the current rating," Tech. Rep., 2014.
[6] ——, "IEC-60853-2: - Calculation of the cyclic and emergency current rating of cables," Tech. Rep., 2008.
[7] CIGRÉ, "Current Ratings of Cables for Cyclic and Emergency Loads. Part 1. Cyclic Ratings (Load Factor Less Than 100%) and Response to a Step Function," Tech. Rep. 24, 1976.
[8] H. Brakelmann, "Efficiency of HVAC power transmission from offshore-windmills to the grid," *2003 IEEE Bologna PowerTech - Conference Proceedings*, vol. 2, pp. 38–43, 2003.
[9] T. Ackermann and N. B. Negra, "Evaluation of Electrical Transmission Concepts for Large Offshore Windfarms," *Proceedings of Copenhagen Offshore Wind*, no. January 2005, pp. 1–10, 2005.

[10] N. B. Negra, J. Todorovic, and T. Ackermann, "Loss evaluation of HVAC and HVDC transmission solutions for large offshore wind farms," *Electric Power Systems Research*, vol. 76, no. 11, pp. 916–927, 2006.

[11] R. Meere, J. Ruddy, P. McNamara, and T. O'Donnell, "Variable AC transmission frequencies for offshore wind farm interconnection," *Renewable Energy*, vol. 103, pp. 321–332, 2017.

[12] J. Song-Manguelle, M. H. Todorovic, S. Chi, S. K. Gunturi, and R. Datta, "Power transfer capability of HVAC cables for subsea transmission and distribution systems," *IEEE Transactions on Industry Applications*, vol. 50, no. 4, pp. 2382–2391, 2014.

[13] T. Kvarts, "Systematic Description of Dynamic Load for Cables for Offshore Wind Farms. Method and Experience," *CIGRÉ*, pp. 1–13, 2016.

[14] J.-A. Pérez-Rúa, K. Das, and N. A. Cutululis, "Lifetime estimation and performance evaluation for offshore wind farms transmission cables," in *Proceedings of the 15th IET international conference on AC and DC Power Transmission (to be presented)*, 2019, pp. 1–6.

[15] J. J. Grainger and W. D. J. Stevenson, *Power System Analysis*, 1994.

[16] D. Chatzipetros and J. A. Pilgrim, "Review of the Accuracy of Single Core Equivalent Thermal Model for Offshore Wind Farm Cables," *IEEE Transactions on Power Delivery*, vol. 33, no. 4, pp. 1–1, 2017.

[17] R. S. Olsen, J. Holboll, and U. S. Gudmundsdottir, "Dynamic Temperature Estimation and Real Time Emergency Rating of Transmission Cables," *IEEE Power and Energy Society General Meeting*, pp. 1–8, 2012.

[18] R. S. Olsen, G. J. Anders, J. Holboell, and U. S. Gudmundsdottir, "Modelling of Dynamic Transmission Cable Temperature Considering Soil-Specific Heat, Thermal Resistivity, and Precipitation," *IEEE Transactions on Power Delivery*, vol. 28, no. 3, pp. 1909–1917, 2013.

[19] G. J. Anders, A. Napieralski, and Z. Kulesza, "Calculation of the internal thermal resistance and ampacity of 3-core screened cables with fillers," *IEEE Transactions on Power Delivery*, vol. 14, no. 3, pp. 729–733, 1999.

[20] G. Mazzanti, "The Combination of Electro-thermal Stress, Load Cycling and Thermal Transients and its Effects on the Life of High Voltage ac Cables," *IEEE Transactions on Dielectrics and Electrical Insulation*, vol. 16, no. 4, pp. 1168–1179, 2009.

[21] M. Koivisto, K. Das, F. Guo, P. Sørensen, E. Nuño Martinez, N. A. Cutululis, and P. Maule, "Using time series simulation tool for assessing the effects of variable renewable energy generation on power and energy systems," *WIREs Energy and Environment*, no. June, pp. 1–15, 2018.

[22] HELCOM, "Our Baltic Sea," 2017. [Online]. Available: http://stateofthebalticsea.helcom.fi/in-brief/our-baltic-sea/.[AccessedOct29,2018]

APPENDIX C3

"Heuristics-based design and optimization of offshore wind farms collection systems"

J.A. Pérez-Rúa, D. Hermosilla,
K. Das, and N. A. Cutululis

in *Journal of Physics: Conference Series*
Vol. 1356, 012014
16th Deep Sea Offshore Wind R&D conference
Trondheim, Norway

16th–18th January

2019

Heuristics-based design and optimization of offshore wind farms collection systems

Juan-Andrés Pérez-Rúa, Daniel Hermosilla Minguijón, Kaushik Das and Nicolaos A. Cutululis

Technical University of Denmark, Department of Wind Energy, Integration and Planning Section, Frederiksborgvej 399, Building 115, Roskilde 4000, Denmark

E-mail: juru@dtu.dk

Abstract. A parallel-based algorithmic framework for automated design of Offshore Wind Farms (OWF) collection systems is proposed in this paper. The framework consists basically on five algorithms executed simultaneously and independently, followed by a combined analysis aiming to generate the best results in terms of different objective functions. The main inputs of the framework are the location coordinates of the Wind Turbines (WT) and the Offshore Substation (OSS), wind power production time series, and the set cables considered for the collection system design. Four heuristics and one metaheuristic algorithm are considered. The heuristics are based on modified versions of well-known graph-theory algorithms: Kruskal (KR), Prim (PR), Esau-Williams (EW), and Vogel's Approximation Method (VAM); all of them coded in a unified framework with quartic time complexity. The metaheuristic is built upon a Genetic Algorithm (GA) designed using a hierarchical-restricted penalization system. Comparisons between all of these methods are performed from different perspectives, taking into consideration the particular constraints treated for OWF practical applications. In general, primals from heuristics lead to faster and better results when only a single cable is available, and provide collection systems with lower electrical power losses for multiple cables choice, whilst the GA shows better results when the initial investment is prioritized and several cable types are considered.

Acronyms

DCF Discounted Cash Flow.

EW Esau-Williams.

GA Genetic Algorithm.

I Investment.

IL Investment plus losses.

KR Kruskal.

L Length.

LCOE Levelized Cost of Energy.

NPV Net Present Value.

OSS Offshore Substation.

OWF Offshore Wind Farm(s).

PR Prim.

VAM Vogel's Approximation Method.

WT Wind Turbine(s).

1. Introduction

Offshore Wind Farms (OWF) represent one of the fastest and most steadily growing types of renewable energy technologies for electricity generation. The capacity has increased almost five times in the last seven years, reaching a globally total installed power of nearly $19\,\mathrm{GW}$ [1]. Currently, general attention is focused on making this technology more attractive from a financial perspective, therefore different strategies, from multidisciplinary fields, are being designed, tested, proposed, and implemented. Economies of scale play a major role in this aspect, and results are already being obtained, as the Levelized Cost of Energy (LCOE) has dropped recently from $240\ \mathrm{USD/MWh}$ to $170\ \mathrm{USD/MWh}$ [2]. Some of the consequences of massive escalation of OWF projects is the farther moving from shore of Offshore Substations (OSS) towards deeper waters, and deployment over larger areas by Wind Turbines (WT), positioned more asymmetrically in the plane, as a result of Annual Energy Production (AEP) maximization techniques [3]. The interconnection between WT to the OSS, falls into the category of well-known mathematical problems, which have been proved to be computationally NP-Hard [4], meaning there is no certificate on the ability to come up with algorithms to solve it in a polynomial time in function of the problem size. The repercussion of this fact is the expotential growth in solving time for large instances of the problem, i.e., large OWF.

To cope with this, several conceptually different methodologies have been proposed. One could cluster them as: exact global optimization, metaheuristics, and heuristics. Global optimization encompass a large set of different alternatives to model analytically a problem, like Integer Programming (IP) [5], Mixed Integer Linear Programming (MILP) [6], Mixed Integer Quadratic Programming (MIQP) [7], and Mixed Integer Non-Linear Programming (MINLP) [8]; all of these methods permit particular physical modelling choices, and the proper balance between solution and modelling quality is one of the tasks of the designer. Although global optimization in theory can provide the global optimum of a problem, they require the use of expensive commercial solvers, and, in the case of Integer Programming (IP), branch-and-bound methods become infeasible for large instances of a problem, in terms of memory resources and computing time. In this way, abundant metaheuristics approaches are available, such as: Genetic Algorithm (GA) [9], Particle Swarm Optimization (PSO) [10], Simulated Annealing (SA) [11], Ant Colony System (ACS) [12], and others; these optimization methods do not require external solvers and can be implemented independently by the designer, and at the same time, may converge faster than global optimization for primals. The main disadvantage of metaheuristics is the lack of formalities such as time and quality upper bounds. Finally, heuristics represent all those approaches following sequential steps to solve a problem, in general based on deterministic rules, hence vulnerable to fall in a local minimals. In the literature, the works [13], [14], [6] tackle the OWF collection system design problem, by means of Prim (PR), Dijkstra, and Kruskal (KR) algorithms; however, they implement the non-capacitated versions of them, only in [6] the Clarke and Wright, that includes inherently the capacitated constraint is applied, however this heuristic is valid only for totally radial systems [15]. As suggested in [16], heuristics for solving a Capacitated Minimum Spanning Tree (C-MST) are interesting options to get primals almost instantaneously, nevertheless in this work only Esau-Williams (EW) is mentioned, and the application is limited to onshore wind farms, where cables crossings are allowed, and no simulation of power flow is implemented.

To the best of the author's research C-MST heuristics to tackle the OWF collection system design and optimization problem has not been yet addressed in the literature. Consequently, this work presents the design and implementation of modified versions of heuristics, based on algorithms previously applied

in telecommunication networks design [17], in order to infer about their weaknesses, strengths, and appropriateness for OWF. The analysis is complemented by comparing it to a GA; all of these methods are framed in a single parallel solver that gives the best solution in terms of different targets.
This paper is structured as follows: The Section 2 describes the optimization framework, continuing with the methodology depiction in the Section 3, and finally, it is reported the application of the model through computational experiments in the Section 4. Conclusions extracted after this work close the article in the Section 5.

2. Optimization framework

The optimization framework comprises the cost model, the general flowchart of the method, and the set of assumptions made when designing the structure of the solver. The most important assumptions are represented in the Section 2.1, which are all considered admissible and reasonable.

2.1. Assumptions

- The OWF is composed of one OSS and a group of WT. The location of these elements is known.
- Time series of power generation are available. The variability must be taken into account. [18].
- The length of the cables is the horizontal trenching length (i.e. the euclidean distance between two points in the plane). Seabed bathymetry is neglected.
- The topology of the grid is based on a radial network, star network or a combination of both, i.e., spanning trees. Cable crossings are not allowed, except at the endpoints of each segment, where both the OSS and WT are located.
- A predefined list of available cables types is available. Let the set of cables be $\boldsymbol{T}$.
- Let the capacity of a cable $t \in \boldsymbol{T}$ be u_t (in terms of WT number). Hence, let $\boldsymbol{U_t}$ be the set of capacities sorted as in $\boldsymbol{T}$. The capacity of cable t is calculated as $u_t = \left\lfloor \frac{\sqrt{3} \cdot V_n \cdot I_{n_t}}{S_n} \right\rfloor$, where V_n is the system nominal voltage, in this paper equal to $33\,\mathrm{kV}$, I_{n_t} is the nominal current of the cable t calculated with [19], and S_n the WT nominal power.
- The upper bound U is found as $U = \max \boldsymbol{U_t}$, and the corresponding cable type $t_C = \arg\max \boldsymbol{U_t}$.

2.2. Cost model

The solution provided depends a lot on the cost function of the cables, therefore it has to be stated explicitly which one was considered. The unitary cost of a cable (in €/km) is calculated by using the cost function (1) proposed in [20], where C_t is the cost of cable type t in €/km, I_{n_t} the rated current of cable type t in A, V_n the rated line to line voltage level in V, parameters A_{p_t}, B_{p_t}, C_{p_t} are cost constants; these values are given as tables depending on the voltage level, and S_{n_t} is the rated power of cable type t in VA ($S_{n_t} = \sqrt{3} V_n I_{n_t}$).

$$C_t = A_{p_t} + B_{p_t}\, \mathrm{e}^{\left(\frac{C_{p_t} S_{n_t}}{10^8}\right)^2} \tag{1}$$

2.3. General flowchart

The flowchart of the full framework is presented in Figure 1. Required main inputs are: WT and OSS locations, cable database with costs and electrical parameters per unit of length (resistance, capacitance, and inductance), and the offshore wind power production time series. After capturing the inputs, the five methods are run in parallel; the four modified heuristics (PR, KR, EW, and Vogel's Approximation Method, VAM) obtain either a feasible point (primal) or a unfeasible point; in the first case, an algorithm to assign a cable type to each branch is executed (in order to minimize the total investment), whilst for the second case, those solutions are dispensed, and can be useful to provide a warm start to other solvers (for instance, using a global optimization). Unfeasible points are due to the cables non-crossing constraint, hence represented as a forest graph; GA provides primals for the considered instances. Finally, all primals

(with cables assigned) are evaluated by means of a power flow solver for calculating the electrical power losses. In the end, a single solution is displayed in function of the desired economic metric, which can be: total cables length (L), total initial investment (I), and initial investment plus electrical power losses (IL). The way of computing the objective IL can vary as well, for instance, metrics similar to the LCOE or Net Present Value (NPV) can be used, the latter includes the electrical power losses as economical expenses along with the cables total costs, applying Discounted Cash Flow (DCF).
The methods, for which each algorithm is explained along with pseudocodes and big-O notation for the worst-case scenario, are described in Section 3.

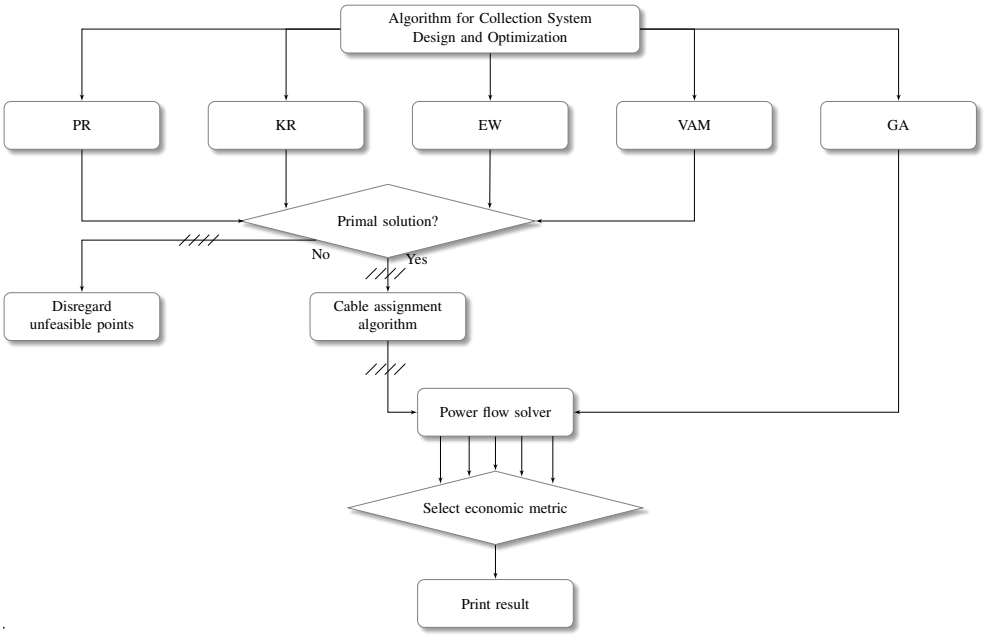

Figure 1. Algorithm's general flowchart.

3. Methodology

A short descriptive explanation of each heuristic, considering their most basic conception, are presented in Sections 3.1 through 3.4. In the Section 3.5 a single pseudocode is proposed, which by varying a single parameter w_i, converges to each of the previous four heuristics; the capacity constraint U, and cables non-crossing constraint are also accounted for. Finally, other sub-blocks of the methodology are provided with their pseudocodes in the following sub-sections.
It is assumed the WT and OSS location are presented as a weighted undirected graph $G(\boldsymbol{V}, \boldsymbol{E}, \boldsymbol{W})$, where $\boldsymbol{V}$ represents the nodes set (WT and OSS), $\boldsymbol{E}$ the set of available edges arranged as a pair-set, and $\boldsymbol{W}$ the associated weight for each element $e \in \boldsymbol{E}$. In general, $G(\boldsymbol{V}, \boldsymbol{E}, \boldsymbol{W})$ is a complete graph.

3.1. PR algorithm

This algorithm is described in detail in [21]. Let $\boldsymbol{N} = \{1, \cdots, w_n + 1\}$ be the set of numbered nodes to form the tree, where w_n is the total number of WT to be connected to a single OSS ($\boldsymbol{N}(1) = 1$). Likewise, let the set $\boldsymbol{S}$ contain the nodes already included in the collection system at a given point of the algorithm; in the first iteration $\boldsymbol{S} = \{1\}$. The idea is to select the shortest edge connecting a node from $\bar{\boldsymbol{S}}$ to $\boldsymbol{S}$, until $\boldsymbol{S} = \boldsymbol{N}$, and $\bar{\boldsymbol{S}} = \emptyset$.

3.2. KR algorithm
The paper proposing this algorithm can be found in [22]. In the first iteration, from $\boldsymbol{N}$ let each element define a set $\boldsymbol{C_i} = \{i\}\ \forall i \in \boldsymbol{N}$. The idea is to choose the shortest edge $\{i, j\}$, such as $j \notin \boldsymbol{C_i}$ and $i \notin \boldsymbol{C_j}$. If $\{i, j\}$ is selected, then $\boldsymbol{C_i} = \{\boldsymbol{C_i}, \boldsymbol{C_j}\}$, and $\boldsymbol{C_j} = \{\boldsymbol{C_j}, \boldsymbol{C_i}\}$. This procedure is repeated until $\boldsymbol{C_i}, \cdots, \boldsymbol{C_{w_n+1}} = \boldsymbol{N}$.

3.3. EW algorithm
This algorithm is described in detail in [23]. For each available edge $\{i, j\}$, two trade-off values are calculated as: $t_{ij} = w_{ij} - w_{i1}$ and $t_{ji} = w_{ji} - w_{j1}$, where w_{ij} is the edge length of $\{i, j\}$, and w_{i1} the edge length from node i to 1 (OSS); for this application $w_{ij} = w_{ji}$. Let $\boldsymbol{T_{to}}$ contain all the calculated trade-off values. Following the definition given in Section 3.2, the idea is in each iteration, to select $\min \boldsymbol{T_{to}}$, while checking $\{u, v\} = \arg\min \boldsymbol{T_{to}}$, conditioned to $u \notin \boldsymbol{C_v}$ and $v \notin \boldsymbol{C_u}$. In case the latest is satisfied, update the pertinent variables and repeat until all components are equal to the full nodes set.

3.4. VAM
This algorithm is described in detail in [24]. As explained for EW algorithm, two trade-off values are defined for each edge: $t_{ij} = w_{ij} + a_i - b_i$, and $t_{ji} = w_{ji} + a_j - b_j$. Where a_i is the nearest feasible neighbor to i, and b_i the second nearest feasible neighbor. Form set $\boldsymbol{T_{to}}$ with all trade-off values. At each iteration, find $\min \boldsymbol{T_{to}}$ and check feasibility. In case the latest is satisfied, update the pertinent variables and repeat until all components are equal to the full nodes set.

3.5. The unified algorithm
Each one of the four previously described heuristics, apparently, follow independent rules to cope with the sequential decision-making problem. Nevertheless, as demonstrated in [17] and [25], all of them converge to a single paradigm which can be unified in a single block of codes. In this work, it is proposed a modified version of the aforementioned unified algorithm, and it is based on the same idea of associating a singular weight parameter p, $\forall\ v \in \boldsymbol{V}$. By establishing the parameter set $\boldsymbol{P}$ in function of the heuristic, the effect is equivalent to changing the sequential order with a branch $e \in \boldsymbol{E}$ is selected into the tree, or, what it is the same, the order of integrating each WT node into the OWF collection system. The unified code, for this case, also takes into account the two main constraints (capacity constraint, U, and cables non-crossing). One of the main advantages of having a single set of code lines is the possibility to, in theory, have infinite variants, by selecting infinite rules for $\boldsymbol{P}$.
For each branch e_{ij}, two trade-off values are assigned: $t_{ij} = w_{ij} - p_i \wedge t_{ji} = w_{ji} - p_j$, where $w_{ij} = w_{ji}$, forming the triple set $\boldsymbol{T}(i, j, t_{ij})$. The nodal weight parameter $p \in \boldsymbol{P}$, $\forall\ v \in \boldsymbol{V}$, must be initialized and updated as the algorithm keeps running. In table 1 the criteria for initializing and updating (at each iteration) the set $\boldsymbol{P}$ are presented; it is noticeable how each different criterion forces the unified algorithm to converge to either any of the previously explained heuristics. A generalization of this rule would be: $p = a \cdot (b \cdot w_{i1} + (1 - b) \cdot w_{lm})\ \forall\ v \in \boldsymbol{V}$, where a and b are constants with $a \geq 0$ and $0 \leq b \leq 1$, w_{i1} is the distance to the OSS, and w_{lm} the distance difference between the first and the second shortest feasible edges. Thus, if a and b are both equal to one, then the general equation is equivalent to the EW' rule; likewise, if a is equal to zero, KR rule is obtained. Therefore, infinite different pairs $\{a, b\}$ lead to infinite different sets $\boldsymbol{P}$. The objective of this paper is to analyze the restricted variant of the four traditional heuristics, without exploring new rules, which can be part of future works.
The unified code is presented in Algorithm 1, which requires Table 1 to be implemented; the main inputs are the original graph (generally considered the complete version), $G(\boldsymbol{V}, \boldsymbol{E}, \boldsymbol{W})$, the geographical coordinates of the WT and the OSS, $Coordinates(\boldsymbol{V})$, the capacity constraint given as upper limit of WT, U, and the specific heuristic type to use $Heuristic = \{PR, KR, EW, VAM\}$. There is certainty about the termination of the algorithm, but primals are not guaranteed. In the last case, the output graph is a forest, whilst in the first case, it is a tree $G_T(\boldsymbol{V_T}, \boldsymbol{E_T}, \boldsymbol{W_T})$, spanning all the vertex-set, $\boldsymbol{V_T} = \boldsymbol{V}$, and using exactly $|\boldsymbol{E_T}| = |\boldsymbol{V}| - 1$ edges.

Table 1. Nodal weight parameter definition.

Heuristic	Initialization	Update when $\{i, j\}$ is chosen
PR	$p_1 = 0 \wedge p = -\infty \; \forall \, v \in \boldsymbol{V} \setminus \{1\}$	$p_j = 0$
KR	$p = 0 \; \forall \, v \in \boldsymbol{V}$	No update
EW	$p = w_{i1} \; \forall \, v \in \boldsymbol{V}$	$p_i = p_j \; \forall \, v \in \boldsymbol{C_{node}(i)}$
VAM	$p = b_i - a_i \; \forall \, v \in \boldsymbol{V}$	$p_i = b_i - a_i$. On the merged new component.

Input: $G(\boldsymbol{V}, \boldsymbol{E}, \boldsymbol{W})$,$Coordinates(\boldsymbol{V})$,$U$,Heuristic
Output: $G_T(\boldsymbol{V_T}, \boldsymbol{E_T}, \boldsymbol{W_T})$
1. *Initialize empty* $\boldsymbol{V_T}$, $\boldsymbol{E_T}$, $\boldsymbol{W_T}$.
2. *Initialize* $\boldsymbol{P}$ *in function of the input: 'Heuristic'.*
3. *Initialize* $\boldsymbol{T}(i, j, t_{ij})$, *in function of* $\boldsymbol{P}$.
4. *Initialize* $\boldsymbol{C}$, $\boldsymbol{S}$, $\boldsymbol{C_{node}}$, $\boldsymbol{R_{node}}$.
5. $go = true$.
6. **while** *(go == true)* **do**
7. $tob = \min_{t_{ij}} \boldsymbol{T}(i, j, t_{ij}) \wedge \{u, v\} = \arg\min_{t_{ij}} \boldsymbol{T}(i, j, t_{ij})$.
8. **if** *(tob* $== \infty$*)* **then**
9. *go == false.*
10. **end if**
11. **if** *(loop-creation constraint with* $\boldsymbol{C_{node}(u)}$ *and* $\boldsymbol{C_{node}(v)}$ *== true)* **then**
12. $t_{uv} = \infty$.
13. $t_{vu} = \infty$.
14. **else**
15. **if** *(capacity constraint with* $\boldsymbol{C}$, $\boldsymbol{S}$, *and* $\boldsymbol{C_{node}}$, $\boldsymbol{R_{node}}$*== true)* **then**
16. $t_{uv} = \infty$.
17. $t_{vu} = \infty$.
18. **else**
19. **if** *(crossing cables constraint with* $\boldsymbol{E_T}$ *and* $Coordinates(\boldsymbol{V})$ *== true)* **then**
20. $t_{uv} = \infty$.
21. $t_{vu} = \infty$.
22. **else**
23. $\boldsymbol{E_T} = \{\boldsymbol{E_T}, \{u, v\}\}$
24. $\boldsymbol{W_T} = \{\boldsymbol{W_T}, w_{uv}\}$.
25. *Update* $\boldsymbol{V_T}$.
26. *Update* $\boldsymbol{P}$ *in function of the input: 'Heuristic'. Update* $\boldsymbol{T}(i, j, t_{ij})$, *in function of updated* $\boldsymbol{P}$.
27. *Update* $\boldsymbol{C}$, $\boldsymbol{S}$, $\boldsymbol{C_{node}}$, $\boldsymbol{R_{node}}$.
28. $t_{uv} = \infty$.
29. $t_{vu} = \infty$.
30. **end if**
31. **end if**
32. **end if**
33. **if** *(columns(*$\boldsymbol{C}$*) == 1)* **then**
34. *go == false.*
35. **end if**
36. **end while**

Algorithm 1: The unified heuristic algorithm

Algorithm 1 is designed following a nested approach. From line 1 to the line 5, the main and auxiliary variables are initialized; variables $\boldsymbol{P}$ and $\boldsymbol{T}(i, j, t_{ij})$ depend strictly on the heuristic type, whilst $\boldsymbol{C}$, $\boldsymbol{S}$, $\boldsymbol{C_{node}}$, $\boldsymbol{R_{node}}$ are useful for running the constraints-checking functions: *loop-creation*, *capacity*, and *crossing-cables*. The cheapest edge in terms of its trade-off function is selected only and only if the aforementioned three constraints are abided and, in this case, the corresponding variables are updated

(line 23 to line 30). If the cheapest edge does not satisfy one of the constraints, then is discarded by forcing its value to infinite. The termination of the full code is guaranteed in line 9 and in line 35; in case line 35 interrupts the code, the final solution is a tree, otherwise a forest.
The worst-case scenario big O notation is given by the expression: $\mathcal{O}(|\boldsymbol{V}|^2 \log|\boldsymbol{V}| + C|\boldsymbol{V}|^2 + |\boldsymbol{V}|^4)$. The first term accounts for the effort, in each iteration, of searching the cheapest trade-off value, the second term is for checking out, in each iteration, the loop and capacity constraints (in constant time), and, finally, the last term represents the crossing-cables evaluation. As the mathematical expression inherently tells, the function is polynomial.

3.6. Cable assignment algorithm
As presented in Figure 1, Algorithm 2 will only be executed for primals; this code requires the tree graph $G_T(\boldsymbol{V_T}, \boldsymbol{E_T}, \boldsymbol{W_T})$, the cables capacity set $\boldsymbol{U_t}$, and the cables type set $\boldsymbol{T}$, and generates as output a set $\boldsymbol{Cable_T}$ sized and sorted as $\boldsymbol{E_T}$, indicating for each branch the selected cable type from $\boldsymbol{T}$. The algorithm is straight-forward and self-explanatory. Worst-case scenario big O notation is: $\mathcal{O}(|\boldsymbol{V_T}||\boldsymbol{T}|(|\boldsymbol{V_T}| - 1))$, showing its polynomial-time bound behaviour.

Input: $G_T(\boldsymbol{V_T}, \boldsymbol{E_T}, \boldsymbol{W_T}), \boldsymbol{T}, \boldsymbol{U_t}$
Output: $\boldsymbol{Cable_T}$
1. *Sort by non-increasing order* $\boldsymbol{U_t}$*, and consequently* $\boldsymbol{T}$.
2. *Initialize* $\boldsymbol{Cable_T}$.
3. **for** *(*$i = 1:1:|\boldsymbol{V_T}|$*)* **do**
4. *Apply Depth-first search (DFS) algorithm in* $G_T(\boldsymbol{V_T}, \boldsymbol{E_T}, \boldsymbol{W_T})$ *for node* i.
5. $\boldsymbol{branch}$ = *Get branches incident to node* i.
6. **for** $(j = 1:1:|\boldsymbol{branch}|)$ **do**
7. $nodes$ = *Get nodes connected through* $\boldsymbol{branch}(j)$.
8. $\boldsymbol{Cable_T}(\boldsymbol{branch}(j)) = \boldsymbol{T}(|\boldsymbol{T}|)$.
9. **for** $(k = 1:1:|\boldsymbol{U_t}|)$ **do**
10. **if** *(*$\boldsymbol{U_t}(k) < nodes$*)* **then**
11. $\boldsymbol{Cable_T}(\boldsymbol{branch}(j)) = \boldsymbol{T}(k-1)$.
12. *Break. Go to step 6*
13. **end if**
14. **end for**
15. **end for**
16. **end for**

Algorithm 2: The cable assignment algorithm

3.7. GA
The detailed description of the GA is presented in [26]; it is designed following a hierarchical-restricted penalization system to facilitate the constraints checking process. The GA optimizes the initial investment cost having the algorithm 2 embedded. Electrical power losses are evaluated after obtaining each solution due to computational costs savings.

3.8. Power flow solver
A power flow solver is called for all the obtained primals; the MATPOWER package [27] is used for these purposes. The main inputs are $G_T(\boldsymbol{V_T}, \boldsymbol{E_T}, \boldsymbol{W_T})$, $\boldsymbol{T}$ (includes electrical parameters per unit of length), $\boldsymbol{Cable_T}$, and wind power time series, while the output is the total electrical power losses for a given collection system design. The OSS is modelled as the slack bus, and the WT as PV busses.

4. Computational experiments
As an exemplification, an OWF following a randomized micrositing is used to apply the method presented in the figure 1. The OWF consists of 51 WT, rated each one at $P_n = 4\,\mathrm{MW}$ and $V_n = 33\,\mathrm{kV}$.

The considered cables are XLPE 3-core copper type. Two instances are considered, first, with only one cable type available ($500\,\mathrm{mm}^2$ with $u_t = 9$) in Section 4.1, and later with two types available ($185\,\mathrm{mm}^2$ with $u_t = 6$, $300\,\mathrm{mm}^2$ with $u_t = 7$) in Section 4.2.

4.1. Single cable type

When only one cable is available the problem is equivalent to finding the minimum length of a spanning tree; in function of the selected cable, different values of U are obtained. After several experiments, it is concluded the EW heuristic presents a larger probability to obtain a feasible solution compared to the other heuristics, evaluating a large set of instances. This can be understood since its trade-off function gives more priority to connect first those WT being farther away to the OSS, hence less chances to get cables crossings. Likewise, the PR heuristic falls the most into unfeasible points, since its approach consists on forming the tree starting from the OSS, getting trapped on those WT located the farthest. A valid strategy to cope with this issue, is to allow the installation of parallel cables, although it is not a so practical option. KR and VAM perform better than PR, but in most of the cases, worst than EW, both in terms of feasibility and solution quality. In general, there is not guarantee that even EW method is able to provide a primal solution; this is totally dependent to the particular WT-OSS relative distribution. Nevertheless, given its fast termination time, it does not represent a high effort to run each of these heuristics to check out their outcome. On the other hand, the GA is designed to overcome the feasibility drawback by applying evolutionary techniques; this algorithm has been tested for OWF instances of up to 70 WT obtaining primals, requiring a computation time in the order of hours. In this regard, additional improvements can be obtained if further strategies to optimize the algorithm are implemented, such as a smart cropping of the search space.

For the particular OWF under analysis, in the table 2 (positive percentages for $LCOE_{cs}$ mean worse objective values) the main numerical results are summarized, while in the Appendix A the graphical results are reported. In this case the four heuristics provide primals, being the EW the cheapest, followed by KR and VAM, and PR provides the worst solution. If electrical power losses are quantified and integrated to the objective function in form of $LCOE_{cs}$ (see equation in [3]), the merit order remains the same, however, when using a NPC_{cs} metric, the difference between KR and VAM with EW is reduced, due to their lower electrical power losses and the gain on value of the unit of energy (NPV_{cs}^{BC} considers a price of 30 €/MWh, NPV_{cs}^{1} 50 €/MWh, and NPV_{cs}^{2} 70 €/MWh); it can bee seen that for NPV_{cs}^{2}, the difference drops to -38% (-100% means the break-even point). EW provides in fraction of seconds a solution very near to the global minimum (when minimizing the initial investment), as experienced by [17] and in several tests in this work for OWF; therefore, it can be used as benchmark with other methods, or combined with global optimization formulations to form a hybrid solver with optimality certificate.

Table 2. Single cable results.

	PR	KR	EW	VAM	GA
Feasible	Yes	Yes	Yes	Yes	Yes
AEP [GWh]			855.36		
Losses [GWh]	4.82	3.75	4.17	3.75	4.41
Initial Investment CS [M€]	41.22	39	38.13	39	39.30
Diff. with best [%]	8.12	2.30	0	2.30	3.08
$LCOE_{cs}$ [€/MWh]	2.96	2.80	2.74	2.80	2.82
Diff. with best [%]	8	2.19	0	2.19	2.92
NPV_{cs}^{BC} [M€]	356.64	359.36	360	359.36	358.75
NPV_{cs}^{1} [M€]	621.89	624.94	625.49	624.94	624.13
Δdiff. with best w.r.t BC [%]	6	−19	–	−19	6
NPV_{cs}^{2} [M€]	887.13	890.52	890.94	890.52	889.50
Δdiff. with best w.r.t BC [%]	12	−38	–	−38	12

4.2. Multiple cables types

In the case of multiple cables types, numerous computational experiments indicate that the initial investment results depend strongly on the capacity and unit price difference among the considered cables. In general, the larger the set of available cables and the larger spread between cables' prices, the greater the difference between the GA and the heuristics, in terms of capital investment; this is because, the GA tends to use longer lengths of smaller cables, forming smaller cluster of WT into feeders groups, giving also higher flexibility to provide feasible solutions, secondly, the heuristics (specially EW method) prioritize forming bigger groups of WT, requiring longer and bigger cables. As a result of the above, the heuristics provide solutions with lower electrical power losses in their favor.

For the OWF under study, in the table 3 and Appendix B the results are presented. The GA gives the best solution in terms of initial investment, albeit with higher electrical power losses than all the other methods, due to the reduction of 66.46% of the cable $300\,\mathrm{mm}^2$, and only an increment of $15.15\,\%$ of the cable $185\,\mathrm{mm}^2$, compared to EW. When using the metric $LCOE_{cs}$ the effect of the electrical power losses is attenuated because this value is compared to the AEP representing likely only 1% of it. However, the NPV_{cs} metric weights out more the electrical power losses, as it can be seen in the table 3 for the NPV_{cs}^{BC}, the EW draws as the best option, and the energy unit price increases this differences almost linearly; in fact, in the case of NPV_{cs}^{2}, the KR method cuts out 51% the difference, which indicates that for certain values of discount rate (or Weighted Average Capital Costs), price of energy, project lifetime, this one can become the solution with the greatest NPV value.

Table 3. Multiple cables results.

	PR	KR	EW	VAM	GA
Feasible	No	Yes	Yes	Yes	Yes
AEP [GWh]			855.36		
Losses [GWh]	–	7	7.3	7	7.99
Initial Investment CS [M€]	–	28.42	27.93	28.42	27.90
Diff. with best [%]	–	1.80	0.05	1.80	0
$LCOE_{cs}$ [€/MWh]	–	2.05	2.01	2.05	2.01
Diff. with best [%]	–	1.99	0	1.99	0
NPV_{cs}^{BC} [M€]	–	368.42	368.77	368.42	368.47
NPV_{cs}^{1} [M€]	–	632.98	633.24	632.98	632.73
Δdiff. with best w.r.t BC [%]	–	−25	–	−25	70
NPV_{cs}^{2} [M€]	–	897.54	897.71	897.54	896.99
Δdiff. with best w.r.t BC [%]	–	−51	–	−51	139

5. Conclusions

The proposed framework provides an algorithmic approach for assessing multi-objective designs for the collection systems in OWF. The framework, composed by four modified versions of graph-theory heuristics, and a GA, presents at which extent each of the methods provide a better solution in function of a particular economic metric. When only a single cable is available, the EW heuristic performs the best in terms of initial investment and feasibility than all the other approaches. If electrical power losses are integrated into the objective in form of the net present value metric, KR and VAM become more and more competitive for higher electricity prices. Whilst for the case of multiple cables, the GA is able to evaluate more design alternatives through evolutionary operators, to combine and modify individuals, leading to improved designs when the capital investment is assessed; however, the deep-rooted nature of the EW leads to a better balance between investment and losses, quantifiable by means of the net present value, with less evident effects over the levelized cost of energy metric; this balance depends strongly on

the values of macroeconomic parameters such as, weighted average capital costs, dynamic energy price throughout the project, and project lifetime. In general, the heuristics terminate in fraction of seconds, they could be implemented in the first planning states of an OWF, and if feasible solutions are found, this work indicates that their quality is high, and hence, can benchmark the GA output, or be combined with global optimization formulations to come up with hybrid solvers.

Acknowledgments
This research has received funding from the Baltic InteGrid Project (http://www.baltic-integrid.eu/).

References

[1] GWEC 2017 Global Wind Report. Annual Market Update 2017 Tech. rep. URL `http://gwec.net/publications/global-wind-report-2/.[Accessed Oct 29, 2018]`
[2] International Renewable Energy Agency 2016 16
[3] Herbert-Acero J, Probst O, Réthoré P E, Larsen G and Castillo-Villar K 2014 *Energies* **7** 6930–7016 ISSN 1996-1073
[4] Godinho M T, Gouveia L and Magnanti T L 2008 *Discrete Optimization* **5** 350–372
[5] Cerveira A, de Sousa A F, Pires E J and Baptista J 2016 *IEEE Transactions on Power Systems* **31** 4319–4329 ISSN 08858950
[6] Bauer J and Lysgaard J 2015 *Journal of the Operational Research Society* **66** 360–368 ISSN 14769360
[7] Hertz A, Marcotte O, Mdimagh A, Carreau M and Welt F 2017 *Journal of the Operational Research Society* **68** 62–73 ISSN 0160-5682
[8] Chen Y, Dong Z Y, Meng K, Luo F, Xu Z and Wong K P 2016 *IEEE Transactions on Sustainable Energy* **7** 1398–1407 ISSN 1949-3029
[9] Jenkins A M, Scutariu M and Smith K S 2013 Offshore wind farm inter-array cable layout *IEEE PowerTech at Grenoble* pp 1–6 ISBN 9781467356695
[10] Hou P, Hu W, Chen Z and Chen C 2017 *Wind Energy* **20** 1017–1032 ISSN 1099-1824
[11] Lehmann S, Rutter I, Wagner D and Wegner F 2017 A Simulated-Annealing-Based Approach for Wind Farm Cabling *Proceedings of the Eighth International Conference on Future Energy Systems* pp 203–215 ISBN 9781450350365
[12] Neagu B and Georgescu G 2014 Wind Farm Cable Route Optimization Using a Simple Approach *Proceedings of the International Conference and Exposition on Electrical and Power Engineering (EPE)* pp 1004–1009 ISBN 9781479958498
[13] Dutta S and Overbye T J 2012 *IEEE Transactions on Sustainable Energy* **3** 339–348
[14] Hou P, Hu W, Chen C and Chen Z 2016 *IET Renewable Power Generation* **10** 175–183 ISSN 1752-1416
[15] Quinonez-Varela G, Ault G, Anaya-Lara O and McDonald J 2007 *IET Renewable power generation* **1** 107–114 ISSN 17521416
[16] Berzan C, Veeramachaneni K, McDermott J and O'Reilly U M 2011 *Massachusetts Institute of Technology* 1–24
[17] Kershenbaum A 1974 *Networks* **4** 299–310 ISSN 10970037
[18] Koivisto M, Das K, Guo F, Sørensen P, Nuño Martinez E, Cutululis N A and Maule P 2018 *WIREs Energy and Environment* 1–15 ISSN 2041840X
[19] IEC 2014 IEC-60287-1: Electric cables - Calculation of the current rating Tech. rep.
[20] Lundberg S 2003 *Configuration study of large wind parks* Ph.D. thesis Chalmers University of Technology
[21] Prim R C 1957 *Bell System Technical Journal* **36** 1389–1401 ISSN 15387305
[22] Kruskal J B 1956 *Proceedings of the American Mathematical Society* **7** 48–50
[23] Esau L R and Williams K C 1966 *IBM Systems Journal* **5** 142–147
[24] Chandy K M and Russell R A 1972 *IEEE Transactions on Computers* **100** 1062–1066
[25] Kershenbaum A and Chou W 1974 *IEEE Transactions on Communications* **com-22** 1762–1772
[26] Hermosilla Minguijón D, Pérez-Rúa J A, Das K and Cutululis N A 2019 Metaheuristic-based Design and Optimization of Offshore Wind Farms Collection Systems *IEEE PowerTech at Milan (submitted)* pp 1–6
[27] Zimmerman R D, Murillo-Sánchez C E and Thomas R J 2011 *IEEE Transactions on Power Systems* **26** 12–19 ISSN 08858950

Appendix

A. Collection system design with a single cable

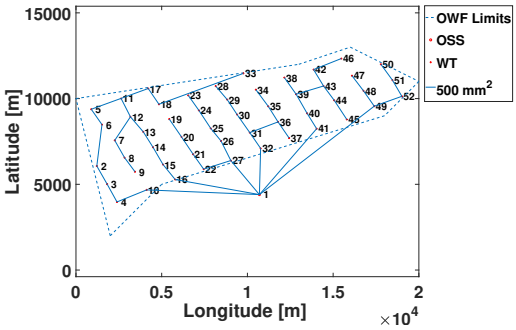

Figure A.1. PR solution for single cable

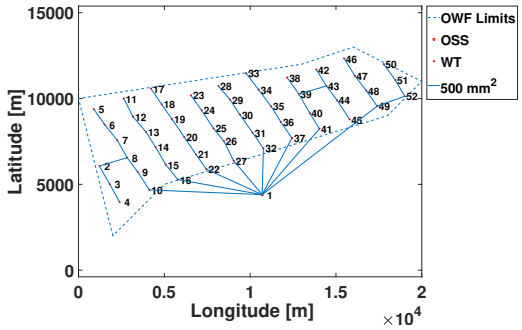

Figure A.2. KR solution for single cable

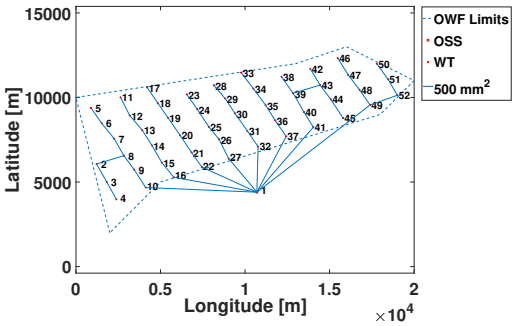

Figure A.3. VAM solution for single cable

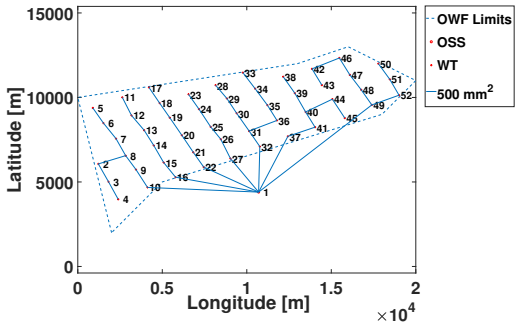

Figure A.4. EW solution for single cable

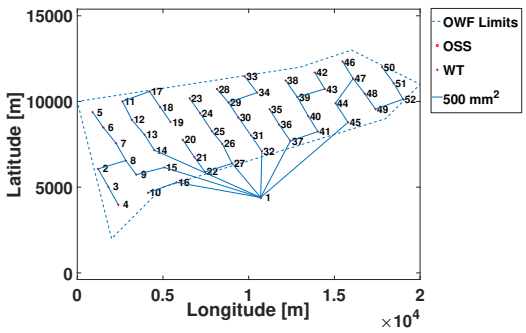

Figure A.5. GA solution for single cable

B. Collection system design with multiple cables

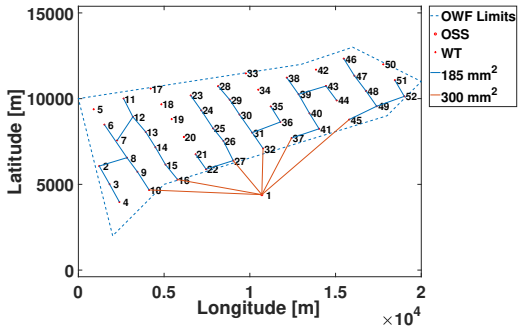

Figure B.1. PR solution for multiple cables

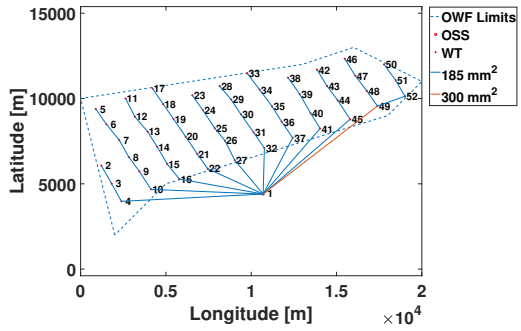

Figure B.2. KR solution for multiple cables

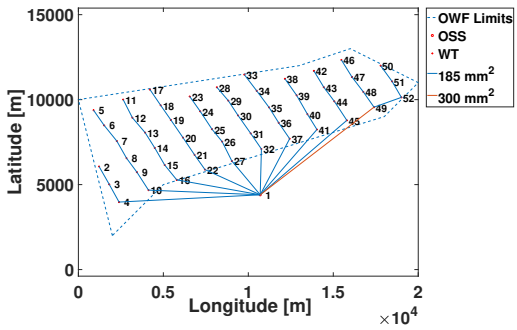

Figure B.3. VAM solution for multiple cables

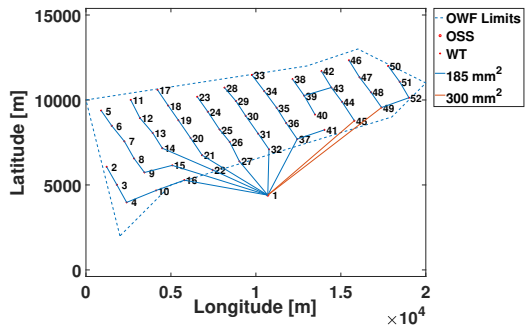

Figure B.4. EW sol. for multiple cables

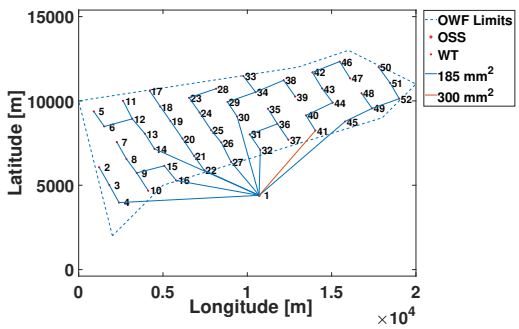

Figure B.5. GA solution for multiple cables

APPENDIX C4

"Metaheuristic-based Design and Optimization of Offshore Wind Farms Collection Systems"

D. Hermosilla, J.A. Pérez-Rúa,
K. Das, and N. A. Cutululis

in *Proceedings of the*
13th IEEE PES PowerTech Conference
Milan, Italy

23rd–27th June

2019

Metaheuristic-based Design and Optimization of Offshore Wind Farms Collection Systems

Daniel Hermosilla Minguijón, Juan-Andrés Pérez-Rúa, Kaushik Das, Nicolaos A. Cutululis
DTU Wind Energy
Technical University of Denmark
Frederiksborgvej 399, 4000 Roskilde, Denmark
Email: dhmi@dtu.dk, juru@dtu.dk, kdas@dtu.dk, niac@dtu.dk

***Abstract*—An optimization framework for automated design of offshore wind farms collection systems is proposed in this paper. The core of the framework consists of a metaheuristic algorithm, namely a Genetic Algorithm (GA). The GA is designed for searching high-quality feasible solutions in terms of the capital expenditure ($CAPEX_{cs}$); a subsequent step runs a power flow in order to calculate electrical power losses for estimating the collection systems share on the Levelized Cost of Energy ($LCOE_{cs}$). Finally, after several executions of the full framework, the feasible solution bringing the cheapest $LCOE_{cs}$ is selected. The main inputs are the coordinate's location of the wind turbines and the offshore substation (OSS), wind power production time series, and the set of considered cables for the collection system design. The proposed approach offers a full search space exploration for feasible solutions, while taking into account cables capacities and disallowing for cable crossings. The results show that this framework can find feasible solutions improving benchmark methods by 8%.**

I. Introduction

Offshore wind energy represents one of the fastest and most steadily growing renewable technologies. The penetration level has increased almost five times in the last seven years, reaching the impressive globally total installed capacity of nearly 19 GW [1]. This growth is mainly explained by reductions in costs of the technology [2]: the LCOE has dropped recently from 240 USD/MWh to 170 USD/MWh. In terms of the total CAPEX, the electrical infrastructure can represent more than 10%, depending whether turbines are fixed-bottom or floating [3]. One of the components of the electrical infrastructure of Offshore Wind Farms (OWFs) is the collection system, for which finding good designs is becoming increasingly more complex, as OWFs tend to move towards coordinate-based design instead of following grid-based pattern (also called symmetrical designs), thanks to advancements on micrositing optimization techniques. This paper focuses on reducing the costs of the collection system, thus contributing to the overall minimization of economic metrics.

The collection system design and optimization problem has been studied with accentuated focus in the last 10 years. This problem is proved to be mathematically NP-hard [4], which means that there is no certificate on the ability to come up with algorithms to solve it in a polynomial time in function of the problem size. One could cluster all the existent methodologies for tackling this problem as follows: exact solutions, branch exchange solutions, C-MST heuristic solutions, metaheuristic solutions, and hybrid solutions. While each of these approaches exhibit advantages and disadvantages, requiring comprenhensive and rigorous studies to determine them, in general, metaheuristic algorithms do not require in-depth mathematical formalities and are a good tool for finding high-quality solutions in combinatorial problems.

In regard to heuristics, in [5]–[7] the authors focus on the development of deterministic techniques for designing the collection systems, such as Quality Threshold Clustering (QT) algorithm for grouping the wind turbines, and followed by the interconnection of them by applying Dijkstra's Minimum Spanning Tree (MST) algorithm. In [6], unsupervised learning algorithms for clustering are applied, which depend strongly on initial conditions, after that by adding Steiner splices, Dijkstra is used leading to a reduction of total length. In [7] is proposed a method for avoiding forbidden areas. All the previous works are intended to cover onshore wind farms. OWFs are the focus of [8]–[10]; in [8] a simple Prim algorithm to form the MST is used, getting solutions for different substation locations. Likewise, in [9], and [10], a deterministic algorithm is proposed using a dynamic objective function depending on the calculated LCOE, modifying in each iteration the cable sizing. In OWFs is preferred by the developers to avoid cable crossings (one installed above the other), because of mainly two reasons: hot-spots can be created due to the contact between those cables, requiring extra thermal insulation to avoid failures, and in case of a single failure on the bottom cable, all those cable on the top would have to be removed due to their physical installation. All the previous works mentioned before have the disadvantage of using deterministic techniques that can get trapped in minimals and disregard cable crossings.

Metaheuristic techniques encompass not only GA, but also others such as Particle Swarm Optimization (PSO). In [11] and [12] a PSO approach is used to optimize not only the collection system, but also the transmission system; through this technique, the main idea is translated from a purely deterministic fashion, to a probabilistic one, where is more likely to find the global minimum, albeit not formal proof in terms of solution quality and time can be formulated. The main disadvantage of the latest works is that the problem is tackled from a MST perspective, meaning that parallel cables can be placed, being this a not-so-common practice by OWF developers. GAs has been used in works such as [4], [13],

and [14]. In [4] is not very clear, among other things, the penalization strategy and how cable crossings can be avoided, therefore their results can not be reproduced. In [13] the search space is artificially restricted, and it seems that crossings are allowed. Similarly, in [14] only radial solutions can be found and it does not optimize for total costs.

The contribution of this paper is to propose a GA algorithm that solves the optimization problem while considering the full search space of the problem. An implementation of genetic algorithm that accounts for cable capacity and cable crossings constraints is proposed and a detailed description of this method is presented. The full proposed method calculates the LCOE_{cs} associated to the collection system of cables in each solution. At the end the best solution is output in a ergodic-fashion.

The paper is structured as follows. The optimization framework is explained in Section II, then in Section III the methodology is explained in detail, in Section IV two case studies are analyzed, and in Section V the conclusions are presented.

II. Optimization Framework

The optimization framework comprises the cost model, the core optimization model, and the general scheme nesting different methods. In developing the framework, several assumptions have been made, as they are presented in the following.

A. Assumptions

- The OWF is composed of one offshore substation (OSS) and a group of wind turbines (WTs). The location of these elements is known.
- The target size of the wind farm is between fifty and sixty turbines.
- The length of the cables is the horizontal trenching length (i.e. the euclidean distance between two points in the plane).
- The topology of the grid is based on a radial network, star network or a combination of both.
- Each cable segment in the collection system must be sized using the standard [15].
- Cable crossings are not allowed, except at the endpoints of each segment, where both the OSS and WTs are located.

B. Cost Model

The cost of the optimization model is given by the cost of the horizontal trenching length of the cables. Given a list of cables with its corresponding electrical parameters, the unitary cost of each cable (in €/km) is calculated by using the cost function (1) proposed in [16]. This cost function uses the rated voltage of the grid, the rated current of each cable, and a set of constants that have been obtained from an empirical study of cable costs. The cost function is scaled to take into consideration macroeconomics phenomenons, such as inflation and exchange rate.

$$C_t = A_{p_t} + B_{p_t}\,\mathrm{e}^{\left(\frac{C_{p_t} S_{n_t}}{10^8}\right)^2} \tag{1}$$

$$S_{n_t} = \sqrt{3} V_n I_{n_t} \tag{2}$$

Where:

- C_t: Cost of cable type t in €/km.
- V_n: Rated line to line voltage level in V.
- I_{n_t}: Rated current of cable type t in A.
- A_{p_t}, B_{p_t}, C_{p_t}: Cost constants. These values are given as tables depending on the voltage level [16].
- S_{n_t}: Rated power of cable type t in VA.

C. Optimization Model

The aim of the optimization model is to find a high quality solution for the OWF collection system design and optimization problem. The following formulation is based on a Capacitated Minimum Spanning Tree (C-MST) problem class, and includes a constraint to restrict cable crossings.

1) Objective Function: Let $G = (V, E)$ be a connected undirected graph with vertex-set V modelling the OSS (root) and WTs locations, and a edge-set E representing the potential connections between them. Introducing the binary decision variable x_e for each element $e \in E$, equal to to 1 if the corresponding edge is selected as part of the solution; the variable x_e defines unequivocally $G_S = (V, E_S)$, a graph forming a solution, with $E_S \subset E$. Following up, for the solution G_S, let G_{S_k} define the set of maximal subgraphs connected to the root by a single edge, such as $G_{S_k} = \{G_{S_{k_1}}, \cdots, G_{S_{k_n}}\}$, and $G_{S_{k_i}} = \left(V_{S_{k_i}}, E_{S_{k_i}}\right)$, $G_{S_{k_j}} = \left(V_{S_{k_j}}, E_{S_{k_j}}\right)$, with $V_{S_{k_i}} \subset V$, $V_{S_{k_j}} \subset V$, $V_{S_{k_i}} \cap V_{S_{k_j}} = \emptyset$, and $E_{S_{k_i}} \subset E_S$, $E_{S_{k_j}} \subset E_S$, $E_{S_{k_i}} \cap E_{S_{k_j}} = \emptyset$.

Additionally, let T be the set of cables considered for the optimization problem. Each cable type $t \in T$ has an associated unitary cost C_t, and an a maximum capacity U_t, expressed in terms of the nodes (turbines) that supports downstream, where $U_{max} = \max U_t$.

$$C_e^t = C_t \cdot length(e) \tag{3}$$

Each edge $e \in E$ has a cost C_e^t that is defined by (3), in function of the cable type and the edge trenching length. Therefore, let x_e^t model the binary decision variable, equal to 1 if the edge e is active through a cable type t, and 0 conversely.

$$\min\left(\text{CAPEX}_{\text{cs}} = \sum_{t \in T}\sum_{e \in E} C_e^t \cdot x_e^t\right) \tag{4}$$

The objective function minimizes the total cable layout cost as defined in (4).

2) Constraints:

$$deg(v) \geq 1 \quad \forall v \in V \tag{5}$$

$$x_e = \sum_{t \in T} x_e^t \quad \forall e \in E \tag{6}$$

$$\sum_{e \in E} x_e = \|V\| - 1 \tag{7}$$

$$\left\| V_{S_{k_i}} \right\| \leq U_{max} \quad \forall G_{S_{k_i}} \in G_{S_k} \tag{8}$$

$$x_q + x_w \leq 1 \quad \forall \{q, w\} \in C \tag{9}$$

$$x_e \in \{0, 1\} \tag{10}$$

$$x_e^t \in \{0, 1\} \tag{11}$$

The enforcement of connectivity between vertices and that the graph is a tree is achieved by satisfying Constraints (5) and (7) simultaneously. The first indicates that all nodes having a degree of at least one. The the second one forces the graph to have the same amount of active edges as the total number of nodes minus one. Constraint (6) enforces that each active edge has one and only one type of cable. To abide the cable capacity restrictions Constraint (8) is implemented. Each set of nodes of the subgraphs G_{S_k} has to have a smaller number of nodes than the maximum capacity cable from the set of cables. Finally, the cable crossings restriction is shown in Constraint (9): It is defined by considering a generic input set, $C \subset E \times E$, of pairs of crossing edges with the property that two crossing edges q and w cannot be active simultaneously.

After the convergence of the GA, a LCOE_{cs} metric is used in order to assess the final quality of the obtained solution, as expressed by (12), where r is the rate of return, an economic factor regarding bank interest and inflation rate (assumed as 5% in this paper), N_y is the project lifetime (assumed as 30 years), and E_{net} is the produced annual energy accounting for power losses (in MWh) [10].

$$\text{LCOE}_{\text{cs}} = \frac{\text{CAPEX}_{\text{cs}} r (1+r)^{N_y}}{((1+r)^{N_y} - 1) E_{net}} \tag{12}$$

D. General framework

The optimization framework is composed by two main processes: the solver and a power flow analysis. The solver is based on GAs and it is described in detail in this paper. The power flow analysis consists on a power flow calculation in order to find the losses associated with the solution given by the solver, allowing the calculation of the LCOE_{cs}.

The optimization framework workflow is described in Figure 1. Since GAs are non-deterministic and do not guarantee finding the optimal solution, the process is ran n times, comparing the LCOE_{cs} of the different solutions in the end.

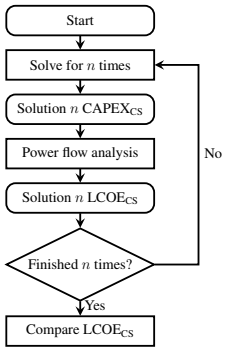

Fig. 1. Optimization framework

III. Methodology

A. Genetic algorithm

Genetic algorithms (GAs) are iterative processes in which a population of candidate solutions, also known as individuals, are evolved towards a better solution. Each individual has a chromosome, which is a set of properties that can be altered through a predefined set of genetic operators. Each individual is a solution to the problem with the variables representing the existence of a cable over an edge of the complete graph using a binary encoding. A more comprehensive explanation of GAs can be found in [17].

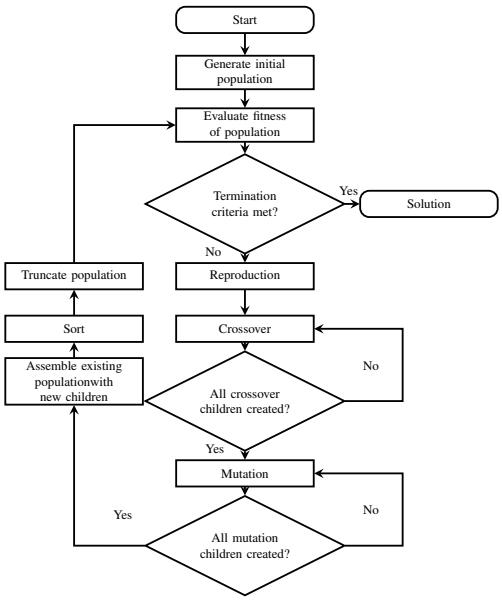

Fig. 2. GA flowchart

B. Fitness assessment

The general work flow of the GA can be seen in Figure 2. The genetic operators implemented are reproduction, crossover and mutation. Reproduction, simulating a roulette

wheel, selects the top performers in a population and forms a mating pool. This will later be used to by the crossover operator to create a new set of individuals. The crossover operator exchanges variables between two parent strings to create individuals. The crossover operator chosen is uniform crossover. The mutation operator creates new children by assigning a random probability for a set of random variables to change their value. The parameter mu controls the mutation rate, which is given in terms of how many variables can be changed each time the operator works.

The genetic algorithm is based on an elitist approach, each iteration represents a new population comprised of the individuals from the previous generation pop_{total} and the new children populations, pop_{cross} and pop_{mu}. The individuals are then ranked according to their fitness value. Finally, the population is truncated to the original population size pop_{total}, eliminating the weakest individuals. This approach allows the algorithm to converge faster as it does not need to re-discover solutions discarded in previous generations.

Each individual goes through a fitness assessment that the determines the cost of the individual. The fitness assessment implements the mathematical formulation proposed in Section II as a fitness function, (13). The fitness function represents the objective function by assessing the cost of the layout of each individual and penalizing its cost if the constraints are violated.

$$Z = \sum_{i=1}^{n} c_i w_i x_i + P \tag{13}$$

Where:

- Z is the fitness of the individual. If no penalizations apply it is also the final cost of the collection system.
- c is the cost of the cable selected, if no cable has been selected the value is 1.
- w is the trenching length of each edge of the complete graph.
- x is the binary string of variables that represent whether an edge of the complete graph is active of not.
- P is the sum of the penalizations that apply to the individual being assessed.

The implementation of constraints from the mathematical formulation is achieved in two ways. Equation (6) is implemented implicitly through the use of binary variables on the x vector, this only allows for only one cable to be built over an edge. The rest of the constraints are implemented via the use of penalizations.

Total connectivity deals with (5), the implementation is achieved doing a depth-first search and checking the connectivity of all nodes. *Tree graph*, checks that the graph is indeed a tree, the condition is described in (7). *Cable capacity* is the implementation of the constrain described in (8). First the tree is transformed into a directional tree rooted at the substation. Then a depth-first search is performed and the number of nodes accessible from each node has to be smaller than the maximum capacity cable available. *Cable crossings restriction*, (9), is implemented by checking intersections in a set composed of all possible pairs of active edges in the solution.

A hierarchy is established among the penalizations for the constraints through the use of conditional functions and through the cost given to each penalization. The need for a hierarchy is two-fold, the first reason being that in order to calculate the number of nodes per branch the graph needs to be a tree. The second reason is that certain functions used to analyze the cable capacity and cable crossings constraints use large amounts of computational power and it is a unproductive to run them if the solution is already known to be unfeasible.

In terms of the order of the constraint assessment, first both the total connectivity and tree graph constraints are determined. If both constraints are met then capacity constraint is calculated. Again if this constraint is satisfied then the cables crossing restriction constrained is analyzed. In this way time is not wasted in computational intensive tasks.

In terms of the penalization cost they are ranked by importance, with the most important constraints having the higher costs. Each penalization is assigned a base cost differentiated by several orders of magnitude from the others, ensuring that, in the case of proportional penalizations the constraints do not interfere with each other.

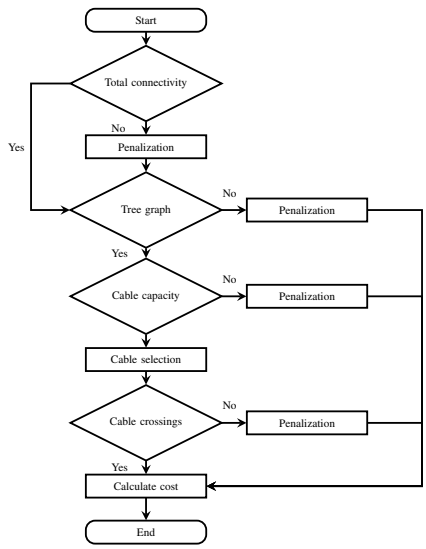

Fig. 3. Fitness assessment flowchart

The total connectivity penalization is assigned the highest cost to ensure that all elements are connected. The tree constraint penalization is proportional to the number of extra edges that impede the formation of a tree graph. The cable constraint penalization is proportional to the number of cables that do not meet the constraint. Finally, the cable crossing restriction penalization has the lowest cost and it is proportional to the number of crossings detected.

After each of the constraint analysis the fitness cost is calculated which includes the addition of the corresponding

penalizations.

The cable selection process is a method for choosing the appropriate cable from a list for each segment. This method is only done once the cable capacity constraint is met, as it requires that at least the highest capacity cable of the list is supported in the solution. The process assigns the smallest cross section possible to each segment according to the number of wind turbines being supported upstream. In doing so the cost is also minimized, as the size of the cross section is correlated to the cost of the cable.

C. Termination criteria

The genetic algorithm finishes the optimization process and outputs a solution when either of the following conditions are met:

- Iteration number: The process stops after a set number of iterations it_{max}
- Stall of the fitness value: The process stops if the fitness value does not change for a fixed amount of iterations it_{stall}, shown in (14) where i is a set that varies each generation according to the iteration number it.

$$Z_i = Z_{i+1} \quad \forall i \in \{it - it_{stall} + 1, it - 1\} \tag{14}$$

IV. Case Studies

Two case studies are analyzed to exemplify the usefulness of the optimization framework here presented, the two OWFs are Ronne Bank North (RBN) and Ronne Bank South (RBS). These are proposals part of the Baltic InteGrid Project and show a grid pattern with bigger spacing between wind turbines on the horizontal axis than in the vertical axis. Each case is presented with three collection system designs; one empirical design (ED) and two solutions given by the GA (GA1 and GA2). Due to the stochasticity of the GA, it converges into different solutions for GA1 and GA2.

Table I contains the list of cables considered for the optimization process, with the $Capacity$ given in terms of the number of WTs rated at 8 MW supported by each cable in a 66 kV grid. Table II summarizes the characteristics of each OWF. Table III shows the key results.

TABLE I
List of available cables

Cross section [mm^2]	95	120	150	185	240	300	400	500	630	800	1000
Capacity [Number of WT]	4	4	5	6	6	7	8	9	10	11	11
Price [k€/km]	270	287	303	327	362	395	440	497	558	628	694

TABLE II
Wind farm characteristics

	RBN	RBS
WTs [number]	27	53
Rated power per WT [MW]	8	8
Grid voltage [kV]	66	66
AEP [MWh]	905,675	1,777,806

TABLE III
Results

	RBN			RBS		
	ED	GA1	GA2	ED	GA1	GA2
Losses [MWh/year]	17.04	26.92	16.26	77.34	64.47	63.37
CAPEX$_{cs}$ [M€]	8.14	7.68	7.80	26.44	24.26	24.34
LCOE$_{cs}$ [€/MWh]	0.638	0.602	0.611	1.055	0.968	0.971
Improvement [%]	-	6	4	-	8	8

The first case study, dealing with RBN, shows that the GA solutions improve both the active power losses and the investment cost, leading up to a 6% decrease compared to the empirical design in terms of the LCOE$_{cs}$. Figure 5 shows that the GA solution prefers vertical connections between the wind turbines as these are shorter than the horizontal ones. The GA uses higher capacity cables by clustering the WT in bigger groups, effectively reducing the number of cables coming out of the OSS. The empirical design, Figure 4, has five cables entering the OSS while the GA solution, Figure 5, has four.

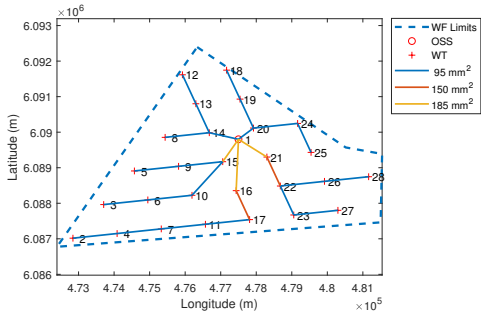

Fig. 4. Ronne Bank North - Empirical Design

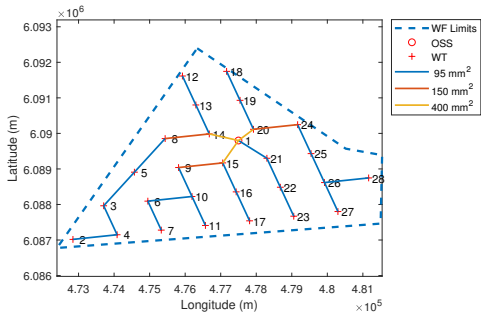

Fig. 5. Ronne Bank North - GA Solution 1

The second case study, RBS, shows reductions both in terms of the losses and of the investment costs. These lead to reductions on the LCOE$_{cs}$ of 8%. Figure 4 shows the empirical design proposed. Figure 7 shows one of the GA solutions. The

GA shows a tendency of using the vertical connections instead of the horizontal ones as they are shorter. It also shows the same behaviour as in the previous case by clustering the wind turbines in groups of 5-8 WT. In areas that are difficult to reach areas it opts for a higher capacity cable, such as the subtree that starts in the OSS and branches at turbine number 36.

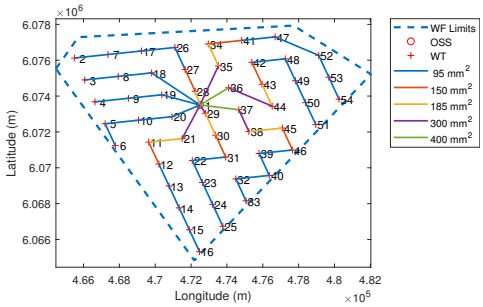

Fig. 6. Ronne Bank South - Empirical Design

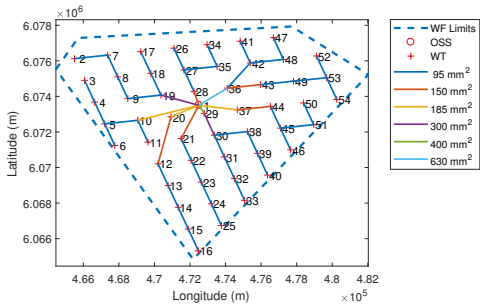

Fig. 7. Ronne Bank South - GA Solution 2

The challenge for solving RBS compared to RBN is twofold, one is the increased amount of connections combinations possible and the other deals with the complexity of the constraints. In terms of the constraints, in both case studies the maximum available cable capacity is 11 WTs. In RBS, with almost double the amount of WTs, it becomes more challenging avoiding cable crossings thus making the process of finding a feasible solution more complicated. Since the framework only deals with one substation, RBN with a total install capacity of 424 MW is indicative of the current upper limit in terms of the number WTs per OSS for a typical OWF.

V. Conclusion

The collection system design of offshore wind farms is becoming increasingly more complex, thus finding economical empirical based solutions has become a more arduous task. This article presents an optimization framework based on GA that is successful in solving the collection system design for a typical OWFs. The framework includes the exploration of the full search space of problem and several realistic constraints. The effectiveness is proven in two case studies showing reductions on the $LCOE_{cs}$ of up to 8% when compared to empirical solutions. Future work includes the analysis of the computational performance of the optimization framework and the inclusion of a reliability analysis to solve looped and meshed topologies.

Acknowledgment

This research has received funding from the Baltic InteGrid Project (http://www.baltic-integrid.eu/).

References

[1] G. W. E. C. GWEC, "Global Wind Report. Annual Market Update 2017," Tech. Rep., 2017. [Online]. Available: http://gwec.net/publications/global-wind-report-2/.[Accessed Oct 29, 2018]

[2] International Renewable Energy Agency, "Innovation Outlook: Offshore Wind, Summary for Policy Makers," p. 16, 2016.

[3] X. Sun, D. Huang, and G. Wu, "The current state of offshore wind energy technology development," *Energy*, vol. 41, no. 1, pp. 298–312, 2012.

[4] A. M. Jenkins, M. Scutariu, and K. S. Smith, "Offshore wind farm inter-array cable layout," in *IEEE PowerTech at Grenoble*, 2013, pp. 1–6.

[5] S. Dutta and T. J. Overbye, "A clustering based wind farm collector system cable layout design," in *IEEE Power and Energy Conference at Illinois (PECI)*, 2011, pp. 1–6.

[6] S. Dutta and T. J. Overbye, "Design Considering Total Trenching Length," *IEEE Transactions on Sustainable Energy*, vol. 3, no. 3, pp. 339–348, 2012.

[7] S. Dutta and T. J. Overbye, "A graph-theoretic approach for addressing trenching constraints in wind farm collector system design," in *IEEE Power and Energy Conference at Illinois (PECI)*, 2013, pp. 1–5.

[8] P. Hou, W. Hu, and Z. Chen, "Offshore substation locating in wind farms based on prim algorithm," in *IEEE Power and Energy Society General Meeting*, 2015, pp. 1–5.

[9] P. Hou, W. Hu, and Z. Chen, "Offshore wind farm cable connection configuration optimization using Dynamic Minimum Spanning Tree algorithm," *50th Power Engineering Conference (UPEC)*, pp. 1–6, 2015.

[10] P. Hou, W. Hu, C. Chen, and Z. Chen, "Optimisation of offshore wind farm cable connection layout considering levelised production cost using dynamic minimum spanning tree algorithm," *IET Renewable Power Generation*, vol. 10, no. 2, pp. 175–183, 2016.

[11] P. Hou, W. Hu, and Z. Chen, "Optimisation for offshore wind farm cable connection layout using adaptive particle swarm optimisation minimum spanning tree method," *IET Renewable Power Generation*, vol. 10, no. 5, pp. 694–702, 2016.

[12] P. Hou, W. Hu, Z. Chen, and C. Chen, "Overall Optimization for Offshore Wind Farm Electrical System," *Wind Energy*, vol. 20, no. 2016, pp. 1017–1032, 2017.

[13] O. Dahmani, S. Bourguet, P. Guerin, M. Machmoum, B. D. Université, P. Rhein, and L. Josse, "Optimization of the internal grid of an offshore wind farm using Genetic algorithm," in *IEEE PowerTech at Grenoble*, 2013.

[14] F. González-Longatt and P. Wall, "Optimal electric network design for a large offshore wind farm based on a modified genetic algorithm approach," *IEEE Systems Journal*, vol. 6, no. 1, pp. 164–172, 2012.

[15] IEC, "IEC-60287-1-1: Electric cables - Calculation of the current rating," Tech. Rep., 2001.

[16] S. Lundberg, "Configuration study of large wind parks," Ph.D. dissertation, 2003.

[17] K. Deb, *Optimization for Engineering Design: Algorithms and Examples, 2nd ed.* PHI, 2013.

APPENDIX C5

"Closed-Loop Two-Stage Stochastic Optimization of Offshore Wind Farm Collection System"

J.A. Pérez-Rúa, S. Lumbreras,
A. Ramos, and N. A. Cutululis

under review
in *Journal of Physics: Conference Series*
EAWE TORQUE 2020
Delft, Netherlands

Closed-Loop Two-Stage Stochastic Optimization of Offshore Wind Farm Collection System

Juan-Andrés Pérez-Rúa[1], Sara Lumbreras[2], Andrés Ramos[2] and Nicolaos A. Cutululis[1]

[1]DTU Wind Energy, Technical University of Denmark, Frederiksborgvej 399, 4000 Roskilde, Denmark.
[2]Institute for Research in Technology, Comillas Pontifical University, Calle de Alberto Aguilera 23, 28015 Madrid, Spain.

E-mail: juru@dtu.dk

Abstract. A two-stage stochastic optimization model for the design of the closed-loop cable layout of an Offshore Wind Farm (OWF) is presented. The model consists on a Mixed Integer Linear Program (MILP) with scenario numeration incorporation to account for both wind power and cable failure stochasticity. The objective function supports simultaneous optimization of: (i) Initial investment (network topology and cable sizing), (ii) Total electrical power losses costs, and (iii) Reliability costs due to energy curtailment from cables failures. The mathematical optimization program is embedded in an iterative framework called PCI (Progressive Contingency Incorporation), in order to simplify the full problem while still including its global optimum. The applicability of the method is demonstrated by tackling a real-world instance. Results show the functionality of the tool in quantifying the economic profitability when applying stochastic optimization compared to a deterministic approach, given certain values of failure parameters.

1. Introduction

Offshore Wind Farms (OWFs) are shaping up as one of the main drivers towards the transition to carbon-neutral power systems. Ambitious targets set by the European Commission see offshore wind power reaching 450 GW by 2050 [1]. Offshore electrical systems have a sizeable weight in the capital investments, reaching 15% of the total initial expenses [2], with the power cables being a backbone component for the Balance of Plants (BoP) value and supply chain. Furthermore, power cables can be single points of failure, leading to strongly undesired contingency [3]. Shallow waters, buried depth, seabed terrain movements [4], and electro-thermal stress, are differential factors in the context of OWFs, giving rise to higher failure rates of submarine cables compared to the reported by other offshore industries, such as oil and gas [5] [6].

OWF export cables are generally built with redundancy, as the high voltage levels and long distances increase the failure probability. Likewise, cables for collection systems may also be arranged to provide greater levels of reliability, typically resulting in a closed-loop topology. However, tailor-made models to design collection system with a closed-loop structure, using global optimization, integrated with analytical methods for reliability assessment, are not readily available in the scientific literature. Radial topology, i.e., without electrical redundancy (trees according to graph theory [7]) has been the most common subject of study in literature in this context, and currently represents the most frequent choice by OWF developers. However, with the increase in the OWFs' capacities and the trend of moving towards subsidy-free operating regimes, quantification of economic suitability for closed-loop or radial topologies is becoming essential.

Radial topology for OWF collection systems falls into a standard class of computational problems, being classified in computational complexity as NP-Hard [8]. Thus, scalability is the main challenge, as state-of-the-art OWFs are in the order of hundred of Wind Turbines (WTs). Mathematical models are proposed and solved through global optimization solvers in [9], [8], [10], [11], and [12]. Nevertheless, a deterministic approach is followed given the assumption of no cable failure over the project lifetime.

Contrarily, studies adopting stochastic techniques are available in [13], [14], and [15]. A Mixed Integer Quadratic Program is presented in [13], which aims to analyze the suitability of having redundancy for system components subject to failure, by solving the full stochastic optimization program including all possible contingencies. Model reduction implementing a Mixed Integer Linear Program along with Progressive Contingency Incorporation (PCI), and decomposition strategies is performed in [14] and [15], proving the ability to decrease computational resources while solving to optimality small-scale OWFs (less than or equal to 30 WTs).

The latter papers provide relevant advances in stochastic optimization supporting several wind power and cable failure scenarios. Nonetheless, the inclusion of practical engineering constraints such as non-crossing of cables, closed-loop topology, and losses inclusion in the objective function are missing in these papers. This gap is covered in this manuscript, where a MILP optimization program based computational tool is presented, supporting decision makers during the design stage of OWFs. An algorithmic framework is developed targeting further computational simplification, supporting an objective function combining simultaneously initial investment, total electrical power losses, and energy curtailment due to cables failures. A recourse problem (the problem of minimizing the expected cost for energy curtailment) is solved to assess the benefits of stochastic optimization compared to the deterministic counterpart.

This paper is structured as follows: In Section 2 the optimization model is explained in detail; followed by Section 2.4, where the algorithmic framework is explained. Finally, a case study is performed in Section 2.4. The work is finalized with the conclusions in Section 5.

2. Optimization model

2.1. Graph and model representation

The aim of the optimization is to design a closed-loop cable layout of the collection system for an OWF, i.e., to interconnect through power cables the n_{w} WTs to the available Offshore Substation (OSS), while providing a redundant power evacuation route.

Let $\boldsymbol{N}_{\mathrm{w}} = \{2, \cdots, 1 + n_{\mathrm{w}}\}$. Besides, let the points set be $\boldsymbol{N} = \{1\} \cup \boldsymbol{N}_{\mathrm{w}}$, where the element $i \in \boldsymbol{N}$, such as $i = 1$ is the OSS.

The Euclidean distance between the positions of the points i and j, is denoted by d_{ij}. These inputs are gathered in a weighted undirected graph $G(\boldsymbol{N}, \boldsymbol{E}, \boldsymbol{D})$, where $\boldsymbol{N}$ is the vertex set, $\boldsymbol{E}$ the set of available edges arranged as a pair-set, and $\boldsymbol{D}$ the set of associated euclidean distances for each element $[ij] \in \boldsymbol{E}$, where $i \in \boldsymbol{N} \wedge j \in \boldsymbol{N}$.

In general, $G(\boldsymbol{N}, \boldsymbol{E}, \boldsymbol{D})$ is a complete undirected graph. It may be bounded by defining uniquely those edges connecting the $\upsilon < n_{\mathrm{w}}$ closest WTs to each WT, and by the $\sigma < n_{\mathrm{w}}$ edges directly reaching the OSS from the WTs.

Likewise, let $\boldsymbol{T}$ be a predefined list of available cable types, and $\boldsymbol{U}$ be the set of cable capacities sorted in non-decreasing order as in $\boldsymbol{T}$, being measured in Amperes (A), such that u_t is the capacity of cable $t \in \boldsymbol{T}$. Furthermore, each cable type $t \in \boldsymbol{T}$ has a cost per unit of length, c_t (including capital and installation costs), in such a way that $\boldsymbol{U}$ and $\boldsymbol{T}$ are both comonotonic. The

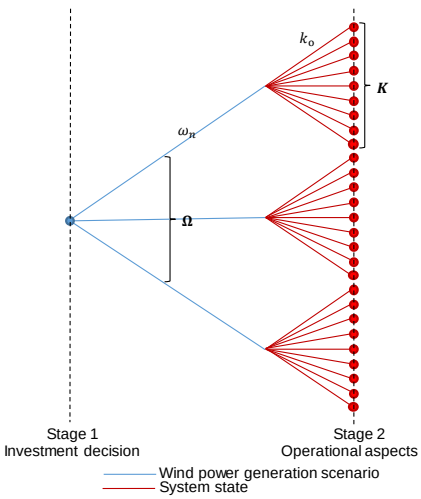

Figure 1. Scenario tree, Υ

set of expenditures per meter is defined as $\boldsymbol{C}$.

The problem is formulated as a stochastic optimization program modelled with two stages: investment (construction) and operation. In Figure 1 is presented a graphical representation of the two stages of the model. In this figure it can be seen that uncertainty is represented by means of a scenario tree (Υ), expressing simultaneously how the stochasticity is developing over time (at the moment of the investment decision, uncertainties of the random parameters are present), the different states of the random parameters (the instances of the random process multiply in function of the generation scenarios and installed cables), and the definition of the non-anticipative decisions in the present (in real-time operation the investment decision can not be changed).

The set of wind power generation scenarios is $\boldsymbol{\Omega}$ (blue lines in Figure 1), they represent power states for bins of wind speed, while the representative system states are $\boldsymbol{K}$ (red lines in Figure Figure 1). The nominal generation scenario is ω_{n}, and the base system state (k_{o}) represents the case of no failures. The base case is therefore represented by the scenario $\{\omega_{\mathrm{n}}, k_{\mathrm{o}}\}$. A wind power generation scenario ω has associated a duration time τ^{ω} (in hours), and power magnitude ζ^{ω} (in per unit, p.u.), and each system state k, a system probability ψ^{k}. The cost of energy in €/Ah is denoted by c_{e}.

The system probability ψ^{k} is calculated using a discrete Markov model to define the cables' complementary states: available, and unavailable. Through this, it is possible to calculate ψ^{k} given the failure statistical parameters Mean Time Between Failures (MTBF) and Mean Time To Repair (MTTR) [16]. In the same way, given the low failure rates of these components a N-1 criterion must be considered in each system state [17]; this means that elements remaining in operation in a contingency are capable of accommodating the new operational situation, and it is very unlikely that other element would fail simultaneously.

The first stage variables are the binary variables $x_{ij,t}$, and y_{ij}; where $x_{ij,t}$ is equal to one if active edge $[ij]$ ($y_{ij} = 1$) uses cable type $t \in \boldsymbol{T}$. The second stage variables are the continuous variables $I_{ij}^{\omega,k}$, $\theta_{i}^{\omega,k}$, and $\delta_{j}^{\omega,k}$. The electrical current in edge $[ij]$ in wind power generation scenario $\omega \in \boldsymbol{\Omega}$, and system state $k \in \boldsymbol{K}$ is represented by $I_{ij}^{\omega,k}$. While the voltage phase at each WT busbar is $\theta_{i}^{\omega,k}$. The curtailed current at wind turbine j in wind power generation scenario $\omega \in \boldsymbol{\Omega}$, and system state $k \in \boldsymbol{K}$ is $\delta_{j}^{\omega,k}$. Note that $\delta_{j}^{\omega,k}$ is bounded by the current generated at j in the same scenario, I_{j}^{ω}, where $I_{j}^{\omega} = \frac{P_n \cdot \zeta^{\omega} \cdot 1000}{\sqrt{3} \cdot V_n}$, where P_n is the nominal power of an individual WT, and V_n the line-to-line nominal voltage of the system.

2.2. Cost coefficients and objective function

2.2.1. Neglecting total electrical power losses The objective function in this section consists of a simultaneous valuation of the total initial investment plus reliability. The investment is intuitively computed as the sum of cables costs installed in each edge $[ij]$; on the other hand, reliability is quantified through the estimation of the economic losses due to cables failures, as the result of undispatched current from each WT. In this way, the objective function is formalized as:

$$\min \overbrace{\sum_{[ij]\in\boldsymbol{E}} \sum_{t\in\boldsymbol{T}} c_t \cdot d_{ij} \cdot x_{ij,t}}^{\text{Investment}} + \overbrace{c_{\mathrm{e}} \cdot \sum_{i\in\boldsymbol{N}_{\mathrm{w}}} \sum_{\omega\in\boldsymbol{\Omega}} \sum_{k\in\boldsymbol{K}} \tau^{\omega} \cdot \psi^{k} \cdot \delta_{i}^{\omega,k}}^{\text{Operation/Reliability}} \tag{1}$$

The sum of system states probabilities must be equal to one, $\sum_{k\in\boldsymbol{K}} \psi^{k} = 1$, given the mutually exclusive nature of the considered events (at most one cable is subject to failure, N-1 criterion).

A system state k represents the failure of a single cable in an active edge $e \in \boldsymbol{E}$, therefore the system probability for the state ψ^{k} is considered equal to this failure probability. This implies that the availability probability of the other installed cables is considered to be equal to one in this scenario [13], representing a conservative approach as the value of the parameter ψ^{k} is slightly overestimated (the system probability is the multiplication of each installed cable state probability).

2.2.2. Considering total electrical power losses Total electrical power losses are non-linear in function of the current, cable type, and total length [7]. The designer must try to find a proper balance between modelling fidelity and optimization program complexity.

A pre-processing strategy is proposed in this manuscript in order to incorporate this factor into the objective function. This consists on calculating the quadratic total electrical power losses in advance of solving the model, by including in the objective function the costs associated to this factor.

The set of cable capacities in terms of number of supportable WTs is defined in the following expression

$$f_t = \left\lfloor \frac{\sqrt{3} \cdot V_n \cdot u_t}{P_n \cdot 1000} \right\rfloor \quad \forall t \in \boldsymbol{T} \tag{2}$$

Let the new cable type set be

$$\boldsymbol{T'} = \left\{ \underbrace{1, 2, \cdots, f_1}_{t_1}, \underbrace{f_1 + 1, \cdots, f_2}_{t_2}, f_2 + 1, \cdots, \underbrace{f_{|\boldsymbol{T}|-1} + 1, \cdots, f_{|\boldsymbol{T}|}}_{t_{|\boldsymbol{T}|}} \right\} \tag{3}$$

This implies that $\boldsymbol{T'}$ is the discretized form of the maximum capacity $U = \max \boldsymbol{U}$. Note that this is translated into the creation of additional variables $x_{ij,t'} : t' \in \boldsymbol{T'}$. Likewise, if the *floor function* in (2) is replaced by a *decimal round down function*, and $\boldsymbol{T'}$ is also discretized using the same decimal steps, then the number of variables will increase accordingly, to the benefit of gaining in accuracy for the cable capacities.

In $\boldsymbol{T'}$ is contained the non-dominated cable sub-types from $\boldsymbol{T}$; this means that each cable sub-type $t' \in \boldsymbol{T'}$ is related to a cable type $t \in \boldsymbol{T}$, inheriting physical properties such as cost per meter (c_t), electrical resistance per meter (R_t), and electrical reactance per meter (X_t); see (3) where this relation is presented graphically. Acknowledging that the investment cost of a cable t exceeds the electrical power losses costs, then the selected cable sub-type to connect n WTs will always be the cheapest (smallest) cable with sufficient capacity, rather than a bigger one with lower electrical power losses as the electrical resistance decreases with size.

As a consequence of the aforementioned, let a new cable capacities set be:

$$\boldsymbol{U'} = \left\{1, 2, \cdots, f_1, f_1 + 1, \cdots, f_2, f_2 + 1, \cdots, f_{|\boldsymbol{T}|-1} + 1, \cdots, f_{|\boldsymbol{T}|}\right\} \cdot \frac{P_n \cdot 1000}{\sqrt{3} \cdot V_n} \tag{4}$$

Let the functions $f(t')$, $g(t')$, and $h(t')$ calculate the cost, electrical resistance, and electrical reactance per meter for cable sub-type t', respectively, which are inherited from a cable type t. Whereby, the objective function for simultaneous optimization of investment, electrical losses, and reliability is:

$$\min \overbrace{\sum_{[ij] \in \boldsymbol{E}} \sum_{t' \in \boldsymbol{T'}} \left(f(t') + \underbrace{3 \cdot 1.5 \cdot g(t') \cdot \left(\frac{c_{\mathrm{e}}}{\sqrt{3} \cdot V_n \cdot 1000} \right) \cdot \sum_{\omega \in \boldsymbol{\Omega}} \left(u'_{t'} \cdot \zeta^{\omega} \right)^2 \cdot \tau^{\omega}}_{=h(t')\text{. Pre-processing for total electrical power losses}} \right) \cdot d_{ij} \cdot x_{ij,t}}^{\text{Investment plus total electrical power losses}} + \overbrace{c_{\mathrm{e}} \cdot \sum_{i \in \boldsymbol{N}_{\mathrm{w}}} \sum_{\omega \in \boldsymbol{\Omega}} \sum_{k \in \boldsymbol{K}} \tau^{\omega} \cdot \psi^{k} \cdot \delta_i^{\omega,k}}^{\text{Operation/Reliability}} \tag{5}$$

The factor $(3 \cdot 1.5)$ in (5) accounts the joule, screen and armouring losses for the three-phase system. The whole term for total electrical power losses ($h(t')$) is calculated for each $t' \in \boldsymbol{T'}$, before launching

the MILP program into the external solver. Therefore, the objective function is a linear weighting of the desired targets: investment, electrical losses, and reliability.

As discussed previously, one of the tasks of the designer is to balance out modelling fidelity and optimization program complexity. The objective function in (5) is a linear function, thus the following simplifications are assumed: (i) integer discretization in (3) which restricts the capacity of cables, and may cause overestimation of electrical losses. This can be diminished by decimal round down, and by increasing discretization steps in (4) at the expense of incrementing the number of variables correspondingly. (ii) Neglection of system states (cables failures) apart of the base state (no failures); however, this is the state with highest probability. (iii) Power flow estimation in a conservative fashion, i.e., overestimating the incoming power flow by neglecting the total power losses downstream. All those simplifications may impact the final layout, however their conservative nature means rather over-designing than impacting the robustness.

2.3. Constraints

In case total electrical power losses are considered, the cable types set is $\boldsymbol{T'}$, otherwise $\boldsymbol{T}$; same logic for $\boldsymbol{U}/\boldsymbol{U'}$, t/t', and $u_t/u'_{t'}$. This applies for the forthcoming mathematical expressions.

The first stage constraints are first presented. These constraints are only defined by the first stage variables, i.e., the investment decision.

In case edge $[ij]$ is active in the solution, then one and only one cable type $t \in \boldsymbol{T}$ must be chosen, as expressed in the next equation

$$\sum_{t \in \boldsymbol{T}} x_{ij,t} = y_{ij} \quad \forall [ij] \in \boldsymbol{E} \tag{6}$$

A closed-loop (sunflower petals) collection system topology is forced through the following expression

$$\sum_{\substack{j \in \boldsymbol{N} \\ j \neq i}} y_{ij} = 2 \quad \forall l \in \boldsymbol{N}_{\mathrm{w}} : l = i \vee l = j \tag{7}$$

Limiting the number of feeders (upper limit of ϕ feeders) connected to the OSS is carried out by means of

$$\sum_{i \in \boldsymbol{N}_{\mathrm{w}}} y_{ij} \leq \phi \quad j = 1 \tag{8}$$

The set $\boldsymbol{\chi}$ stores pairs of edges $\{[ij], [uv]\}$, which are crossing each other. Excluding crossing edges in the solution is ensured by the simultaneous application of the next linear inequalities along with (6)

$$y_{ij} + y_{uv} \leq 1 \quad \forall \{[ij], [uv]\} \in \boldsymbol{\chi} \tag{9}$$

The no-crossing cables restriction is a practical requirement in order to avoid hot-spots, and potential single-points of failure caused by overlapping cables [9]. Constraint (9) exhaustively lists all combinations of crossings edges. The constraints in (6) ensure that no active edges are crossing or overlapping between each other. These constraints thus link the variables y_{ij} and $x_{ij,t}$.

The second stage constraints are now deployed. These constraints are only defined by the second stage variables, i.e., the operational aspects. They are defined by the flow conservation, which also avoids disconnected solutions, and is considered by means of one linear equality per wind turbine as per

$$\sum_{\substack{i \in \boldsymbol{N} \\ j \neq i}} \sum_{\omega \in \boldsymbol{\Omega}} \sum_{k \in \boldsymbol{K}} I_{ji}^{\omega,k} - I_{ij}^{\omega,k} + \delta_j^{\omega,k} = I_j^{\omega} \quad \forall j \in \boldsymbol{N}_{\mathrm{w}} \quad \forall \omega \in \boldsymbol{\Omega} \quad \forall k \in \boldsymbol{K} \tag{10}$$

The set of tender constraints, useful to link first and second stage constraints, are lastly presented.

A DC power flow model is applied in this manuscript, in order to calculate the power flow distribution along the resultant electrical network. This model assumes no active power losses, nominal voltage at each bar, and no reactive power flow [18]. The DC power flow is forced with the following equations

$$I_{ij}^{\omega,k} - \frac{1000 \cdot V_n \cdot (\theta_i^{\omega,k} - \theta_j^{\omega,k})}{\sqrt{3} \cdot X_t \cdot d_{ij}} - M \cdot (1 - x_{ij,t}) - M \cdot r_{ij}^k \leq 0 \quad \forall [ij] \in \boldsymbol{E} \quad t \in \boldsymbol{T} \quad \forall \omega \in \boldsymbol{\Omega} \quad \forall k \in \boldsymbol{K} \tag{11}$$

$$-I_{ij}^{\omega,k} + \frac{1000 \cdot V_n \cdot (\theta_i^{\omega,k} - \theta_j^{\omega,k})}{\sqrt{3} \cdot X_t \cdot d_{ij}} - M \cdot (1 - x_{ij,t}) - M \cdot r_{ij}^k \leq 0 \quad \forall [ij] \in \boldsymbol{E} \quad t \in \boldsymbol{T} \quad \forall \omega \in \boldsymbol{\Omega} \quad \forall k \in \boldsymbol{K} \tag{12}$$

Where r_{ij}^k is a parameter equal to one if edge $[ij]$ is failed, or zero if otherwise, X_t is the electrical reactance per meter of cable t (in case of inclusion of total electrical power losses, let $X_{t'} = h(t')$), and M is a big enough number to guarantee feasibility for those inactive or failed components.

The cable capacities are not exceeded by including the next bilateral constraints.

$$\sum_{t \in \boldsymbol{T}} u_t \cdot x_{ij,t} \cdot (1 - r_{ij}^k) \geq I_{ij}^{\omega,k} \quad \forall [ij] \in \boldsymbol{E} \quad \forall \omega \in \boldsymbol{\Omega} \quad \forall k \in \boldsymbol{K} \tag{13}$$

$$\sum_{t \in \boldsymbol{T}} -u_t \cdot x_{ij,t} \cdot (1 - r_{ij}^k) \leq I_{ij}^{\omega,k} \quad \forall [ij] \in \boldsymbol{E} \quad \forall \omega \in \boldsymbol{\Omega} \quad \forall k \in \boldsymbol{K} \tag{14}$$

The current $I_{ij}^{\omega,k}$ may circulate either from i to j or viceversa.

Finally, Constraints (15) to (19) define the nature of the formulation by the variables definition, a MILP optimization program.

$$x_{ij,t} \in \{0, 1\} \quad \forall t \in \boldsymbol{T} \quad \forall [ij] \in \boldsymbol{E} \tag{15}$$

$$y_{ij} \in \{0, 1\} \quad \forall [ij] \in \boldsymbol{E} \tag{16}$$

$$-0.1 \leq \theta_i^{\omega,k} \leq 0.1 \quad \forall i \in \boldsymbol{N} \quad \forall \omega \in \boldsymbol{\Omega} \quad \forall k \in \boldsymbol{K} \tag{17}$$

$$-U \leq I_{ij}^{\omega,k} \leq U \quad \forall [ij] \in \boldsymbol{E} \quad \forall \omega \in \boldsymbol{\Omega} \quad \forall k \in \boldsymbol{K} \tag{18}$$

$$0 \leq \delta_i^{\omega,k} \leq I_i^{\omega,k} \quad \forall i \in \boldsymbol{N}_{\mathrm{w}} \quad \forall \omega \in \boldsymbol{\Omega} \quad \forall k \in \boldsymbol{K} \tag{19}$$

2.4. The stochastic optimization program

To summarize, the formulation of the MILP optimization program consists of the objective function (1) or (5), and the constraints defined in (6) - (19). Let this stochastic optimization program be denoted $P^{\boldsymbol{\Omega},\boldsymbol{K}}$.

3. Optimization framework

Since the two-stage variables scale-up exponentially as a function of the scenario tree size, the representative systems states must be limited [14]. The basic version of the stochastic optimization program presented in Section 2 encompasses the full set $\boldsymbol{E}$; each element $[ij]$ gives place to a system state k to form the system states set $\boldsymbol{K}$ (using the transformation function $\boldsymbol{K} = \Phi(\boldsymbol{E})$ which maps from edges set to system states set).

Nevertheless, the actual selected edges in a solution (i.e. a feasible point satisfying the optimality criteria) is only a subset $\boldsymbol{E'} \subset \boldsymbol{E}$; let the complement set $\boldsymbol{E''}$ contain the unused elements from $\boldsymbol{E}$, and let define the subset $\boldsymbol{E'''} \subset \boldsymbol{E''}$.

Trough an inactive edge $[ij]$ ($y_{ij} = 0$) there is no electrical current in any of the system scenarios according to (13) and (14). If there is no current through an edge, then its failure has no impact over the network power flow. This can be intuitively understood as comparing it with an open water tap which

causes no spill when pipes are broken, as there is no flow of water. As a consequence, only the subset $\boldsymbol{K'} \subset \boldsymbol{K}$ (related to) is necessary and sufficient to obtain the optimum in $P^{\boldsymbol{\Omega},\boldsymbol{K}}$.

Let the necessary and sufficient set $\boldsymbol{K'}$ encompass:

$$\boldsymbol{K'} = k_{\mathrm{o}} \cup \boldsymbol{K}_{\boldsymbol{E'}} \cup \boldsymbol{K}_{\boldsymbol{E'''}} \tag{20}$$

Where $\boldsymbol{K}_{\boldsymbol{E'''}}$ is the system states linked to the subset of unused edges $\boldsymbol{E'''}$, and $\boldsymbol{K}_{\boldsymbol{E'}}$ to $\boldsymbol{E'}$.

The formal mathematical proof is not deployed in this article, but this particular characteristic reveals a contingency structure which can be exploited in order to simplify the full problem $P^{\boldsymbol{\Omega},\boldsymbol{K}}$. This contingency structure opens the door for a Progressive Contingency Incorporation (PCI) strategy, aiming to find a proper set $\boldsymbol{K'}$ following an iterative approach. Algorithm 1 is presenting the PCI implementation.

In the first line a deterministic instance of the full problem is tackled. This means considering uniquely the scenario $\{\omega_{\mathrm{n}}, k_{\mathrm{o}}\}$. For this problem a valid assumption is to consider zero curtailed power. After this, the active edges of interest corresponding to the first stage optimization variables are stored as $\boldsymbol{E'}$, along with the obtained solution variables in $\boldsymbol{X}_{\mathrm{ws}}$ (where $\boldsymbol{X}_{\mathrm{d}}$ and $\boldsymbol{Y}_{\mathrm{d}}$ contains the solution sets corresponding to $x_{ij,t}$, and y_{ij} for the deterministic case, respectively). As no previous iteration has been conducted, cumulative solution variables are unavailable ($\boldsymbol{E}'_{\mathrm{o}}$). Since the second stage variables express contingency scenarios of the components delimited by the first stage variables, the tree Υ uniquely considers the failure states associated to those components. For the case presented in Algorithm 1, solely those feeders which satisfy the reliability level r_{c}, are subject to fail.

Parameter r_{c} defines the degree of connection towards the OSS, so for example, $r_{\mathrm{c}} = 1$ brings along the main feeders (rooted at $i = 1$), and $r_{\mathrm{c}} = 2$ includes the last ones together with the feeders connected to the main ones, and so on for $r_{\mathrm{c}} > 2$. By means of those parameters, the model can be further relaxed for large instances.

The Progressive Contingency Incorporation routine is started at line 4. The opening step is to intersect the current active edges set $\boldsymbol{E'}$, and the cumulative set $\boldsymbol{E}'_{\mathrm{o}}$. If the intersection set is equal to the current active edges $\boldsymbol{E'}$, then the process is terminated, otherwise more iterations are attempted. For the former case, the algorithm is stopped, with solution $[\boldsymbol{X}, \boldsymbol{Y}]$; for the latter case, the iterative process is continued to the subsequent iteration κ. Trivially, for $\kappa = 1$, $\boldsymbol{A} = \emptyset$. Therefore, in line 9 the union set is obtained to update $\boldsymbol{E}'_{\mathrm{o}}$. A new instance of the main problem is solved in line 10, using the initial point $\boldsymbol{X}_{\mathrm{ws}}$ (warm-start point), while considering the full wind power generation scenarios indicated by the user Ω, and the system states related to edges cumulatively installed in all iterations, ($\boldsymbol{K'} = \Phi(\boldsymbol{E}'_{\mathrm{o}})$).

When the Algorithm 1 converges, the scenario criterion is met: obtention of the proper set $\boldsymbol{K'}$; meaning that all representative systems states have been already considered.

1. $[\boldsymbol{X}_d, \boldsymbol{Y}_d] \leftarrow \arg P^{\boldsymbol{\Omega},\boldsymbol{K'}} : \Omega = \omega_n, \boldsymbol{K'} = k_o$
2. $\boldsymbol{E'} \leftarrow \boldsymbol{Y}_d = \{[ij]\} : y_{ij} = 1 \quad \forall [ij] \in \boldsymbol{E} : [ij]$ *satisfies reliability level* r_c
3. $\boldsymbol{E}'_o \leftarrow \emptyset, \boldsymbol{X}_{ws} \leftarrow \boldsymbol{X}_d \cup \boldsymbol{Y}_d$
4. **for** $(\kappa = 1 : 1 : \kappa_{max})$ **do**
5. $\quad \boldsymbol{A} \leftarrow \boldsymbol{E'} \cap \boldsymbol{E}'_o$
6. $\quad$ **if** $(\boldsymbol{E'} == \boldsymbol{A})$ **then**
7. $\quad\quad$ *Break*
8. $\quad$ **end if**
9. $\quad \boldsymbol{E}'_o \leftarrow \boldsymbol{E'} \cup \boldsymbol{E}'_o$
10. $\quad [\boldsymbol{X}, \boldsymbol{Y}] \leftarrow \arg P^{\boldsymbol{\Omega},\boldsymbol{K'}} : \Omega, \boldsymbol{K'} = \Phi(\boldsymbol{E}'_o) \cup k_o$ *with initial point* $\boldsymbol{X}_{ws}$. $\Upsilon = \{\Omega, \boldsymbol{K'}\}$
11. $\quad \boldsymbol{E'} \leftarrow \boldsymbol{Y} = \{[ij]\} : y_{ij} = 1 \quad \forall [ij] \in \boldsymbol{E} : [ij]$ *satisfies reliability level* r_c
12. $\quad \boldsymbol{X}_{ws} \leftarrow \boldsymbol{X} \cup \boldsymbol{Y}$
13. **end for**

Algorithm 1: Progressive Contingency Incorporation (PCI) Algorithm

4. Case study

The applicability of the method explained in Section 2.4 is illustrated using Ormonde OWF [19] as case study. The experiments have been carried out on an Intel Core i7-6600U CPU running at 2.50 GHz and with 16 GB of RAM. The chosen solver is IBM ILOG CPLEX Optimization Studio V12.7.1 [20]. The main input parameters are shown in Table 1. A Mean Time To Repair (MTTR) per failure of 30 days (720 hours) is considered in this study [4]. The objective function (1) is applied in this case study as the main aim is to present the model's performance and quantitative comparison versus a deterministic version.

Table 1. Data inputs

P_n	V_n	Life	c_e	MTTR	$\boldsymbol{U}$	$\boldsymbol{C}$	n_w	υ	σ	ϕ	r_c
5 MW	33 kV	30 y	2.86 $\frac{€}{Ah}$	720 h	$\{530, 655, 775\}$ A	$\{450, 510, 570\}$ k€/km	30	6	10	4	1

The power magnitudes are $\zeta^1 = 1$ (ω_n), $\zeta^2 = 0.5$, $\zeta^3 = 0.2$, and $\zeta^4 = 0$. The duration times account for the project lifetime (30 years) and considering 8760 hours per year: $\tau^1 = 65700$ hours (ω_n), $\tau^2 = 91980$ hours, $\tau^3 = 91980$ hours, and $\tau^4 = 13140$ hours. A cable failure probability is calculated as per $\psi^k = \frac{MTTR}{MTTR+MTBT\cdot\frac{8760}{d_{ij}}}$, with d_{ij} being the edge length where the component is installed. The results for this case study are obtained by varying the MTBF from 10 to 178 years kilometres per failure, with the latter value being listed as the most critical for OWFs medium voltage cables under operation in [4]. Early stage in offshore projects maturity and the consequent scarcity of available data cast uncertainty over the accuracy of this parameter, implying that more critical situations can be faced in future projects. Each MTBF value represents a different stochastic problem meaning that the model is run individually.

Quantitative assessment for the comparison between the output of the stochastic model ($[\boldsymbol{X}, \boldsymbol{Y}]$), and the output of the deterministic model ($[\boldsymbol{X}_d, \boldsymbol{Y}_d]$) is carried out. For the latter, a recourse problem is tackled $Q([\boldsymbol{X}_d, \boldsymbol{Y}_d])$, defined as minimization of the expected costs (reliability costs) given the scenario tree (Υ) obtained from the wind power generation scenarios Ω, and the system states linked to $\boldsymbol{Y}_d$.

For all the launched instances of MTBF an optimality gap of 0% has been set up, and a reliability level of $r_c = 1$ is assumed; this means that only those feeders connected directly to the OSS are subject to failure (the main feeders).

In-detail cable layout results for a MTBF of 10 are shown in Figure 2. Due to the rather straightforward layout of the wind farm, the main difference between the deterministic and stochastic technique is the use of larger cables on the connections close to the OSS. For OWFs with more wind turbines and/or more irregular layout, the changes would likely expand to the connections between the wind turbines.

The economic comparison between deterministic and probabilistic model (see Figure 3(a)), indicates that for MTBF values inferior to 30, the stochastic model provides a cheaper system in overall terms; this is achieved as reliability costs are lower at the expense of more costly cable infrastructure (in this particular case only due to cable sizing). The values in Figure 3(a) are expressed as the percentage difference between the deterministic and stochastic model relative to the latter. The associated reliability costs for the deterministic designed layout are calculated through the aforementioned recourse problem; a DC power flow and undistpached energy are the main results for this particular task.

Conversely, beyond MTBF=30, the failures probabilities drop considerably, resulting in an equal weight for each cost unit (initial investment and reliability costs) in the objective function of the deterministic model. This basically means that the reliability costs become trivial, and hence the focus is merely on the investment costs reduction. To compare the overall costs, the deterministic layout solution is run with the scenarios analyzed in the stochastic.

For large enough values of r_c, for instance such that all edges are covered, one could expect that the MTBF break-even point would move further right, that is, stochastic programming would provide overall more economic benefits for less frequent failures rates.

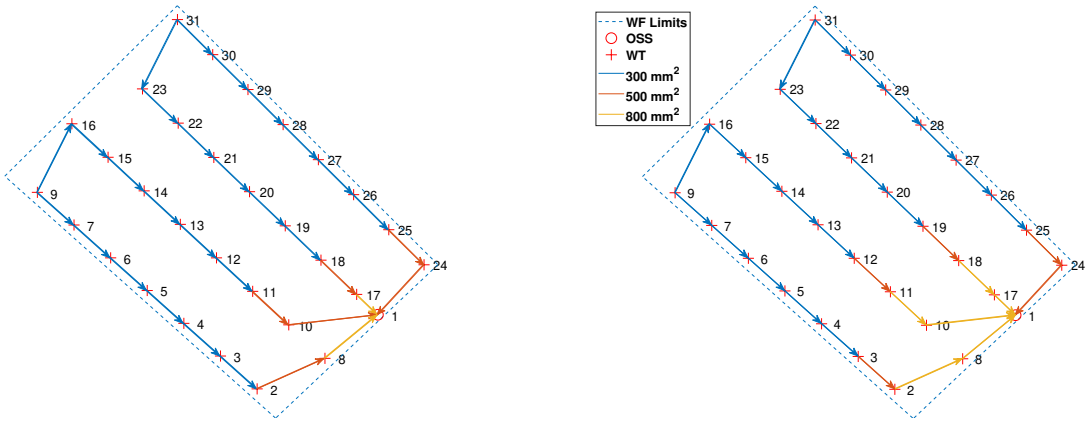

(a) Deterministic designed layout

(b) Stochastic designed layout

Figure 2. Designed cables layouts for MTBF=10

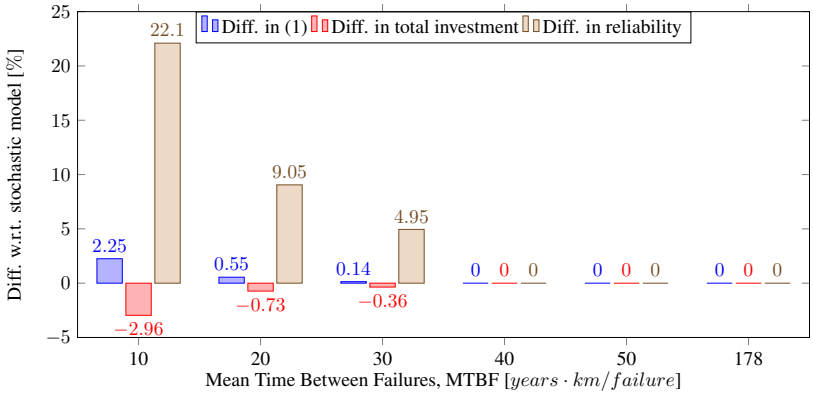

(a) Economic comparison. (Positive percentages mean savings using stochastic optimization)

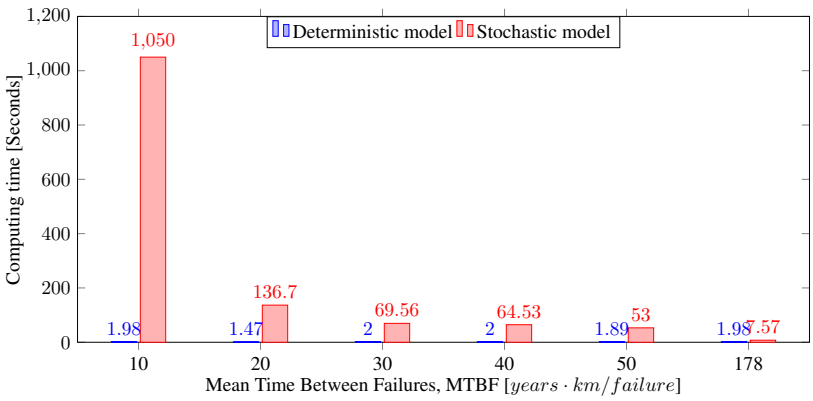

(b) Computing time comparison

Figure 3. Deterministic vs Stochastic Model for Closed-Loop Structure

Regarding computing time, in Figure 3(b), it is noticeable that the stochastic model for each MTBF instance is more complex computationally, as for instance, for a value of 10 the computing time is 530 times larger than the deterministic version. The small variations of computing time among the

deterministic cases is merely due to CPU's performance. Likewise, the larger the MTBF, the more simplified the model becomes as the reliability costs share are decreasing. The deterministic cases on the other hand are independent to the failures rate and converge in couple of seconds.

5. Conclusions

A stochastic model to quantify the economic suitability of building closed-loop collection system for OWFs is introduced in this manuscript. The objective function allows for a simultaneous consideration of initial investment, total electrical power losses costs, and reliability costs. The focus of this work has been to describe the proposed model, while presenting its application in a case study.

Results of this article point out that in function of failure parameters, network topologies with redundant power corridors may bring along significant cost benefits when applying stochastic optimization, compared to a simple deterministic approach. Additionally, the stochastic model presents a complex mathematical structure impacting considerably the required computational resources. Lastly, the contingency structure of the problem has been exploited analytically in order to simplify its complexity. Future work will present the application of this method for comparing quantitatively different network topologies, such as closed-loop and radial systems.

References

[1] BVG Associates, Recognis and WindEurope 2019 Our Energy Our Future Tech. rep.

[2] Sun X, Huang D and Wu G 2012 *Energy* **41** 298–312 URL https://doi.org/10.1016/j.energy.2012.02.054

[3] ReNEWS 2017 Rampion suffers cable fault URL http://renews.biz/105889/rampion-suffers-cable-fault/.[Accessed Oct 29, 2018]

[4] Warnock J, McMillan D, Pilgrim J and Shenton S 2019 *Energies* **12** 1–12 URL https://doi.org/10.3390/en12142682

[5] CIGRE: Working Group B110 2009 Update of service experience of HV underground and submarine cables Tech. rep. URL https://e-cigre.org/publication/ELT_243_3-update-of-service-experience-of-hv-underground-and-submarine-cable-systems.[Accessed March 30, 2020]

[6] CIGRE: Working Group B121 2009 Third-Party Damage to Underground and Submarine Cables Tech. rep. URL https://e-cigre.org/publication/398-third-party-damage-to-underground-and-submarine-cables.[Accessed March 30, 2020]

[7] Pérez-Rúa J A and Cutululis N A 2019 *IEEE Access* **7** 85796–85811 URL https://doi.org/10.1109/ACCESS.2019.2925873

[8] Fischetti M and Pisinger D 2018 *European Journal of Operational Research* **270** 917–930 URL https://doi.org/10.1016/j.ejor.2017.07.061

[9] Bauer J and Lysgaard J 2015 *Journal of the Operational Research Society* **66** 360–368 URL https://doi.org/10.1057/jors.2013.188

[10] Pillai A C, Chick J, Johanning L, Khorasanchi M and De Laleu V 2015 *Engineering Optimization* **47** 1689–1708 URL https://doi.org/10.1080/0305215X.2014.992892

[11] Klein A and Haugland D 2017 *Annals of Operations Research* **272** 373–388 URL https://doi.org/10.1007/s10479-017-2581-5

[12] Pérez-Rúa J A, Stolpe M, Das K and Cutululis N A 2020 *IEEE Transactions on Power Systems* **35** 2256–2267

[13] Banzo M and Ramos A 2011 *IEEE Transactions on Power Systems* **26** 1338–1348 URL https://doi.org/10.1109/TPWRS.2010.2075944

[14] Lumbreras S, Ramos A and Cerisola S 2013 *IEEE Transactions on Power Systems* **28** 1452–1460 URL https://doi.org/10.1109/TPWRS.2012.2225077

[15] Lumbreras S and Ramos A 2013 *IEEE Transactions on Power Systems* **28** 1434–1441 URL https://doi.org/10.1109/TPWRS.2012.2204906

[16] Calixto E 2016 *Gas and Oil Reliability Engineering* 2nd ed (Gulf Professional Publishing) URL https://www.sciencedirect.com/book/9780128054277/gas-and-oil-reliability-engineering#book-info[Accessed March 05, 2020]

[17] Billinton R and Allan R N 1992 *Reliability Evaluation of Engineering Systems: Concepts and Techniques*

[18] Grainger J J and Stevenson W D J 1994 *Power System Analysis* 2nd ed (McGraw-Hill Education)

[19] Vatenfall Ormonde Offshore Wind Farm URL https://powerplants.vattenfall.com/ormonde.[Accessed Feb 5, 2020]

[20] IBM 2015 IBM ILOG CPLEX Optimization Studio CPLEX User Manual Tech. rep. URL https://www.ibm.com/support/knowledgecenter.[Accessed April 11, 2019]

{2.7182818284} ϑφερτυθιοπσδφγηξκλ